



UNIVERSITY OF
BIRMINGHAM

The Tribological Properties of PEEK Machine Elements

By

Zainab Mohammed Shukur

B.Sc.M.E M.Sc.M.E



A thesis submitted to the University of Birmingham for the degree of:

DOCTOR OF PHILOSOPHY

**Department of Mechanical Engineering
School of Engineering
University of Birmingham**

2020

UNIVERSITY OF
BIRMINGHAM

University of Birmingham Research Archive

e-theses repository

This unpublished thesis/dissertation is copyright of the author and/or third parties. The intellectual property rights of the author or third parties in respect of this work are as defined by The Copyright Designs and Patents Act 1988 or as modified by any successor legislation.

Any use made of information contained in this thesis/dissertation must be in accordance with that legislation and must be properly acknowledged. Further distribution or reproduction in any format is prohibited without the permission of the copyright holder.

Abstract

This research reports on the relative dynamic performances of laser-sintered and injection-moulded poly-ether-ether-ketone (EOS PEEK HP3) gears and discusses the possibility of producing high performance polymer gears, manufactured by laser-sintering.

Recent developments in laser-sintering of EOS PEEK HP3 have substantially improved its mechanical properties, and these are now comparable with injection-moulded PEEK.

Here the wear rates and failure mechanisms, including contact fatigue and surface melting of laser-sintered and injection-moulded EOS PEEK HP3 were tested under conditions of relatively high loads and high slip-ratios through Twin Disc test rig and TE77 EP-GEAR DYNAMICS test rig high frequency reciprocating tribometer to simulate polymer gears contact unlubricated and lubricated in addition to gears direct testing.

It was observed that the coefficient of friction and wear rates were significantly below that of injection moulded PEEK. However, when using of laser sintered EOS PEEK HP3 for gears for transmission of power, the predominant failure mechanism was bending fatigue, and this meant using this material limited power transmission to low levels.

The use of a laser-sintered EOS PEEK HP3 in gears power transmission effects by the improving the tribological performance of gear teeth with surface lubricated conditions.

Despite the advances made in laser-sintering of EOS PEEK HP3 further advances are required before it can be used for gears in power transmission.

TABLE OF CONTENTS

Introduction	i
1 Introduction	1
1.1 Polymer Machine Elements.....	2
1.2 Gearing	3
1.2.1 Theory of Gearing.....	4
1.2.2 Terminology	5
1.3 Thesis Outline.....	8
1.4 Project Aims and Objectives	8
1.5 Thesis Structure	9
2 Literature Review	11
2.1 Engineering Polymers	11
2.2 Tribology of Polymers	13
2.2.1 Lubrication.....	14
2.2.2 Friction	16
2.2.3 Frictional Heating.....	17
2.2.4 Wear 18	
2.3 Introduction- Polymer Gearing.....	27
2.3.1 Polymer Gear Temperature.....	27
2.3.2 Polymer Gear Wear.....	29
2.3.3 Polymer Gear Failure	31
2.3.4 Wear and Failure of Polymer Gears	33
2.4 CONCLUSIONS	36
3 Methodology Testing and Material	37
4.1 Introduction:	37
4.2 Theory of Polymer Gear Contact.....	37
4.3 Gear Kinematics	38
4.4 Gear Contact Calculations.....	41
4.4.1 Tribological Tests.....	44
4.4.2 Twin-Disc Technique; Rolling – Sliding Test Rig.....	44
4.4.3 Principles of TE77 (Replicating Gear Contact Conditions)	47
4.4.4 Gear Testing.....	59
	ii

4.5	Physical Properties of Polymers (Surface Microscopy).....	64
4.5.1	Scanning Alicona Microscopes.....	64
4.5.2	Scanning Electron Microscopes (SEM).....	64
4.5.3	Thermal Camera.....	64
4.5.4	Crystallinity	64
4.6	Materials.....	65
4.6.1	Injection model	65
4.6.2	Selective Laser Sintering.....	66

4 Tribological Properties of Twin Discs Simulation Additive

Manufacture Gears

72

4.1	Twin Disc Testing.....	72
4.2	Friction Coefficient and Temperatures Results for un-lubricated tests	73
4.3	The Steady State Friction Coefficient: Non-lubricated Tests.....	76
4.4	Wear Mechanisms and Topographical Analysis: Non-lubricated Tests	78
4.5	Wear Tracks.....	81
4.6	Average wear rate versus test severity	83
4.7	Measured Temperature, Non-lubricated Tests	86
4.8	Bulk Temperature	88
4.9	Crystallinity Measures	92
4.10	The Properties of Lubricated EOS PEEK HP3	94
4.11	Wear Mechanisms and Topographical Analysis: Lubricated Tests.....	95
4.12	Friction Coefficient Properties for EOS PEEK HP3: Lubricated Conditions.....	99
4.13	Measured contact temperature.....	102
4.14	Conclusions	102

5 Tribological Simulation of PEEK Gears Using Energy pulse method

5.1	Materials & Methods	107
5.2	Tribological tests.....	107
5.3	Theoretical Estimation of Film Thickness for The EP Kinematic Conditions..	108
5.3.1	Effect of the Slide/ Roll Ratios on the Film Thickness for the EP Kinematic Conditions.....	110
5.3.2	Effect of the Frequency on the Film Thickness for the EP Kinematic Conditions	111
5.3.3	Effect of the Loads on the Film Thickness for the EP Kinematic Conditions ..	112

5.3.4	Effect of Stroke Length on the Film Thickness for the EP Kinematic Conditions.	113
5.4	Tribological Properties of Polymer vs. Steel Simulation of lubricated Gear. ...	114
5.4.1	Frictional Results of PEEK lubricated.	114
5.4.2	Results of Wear and Energy Pulse.....	116
5.5	Tribological Properties of Polymer Vs. Steel in the Simulation of Gear Un- Lubricated.	120
5.5.1	Results – Friction Coefficients	120
5.5.2	Results – Wear.....	122
5.6	CONCLUSIONS	125

6 THE SUITABILITY OF LASER-SINTERED PEEK FOR GEAR APPLICATIONS 127

6.1	Gear Production.....	127
6.1	Test Methods	129
6.2	Results	130
6.2.1	Gear Failure	130
6.2.1	Gear Wear.....	135
6.3	CONCLUSIONS	148

7 CONCLUSIONS AND FUTURE WORK 149

7.1	Chapter 4 Conclusion.....	149
7.2	Chapter 5 Conclusion.....	150
7.3	Chapter 6 Conclusion.....	151
7.4	Summary	153
7.5	Future Work.....	153
7.5.1	Tribological Testing and Mechanical	154
7.5.2	Gear Design	154

FIGURES INDEX

Figure 1.1:Characterising non-conformal machine elements.....	3
Figure 1.2: (a) Construction of an involute curve (b) Conjugate action, (after Shigley, et al., [5, 10])	5
Figure 1.3: Showing gear nomenclature (after Shigley, et al., [10]).....	5
Figure 1.4: Nomenclature associated with a pair of meshing gears (after Shigley, et al., [10]).....	7
Figure 1.5: Definition of contact ratio (after Merritt, [11]).....	8
Figure 1-6 summarises the development steps to be used in the development of optimised laser sintered PEEK gear geometry.	10
Figure 2.1: The stages of thermoplastic transitional as a function of temperature [13].....	12
Figure 2.2. A random surface showing the roughness after [16].	13
Figure 2.3: Cross-section of boundary lubrication regimes for two notional surfaces:.....	14
Figure 2.4 Schematic diagram of energy losses due to friction after [16].	16
Figure 2.5: Illustration of physical contact area and contact surface, after [16].	17
Figure 2.6: Two-zone model of friction and wear processes. after [33].	20
Figure 2.7: Transitions in cohesive wear mechanisms, after [32, 44].	22
Figure 2.8: A Comparison of the energy calculated from friction and hysteresis for a pair of polyamide meshing gears (after [7]).	28
Figure 2.9: wear damage of polymer gear: [25].	30
Figure 2.10: Typical wear, generally material independent {Dearn, 2009 #197}.....	31
Figure 2.11: Gear wall and Root failure [73].	32
Figure 2.12: gross wear [28].	32
Figure 2.13: Pitch line failure in Nylon 6/6 composite (glass fibre) [28].	33
Figure 2.14: gear pitting [28].	33
9 Figure 3.1: Actual and hypothetical contact paths for two polymer gear teeth as they mesh [84].	38
Figure 3.2: Load share ratio as a function of roll angle for a perfectly stiff gear tooth, and polymer gear with deflection (after Karimpour, et al. [6])	39

Figure 3.3: a) Rolling (V_{roll}) and sliding (V_{slide}) velocities, and b) Resulting Slide-roll ratio, for polymer gear contact.....	40
Figure 3.4: Contact paths of perfectly stiff gear, with A-P the approach path, and P-B the path of recess [10].	43
Figure 3.5: Schematic of the twin-disc test rig (after [14, 75]).	46
Figure 3.6: Twin-disc test geometry and a sample disc.....	46
Figure 3.7: EP-Gear Slide-roll adaptor for the TE 77 EP-GEAR DYNAMICS high frequency reciprocating tribometer (after [23]).	47
Figure 3.8: Schematic diagram of disc-on-plate setup with rolling-sliding motion.	49
Figure 3.9 Operating Envelopes of TE 77 EP-GEAR DYNAMICS (after [23]).	50
Figure 3.10: Slide-roll ratio for polymer gear contact, continuous blackline. The grey rectangle on the left shows the area of simulated twin-disc testing, and the blue rectangle shows the area for the EP/Gear adaptor (after [[27])	52
Figure 3.11: The three rolling-sliding ratios (after [4]).	53
Figure 3.12: A schematic of the equipment used and the variable, EP gear Slide-roll adaptor [87].	53
Figure 3.13: The process of gear tooth engagement, represent rolling velocities relative to the contact point (after Plint [88]).	57
Figure 3.14: Tooth contact condition, driving gear, two 30-tooth 20 deg. Pressure angle spur gears (after Plint [88]).	58
Figure 3.15: Birmingham standard rack geometry [89].....	59
Figure 3.16: Birmingham standard gear 20° pressure angle[89].	60
Figure 3.17: Mark II test rig, designed by White, 1999 [89].	62
Figure 3.18 the pylon 6 Camera.	63
Figure 3.19: selective laser sintering process.....	67
Figure 3.20: Electro Optical Systems (EOS) P800 High Temperature Laser Sintering (HTLS) system, (source EOS).....	67
Figure 3.21: the mechanical properties of various selectively laser sintered polymeric materials [95].	68

Figure 3.22: Effect of (X,Y,Z) orientations on ultimate tensile strength, and percentage elongation-to-break, for HT-LS EOS PEEK HP3 compared with IM PEEK specimens [103].....	69
Figure 4.1 : Results obtained for surface temperature, wear and friction coefficient for EOS PEEK HP3 disc running against EOS PEEK HP3, contact pressure 56 MPa and slip ratio 14.29%.....	74
Figure 4.2: Results obtained for surface temperature, wear and friction coefficient for EOS PEEK HP3 disc running against steel disc under contact pressure of 56 MPa and slip ratio of 14.29%.....	75
Figure 4.3: Results obtained for surface temperature, wear and friction coefficient for PEEK disc running against steel disc under contact pressure of 56 MPa and slip ratio of 14.29%.....	75
Figure 4.4: The time steady state average friction coefficient EOS PEEK HP3 vs. EOS PEEK HP3 disc for three applied pressures (39, 48, and 56 MPa), three slip values (3.94, 14.29, and 28.57%) showing the test duration at which peak value was attained.....	77
Figure 4.5: The time steady state average friction coefficient EOS PEEK HP3 disc vs. steel disc for three applied pressures (39, 48, and 56 MPa), three slip values (3.94, 14.29, and 28.57%) showing the test duration at which peak value was attained.....	78
Figure 4.6: The time steady state average friction coefficient for PEEK vs. steel disc for three applied pressures (39, 48, and 56 MPa), three slip values (3.94, 14.29, and 28.57%) showing the test duration at which peak value was attained.....	78
Figure 4.7: Surface damage incurred in EOS PEEK HP3 vs. EOS PEEK HP3, EOS PEEK HP3 vs. steel, PEEK vs. steel and PEEK vs. PEEK tests with 14.29% slip-ratio and contact pressure 56 MPa.....	80
Figure 4.8: Wear as seen by an optical microscope for EOS PEEK HP3 disc vs. EOS PEEK HP3 disc, for contact pressure of 56 MPa and three slip-ratios, 28.57%, 14.28% and 3.9%.....	81
Figure 4.9: Wear as seen by an optical microscope for EOS PEEK HP3 disc vs. steel disc, for contact pressure of 56 MPa and three slip-ratios, 28.57%, 14.28% and 3.9%.....	82
Figure 4.10: Wear as seen by an optical microscope for PEEK disc vs. steel disc, for contact pressure of 56 MPa and three slip-ratios, 28.57%, 14.28% and 3.9%.....	82
Figure 4.11: Average wear rate verses test severity for EOS PEEK HP3 disc vs. EOS PEEK HP3 disc twin disc tests.....	83
Figure 4.12: Average wear rate verses test severity for EOS PEEK HP3 disc vs. steel disc twin disc tests.....	84

Figure 4.13: Average wear rate verses test severity for PEEK disc vs. steel disc twin disc tests. .84	84
Figure 4.14: Infrared temperature profile for EOS PEEK HP3 disc vs. EOS PEEK HP3 disc, along lines A and B measured at the end of the test under the conditions of 14.29% slip- ratio and contact pressure 56 MPa.....87	87
Figure 4.15: Infrared temperature profiles for EOS PEEK HP3 disc vs. steel disc along lines A and B measured at the end of the test under the conditions of 14.29% slip-ratio and contact pressure 56 MPa.87	87
Figure 4.16: Maximum measured temperature and coefficient of friction for all test conditions: EOS PEEK HP3 disc vs. EOS PEEK HP3 disc.90	90
Figure 4.17: Maximum measured temperature and coefficient of friction for all test conditions: EOS PEEK HP3 disc vs. steel disc.91	91
Figure 4.18: Maximum measured temperature vs. coefficient of friction for all test conditions: PEEK disc vs. steel disc.....91	91
Figure 4.19: SEM micrographs of the surface of EOS PEEK HP3 (as produced). Where SEM is the Scanning Electron Microscope), and SOM is the Scanning Optical Microscope.....95	95
Figure 4.20: SEM micrographs of the surface of EOS PEEK HP3.....96	96
Figure 4.21: Measured EDS spectrum on the surface of the disc EOS PEEK HP397	97
Figure 4.22: shows the location of silicone oil on the surface of the disc EOS PEEK HP3 Mixed map: Silicon (red), Iron (green) by EDS,.....97	97
Figure 4.23: Frictional coefficient for EOS PEEK HP3 vs. EOS PEEK HP3, for contact pressures 56 and 39 MPa, with slip ratio 28.57% for lubricated (L) and non- lubricated conditions (Un-L).99	99
Figure 4.24: Frictional coefficient for EOS PEEK HP3 vs. steel, with contact pressures 56 and 39 MPa, and slip ratio 28.57%, lubricated (L) and non-lubricated (Un-L) conditions.....100	100
Figure 4.25: Frictional coefficient for PEEK vs. steel, with contact pressures 56 and 39 MPa, and slip ratio 28.57%, lubricated (L) and non-lubricated (Un-L) conditions.100	100
Figure 5.1: showing the film thicknesses for the three lubricants tested for the slide/roll ratios 83% using the TE77 EP/Gear adaptor during a single reciprocating stroke 10mm, 2 HZ.109	109
Figure 5.2: showing the film thicknesses for the three lubricants tested for the slide/roll ratio 43%, using the TE77 EP/Gear adaptor during a single reciprocating stroke 10mm, 2 HZ.....109	109

Figure 5.3: showing the film thicknesses for the three lubricants tested for the slide/roll ratios 25%, using the TE77 EP/Gear adaptor during a single reciprocating stroke 10mm, 2 HZ.	110
Figure 5.4: showing the film thicknesses for the three slide/roll ratios for oil lubricants tested using the TE77 EP/Gear adaptor during a single reciprocating stroke 10mm, and 2 HZ. .	111
Figure 5.5: showing effect the different frequency on the film thicknesses oil lubricants for the slide/ roll ratio 83.8% by using the TE77 EP/Gear adaptor during a single reciprocating stroke 10 mm.....	112
Figure 5.6: showing effect the contact pressures on the film thicknesses oil lubricants for the slide/ roll ratio 83.8% by using the TE77 EP/Gear adaptor during a single reciprocating stroke 10 mm, 2HZ.....	112
Figure 5.7: showing effect the load on the film thicknesses oil lubricants for the slid/ roll ratio 83.8% by using the TE77 EP/Gear adaptor during a single reciprocating for contact pressure 39 Nm, and 2HZ.	113
Figure 5.8: showing the average friction coefficient plotted against time for PEEK-Steel, where the initial represents the lubricants (W- deionised water, O- SN100 base oil and S-Silicone oil), and the percentage is the slide/ roll ratio.	114
Figure 5.9: showing the average time taken to reach steady-state frictional conditions for each of the three lubricants and three slide/roll ratios for PEEK-Steel Contact.....	115
Figure 5.10: showing (a) a sample of the measured wear track and (b) the profile of the same wear scar, generated on the PEEK plate at a slide/ roll ratio of 83.3% and lubricated with deionised water.....	117
Figure 5.11: showing the calculated energy pulse with volume of wear during the two hours. ..	118
Figure 5.12: showing SEM micrographs of the worn PEEK surfaces at a slide/ roll ratio of 83.3%, when lubricated with (a) deionised water, (b) SN100 base oil, and, (c) silicone oil. Note: images were taken from the centre of the wear scar from each sample.....	119
Figure 5.13: showing the average friction coefficient plotted against time for EOS PEEK HP3 - Steel, PEEK-Steel, and PEEK CA30%-Steel, where the slide/ roll ratio was 83.3% , contact pressure 39 MPa and 2 HZ	121
Figure 5.14: Friction coefficient (EOS PEEK HP3 vs Steel) unlubricated.....	121
Figure 5.15: friction Coefficient (Steel vs. EOS PEEK HP3 – lubricated).....	122

Figure 5.16: Profile of surface depth of scars generated on non-lubricated EOS PEEK HP3, PEEK, and PEEK CA 30% plates (frequency 2 Hz, contact pressure 39 MPa, and slide/ roll ratio 83.3%).....	123
Figure 5.17: : Smearing of the surface asperities of EOS PEEK HP3: A) contact pressure 39 MPa, frequency 2 Hz, non-lubricated, B); as A but lubricant added; and C) contact pressure 56 MPa and frequency 2 Hz with lubricant added.	124
Figure 5.18: Wear of surface asperities of EOS PEEK HP3 for A) unlubricated and B) lubricated tests; contact pressure 56 MPa and frequency 2 Hz.	125
Figure 6.1: Keyway re-design to allow for removal of the steel hub [after [2]].	128
Figure 6.2: Manufactured gear geometry [after [2]].....	128
Figure 6.3: EOSINT P800 laser-sintering machine.....	129
Figure 6.4: Hub assembly.	129
Figure 6.5: Root failures of EOS PEEK HP3 with dry running.....	131
Figure 6.6: Regions of failure: Region A and Region B, surface fracture.....	131
Figure 6.7: Regions of failure: Region A, and; Region B.....	132
Figure 6.8: Failure surface fracture on the boundary surface for EOS PEEK HP3 vs steel test at 1000 rpm and load 8.2 Nm.....	132
Figure 6.9: Failure surface (Region A).....	133
Figure 6.10: Partially sintered on the surface. (Region A)	134
Figure 6.11: Failure surface gear teeth at Region B.	135
Figure 6.12: Differential wear scan using pylon 6 Camera, the direction of rotation clockwise .	137
Figure 6.13: wear loss for the EOS PEEK HP3 vs. EOS PEEK HP3 gears lubricated tested.	139
Figure 6.14: wear loss of the EOS PEEK HP3 vs. Steel gears lubricated tested.	139
Figure 6.15: wear loss for the un-lubricated tested	140
Figure 6.16: scuffing on addenda of gear tooth	141
Figure 6.17: EOS PEEK HP3 gear the pitch line	142
Figure 6.18: material build-up and smearing at the end of the mesh.....	142
Figure 6.19: EOS PEEK HP3 transfer to the metal (non-lubricated conditions)	143
Figure 6.20: EOS PEEK HP3 vs. Steel gear teeth lubricated.	144

Figure 6.21: Lubricated wear of EOS PEEK HP3 vs. EOS PEEK HP3 gear teeth.	144
Figure 6.22: EDS of the surface EOS PEEK HP3 gear for Test 6, around the pitch line [Platinum coating]	145
Figure 6.23: EDS of the surface EOS PEEK HP3 surface tooth for the Test 5, around the pitch line [Platinum coating].....	145
Figure 6.24: EOS PEEK HP3 gear tooth lubricated, Test 6.....	146
Figure 6.25: EOS PEEK HP3 of gear tooth lubricated Test 5.	146
Figure 6.26: EOS PEEK HP3 gear in Test 6 (with lubricant).....	147
Figure 6.27: the pitch line of EOS PEEK HP3 gear in Test 5 (with lubricant).....	147

Nomenclature

A	Area	m m ²
a	Semi width of contact	m
b	width	m
C	Centre distance	m
\dot{C}	Maximum sliding velocity (gears)	m m /s
D	Pore diameter	μ m
d_p	Pitch circle diameter	mm
E	Elastic modulus	MPa
E^*	Reduced modulus	MPa
E'	In-phase storage modulus	MPa
E''	Out-of-phase loss modulus	MPa
E_f	Flexural modulus	MPa
E_t	Tensile modulus	MPa
F	Force	N
f	Frequency	Hz
GIC	Critical energy release rate	J/m ²
H	Hardness	----
h	Thickness	mm
l_a	Path of approach	mm
l_r	Path of recess	mm
KIC	Critical stress intensity factor	MPa/m ²
l	Length	mm
Lab	length of contact	mm
m	Gear tooth module	mm
N	Number of gear teeth	----
P	Pressure	MPa
Pc	Circular pitch	mm

r	Strain rate	%/min
R	Effective radius	mm
T	Torque	Nm
T	Temperature	C°
$\tan \delta$	Loss tangent	---
T_f	Flash temperature	C°
T_g	Glass transition temperature	
T_i	Interfacial temperature	C°
T_m	Melting temperature	C°
v	Velocity	mm/s
V_{max}	Maximum sliding velocity	mm/s
α	Plasticity index	---
β	Asperity tip radius	mm
γ	Surface tension	N/m
ΔH	Change in enthalpy Contact	J
ε	Contact ratio	---
ε	Strain	---
ν	Poisson's ratio	---
ρ	Radius of curvature	mm
σ	Standard deviation of asperity heights	---
σ	Stress	MPa
ϕ	Pressure angle	Degree
ψ	Working pressure angle	
ω	Rotational speed	rpm

Subscripts

1	Pinion (driver)
2	Wheel (driven)
0	Initial value
f	Flexural
c	Compressive
t	Tensile

Abbreviations

ALM	Additive Layer manufacturing
DMTA	Dynamic Mechanical Thermal Analysis
DSP	Differential Scanning Calorimetry
EDI	Energy Dispersive X-ray Spectroscopy
TE77	High Frequency Reciprocating Rig
HT-SLS	High Temperature Selective Laser Sintering

EOS PEEK HP3	laser-sintered and injection-moulded poly-ether-ether-ketone
L	Lubricated
LSR	Load Share Ratio
LVDT	Linear Variable differential transformer
PA	Polyamide
PAEK	Poluaryletherketone
PC	Path of Contact
PEEK	Poly-ether-ether-ketone
PLF	Pitch-Line-Fracture
POM	Polyoxymethylene
PTFE	Polytetrafluoroethylene
RTI	Relative Thermal Index
SEM	Scanning Electron Microscopy (Scanning Electron Microscope)
Unl	Unlubricated

Acknowledged

Firstly, I would like to thank Prof. Karl Dearn and Dr. Stephen Kukureka for their continual assistance and supervision throughout this project.

With regards to the collaborating partners in this research project, I would like to express my gratitude to Prof. Yongkang Chen of the University of Hertfordshire for your efforts and hospitality.

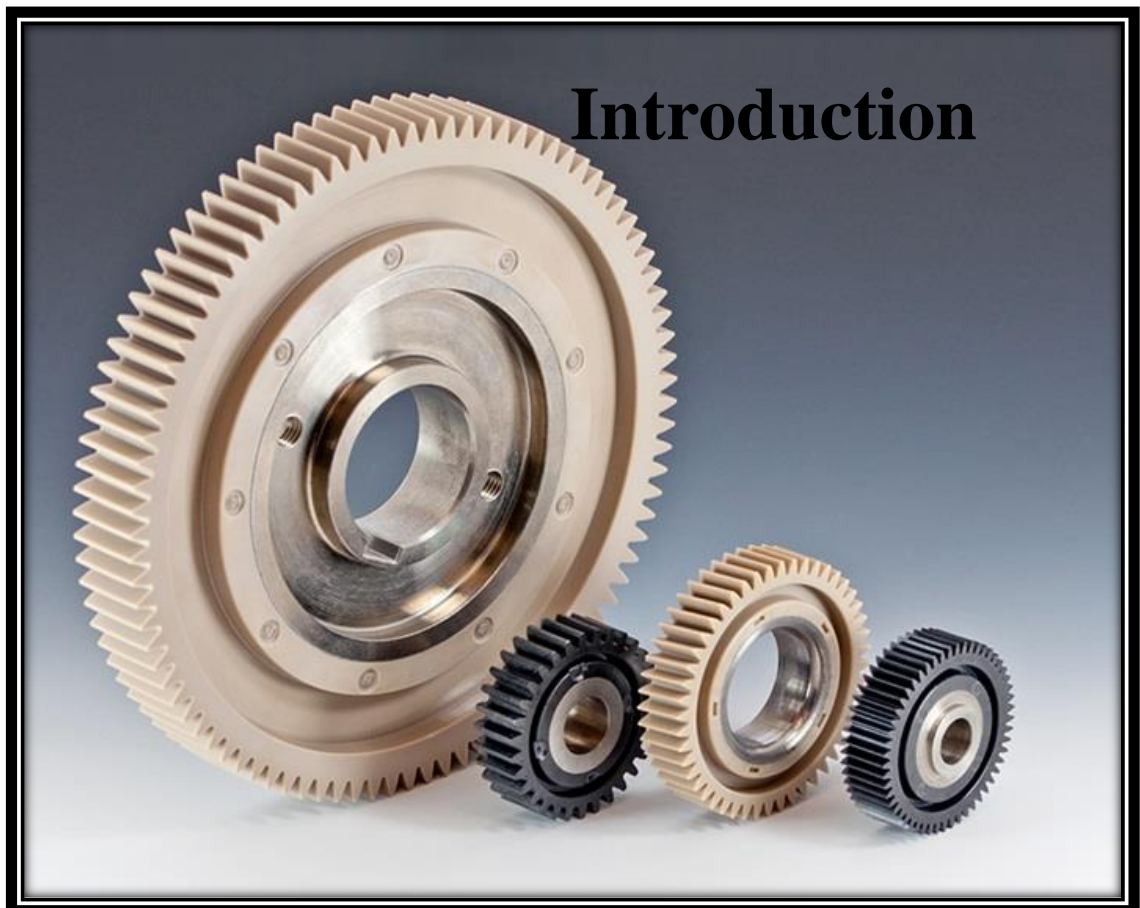
I would also like to thank my friends and my group (Dr David Eckold's, Dr. Iestyn Stead and Miss. Sutartip Wittayapiyanon) for your help and advice and support...

I would also like to thank gratefully, the Ministry of Higher Education and Scientific Research (MHE) and University of Kufa in Iraq for the financial support.

Finally, I would like to thank my family and my dear friend from Iraq for his ongoing and support... I couldn't have done it without you.

Chapter One

1



1

“To raise new questions, new possibilities, to regard old problems from a new angle, requires creative imagination and marks real advance in science”

Albert Einstein, scientist (1879-1955)

Introduction

Gears have been a fundamental engineering component used to transfer motion and energy from on shaft to another. In 4th Century BC, Aristotle wrote about wheels in order to transmit motion using friction. Some evidences of Ancient Greeks described metal gears with wedge shaped teeth, and gear wheel drives in windlasses [1]. Nevertheless, modern gear theory wasn't established until the 17th century, in which the accurate movement transmission is a central part. And since Philipe de la applied it to gearing in 1694; for the most conformal (constant speed ratio) applications, the involute has become the criterion method [2, 3].

Romans used gears in water-powered mills lifting loads such as buildings and ship anchors because of the ability of gears to amplify torque. In 18th Century, gears were also used, in order to increase rotational speeds of power textile machinery and mills, and animal fats were used in these machines as a lubricant. In modern material science, the polymeric material and its reinforcement were developed and became more widespread because of the advantages of these materials, a growing appreciation of the economic and technical advantages, and deepened understanding of polymer gear characteristics. Plastic gears are one of these materials used in power transmission in different engineering applications.

This chapter will introduce polymer machine elements; it will also consider spur gear geometry and gear theory.

1.1 Polymer Machine Elements

In general, many machine elements have contact surfaces non-conformal to each other wherever a load is carried on a small contact area. This means that the load per unit zone in conformal machine elements is lower than in elements of machines that are non-conformal because the contact areas between conformal surfaces are greater than for non-conformal machine elements. This may also be expressed as; the load per unit contact area between the elements of non-conformal machine surfaces can be much higher than for the elements of conformal machine.

The contact between components such as piston rings, journal bearings, clutches, bearings, power screws, chain linkages, V-belts and deep groove etc., is, fundamentally, machine elements conformal, and non-conformal such as gears, roller element bearings in addition to cams [4].

With non-conformal machine elements lubricated by oil, the high pressure generated results in a major increase in lubricant viscosity. Viscosity is a function of how readily the fluid flows and a substantial increase in its value will considerably promote the ability of the oil to support the load without the contact area being compressed.

Describing machine elements based on their conformity makes it possible to simulate their basic motions. Figure 1.1 illustrates a method of describing the non-conformal machine elements based on their roll-slide interactions, and testing methods that.

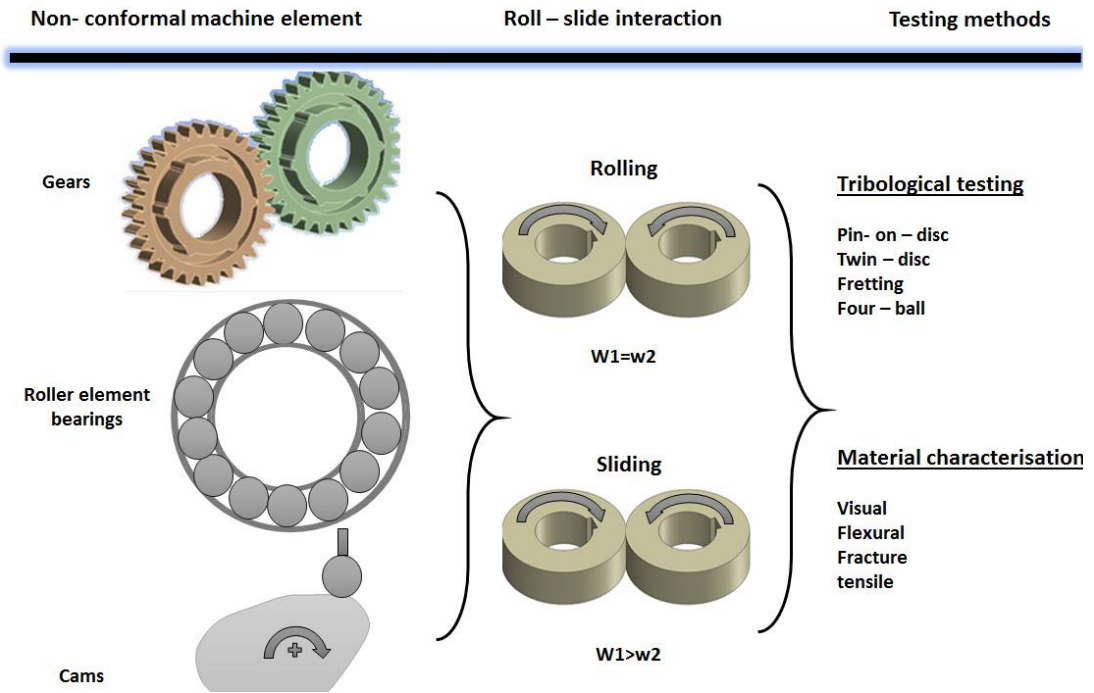


Figure 1.1:Characterising non-conformal machine elements.

1.2 Gearing

In machine elements, practical limitations need to be considered, especially when polymers are used to transmit a load [5]. Recently, this type of material has been used in numerous applications which are noticeably different from those of metal applications because of their lower strength, modulus, melting point and thermal conductivity. Their properties have meant that polymer gears are considered operationally and economically beneficial and environmentally friendly [6]. Wear and friction of the polymer results from the dissipation of mechanical energy resulting from frictional heating and deformation (hysteresis) [7]. Therefore, the progress of high-performance polymer gears focused primarily on developing a material capable of handling high interface temperatures [7].

The process of selecting the best polymer is not well understood for a particular mechanical application because of the complex interactions between such factors as friction, temperature, wear and geometry. This means that for a given mechanical operation, the only way to define polymer with confidence is to test it physically, matching its parameters as close as possible to the real operation needs.

Plastic gears are used in low speed, low load, motion-controlled applications such as those found in office equipment, automatic telling machines and domestic appliances. The advantages of the use of plastics as machine elements can be summarised as:

1. High resilience.
2. Ability to run un-lubricated.
3. Low cost (particularly when injection moulded in high volumes).

Limitations on the applications of plastic gears are [6]:

1. High initial tooling costs.
2. Susceptibility to temperature.
3. Environmental sensitivity (thermal expansion and moisture absorption).
4. Lower load capacity and stiffness.

The use of polymeric gears gives economic, operational and environmental benefits. The relatively lower costs of production and their efficiency in use have meant increased acceptance of plastics as gear materials and production of plastic gears is increasing by approximately 5.3% per year [8].

1.2.1 Theory of Gearing

The main function of gears is to transmit both rotational motion and power, and they are usually required for use where the speed of rotation is non-fluctuating. This is achieved when the meshing gears have constant angular velocities with a motion that is geometrically constrained between specified boundary surfaces, which is the motion of most involute gear teeth profiles. The most important terms used for spur gears are given in Figure 1.2 [9].

In gear design, when two gears are meshed together, there is invariably a driver and a driven part. The pinion is usually both the driver and the smaller size gear, while the larger driven is the “gear”, also known as “wheel”, and this difference in the size is the reason for their difference in speed.

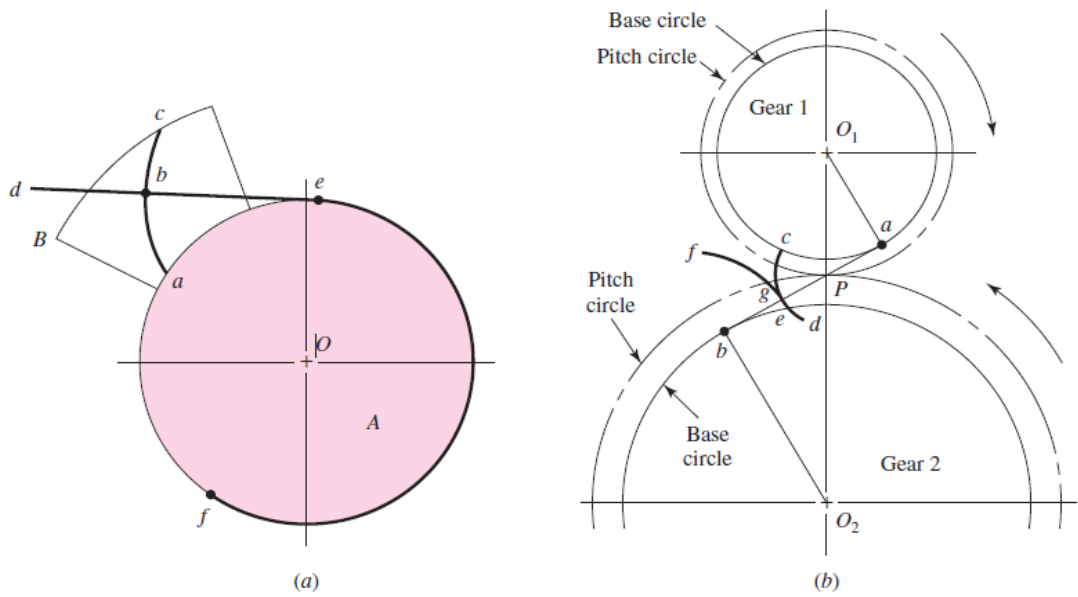


Figure 1.2: (a) Construction of an involute curve (b) Conjugate action, (after Shigley, et al., [5, 10])

1.2.2 Terminology

The nomenclature associated with spur gears and used in this project is shown in Figure 1.3, including several parameters concerned with shape of spur gear teeth such as addendum, dedendum, circular pitch, pitch circle and face width and others. These parameters will be referred to when calculating sliding and rolling velocities [10].

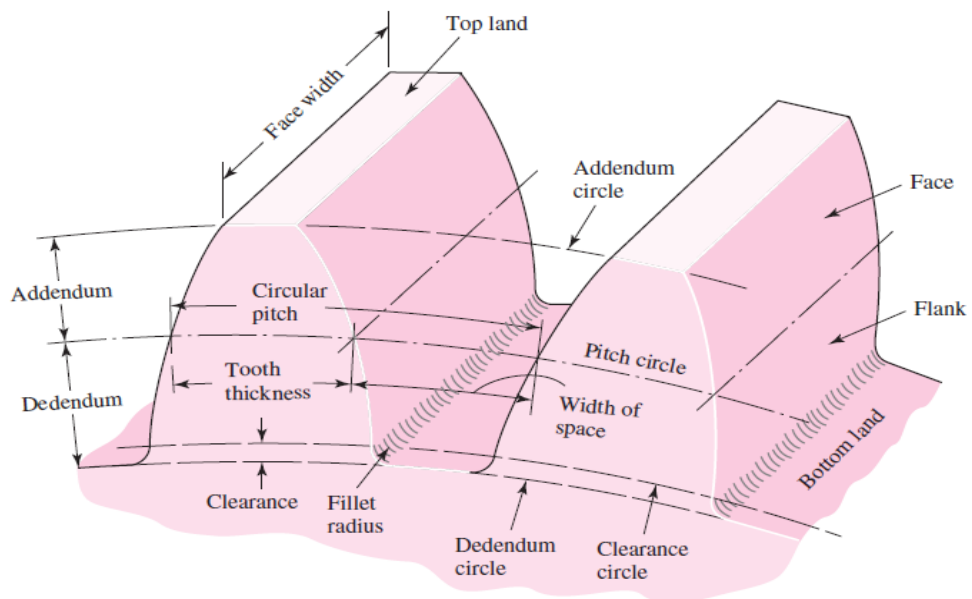


Figure 1.3: Showing gear nomenclature (after Shigley, et al., [10])

Gear Tooth Dimensions

In this section, the required gear tooth dimensions are presented in Figure 1.4:

- Centre distance, C is defined as the distance between parallel axes of the gears or the distance between centers of the diameter pitch of pinion, d_p and wheel, d_g . Mathematically this is expressed as in Equation 1.1.

$$C = \frac{d_p + d_g}{2} \quad \text{Equation 1.1}$$

- Pitch point, P is a common point of a pair gear contact between two pitch circles.
- Circular pitch p_c is the distance measured along the pitch circumference circle from a one point of tooth to the corresponding point on the next tooth, and it is calculated using Equation 1.2.

$$p_c = \frac{\pi d_p}{N_p} \quad \text{Equation 1.2}$$

- Number of teeth for pinion, N_p and wheel, N_g
- The size of a gear tooth is indexed by its module, m , the ratio of the pitch circle diameter in millimeters to the number of teeth. It is usually denoted by module. Mathematically,

$$m = \frac{d_p}{N_p} = \frac{d_g}{N_g} \quad \text{Equation 1.3}$$

- Addendum, a_e is the radial distance from the pitch circle to the top of the tooth.
- Dedendum, d_e is the radial distance from the pitch circle to the bottom of the tooth.
- The total tooth depth or working depth is the sum of the addendum and dedendum.

The clearance is the distance by which the dedendum, of one gear tooth exceeds the addendum of its mating gear tooth shown in Figure 1.3 - Figure 1.5, the nomenclature associated with two gears in mesh. When the two gears mesh, there are new considerations such as:

- The pressure angle, ϕ is the angle between the pressure line and the tangent to the pitch circle at the pitch point.
- Face width, b
- The path of contact is the path travelled between the first point of contact, a and last point of contact, b .
- The angle subtended between the first point of contact and the pitch point is the arc of approach. The angle subtended between the last point of contact and the pitch point

is the arc of recess. Summing these two arcs gives the arc of contact, ϵ which is the distance travelled by one tooth whilst in contact with another.

- The contact ratio, m_g of a pair of meshing gears is the average number of pairs of teeth in action. Mathematically, the contact ratio is a function of the ratio of the arc of contact to the circular pitch, p_c . Expressed in terms of the line of action or Pressure line, L_{ab} (see Figure 1.5) this gives:

$$\epsilon = \frac{L_{ab}}{p_c \cdot \cos \phi} \quad \text{Equation 1.4}$$

- The pressure line is showing the first and last contact of a pair of meshing gear on tooth surface at the position points of a and b , respectively. Therefore, the pitch points on tooth gear are found as A, P and B (see figure 1.5).

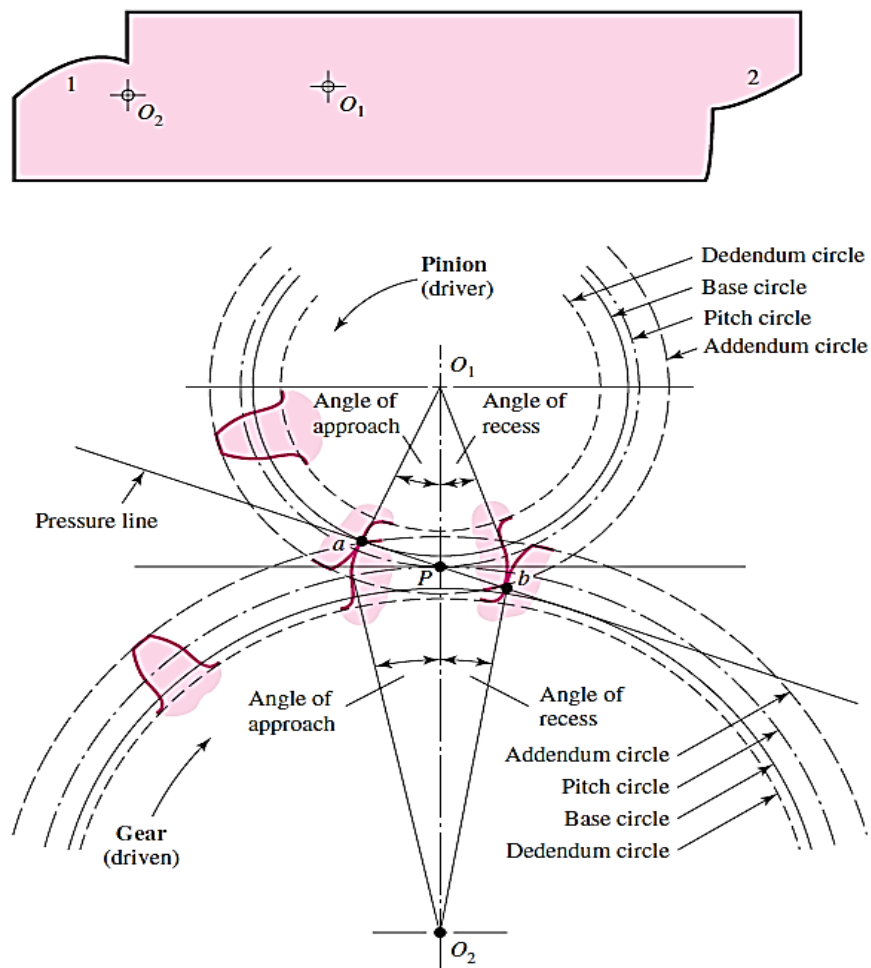


Figure 1.4: Nomenclature associated with a pair of meshing gears (after Shigley, et al., [10])

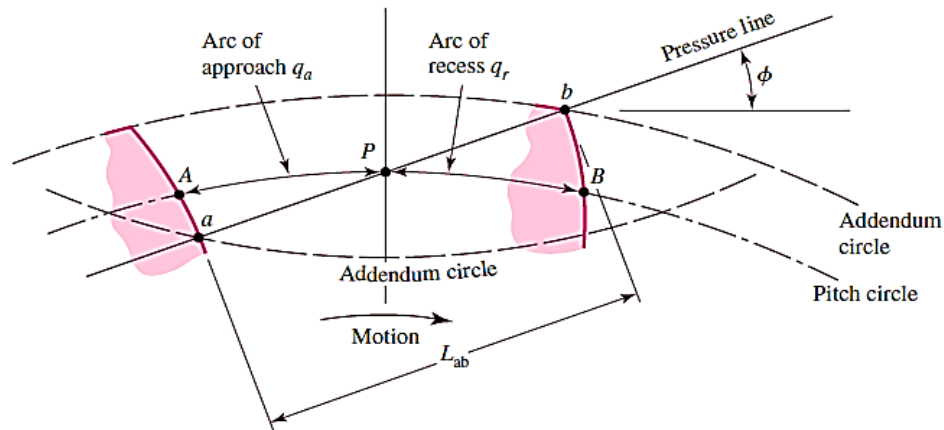


Figure 1.5: Definition of contact ratio (after Merritt, [11]).

1.3 Thesis Outline

The development of polymer gears needs improvement in the understanding of the tribological and material characteristics of polymers. Therefore, the dynamic and tribological performance of the injection moulded polyether-ether-ketone (PEEK), PEEK Composite PMCs (Vitrex, 450CA30) and laser-sintered polyether-ether-ketone 3D printing (EOS PEEK HP3) will be studied experimentally using a TE77 under replicating gear contact conditions (Energy Pulse (EP) -Gear Roll-Slide Adaptor) and the twin-disc tribometer under different conditions. Similar and dissimilar gears (or discs) are to be tested lubricated and unlubricated where four types of lubricants (water, oil SN100, and silicone oil) will be used.

1.4 Project Aims and Objectives

This thesis has main aims to study the dynamic and tribological properties of injection moulded PEEK, PMCs and laser sintered PEEK (EOS PEEK HP3) polymers used in power transmission under different operational conditions and with and without lubricant.

To do this, several objectives have been outlined:

- Review the current ‘state of the art’ of: polymer machine element wear and tribology; laser sintered materials and their application; and, the principles and mechanisms of polymer gear failure
- Investigate the tribological properties of highly loaded polymers; fundamental assessments will be made using Twin Disc test rig and TE77 EP-GEAR DYNAMICS test rig high frequency reciprocating tribometer to simulate gears in an attempt to
- Establish and characterise their properties, and to provide a benchmark for tests comparing laser sintered materials.
- Investigating the tribological properties of EOS PEEK HP3 under varying condition such as load and speed with and without lubricant by gear direct testis, mechanical performance, modes of failure and tribological response.

1.5 Thesis Structure

The present study will be consisting of seven chapters. Following this introductory section, the next chapters will be as follows:

- **Chapter two:** Review the present work of wear and tribology of polymer machine elements components and the principles and mechanisms of failure of polymer gears.
- **Chapter three:** Offers descriptions of the testing devices, the methods used to measure the friction coefficient.
- **Chapter four:** The frictional properties of PEEK HP3 EOS are evaluated using experimental twin-disc arrangements to simulate the complexities of gear loading mechanisms.
- **Chapter five:** Investigate the tribological properties of slide/roll ratios (25%, 43% and 83%) and under a variety of lubrication conditions including silicone, base oil and water; fundamental assessments will be made using TE77 replicating gear contact conditions (Energy Pulse (EP) -Gear Roll-Slide Adaptor). It was attempted to establish and characterise of the PEEK, PMCs and laser sintered PEEK (EOS PEEK HP3).

- **Chapter six:** Investigate the failure modes and tribological reaction of PEEK HP3 EOS gears to understand and develop specific gear for PEEK HP3 EOS materials.
- **Chapter seven:** Conclusions, recommendations, and suggestions for future work.

Figure 1-6 summarises the development steps to be used to optimise laser sintered PEEK gear geometry.

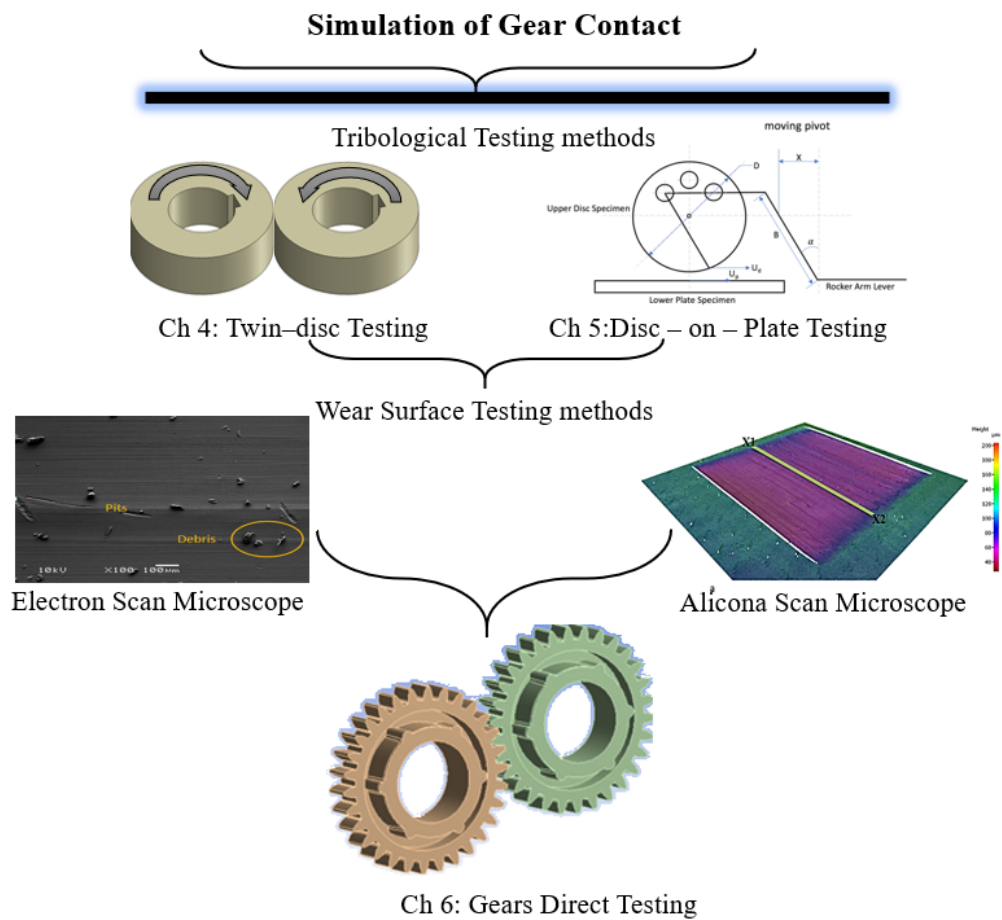
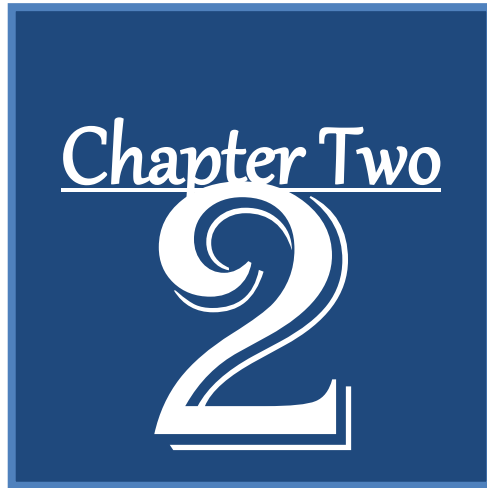


Figure 1-6 summarises the development steps to be used in the development of optimised laser sintered PEEK gear geometry.



LITERATURE REVIEW

2

“We can create a more sustainable, cleaner and safer world by making wiser energy choices.”

Robert Alan Silverstein

Literature Review

Polymers are now widely applied in mechanical systems because of ease and low cost of production, and their range of mechanical, material and tribological properties [12].

This chapter will introduce the significance of the tribological properties of polymers, their wear mechanism, friction coefficients and temperatures at area of contact, in addition to the application of polymer gears.

2.1 Engineering Polymers

In most mechanical systems it is necessary that the materials used retain certain essential characteristics at high temperatures. However, as Figure 2.1 displays, thermoplastic polymers experience a severe loss of stiffness when the operating temperature rises close to the glass transition temperature (T_g). The temperature at which the polymer structure transforms when an amorphous polymer is heated “viscous liquid or rubbery” is the Glass Transition Temperature, T_g . It could be defined as “a temperature at which amorphous polymer takes on characteristic glassy-state properties like brittleness, stiffness and rigidity (upon cooling)” [12].

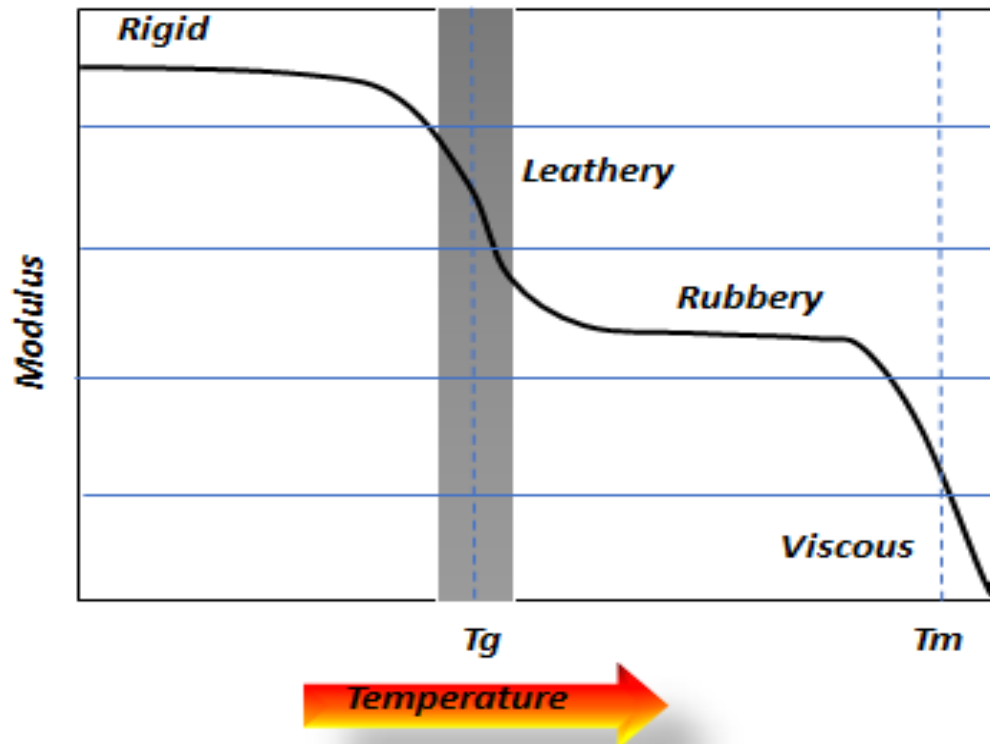


Figure 2.1: The stages of thermoplastic transitional as a function of temperature [13].

Figure 2.1 shows two distinct transition regions: around T_g , the glass temperature which marks a transition in the polymer's behaviour, and when the working temperature approaches the melting point of the polymer (T_m). Below T_g the polymer will be more glass-like - relatively hard and brittle; above T_g the polymer will be relatively soft and flexible. T_g is well above room temperature for most common polymers (rubber and Polyoxymethylene (POM) are the exception), and is the temperature at which the van der Waals forces, the inter-atomic and inter-molecular forces, are no longer sufficient to outdo the thermal energy of the molecular chains comprising the polymer, which acquire a higher level of movement [13].

Thermoplastic materials, in their great majority, are adversely affected by the changes in material properties, particularly mechanical properties, that take place around T_g . Thus, attempting to operate a polymer beyond its T_g is undesirable [14].

The polymer chains which are a key factor in the behaviour of plastics comprise a base of carbon atoms with other atoms such as hydrogen bound at several points [15].

Above T_m the polymer exists as a liquid within which the chains move easily. There are different molecular orders at temperatures under the melting point (referring to the geometry of the molecular chains).

Choosing a polymer suitable for a specific engineering purpose is a process that is neither well documented nor understood. The factors influencing the final choice will include uncertainties such as frictional wear, effect of lubrication and material temperatures. To be sure the correct selection has been made when specifying a polymer for any industrial process; the polymer must be physically tested at conditions that mirror the application. Preliminary investigation of polymer characteristics such as its T_g , T_m and crystallinity will provide an initial screening and give an indication of likely material performance. But this needs to be combined with physical tests in order to fully grasp the likely in-situ limitations of the polymer.

2.2 Tribology of Polymers

The tribological performance of two surfaces in contact depends very much on their surface structures at the microscopic level; material properties, surface roughness, and the quality of the lubricant separating them. Typically, the material properties and the microstructure will be determined by the bulk properties of the material, thus a first step in optimising the performance of a mechanical system is to choose suitable materials. One important aspect is the material surface roughness. Typically, the description of the surface structure (roughness) is simplified to two distinct scales following Eckold who described them as [16];

- i. “Waviness is the fluctuations on the macro scale, and
- ii. Roughness on the micro scale.
- iii. An example of a material displaying both waviness and roughness is shown in Figure 2.2”.



Figure 2.2. A random surface showing the roughness after [16].

2.2.1 Lubrication

Typically, lubrication is the addition of a material between two or more surfaces in contact for reducing the frictional forces. In mechanical systems the lubricant is generally a semi-solid such as grease, a fluid such as purpose-designed oil, or fluid carrying specialist additives such as nanoparticles.

Lubrication can be divided into three general regimes, see Figure 2.3: (a). boundary, (b) hydrodynamic, and (c). elastohydrodynamic lubrication.

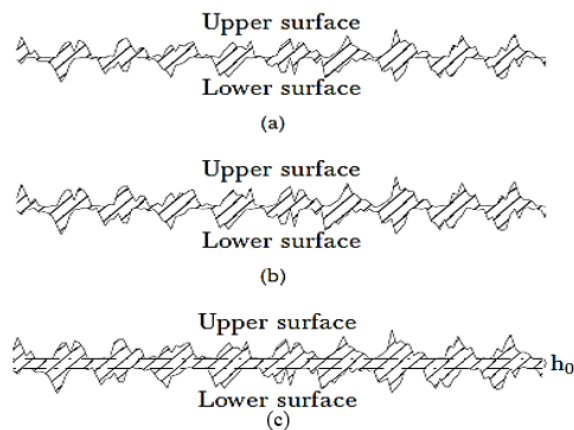


Figure 2.3: Cross-section of boundary lubrication regimes for two notional surfaces: (a) Mixed lubrication: asperities in contact, (b) Hydrodynamic lubrication: asperities mostly separated by a small proportion will touch, and (c) A distinct film of lubricant of thickness h_0 is present, asperities separated after [16].

Boundary lubrication: happens if the hydrodynamic pressure is insufficient to support the load, instead asperity on asperity contact will support the load; see Figure 2.2 & Figure 2.3 (a). This is usually due to a sliding velocity that is too low to support the full film development [17].

Hydrodynamic lubrication: the sliding velocity is adequate to generate a lubricant pressure that will support the load; there is little or no asperity on asperity contact. For hydrodynamic lubrication to occur, in addition for the sliding velocity to be sufficient to generate a pressure to support the load, the surfaces in contact must not be parallel [17]. Hydrodynamic lubrication was first noted in 1883, and shortly after in 1886, was analysed by Reynolds who produced the well-known Reynold's equation for the modelling of hydrostatic effects [18].

Elastohydrodynamic lubrication: the pressure exerted by the lubricant fully supports the load and there is complete separation of the sliding surfaces by a film of lubricant. In the performance of the system there are two additional necessary elements: where the pressure is of importance fundamental to lubricated viscosity, and the elastic properties of the sliding bodies must be known.

Because the lubricant film separated the sliding surfaces completely, bearings - for example - could operate almost indefinitely with little or no wear; provided, of course, there was no chemical attack on the bearings. Thus, in most bearing systems elastohydrodynamic lubrication is preferred.

Mixed lubrication: is a transitional state between boundary and hydrodynamic lubrication. The lubricant pressure partially supports the load, but some cases of asperity-on-asperity contact do occur.

Tribological tests in a of this research were carried out dry and with 15 ml of each of three lubricants: water, a light base oil of SN 100 used a basis for numerous industrial lubricants, and Wacker® AK 1000 silicone fluid. Stribeck curves have been presented in Chapters 4& 5 and can be used to determine in more detail the lubrication regimes occurring for the different sliding-rolling velocities.

2.2.1.1 Theoretical estimation of film thickness for the TE 77 Energy Pulse - GEAR DYNAMICS (EP).

Elastohydrodynamic lubrication theory describes the conditions of lubrication such as those found in machine elements, where contact between the surfaces occurs over a small region and is usually non-conformal. It incorporates and assesses the effects of normal load, sliding/rolling velocity, and geometry, on the theoretical film thicknesses for wide conditions range. Elastohydrodynamic Lubrication (EHL) theory also describes the change in viscosity of the lubricant due to pressure and the extent of elastic deformation in the surfaces of the bearing. [19-22], it describes the lubrication conditions typically between non conformal surfaces, like those found in elements of machines (cams, rolling-element bearings and gearing). Normal thicknesses of oil films are determined and consideration was given to the effect these have on the

performance of steel / polymer and polymer / polymer meshes. The film thicknesses are depended on the rolling velocity (entrainment speeds) that was depended on the slip ratio [23-26].

The theoretically film thickness in chapter 4 will be shown for the three slide/ roll ratios 83%, 43%, and 25%, for the three lubricants. The figures in chapter 4 offers an indication of the effect of slide/ roll ratio on generated lubricant film thicknesses for different types of lubrication by the TE77 EP/Gear adaptor during a single reciprocating stroke. The experimental conditions have been selected to simulating a PEEK/steel gear contact of the Birmingham standard benchmark geometry defined in [27] transmitting a torque of 7 Nm. As the slide/ roll ratio was increased so the film thicknesses and the entrainment velocities decreased.

2.2.2 Friction

Friction is a primary concern in mechanical systems because it is a source of loss of efficiency in the system. Energy losses due to friction are usually in the form of heat (e.g. plastic deformation/wear/fracture), see Figure 2.4. Friction can generate considerable levels of sound and vibration, but these rarely carry more than a minute fraction of the energy being lost. Of course, reducing friction will reduce the degradation of surfaces due to wear, but factors that reduce friction do not necessarily reduce wear.

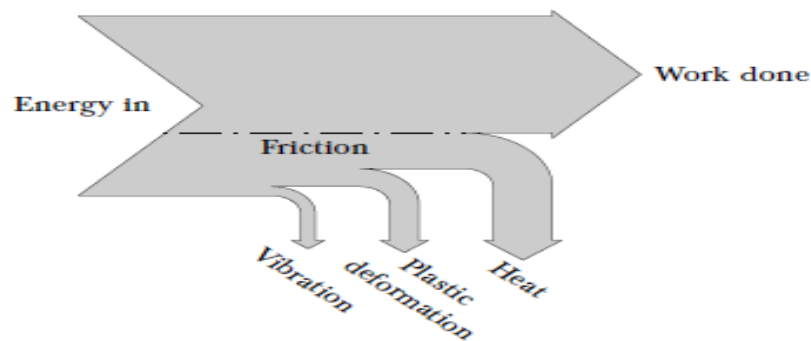


Figure 2.4 Schematic diagram of energy losses due to friction after [16].

However, friction is a complex phenomenon and the above hold in only a limited number of cases. An implicit assumption is that the geometric area of contact is the actual area of contact between the surfaces. However, the geometric area greatly exceeds the actual area of contact (the sum of those areas where the asperities of the two surfaces are in contact), see Figure 2.5.

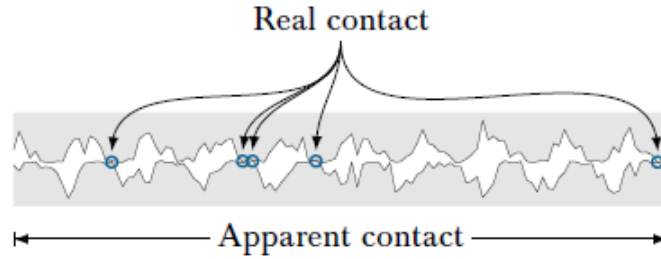


Figure 2.5: Illustration of physical contact area and contact surface, after [16].

The final law depends on the local flash temperatures (a measure of the frictional heat generated and which depends on sliding velocity) being sufficiently low, that there is no significant change in local material properties, e.g., no local thermal expansion [17]. Additionally, because polymers are viscoelastic and temperature sensitive they do not, generally, follow the laws of friction listed [28].

2.2.3 Frictional Heating

The mechanical behaviour of polymers is very much influenced by the properties of the surfaces that are interacting. This, in turn, means the polymer's properties will be a function of surface operating conditions.

Frictional heating is assumed to take place instantaneously as one surface slides over a specific point on the other; the consequent flash increase in temperature is assumed to dissipate rapidly. Thus the actual temperature at any contact point between the surfaces is the sum of the material's flash temperature and bulk temperature [29]:

$$T_{\text{interface}} = T_{\text{flash}} + T_{\text{bulk}} \quad \text{Equation 2.1}$$

where T_{flash} : the instantaneous increase in temperature as a result of frictional heating and T_{bulk} : 'the bulk temperature of the two bodies' in contact which will be a function of the measured bulk temperatures, the ambient temperature and effects of physical heating.

Blok's equation [29] (Equation 2.2), is used to calculate the flash temperature, this assumes the system to be in a condition of steady-state sliding so constraints such as sliding speed, normal pressure and heat intensity may be observed as constants:

$$\delta T_{\text{flash}} = \frac{1.11 * \mu * F(V_1^{1/2} - V_2^{1/2})}{b\sqrt{2} * k * \rho * c * a} \quad \text{Equation 2.2}$$

Where the two discs of twin disc have a semi-width of contact, a , and could be calculated as:

$$a = \sqrt{\frac{4 \cdot F \cdot R}{b \cdot \pi \cdot E}} \quad \text{Equation 2.3}$$

and contact modulus calculated as:

$$\frac{1}{E} = \frac{1 - \nu_1^2}{E_1} + \frac{1 - \nu_2^2}{E_2} \quad \text{Equation 2.4}$$

where E and ν are, Young modulus and Poisson ratio respectively.

The effective curvature can be calculated as:

$$\frac{1}{R} = \frac{1}{R_1} + \frac{1}{R_2} \quad \text{Equation 2.5}$$

These equations may be used to predict the likely peak temperature of the surfaces for two sliding surfaces in contact. It is necessary to state that Equation 2.2 assumed the sliding velocity and normal pressure were constant so that such parameters as the rate of generation of heat intensity, bandwidth sliding speed could be treated as constant. It is also necessary to note that these assumptions are not valid in the case of meshing gear teeth [30].

2.2.4 Wear

Wear results from friction forces acting on two surfaces in contact and relative movement. To design machine elements of polymer that are used to transmit load, there are specific limits that should be considered. Wear is known to be a complex process but polymer wear is generally different from metals, with much lower melting points, lower strengths and modulus. Furthermore, less thermal conductivity also suggests more severe thermal effects [12].

Initially, the surface resistance to wear was considered to be dependent principally on the hardness of the material [31]. Generally, the high value of elastic modulus associated with hard materials does mean low wear, but it has also been shown that certain polymers, even though they possess a relatively low value of elastic modulus,

can deliver significant wear resistance. It has been long recognised that to characterise the wear rate of materials the ratio of elastic modulus (E) to hardness (H), is vital [31]. The plasticity index α , as defined in Equation 2.6 is directly proportional to the ratio E/H, and is valuable for minimising wear:

$$\alpha = \frac{E}{H} \left(\frac{\sigma}{\beta} \right)^{\frac{1}{2}} \quad \text{Equation 2.6}$$

“where σ : asperity heights ‘standard deviation’

β : Asperity tip radius

E: Elastic modulus

H: Hardness

The absolute and relative motions to which the surfaces in contact are subjected, and the interactions of those surfaces are required to understand the importance of the interactions to which the contacting materials are subjected. Equation 2.6 shows that the wear resistance of a material does not depend only on the ratio E/H. But when considering E/H it must be recognised that H for polymers cannot be clearly defined because their behaviour is invariably viscoelastic and rate-dependent at the likely temperatures of interest. Any attempt to use a hardness value for a polymer must include time dependent effects. The situation is made further more complex because E will also be time dependent for polymers, because they are viscoelastic [13].

Figure 2.6. Hutchings has defined the processes thus [32]: “If the counterface is smooth, then wear may result from adhesion between the surfaces, and involve deformation only in the surface layers of the polymer. On the other hand, if the counterface is rough then its asperities will cause deformation in the polymer to a significant depth; wear then results either from abrasion associated with plastic deformation of the polymer, or from fatigue crack growth in the deformed region. These two classes of wear mechanism, involving surface and subsurface deformation respectively, have been termed ‘interfacial’ and ‘cohesive’ wear processes”.

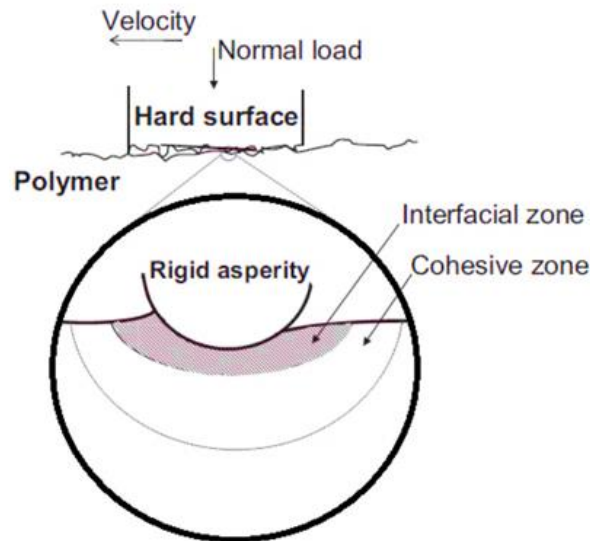


Figure 2.6: Two-zone model of friction and wear processes. after [33].

Cohesive wear takes place in the comparatively large volumes in the cohesive zone close to the polymer surface, see Figure 2.6. Cohesive wear is the dissipation of frictional energy, with damage usually caused by an asperity in the contacting surface digging into the polymer's surface. The degree of wear will obviously depend on the level to which the surface feature penetrates the polymer and the consequent stresses which occur in and across the contact area and cohesive zone and, of course, the strength and other mechanical properties of the polymer [12]. The processes taking place include the fatigue that accompanies repeated elastic, recoverable deformation (which may include consequential cracking), and abrasive processes resulting in permanent plastic deformation [34].

As frictional energy is dissipated, the interfacial wear happens in a thin region adjoining the surface (see Figure 2.6). Material moved from one surface to the other is very significant; in addition, surface adhesion can be reduced by local chemical effects.

2.2.4.1 Adhesion Wear

If two moving surfaces come into contact such that there is relative movement between them, friction is likely to be generated, mainly by adhesion but also by deformation of asperities [34].

Interfacial wear is closely connected with adhesion in sliding friction. When two materials with a relative velocity come into contact, molecular forces act across the contact interface triggering the generation of adhesive connections and interfacial bonding. These local adhesive bonds create both elastic as well as plastic deformations in the polymer uppermost layer. The breaking of cohesive bonds in the polymer body subsequent to the adhesion causes formation of wear debris, or material transfer or both.

Material transfers by friction plays a very important role in the mechanical behaviour of polymers. Wear, self-lubrication and frictional forces all depend on the the polymer ability to produce the transfer film on the counterface and on the wear life and effectiveness of the film.

Laux and Schwartz studied the influence of sliding on transfer film and wear performance of PEEK. They showed that decreased wear was closely associated with the transfer film; increasing the film thickness reduced asperity abrasion [35]. How quickly the film is generated, its durability, and its lubrication properties depend primarily on its structure and the adhesive force between the contact surface and the transfer layer.

It has also been demonstrated that in certain circumstances large amounts of material can transfer with a consequential detrimental effect on rolling performance [36]. This retention of transferred material is significantly affected by operating conditions and by the surface roughness counterface, and smooth counterfaces that allow greater transfer [37, 38]. Nunez et al., demonstrated that when polymer pins were tested against metal disks with smooth counterfaces, the transfer layers on the discs were uniform and continuous, suggesting that the increased thickness of the transfer layer was due to adhesion forces of large magnitudes [39].

Adhesion interactions are often presented in terms of the free surface energy (Y_n); the necessary energy to generate a new surface layer. Wieleba has shown that for solid surfaces under conditions of dry friction the larger the surface energy in either material, the more durable will be the bonds formed with the mating material [40].

Crediting the transfer of material to the difference in surface energies has been confirmed by twin-disc test notes made by Hoskins et al., who investigated the acoustic

noise radiated from adhesive wear in POM gears against steel for unlubricated contact [41]. It was confirmed that thermal and mechanical effects significantly affected the adhesion processes.

Additional studies by Moore and Tabor on adhesive properties of polymers have demonstrated that for PEEK slower sliding speeds increased adhesion, suggesting that a slower sliding speed would increase adhesive wear and temperatures. A possible explanation of this phenomenon is that viscoelastic deformation under load increases the contact area, and this leads to an increase in adhesion [14].

2.2.4.2 Abrasive Wear

There can be no clear-cut distinction between interfacial and cohesive wear because counterface surface roughness and the polymer's specific surface combine to determine generally the mechanisms of wear.

Lancaster and Hutchings have endeavoured to explain these influences schematically for elastomers, thermoplastics and reinforced thermosets, [32, 34, 43, 44] see Figure 2.7. For elastomers with low modulus, the figure shows that for both smooth and rough surfaces their deformation can usually be almost wholly elastic. In elastomers fatigue mechanisms dominate cohesive wear.

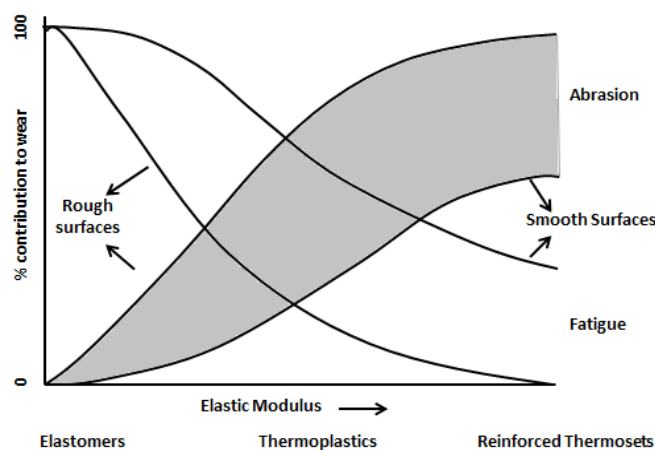


Figure 2.7: Transitions in cohesive wear mechanisms, after [32, 44].

Generally, abrasive wear of thermoplastics, including thermoplastics reinforced with, e.g., carbon fibre is based on one or more of the following:

- 1- Two-body abrasion; abrasive particles protrude out of the surface of one of the bodies (the stronger) causing abrasive wear on the second (weaker) body.
- 2- Three-body abrasion; stand-alone abrasive particles are entrained between two non-abrasive surfaces and cause abrasive wear on both.
- 3- Erosion; hard, fast moving particles impact on a surface, generating wear.

Typically, abrasive wear of polymers will be a function of surface roughness of both the surfaces in contact and any filler between them [45-49]. Adding reinforcing filler where particles of the reinforcing element act as hard filler in a matrix of softer material will change the wear mechanism into abrasion wear.

Hooke et. al., added glass fibre reinforcement to polyamide discs and gears and determined the resulting changes in wear properties [50]. They observed that the glass fibre reinforcement was scattered within the polymer matrix and found that abrasion was the dominant mode of wear once an initial layer surface has been removed. They also found that the alignment of the reinforcement in the polymer had a significant effect on the degree of observed abrasion [51].

Many researchers have investigated the wear and friction properties of PEEK and its composites but PEEK's high performance potential was not realised as PEEK-ferrous metal contacts tend to fail through scuffing and/or two- and three-body abrasion [49]. Ovaert and Cheng found that for unlubricated PEEK running against mild steel, a transition from a relatively low to a relatively high abrasion wear rate was found for a counterface with Rots Mean Square of surface (RMS) surface roughness (Ra) in the range between 0.13 μm (considered smooth) to 0.76 μm (considered rough) [52]. It was also shown that for PEEK reinforced with carbon fibre, again running against mild steel, the presence of the carbon fibre minimised plastic deformation and in so-doing, improved protection against abrasion [49]. It was noted that the observed damage of the mild steel counterface was increased.

The influence sliding speed has on the measured polymers friction will depend on the major wear mechanism and the polymer's tribological properties (i.e. fatigue limits, strength and toughness), the surface penetration level and the stresses across the

cohesive region, above and under the area of contact [12]. The resulting failure processes will include abrasion (permanent deformation) and fatigue (elastic deformation) with subsequent cracking [34].

2.2.4.3 Fatigue Wear

When asperities two surfaces impact one on another then, as in the case of an engineering polymer at a high temperature, they deflect elastically and the wear regime will tend towards fatigue.

For polymeric materials fatigue studies have primarily been for rolling contact. Kukureka et al., found that for a surface formed of POM (acetal) running against POM in unlubricated contact roll-slide conditions, in the mild wear regime the wear seems to be partly due to mechanical fatigue and the flaking of the surface with pitting is due to adhesion [53]. However, the surface manifested itself differently, depending on the relative speeds of the discs. When this sliding speed was low, there was negligible wear rate, but shallow pits and flakes were seen on the surfaces of both discs. However, as the sliding speed was increased, lateral cracks in the surface were seen perpendicular to the direction of the sliding. Kukureka also studied the surface temperature due to frictional heating and found that the lateral cracking coincided with a sliding temperature of about 110 °C, close to the onset of thermal softening.

However, the response of Nylon 66 subject to wear under roll-slide, for similar conditions to those described above, was very different. Deep surface cracks about 0.5 mm long, parallel to the direction of slide, appeared after only a relatively short period of testing [46, 50, 54]. The cracks appeared independently of sliding speed (except for pure rolling) and were thus treated as an inherent property of this polymer.

Avenzi et al., have presented a discussion on the fatigue properties of unfilled PEEK, a general-purpose unreinforced grade, and three PEEK composites, where the PEEK was reinforced with short fibres [55]. The fatigue mechanisms were found to be different for unfilled PEEK compared to the PEEK-based composites; micro pitting with deep transverse cracks were observed in unfilled PEEK rollers, whilst delamination and spalling were observed in the PEEK-composite rollers. Avenzi et al.,

also concluded that rolling contact fatigue of PEEK roller bearings demonstrated the importance of the self-lubrication capability of this material (which is powerfully affected by the adhesion processes) for determining the length of the component's life, [55].

Not only mechanical fatigue can have a substantial influence on the polymers tribological performance. Simazcelic and Yilmaz have shown that the isothermal ageing of PEEK produced a significant decrease in crystallinity [56], however the resulting crystallinity had a more organized structure with the increase in flexural modulus due to the formation of a trans-crystalline layer. For both unfilled and filled PEEK there was a noticeable decrease in material toughness after being subject to thermal ageing. In particular the impact properties of PEEK (unfilled and filled) were dramatically affected because the force required for crack initiation, and the total fracture energy, were severely reduced [56, 57].

2.2.4.4 Impact Wear

The ability of unlubricated polymer to undergo substantial plastic deformation before cracking or breaking inevitably means that they have low susceptibility to impact loads. However, the addition of lubrication can change the impact response and wear of a surface. Generally, the addition of a lubricant dampens any loading effect, but it has also been demonstrated that lubrication increases the likelihood of pitting under high loads.

Pitting is often ascribed to repetitive loading of a tooth's surface under circumstances where the contact stress is greater than the material's surface fatigue strength and crack growth is initiated [4]. Subsequently, lubricant is forced into these surface cracks by hydrostatic pressure, eventually material is removed resulting in the formation of a pit.

After investigating the behaviour of injection moulded PEEK rolls, Berer et al., reported that increased pitting wear occurred with lubricated contact [58]. 'Pre-cracks' in the surface of the PEEK due to the injection moulding process were deemed the cause of the increased pitting observed. Improvement of the moulding process improved PEEK roll fatigue life by a factor of 2-3.

Severe pitting has been found on PEEK gears subject to large loads [4, 6, 30]. Kono in his studies of PEEK gears lubricated with heated oil confirmed that the pitting was largely due to hydrostatic forces; this time between the gear teeth as they meshed [4]. The pitting was spread over the entire tooth flank, not confined to the pitch line and the lowest/highest points of tooth contact, as would be likely in lubricated metal-to-metal contact. It was also found that for polymer gears subject to large loads the resulting high temperatures at the contact point(s) can produce friction coefficients higher than 0.8, which are very much greater than the friction coefficients for metal - to- metal contacts lubricated with oil, and are believed to make a significant contribution to the generation of acute pitting damage.

Reinforcing ductile polymers with rigid fillers can significantly improve impact strength and increase the magnitude of the initiation force required to generate a crack in the polymer. However, there was a sharp reduction in the energy required to initiate a crack, and in the polymer's fracture energy [56].

2.2.4.5 Tribochemical Wear

Lubrication is known to decrease abrasive wear by reducing friction, helping dissipate heat generated by friction, and lessening shear stresses in the materials' surfaces [59]. However, the forces exerted by the lubricant on the surface layer of the polymer can be so large as to break the long polymer chains, generating new materials that may be chemically active and help degrade the surface [40]. When the contact is between steel and a polymer, the surface of the steel will contain oxides which could be transferred to a polymer molecule by chemical action. These oxygen containing polymer molecules could adhere to the metal surface due to their strong chemical polarities, increasing material transfer by adhesion [60]. Nevertheless, if the lubricant present prevents asperity contacts it is to be expected that the amount of material transfer will, overall, be significantly reduced.

2.3 Introduction- Polymer Gearing

This section will introduce polymers in engineering including, polymer manufacture aspects, polymer machine elements, polymer gear wear and polymer gear failure.

2.3.1 Polymer Gear Temperature

Generally, the mechanical energy generated by material deformation and friction results in wear and a temperature increase. In polymers, the frictional performance results to the transformation from glassy to rubbery and carry on to the melting phase and has an influence on sliding temperature. Normally, the polymers sliding properties are denoted as “ p_v ” (meaning contact pressure x sliding velocity). Frictional heating between mating gear teeth, can cause problems due to high surface temperatures, because its effect can limit power levels obtainable using gears of polymer [50, 61]. Temperature generally has a determining influence on the mechanical performances and failure modes of polymer gears. Therefore, temperature limits the application and operation of polymer gears [61-63].

In meshing polymer gears, the tooth contact generates heat due to a complex combination of mechanisms, including:

- 1- Frictional heating: produced by the kinematics of the meshing cycle.
- 2- Hysteresis losses: caused by viscoelastic deformation, this is converted mainly into heat.
- 3- Heat conducted: through the gears drive shafts (normally, this is negligible, and may act to remove heat from the gears).
- 4- Ambient radiation (In most applications this is negligible and will usually act to remove heat from the gears).

The modelling of heat generation due to contact was begun by Koffi, et al. [7]. These researchers modelled the components of heat generation per unit face width for a polyamide 66 gear, and their results are shown in Figure 2.8,. It was found that heat generated due to friction is larger than heat generated by hysteresis even in the case of pure rolling (i.e. when sliding velocities are zero at the pitch point of the gears) and during tooth contact outside the action line where deformation of the tooth is increased [27].

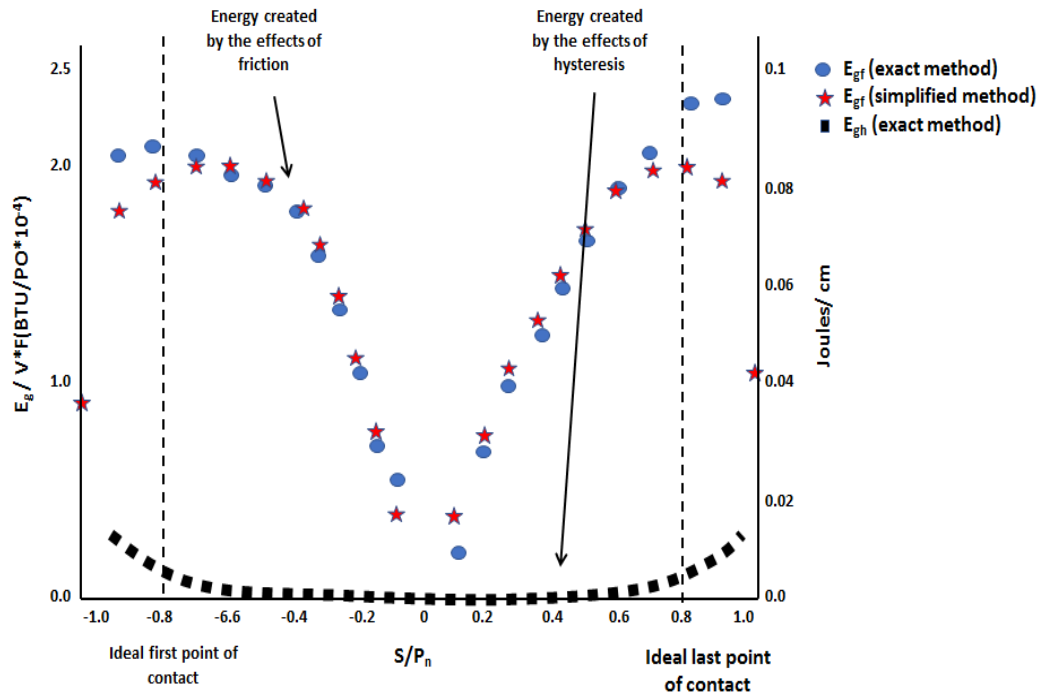


Figure 2.8: A Comparison of the energy calculated from friction and hysteresis for a pair of polyamide meshing gears¹ (after [7]).

Numerous researchers of polymer gears have studied the surface temperature experimentally and theoretically:

Letzelter, et al., presented a new model for recording the distribution of meshing temperature as a time function and used this to study the mechanical behaviour of polyamide 66. They measured thermal behaviours of the polymer gears by using an infrared camera [61].

Zhang, et al., used a coupled thermo-elasto-hydrodynamic analysis to measure the increase in tooth temperature due to friction heat in a mixed elasto-hydrodynamic lubrication (EHL). They considered the, heat generation, mixed lubrication, and shearing load in the contact area. They have improved the current spiral bevel gear thermal analysis method by taking into account the lubrication condition of the tooth surface and claim to have solved a problem of a moving heat source applied to a complex curved surface. They conducted transient thermal analyses and steady-state based on loaded tooth contact analysis of spiral bevel gears and point contact EHL

¹ Gears modelled with 20 teeth, 53 Nm load and 2.07 GPa storage modulus, a loss modulus of 0.05 and a friction coefficient is 0.1.

analysis. They compared the experimental and analytical results and found a good agreement between them [64].

Wen Tang, et al., combined the frictional heat generation and transient thermal behaviour of spiral bevel gears, a hybrid thermo-elastic 3D finite element model was developed. They investigated prediction of transient temperature and thermal characteristics of polymer by analysing the heat fluxes as a result to friction effects on the gear tooth. They compared their results with earlier work on thermal characteristics in order to different the model and numerical approach and found good agreement between them. Their study presented an in-depth understanding of the frictional heat generation process and temperature fields. They investigated the transient thermal performance of a variety of pinion machine-setting parameters in order to study an optimal tooth contact pattern to produce a uniform temperature area of significantly lower value [65].

Bravo, et al., suggested two types of advanced gear materials. The first is a semi-ecological polyethylene composite gear reinforced by birch fibres, and the second is a fully bio-sourced natural polyethylene gear with birch fibres. They tested the fully ecological composite-plastic gears and recorded, under different operating conditions, the evolution of fatigue and temperature. They used acoustic emissions to evaluate the development of fatigue cracks and found that completely ecological gears offer a viable another to conventional materials, like plastics engineering, possibly at a lower cost. [66].

Zhen, et al., studied polymer gears and analysed the instantaneous temperature rise of the tooth surface in the polymer gear through systematic and combined approach of theoretical and finite element analysis. They found that the effect of the loading torque on the instantaneous temperature was more important than the rotational speed. They predicted the life of the meshing polymer gear by considering the influence of speed and loading torque. They verified their model with experimental tests [67].

2.3.2 Polymer Gear Wear

Generally, the most common failure mode in unlubricated polymer applications is wear, due to the direct contact of polymer machine elements, but the resistance of a polymer to wear does not depend on the ratio E/H only. This is clear if one takes into

account the essential motions included in certain elements of machine. Wear is one of the hardest forms of predicting failures [53, 68-70] because the wear rate in polymer gears depends on many different factors, including:

1. Material factors - consequences of choice of materials for polymer pinions and gears (e.g., surface energy, effect of similar and dis-similar materials meshing), plus the effect of properties of the added internal lubricant on the wear rate.
2. Operational factors – These factors represent effects of the operational circumstances on the wear rate of polymer gears, including: sliding speed, pressure of contact and ambient temperature.
3. Geometry of gear – the angle of the pressure, module and width of the face.

The reduction of friction at the meshing stage undoubtedly has a positive effect on the wear resistance of polymer gears [68], and dropping flash temperatures also decreases gear wear.

Figure 2.9 show the regions of approach and recess. Cropper [30] discovered that certain polymers were vulnerable in the transition between approach and recess, to such an extent that there were noticeable wear variations between driver and gear drive

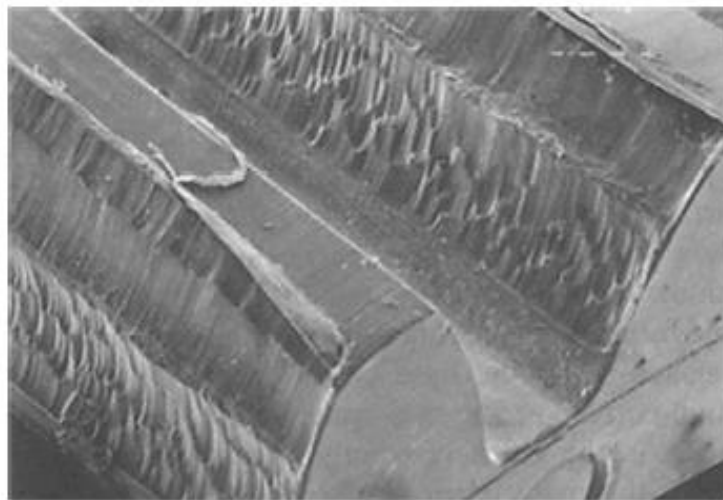


Figure 2.9: wear damage of polymer gear: [25].

Despite the vast variety of polymer materials that have been established, experimentally wear in polymer gears displays similar characteristics.

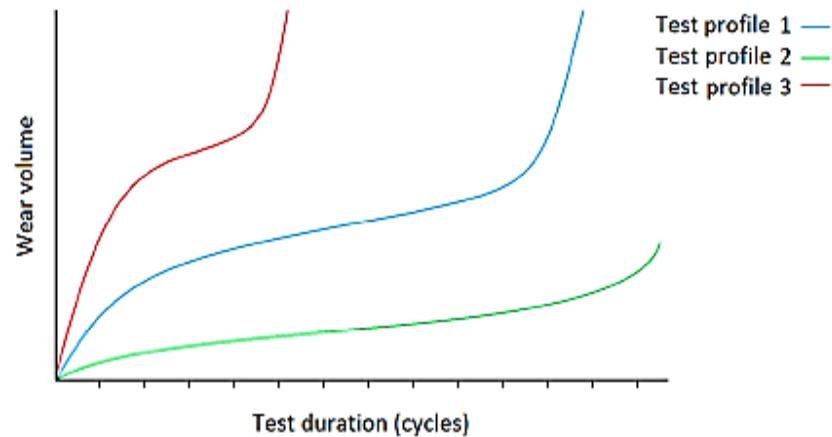


Figure 2.10: Typical wear, generally material independent [12].

Profile 1 in Figure 2.10 shows the most likely wear record, and three clear regions can be seen. Initially the gear undergoes a ‘running-in’ period during which the tooth profile adapts itself to its optimal geometry (here manufacturing errors are being reduced and even eliminated). Running-in is followed by a much longer second period which represents the gear in its “steady-state”, subject to gradual wear. Finally, there is a relatively short period of rapid wear and eventual failure.

Profile 2, appears similar to Profile 1 but the running-in period is very much shorter, indicating a gear set designed for special application. Profile 3 presents data for the usual wear of a poorly designed machine, in which neither gear material nor geometry are suited to the given working conditions.

With polymer gears the sudden commencement of rapid wear is usually coupled with melting of the tooth surface at the active flanks, as the material’s temperature reaches its point of melting.

Hooke, et al. [50] have shown that this operational limit is weakly related to rotational speed and much more strongly related to the applied load.

2.3.3 Polymer Gear Failure

As mentioned above, there are limits to the use of polymeric material in mechanical applications because these materials response is very different from the response of a metal. Deflection, load, temperature, sliding velocity and lubrication, all, have major

influence in the reaction of the polymeric material, and its tribological performance in a mechanical application.

In polymeric materials, there are four keys of failures [4]:

- 1- Root Bending Fatigue, at both active and non-active root gear flanks, in addition to rim failure, which is shown in Figure 2.11 for a PEEK gear. It is very clear after removal of the load, a tooth was permanently deformed [30].

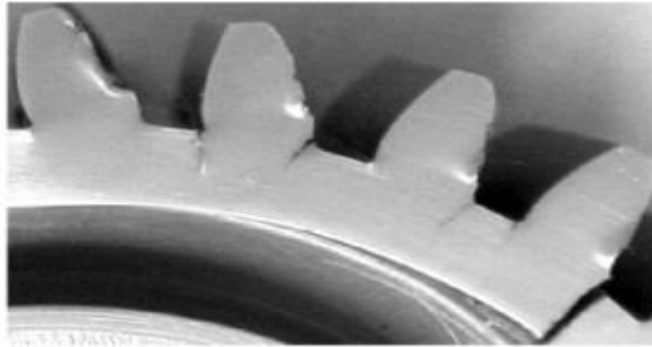


Figure 2.11: Gear wall and Root failure [4].

- 2- Excessive Wear: thermally failed resulting in gross wear - Nylon 6/6 composite gear (30% Glass fibre and 15% PTFE), see Figure 2.12.

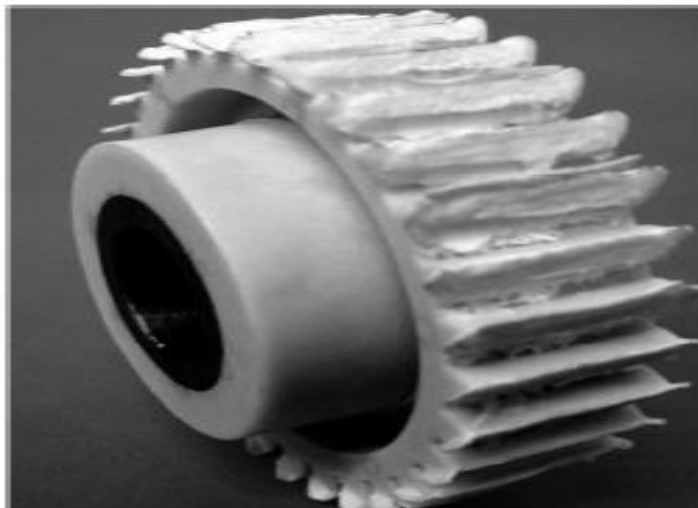


Figure 2.12: gross wear [30].

- 3- Pitch-Line Fracture: a type of primarily failure related to unlubricated polyamide and polyamide composites but can be noticed in PEEK gears for the both unlubricated and lubricated test (see Figure 2.13) [70].

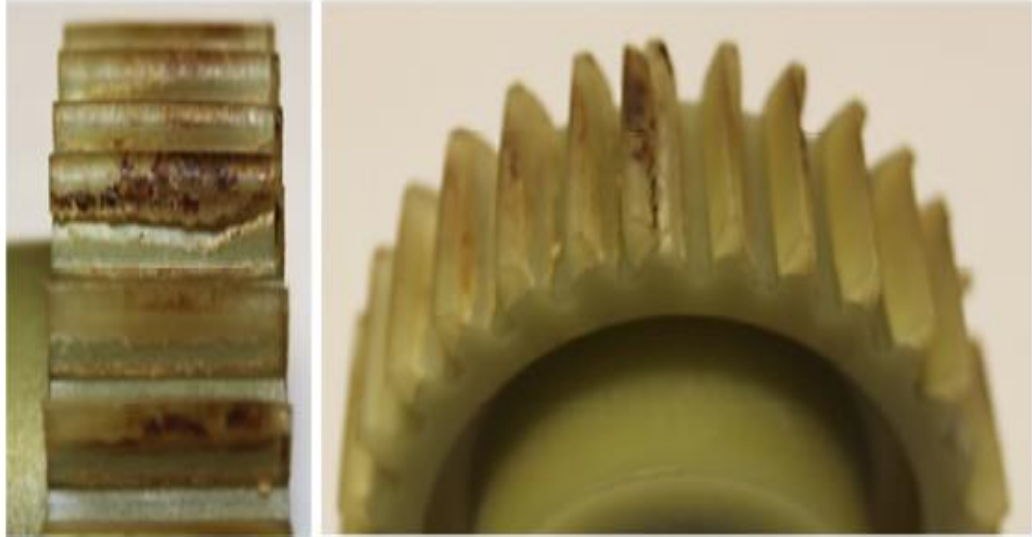
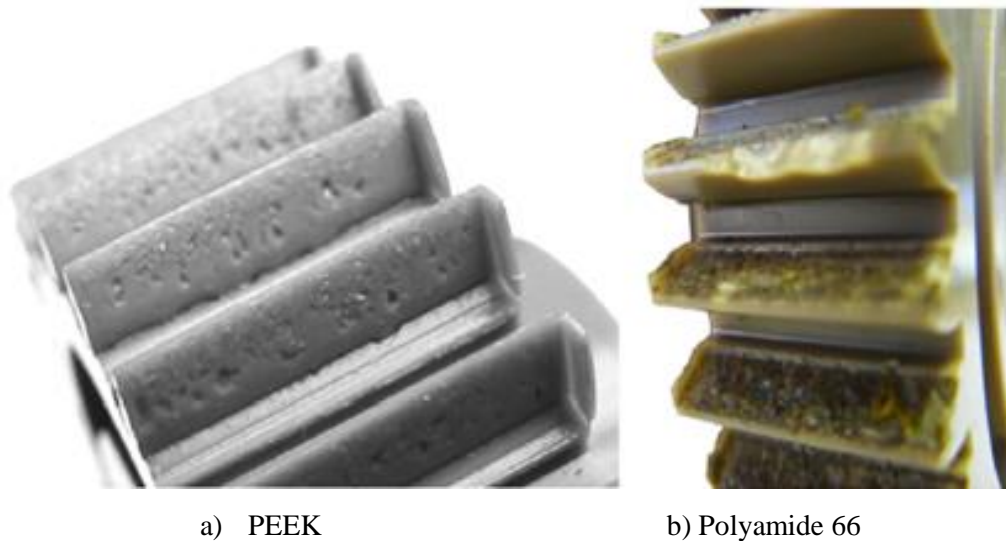


Figure 2.13: Pitch line failure in Nylon 6/6 composite (glass fibre) [4].

- 4- Pitting Damage: Severe gear pitting run under (high loads and lubricant) (see Figure 2.14).



a) PEEK

b) Polyamide 66

Figure 2.14: gear pitting [30].

Note the failure mechanisms presented here were all affected by the temperatures.

2.3.4 Wear and Failure of Polymer Gears

Because wear and failure are usually combined in the reported studies of polymer gears, wear and failure are reviewed together in this section:

Chen, et al., studied the performance of various metallic surface treatments and counterface materials on the tribological effect of polymer and polymer composites roll/ slide contact and un-lubricated. The polymer materials used were (PA66) and its composite (RFL4036). They conducted tests at a 300 N load with various slip ratios and a rotational speed 1000 rpm using twin-disc rig. For the results presented when running against steel and aluminium counterfaces, the unreinforced PA66 exhibited greater friction and more wear than the polyamide composite. When tested against a brass counterface, the PA66 exhibited lower wear than the polyamide composite. The surface treatment of steel had an important impact on the friction coefficient and wear rate of polyamide composites as well as on the tribological mechanisms. A thin film on the contact surface had been observed to play a dominant role in reducing the composite's friction and wear and in doing away with the initiation of transverse cracks [71].

Harsha, et al., presented tribological studies of smooth polyetherketone (PEK) and composite PEK by glass fibre reinforcement at 23 °C & 1200 °C high temperature. The investigated the wear and friction properties with sliding velocity and unlubricated under different experimental parameters. It was found that at room temperature, and at the elevated temperature, wear behaviour and the friction for both PEEK and composite were relatively different. The presence of glass fibre reinforcement was found to be more beneficial in controlling PEK matrix wear at room temperature than at high temperature. Using Scanning Electron Micrographs (SEM) and optical microscopy of the damaged polymer/ steel contact, material removal and film transfer formation was used to test wear mechanisms [72].

Mbarek, et al., studied temperature, friction and wear near the pitch point regions of the contact using a twin-disc test configuration with a PA66 disc and non-alloyed C45 structural steel disc. For any one test the diameters of corresponding discs were the same, but discs of different diameters were used in different tests. The effect of slip ratios of 4%, 12%, 20%, and 28% were considered for a 34 MPa a contact pressure, and 300 rpm rotational speed. The surface temperatures of the two discs were measured using a thermal imager. It was found that friction and wear are narrowly concerned to the temperature created by sliding, and friction coefficients and temperature was behavior by a quasi-linear increase in time at points close the pitch point [73].

Kalin and Kupec presented the results of the tests for polyoxymethylene (POM) gears against steel gears, under well-controlled temperature conditions were reported and given that different S-N curves at 300 °C, 500C and 700 °C that were kept constant for three torque values at the gear root (1.0 Nm, 1.2 Nm and 1.4 Nm). Their found significant influence of the temperature on the fatigue life of POM gears, i.e., the fatigue life of the POM gears improved considerably at lower temperature (300 °C) [74].

Singh and Singh examined the thermal and wear behaviour of gears made from POM, high density polyethylene (HDPE) and acrylonitrile butadiene styrene (ABS). They used verity torques (0.8, 1.2, 1.6 and 2.0 Nm) and various rotational velocities (600, 800, 1000 and 1200 rpm). They performed a steady state gears analysis when the applied torque was 1.4 Nm and the rotational speed was 900 rpm in order to measure the durability and determine failure modes occurring in the gears. They found that the ABS gear failed after 0.5 million cycles due to excessive wear of the teeth. The HDPE gears completed 1.1 million cycles before failing due to cracking at the root of gear teeth. The POM gear completed 2 million cycles and there was no indication of failure [75].

Moder et al, experimentally studied three different composite polymers with high-performance PTFE filling, in rolling-sliding against steel counterparts, in unlubricated contact. They investigated the effect of electroless nickel plating on the tribo-system in addition to the effect of the counterpart's surface roughness. For the experimental part of this study, they employed a pin-on-plate test setup, with reciprocating motion and a two-disc machine. They used a microscope for investigating the phenomena taking place in the contact zone. The results showed that PTFE played a vital role in the functionality of these systems and the counterparts roughness strongly affected friction and wear [76].

2.4 CONCLUSIONS

Material testing was shown to provide an indicator of material efficiency for an application; however the use of simulated mechanical tests to simulate the operating conditions of polymer gears is currently limited to investigation by the rolling / sliding contact twin-disc rig close to the pitch line.

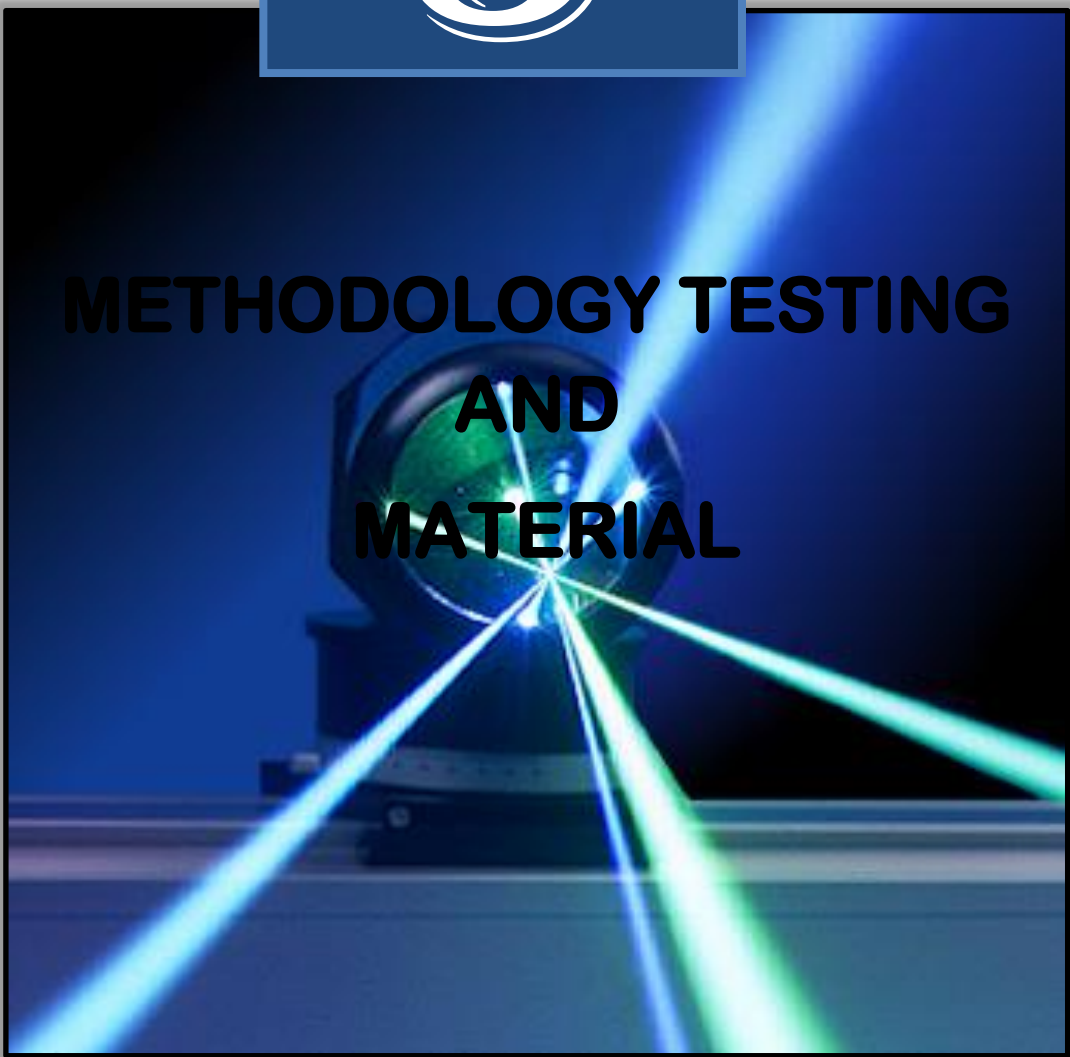
Therefore, to investigate the polymer applicability for a particular mechanical application, attention must be given to the kinematics of the gear system and their effect on material properties.

In conclusion the material's physical and mechanical properties result in a kinematic reaction materials of the polymer gear that do not conform to present gear selection techniques, the only method to reliably specify a polymer is by physical testing for a particular mechanical application.

Chapter Three

3

**METHODOLOGY TESTING
AND
MATERIAL**



3

“For ever fact, there is an infinity of hypotheses”

Robert Maynard Pirsig

Methodology Testing and Material

3.1 Introduction:

Polymers and polymer composites are widely used to produce machine elements including roller bearings, gears and cam mechanisms. Polymers have many advantageous characteristics, but their responses are very complex under contact conditions which usually include high loads, velocities, contact pressures and even temperatures. To gain the knowledge required for informed design necessitates physical testing in order to identify polymeric materials suitable for the manufacture of individual gear components. Which means that the only way of being sure of the combined effects of such factors as geometry, friction, temperature and wear on a polymer is to physically test it before any specific mechanical application.

3.2 Theory of Polymer Gear Contact

While such mechanical/physical tests remain the best method of establishing the specific polymer performance for a given application, it is essential that the test conditions match the working conditions because the response of a polymer gear will change significantly with operational conditions; load, rotational speed, and geometry. To develop relevant tests, it is necessary to understand the interactions that take place when polymer gears are in dynamic contact, and the consequential tribological effects.

3.3 Gear Kinematics

The compliance (deflection) of the polymer materials used in gears results in a contact path from the start to the end of meshing, that extends outside the notional path of a perfectly stiff gear, see Figure 3.1 [77, 78]. In such a situation, the real sliding velocity and distribution of load across the teeth as they mesh will also change.

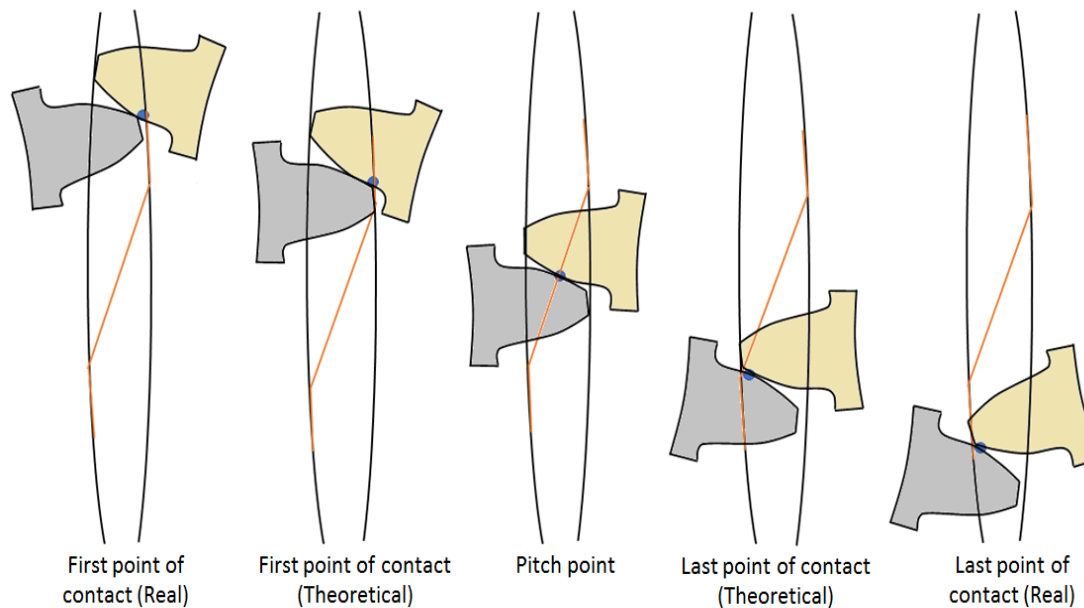


Figure 3.1: Actual and hypothetical contact paths for two polymer gear teeth as they mesh [79].

The geometry of Birmingham standard gear (BSG) provides the hypothetical 1.653 contact ratio, meaning that there are periods when only one tooth pair transmits the torque as the teeth mesh. Karimpour, et al. have demonstrated, using finite element models, that the contact paths of gears made of high compliance polymers are lengthened due to tooth deflections, which means the actual contact ratio is increased, and the division of the applied load between different pairs of meshing teeth will differ from standard assumptions [27]. Figure 3.2 shows results obtained by Karimpour, et al. compared with the theoretically assumed load sharing ratio " *the helical gear, the additional contact ratio is created due to face advance which is called face contact ratio and it provides the higher contact ratio than that of spur gear* " as a function of roll angle for a gear made of a polymer of high compliance. The gear geometry used was the BSG [27].

Figure 3.2 shows that for a single, perfectly rigid tooth gear the theoretical contact takes place above only 12°. The corresponding path length of the contact is 5.904 mm. In fact, as Figure 3.2 shows, the real profile is nearer to a parabola, due to the tooth movement that takes place in polymer gears, which implies multiple tooth contact rather than single tooth contact. The compliance inherent in a polymer introduces a deflection ‘lag’ for successive teeth mating. This extends the contact path, as increases the actual contact ratio to more than 2 in certain cases for BSG geometry [53].

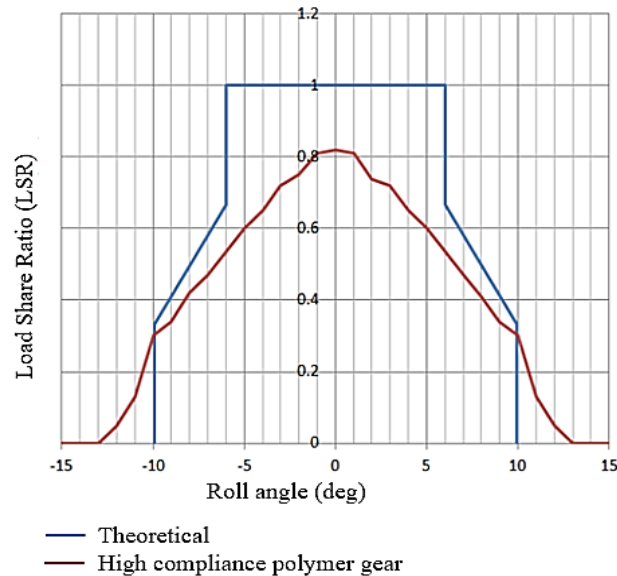


Figure 3.2: Load share ratio as a function of roll angle for a perfectly stiff gear tooth, and polymer gear with deflection (after Karimpour, et al. [27])

If the path of contact is increased, then the gear mesh dynamics will also change. For meshing gears the slip ratio (also known as the slide-roll ratio) is “the ratio of the sliding velocity at the point of contact along the line of action, to the rolling velocity” [7]. With two discs rotating with rotational speeds of V_1 and V_2 respectively, at the point of contact the slip ratio is given by [7]:

$$\text{Slip ratio (\%)} = 2 \times \frac{V_2 - V_1}{V_2 + V_1} \times 100 \quad \text{Equation 3.1}$$

When simulating gear performance, such as when investigating polymer behaviour at the pitch point, twin-disc tests are in common use. In such set-ups the contact will have low sliding and high rolling velocities, so the slip-ratio (slide-roll ratio) will be small, possibly close to zero.

Figure 3.3 presents the theoretical rolling (V_{roll}) and sliding (V_{slide}) velocities determined for a pair of gears without deflection meshing gear teeth, including the effect due to extended contact path. Also shown is the resulting slip-ratio. But this occurs as a result of deflection

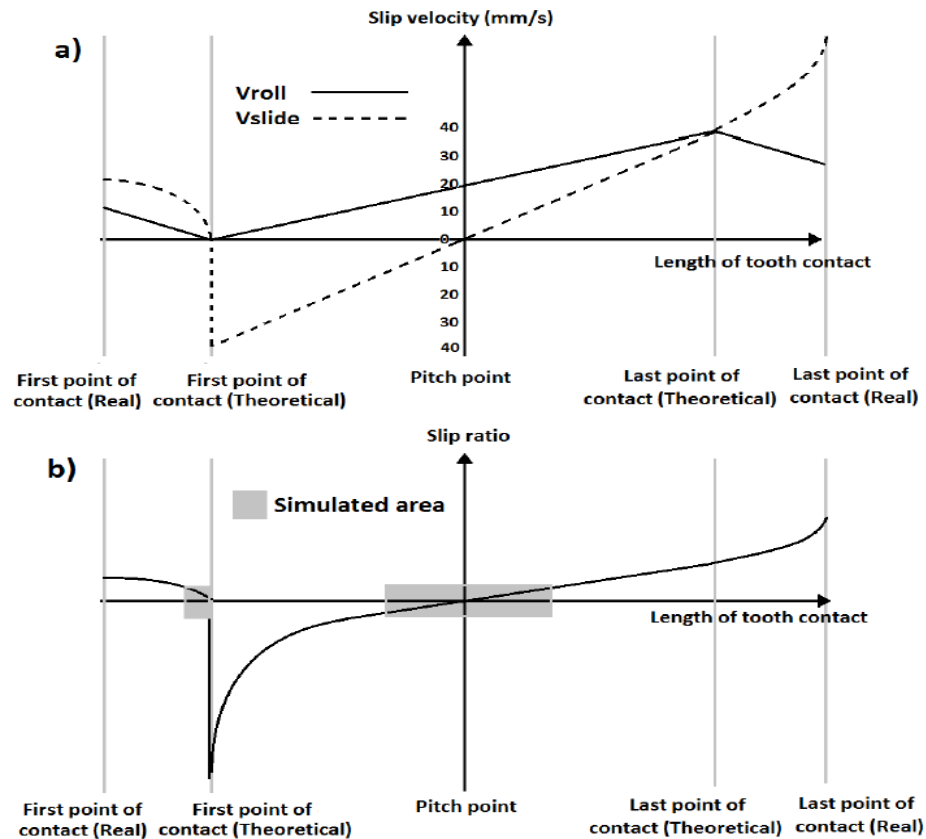


Figure 3.3: a) Rolling (V_{roll}) and sliding (V_{slide}) velocities, and b) Resulting Slide-roll ratio, for polymer gear contact.

Grey areas are the areas simulated in twin-disc testing [14].

Tests using twin-discs have successfully modelled meshing of the gear and simulated the effect of tooth deflection on the system. In Figure 3.3 the twin-disc tests can produce slip ratios as high as 30%, and can replicate both the theoretical contact point at which significant deflection takes place, as well as the area around the pitch-point. It can be seen that when large deflections occur this kinematic model shows an extended path of contact; which allows conditions for both premature and extended tooth contact to be modelled.

3.4 Gear Contact Calculations

When gear teeth mesh they will be subject to both contact and bending stresses. Hertz' theory can be used to find contact stress at the pitch point in contact for spur gears, [80]. Under such simplified conditions, the pitch point value of the radius of gear curvature (ρ) is found using:

$$\rho = \frac{d_p \cdot \tan \varphi}{2} \quad \text{Equation 3.2}$$

where φ is the working pressure angle, and d_p is the gear base circle diameter.

The load of contact per unit width, P, is provided to the face by:

$$P = \frac{2 \cdot T_r}{d_p \cdot w \cdot \cos \varphi} \quad \text{Equation 3.3}$$

where T_r is the nominal torque transmitted by the gears, and w is face width of the gears.

Note that P in Equation 3.3 assumes the gear tooth is perfectly stiff. But in polymer gears with high compliance, the load is shared and the contact path is lengthened, both of which increase the actual contact ratio. This means the actual face contact load per unit width is:

$$P = \frac{2 \cdot T_r}{d_p \cdot w \cdot \cos \varphi} \text{LSR} \quad \text{Equation 3.4}$$

Where: LSR is the load share ratio, due to the deflection of the gear material. Using Hertz' theory, the semi-width of contact of a gear set, a, can be calculated as:

$$a = \sqrt{\frac{2 \cdot F \cdot R_{eq}}{\pi \cdot l \cdot E}} \quad \text{Equation 3.5}$$

Contact modulus is given by:

$$\frac{1}{E} = \frac{1-v_1^2}{E_1} + \frac{1-v_2^2}{E_2} \quad \text{Equation 3.6}$$

Effective radius is given by:

$$\frac{1}{R_{eq}} = \frac{1}{R_1} + \frac{1}{R_2}$$

Equation 3.7

It follows that the maximum contact pressure is:

$$P_0 = \frac{2.F}{\pi.a.l}$$

Equation 3.8

P: applied load

E₁, E₂: elastic moduli for disc 1 and plate 2 respectively.

R₁: radius of gear 1,

R₂: radius of gear 2,

R_{eq} = effective radius

Having established an expression for the contact pressure, it is necessary to determine the length of the contact path and maximum value of V_{slide} in order to find the most appropriate lengths of stroke and operating frequencies.

We must find the approach path and path of recess, for a wholly stiff gear, to determine V_{slide} maximum value for gear tooth, see Figure 3.4.

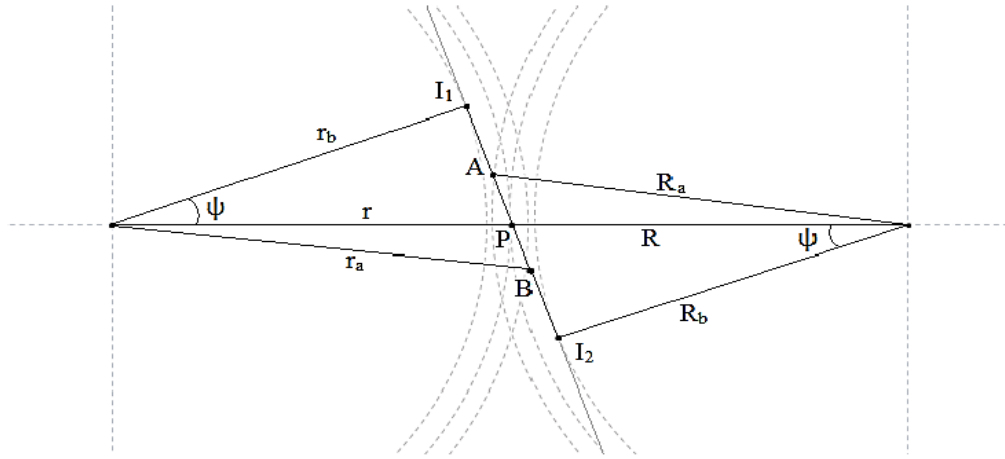


Figure 3.4: Contact paths of perfectly stiff gear, with A-P the approach path, and P-B the path of recess [10].

From Figure 3.4, a geometric expression can be found to describe the path of contact as the sum of the paths of approach (AP) and recess (BP).

$$\begin{aligned}
 AP &= AI_2 - PI_2 = \sqrt{(R_a^2 - R_b^2)} - R \sin \varphi \\
 &= \sqrt{(R_a^2 - R^2 \cos^2 \varphi)} - R \sin \varphi
 \end{aligned}
 \tag{Equation 3.9}$$

Thus path of contact is:

$$PC = AP + PB = 2 \cdot AP
 \tag{Equation 3.10}$$

The maximum sliding velocity (\hat{C}) is found as:

$$\hat{C} = (\omega + \Omega) \cdot PC
 \tag{Equation 3.11}$$

Assuming a perfectly stiff gear, the maximum length of PC is the distance between the first and last points of contact. Thus:

$$\hat{C} = (\omega + \Omega) \cdot \left(\frac{PC}{2} \right)
 \tag{Equation 3.12}$$

3.4.1 Tribological Tests

The tribological tests used were twin-disc tests, TE 77 EP-GEAR DYNAMICS high frequency reciprocating tribometer for replicating gear contact conditions with (Energy Pulse (EP) - Gear Slide-roll Adaptor) and a Mark II Gear Test Rig.

3.4.2 Twin-Disc Technique; Rolling – Sliding Test Rig

Twin-disc test rig tests can simulate gear contact with sliding/rolling dry and un-lubricated. Two parallel axes each carried a disc of equal diameter, 30 mm, and width, 10 mm, loaded one above the other in contact, as shown in Figure 3.5. These two discs were run with specified slip ratios obtained by changing the drive gears.

The input shaft was driven by an electric motor, a pair of gears were used to control toothed drive belts and speed changing, see item 7, in Figure 3.5 which is a schematic representation of the system. The relative slip ratio could be balanced for the two discs in contact by controlling the speed at which the discs were driven.

$$\frac{\text{Slide}}{\text{roll}} \text{ ratio} = 2$$

$$* \frac{\text{sliding velocity}}{\text{rolling velocity}}$$

Equation 3.13

The upper disc (item 9) is supported in a pivoted block (item 4), and the lower disc (item 10) is mounted in a rigid block (item 6). Thus, the system can simulate conditions of non-conformal contact as might be present in gears and bearings in machines.

A pivoted and sprung lever arm (item 5) provides a load on the upper disc which results in a normal force acting between the two discs. Strain gauges on the lower disc measure the tangential force, and thus the sliding frictional force [14, 71]. This system could measure the wear of the upper block by detecting the movement of the disc centres using a LVDT (Linear Variable Displacement Transducer).

Figure 3.6 presents the geometry of the test sections. The specimen discs were set on the test-rig shafts in pairs. During test runs a number of different loads and slip ratios were used. The data acquisition system recorded wear, friction and temperature of the area contact.

The experimental parameters are given in Table 3.1, for the contact pressures calculated to match contact conditions for gears transmitting torques of 7.0, 10.0 and 13.5 Nm.

Table 3.1: Test conditions for EOS PEEK HP3 twin-disc tests

Max. Contact Pressure / MPa	Slip Ratios		
	3.9%	14.29%	28.59%
56	√	√	√
48		√	√
39			√

The twin-disc tests simulate the instantaneous mechanical response of material for a gear pair in the pitch point area and the first and last theoretical points of tooth contact (as a result of tooth deformation as defined in the previous paragraph). These are instances of the meshing cycle where the sliding velocity is low [73, 79] and so when the maximum slip-ratio is below approximately 30%. The test specimens in this research were designed to simulate a spur gear with the geometry module = 2 mm, number of teeth = 30, pressure angle = 20°, speed ratio= 1:1 (a Birmingham standard gear [81]).

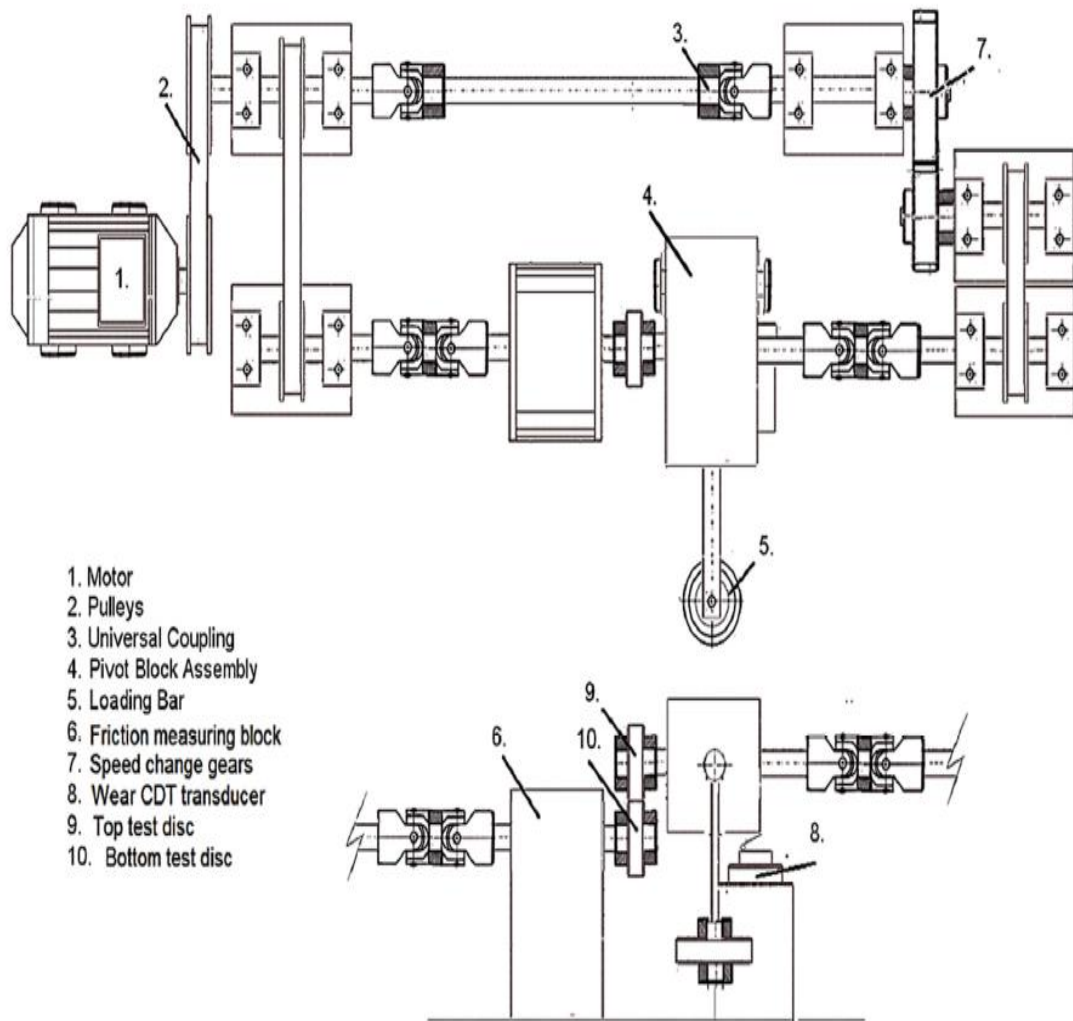


Figure 3.5: Schematic of the twin-disc test rig (after [14, 71]).

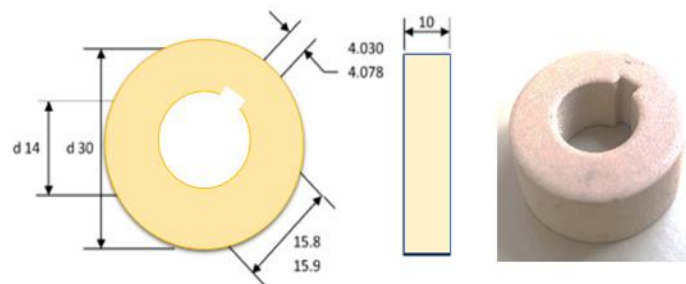


Figure 3.6: Twin-disc test geometry and a sample disc.(all dimension in mm)

3.4.3 Principles of TE77 (Replicating Gear Contact Conditions)

The TE 77 with EP - Gear Slide-roll adaptor fitted, is shown in Figure 3.7. When configured in this manner, the upper specimen disc rotates under load against a lower specimen plate. The load is varied by adding mass to, or removing mass from, the load bridge. Additionally, a sinusoidal rocking motion is induced by a linkage mechanism.

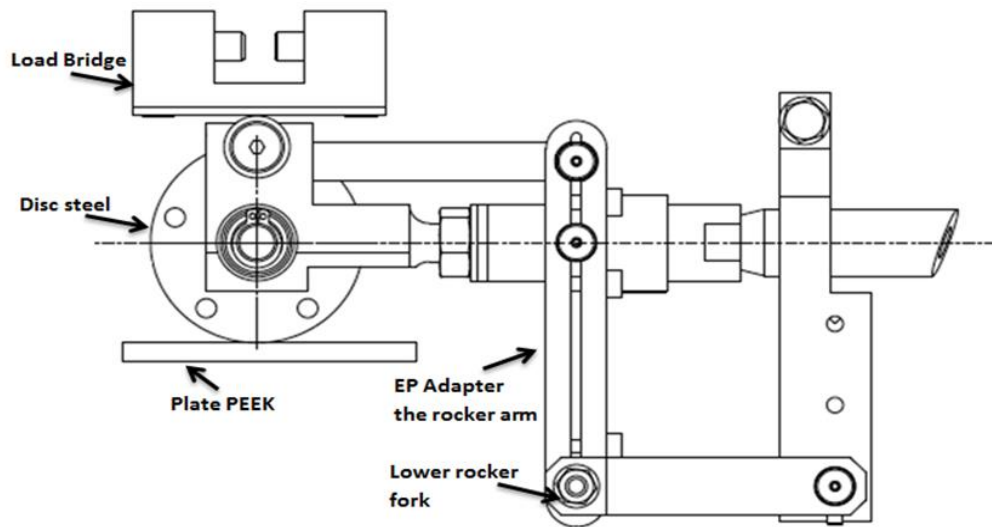


Figure 3.7: EP-Gear Slide-roll adaptor for the TE 77 EP-GEAR DYNAMICS high frequency reciprocating tribometer (after [23]).

However, we need to consider a number of limiting assumptions when using a EP-Gear Slide-roll adaptor for the TE 77 EP-GEAR DYNAMICS test rig (TE77) high frequency reciprocating tribometer to simulate gears:

- The action of the gear is simulated only as the cyclic engagement of a single tooth; the major drawback of such a process is that the cooling of the gear that takes place during the non-interactive part of the cycles is not included.
- The value of $V_{\text{slide/roll max}}$ is calculated for the distance between the contact extremities, so the contact pressure will approach zero for teeth which are perfectly stiff. But for TE77 tests it is assumed that the contact pressure is constant for the entire length of the stroke.
- The contact pressure changes with disc wear.

- Where tribological tests are performed within a closed system, the debris of wear that is retained during the contact region can change the measured tribological performance.
- A stroke length of the TE77 between (1-25) mm.

However, the TE77 frequencies reflect $V_{\text{slide/roll max}}$ for contact of gear tooth, demonstrating the applicability of this test type.

3.4.3.1 Contact Area for TE 77

The TE77- EP can be used to simulate high performance gears, testing the physical properties of materials; not directly simulating a gear's operating conditions.

To use a reciprocating test to usefully model the behaviour of a polymer gear tooth requires appropriate standards of stroke length, load contact and reciprocating frequency. The theory of Hertz assumes that the initial contact is at a point or along a line is made when two curved bodies contact together. Once a load is applied, there will be contact which extends onto a minute and elastic deformation but limited region. Hertz described a means of determining the likely area of this region [80] based on a number of assumptions:

- The area of contact is small relative to the curved bodies size,
- The contact surfaces, it should be smooth, frictionless as well as continuous,
- The separation (h) of non-deformed surfaces such as cylinders spheres and ellipsoids may be expressed in the form $h = Ax^2 + By^2$ (where A and B are constants).
- The elastic load deformation could be observed if each body is recognized as an elastic half-space. It could be measured the contact pressure and contact area for the load 'F' by using Hertz's theory [80].

Hertz's theory (normal contact of elastic solids) was used to calculate a measure of the contact area - the so-called radius (a), for the configuration shown in Figure 3.8; a disc in flat contact with a plate. With the TE77 the disc is in contact with a plate lying in a plane parallel to the y-axis, in the given coordinate system. The disc presses on the

plate with load (P) per unit length. To determine the contact pressure (P_0), contact modulus and effective radius are needed:

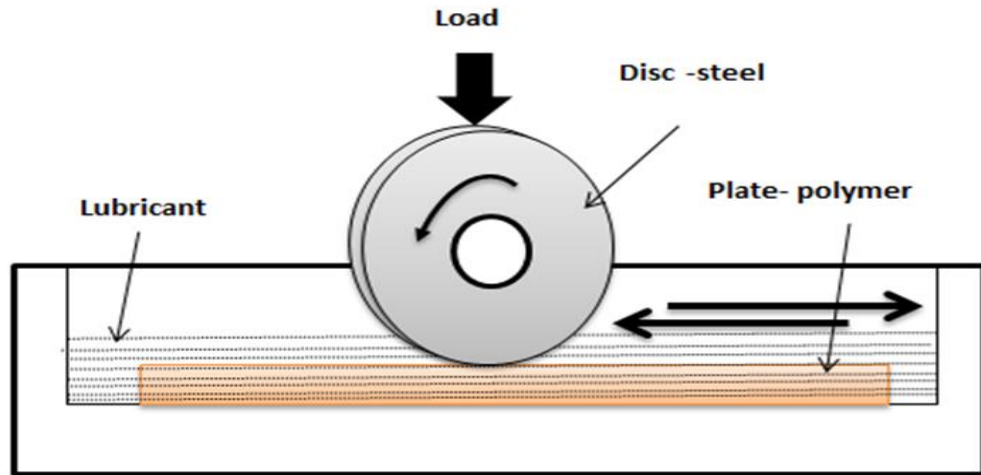


Figure 3.8: Schematic diagram of disc-on-plate setup with rolling-sliding motion.

Contact modulus is given by: $\frac{1}{E} = \frac{1-\nu_1^2}{E_1} + \frac{1-\nu_2^2}{E_2}$ **Equation 3. 14**

Effective radius is given by: $\frac{1}{R_{eq}} = \frac{1}{R_1} + \frac{1}{R_2}$ **Equation 3. 15**

The contact area can be approximated to be rectangle with semi-width [80]:

$$a = \sqrt{\frac{2 \cdot F \cdot R}{\pi \cdot l \cdot E}}$$
Equation 3. 16

The peak contact pressure can then be calculated using [80]:

$$P_0 = \frac{2 \cdot F}{\pi \cdot a \cdot l}$$
Equation 3. 17

where: P: applied load, E_1 , E_2 : elastic moduli for disc 1 and plate 2 respectively.

R_1 : radius of disc 1, $R_2 = \infty$: radius plate 2, flat plate, R_{eq} = effective radius.

3.4.3.2 Length, Stroke and Frequency for TE77 EP Gear Slide-roll

Figure 3.9, presents the frequency and stroke length of the EP-Gear Slide-roll adaptor in the TE 77. For example: the maximum length stroke of 25 mm, can be maintained up to a frequency of 20 Hz. Above this frequency the length of the stroke decreases with increase in frequency, approximately as $1/f$ [23].

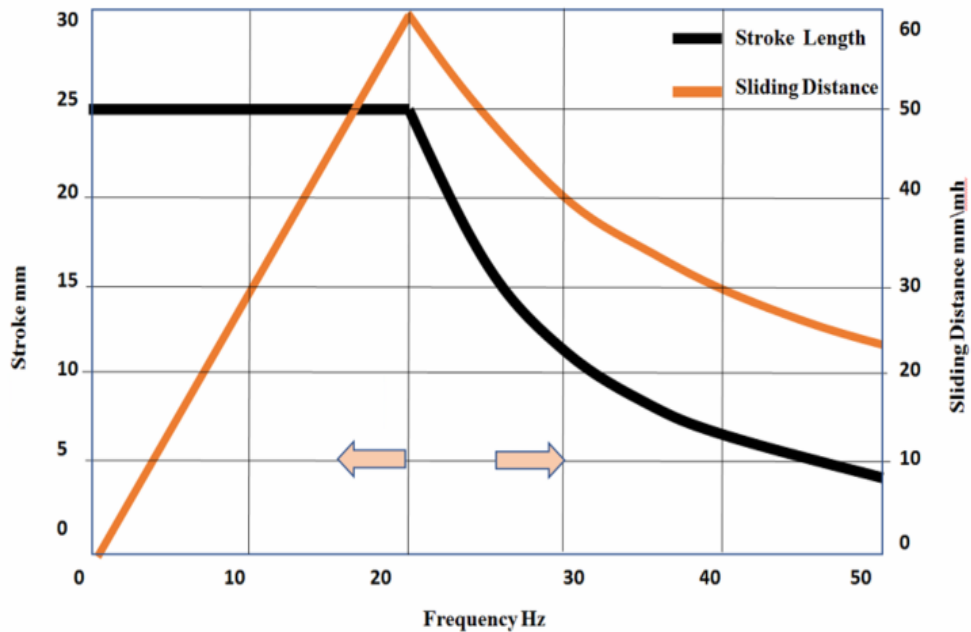


Figure 3.9 Operating Envelopes of TE 77 EP-GEAR DYNAMICS (after [23]).

Figure 3.9 also shows the relation between sliding distance and frequency. Assuming the TE77 operates under simple reciprocating motion the maximum sliding and rolling speeds can be compared. If l is the length of the stroke, f is the frequency, then V_{max} , the maximum sliding velocity is given by:

$$V_{max} = 2 \cdot \pi \cdot f \cdot \frac{l}{2} \quad \text{Equation 3. 18}$$

3.4.3.3 Slide-roll Ratios for TE 77 EP-GEAR DYNAMICS

The slide-roll ratio is the ratio of rolling to sliding velocities at a contact point and the TE77 can be used to simulate gears during tooth engagement, see Equation 3.19, [23, 82]:

$$\text{Slide-roll ratio (\%)} = 2 \times \frac{U_2 - U_1}{U_2 + U_1} \times 100 \quad \text{Equation 3.19}$$

Where:

$$\text{Sliding Velocity} = U_2 - U_1$$

$$\text{Rolling Velocity} = (U_2 + U_1)/2$$

The slide-roll ratio is the ratio of sliding/rolling velocities, and Figure 3.10 presents a schematic of the transient slide-roll ratio. This includes extensions to the theoretical path of contact as a result of a lag generated by deflections in the polymer gear teeth [83]. This results in a reversal of the direction of the slide at the hypothetical first point of tooth contact.

Also included in Figure 3.10 are the limits of the simulated regions along the path of contact for each of the potential test methods. Twin-disc tests are limited to a single slide-roll ratio value up to 30%, shown as the grey zone. Once set, this does not change during a test.

Using the TE 77 EP-GEAR DYNAMICS (TE77 EP/Gear adaptor), see the blue area in Figure 3.10, allows a much wider range of slide-roll ratios to be simulated, up to 83.3%, but crucially the method is transient, simulating the critical reversal of the sliding direction. This means that the kinematics at the pitch-point and its surrounding region, as well as the first point of contact, can be analytically examined using the TE 77 EP/Gear adaptor.

The specifications of the simulated gears investigated were a spur gear of 2 mm pitch, 30 teeth, 20° pressure angle, and running under a ratio of 1:1 [27], this is the BSG geometry.

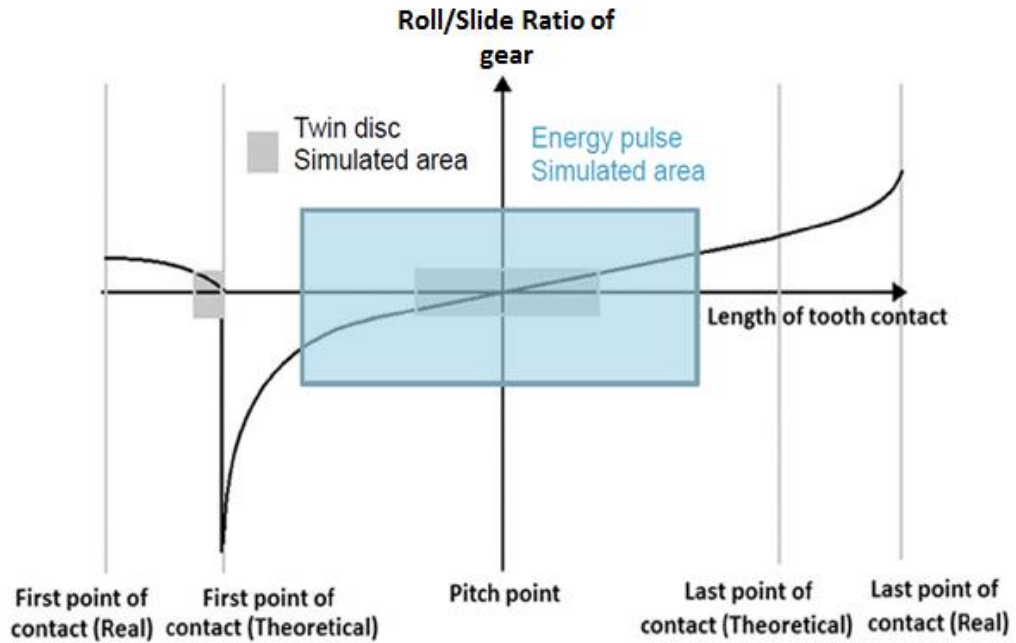


Figure 3.10: Slide-roll ratio for polymer gear contact, continuous blackline. The grey rectangle on the left shows the area of simulated twin-disc testing, and the blue rectangle shows the area for the EP/Gear adaptor (after [[27])

The slide-roll ratio for each of the Birmingham spur gears is very large as shown in Figure 3.10, where the slide-roll ratio value for the TE 77 EP-GEAR DYNAMICS was ($\pm 83.3\%$) [23].

The theoretical slide-roll ratio of a polymer gear neglects deflections and the effect of any extension in the contact line of the two meshing gear teeth. TE 77 and the twin-disc tests will provide different evaluations when simulating a gear tooth, contingent on the degree that the deflection impacts on the system. It could be that using the TE 77 test, simulates the area adjacent to the theoretical first point of contact area deflections happens.

The relative velocities between the samples vary symmetrically about the midpoint and throughout the stroke, such kinematics replicate a wide range of tribological conditions [27]. The relative slip ratios were set as 25.3%, 43.1%, and 83.3%, (determined by the positions of the rocker arm and lower rocker fork, see Figure 3.11). Where the lower rocker fork $B = 13 \text{ mm}$ the slip ratio is 25.3%, when the lower

rocker fork $B = 34 \text{ mm}$ the slip ratio is 43.1%, and for the slip ratio 83.3% the lower rocker fork $B = 51 \text{ mm}$.

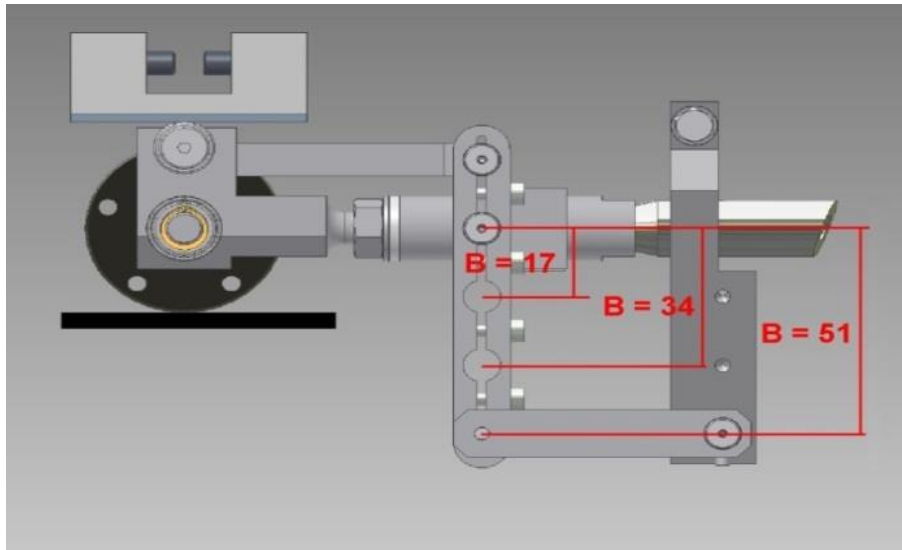


Figure 3.11: The three rolling-sliding ratios (after [4]).

Figure 3.12 shows a schematic of the equipment used and its various elements, including three sliding-rolling ratios and sliding velocities. A good estimate of the motion can be made by assuming that the adjustable link remains horizontal, resulting in the simplified relationship shown below.

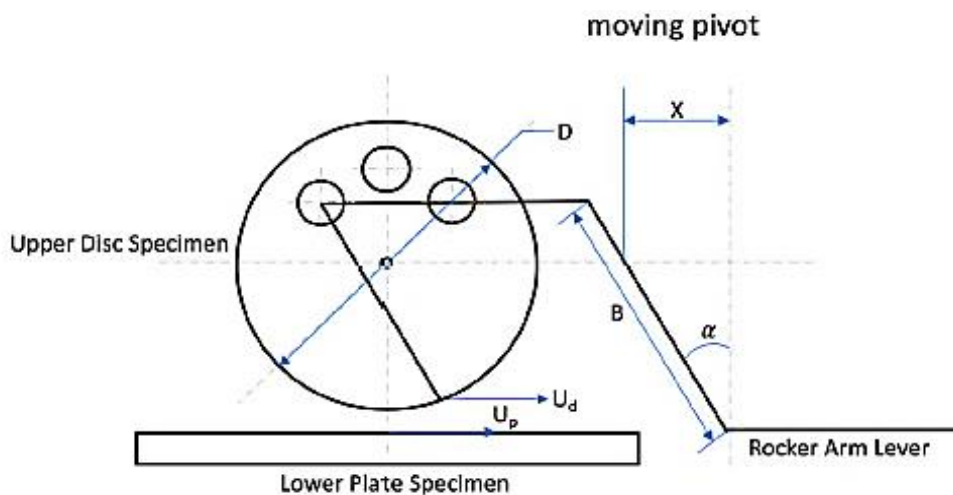


Figure 3.12: A schematic of the equipment used and the variable, EP gear Slide-roll adaptor [82].

In Figure 3.12:

B = Distance from moving pivot point to adjustable link

D = Disc diameter

A = R = Scotch yoke amplitude

x = Reciprocating stroke position

ω = Scotch yoke frequency

t = Time

α = Angular rotation

U_d = Disc surface speed relative to O; $\mathbf{U}_d = \frac{D}{2} \cdot \frac{d\alpha}{dt}$

U_p = Plate surface speed relative to O: $\mathbf{U}_d = \frac{d}{dt} (\mathbf{x})$

Reciprocating motion $x = A \sin \omega t$

Geometry: $\sin \alpha = x/D = (A \cdot \sin \omega t) / B$

$$\cos \alpha \cdot \frac{d\alpha}{dt} = (A \cdot \omega / B) \cdot \cos \omega t$$

$$\frac{d\alpha}{dt} = (A \cdot \omega / B) \cdot \frac{\cos \omega t}{\cos \alpha}$$

$$\cos 2\alpha = 1 - \sin^2 \alpha = 1 - (A^2 \cdot \sin^2 \omega t / B^2)$$

$$\text{Hence: } d\alpha/dt = \left(A \cdot \frac{\omega}{B} \right) \cdot \cos \omega t / \text{SQRT}(1 - A^2 \cdot \sin^2 \omega t) / B^2$$

$$\text{Hence: } U_d = \frac{D}{2} \cdot \left(A \cdot \frac{\omega}{B} \right) \cdot \cos \omega t / \text{SQRT}(1 - A^2 \cdot \sin^2 \omega t) / B^2$$

$$\text{Slide - roll ratio} = \frac{|U_d - U_p|}{|U_d + U_p|}$$

$$= \frac{\left[\frac{D}{2} \cdot \left(A \cdot \frac{\omega}{B} \right) \cdot \cos \omega t / \text{SQRT}(1 - A^2 \cdot \sin^2 \omega t) / B^2 \right] - A \omega \cos \omega t}{\left[\frac{D}{2} \cdot \left(A \cdot \frac{\omega}{B} \right) \cdot \cos \omega t / \text{SQRT}(1 - A^2 \cdot \sin^2 \omega t) / B^2 \right] + A \omega \cos \omega t}$$

Entrainment Velocity according to [82]

$$= 0.5 * (U_d - U_p)$$

$$= 0.5 \left(\left[\frac{D}{2} \cdot \left(A \cdot \frac{\omega}{B} \right) \cdot \cos \omega t / \text{SQRT}(1 - A^2 \cdot \sin^2 \omega t) / B^2 \right] - A \omega \cos \omega t \right)$$

The slide-roll ratio % = $(U_1 - u + R\omega) / (U_1 - u - R\omega) * 100\%$

If $\omega = 0$ then (R/S) % = 100%, hence pure sliding.

If $U_d = u + R\omega$ then (R/S) % = 0%, hence pure rolling.

Table 3.2 presents the experimental parameters: load 100 N, stroke 10 mm, and frequency 2 Hz as well as test duration and room temperature. simulates the equivalent perfectly rigid gear teeth for a load of 7 Nm applied in gear tests at contact pressures 39 MPa as Eq 3.8 for contact pressures gears and Eq 3.17 for contact pressures TE77.

Table 3.2: Experimental parameters used for the TE77 EP Gear Slide-roll tribological tests, selected gear test conditions on 7Nm steel vs. PEEK.

Parameter	
Contact pressure	39 MPa
Stroke	10 mm
Reciprocation frequency	2 Hz
Temperature	22±2 °C
Test duration	2 hours

3.4.3.4 Energy Pulse and Wear

The Energy Pulse (EP) of the Gear Slide-roll Adaptor was also used to evaluate the Archard wear equation, which explains sliding wear in terms of asperity interactions. This was not as simple as might appear because there is a major difference between them. The EP considers the length of time that the materials have been subjected to heat energy input when the surface elements pass the contact point. Thus, the EP takes into consideration the growth of wear or damage where the surfaces are in contact, the EP can be written as [83]:

$$\mathbf{EP} = \frac{\mu P U_s t_t}{2a} \quad \frac{\mathbf{J}}{\mathbf{mm}^2} \quad \mathbf{Equation\ 3.20}$$

Where:

μ - The coefficient of friction,

P - Applied load (N)

a - Contact area (mm²).

t_t - Transit time of the contact point (s) and,

U_s - Relative sliding velocity (m/s).

Equation 3.20 can be rewritten to account for combined sliding and rolling motion, (see Equation 3.21). Here the EP will be proportional to the frictional force (μP), inversely proportional to the “radius” of the contact area, and would be expected to vary only slightly with slide-roll ratio, S (see [83]).

$$\mathbf{EP} = \frac{\mu P}{2a} \left(\frac{2S}{1+S} \right) \times 10^{-3} \quad \frac{\mathbf{J}}{\mathbf{mm}^2} \quad \mathbf{Equation\ 3.21}$$

3.4.3.5 The Link Between Energy Pulse and Wear Gear Tooth Contacts

In polymer gears, the contact path extends beyond the theoretical path; see Figure 3.1, as a result of large tooth deflections and the epitomized process engagement of two gear tooth of conventional involute form. Due to the relatively high compliance of the polymer, large tooth deflections occur and this means the contact path is extended.

This extended contact means sharing the rising load done by a single pair of tooth between multiple teeth (in effect increasing the contact ratio)[19]. The consequence of this extension is alteration of the sliding velocity and load distribution between meshing teeth [14, 19, 27, 73].

Figure 3.13 shows the gear tooth engagement process for two conventional form of involute teeth. At point 1, shortly after engagement, the driving gear surface moves at a small speed relative to the contact point, while the driven gear moves faster. At point 2, the pitch point, the rolling speeds are the same, and we have a pure rolling condition without slipping. At point 3, near the end of the path of contact, the conditions are reversed, with the driving gear surface moving rapidly and the driven gear more slowly.

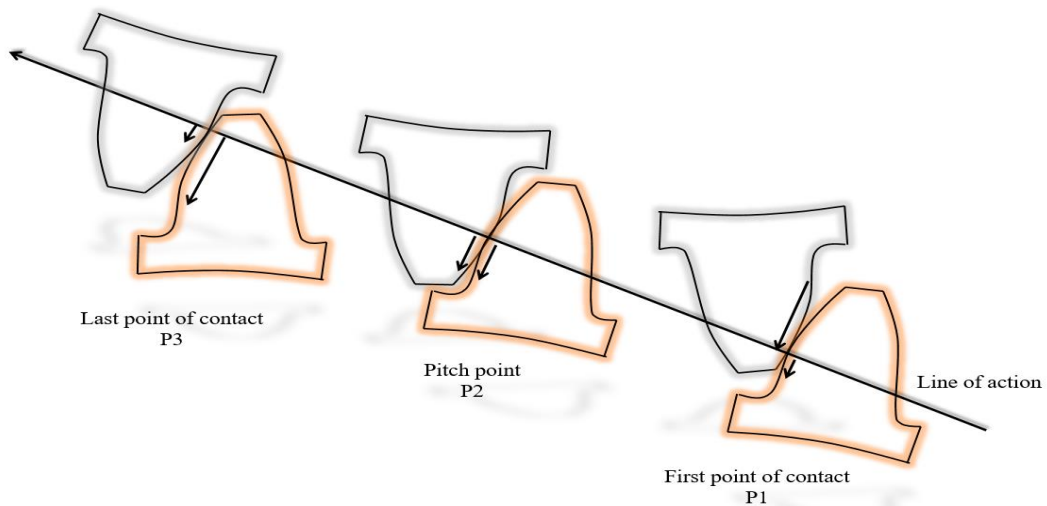


Figure 3.13: The process of gear tooth engagement, represent rolling velocities relative to the contact point (after Plint [83]).

Figure 3.14 shows the driving tooth contact conditions for a pair of 30-tooth, 20 deg. pressure angle gears of traditional forms. The contact point moves from root to tip along the tooth surface, with steadily increasing (rolling) speed. The rolling velocity

ratio has an initial value of 0.37, rising to 1.0 at the pitch point, where pure rolling occurs, and then falling to a final value of 0.37.

At the start of the touch, the energy pulse has a high initial value, falls to zero at the point of pitch, and increases to a level of about one third of its maximum value at the tip. The whole load is transmitted by a single pair of teeth between points A and B. Outside this zone the load is shared, between two pairs of teeth is assumed to be equally shared. Therefore the energy pulse, which is proportional to the tooth load, is doubled between A and B, but remains very low, as sliding velocity is also low in this zone.

It is evident, in quality, that the EP profile along the gear surface resembles the normal scuffing damage profile, which tends to be concentrated in the gear tooth's dedendum region. It is also evident that the impact of tip relief at the start of the contact is to reduce the level of EP in the critical area.

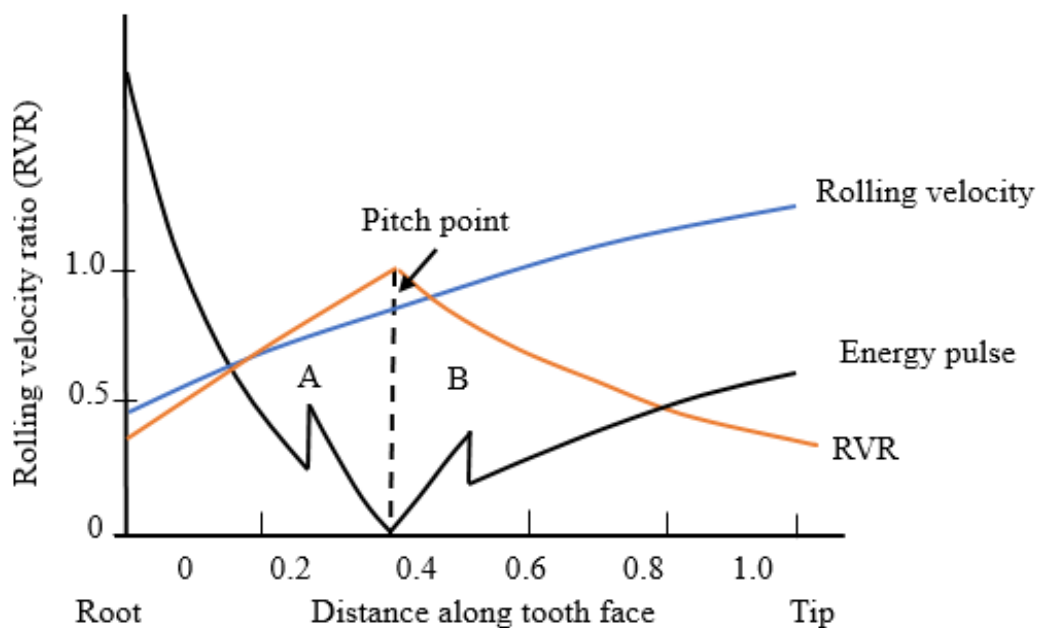


Figure 3.14: Tooth contact condition, driving gear, two 30-tooth 20 deg. Pressure angle spur gears (after Plint [83]).

The TE77 tests simulate the instantaneous mechanical response of material for a gear pair in the region of the pitch point and the first and last theoretical points of tooth contact (as a result of tooth deformation as described in the previous paragraph). These are instances of the meshing cycle where the sliding velocity is low [73, 79] and so when the maximum slip-ratio is below approximately 30%. The test specimens in this

research were designed to simulate a spur gear with the geometry module = 2 mm, number of teeth = 30, pressure angle = 20°, speed ratio= 1:1 (a Birmingham standard gear [81]).

3.4.4 Gear Testing

This section describes the application of the test rig to a specific polymer gear, (EOS PEEK HP3) and its main operating essentials. A comprehensive description of the fundamental principles and operation of the test rig is given by White [84].

3.4.5 Gear Geometry (Birmingham Standard Gear)

In all the tests, the polymer gears used were BSG geometry. Figure 3.15 shows comprehensive details of the geometry, see [30, 84].

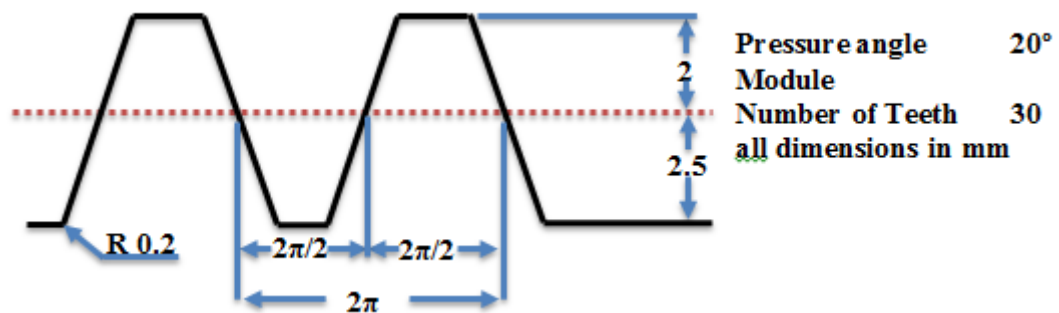


Figure 3.15: Birmingham standard rack geometry [84].

It was essential with a moulded Mark II test rig, when connecting injection moulded gears to the shaft, to have a metallic hub which was fastened using a knurl and keyway to prevent failure of the link gears, figure 3.16.

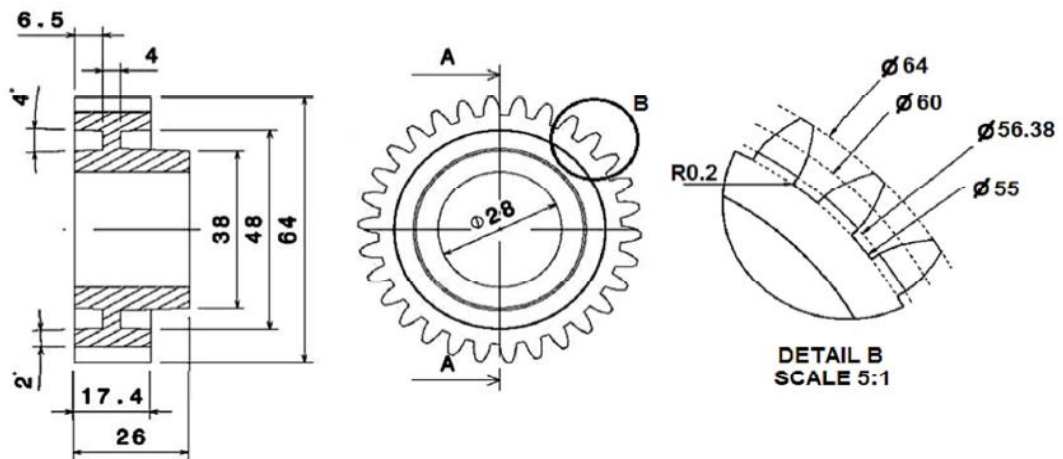


Figure 3.16: Birmingham standard gear 20° pressure angle[84].

3.4.5.1 Mark II Gear Test Rig

Figure 3.17 is a schematic of the Mark II gear test rig, used with the polymer gears, see White [84]. This test rig is of the type that re-circulates mechanical power, which reduces power consumption and improves the dynamic performance of the loading mechanism.

3.4.5.2 Loading Mechanism for Mark II Gear Test Rig

Test gears are loaded by hanging masses on the load-arm mechanism and a master gearbox (containing three helical gears). An axial force is obtained from the mass suspended on the load arm; it is transferred to the master gearbox of the test rig through the housing assembly. A mechanical advantage of 4:1 is given by the configuration therefore the conciliated axial force is:

$$F = 4mg$$

Equation 3.22

The load was transmitted within the lead gearbox via the load shaft, load collar and a piston, then to a helical gear (the load gear which was allowed to slide freely up and down its shaft). The helical gear meshed via a helical coupling gear. The rotation of the load shaft induced a torque and rotational movement in the polymer test gears. The induced torque T_r , was given by [84]:

$$T_r = \frac{F \cdot D_p}{\tan \beta} \quad \text{Equation 3.23}$$

Where:

F: axial force,

D_p : pitch circle diameter of loading gear, and

β : helix angle of the gears (30°)

Introducing Equation 3.22 into 3.23 gives:

$$T_r = \frac{4 \cdot m \cdot g \cdot D_p}{\tan \beta} \quad \text{Equation 3.24}$$

Cropper, [30] calibrated the Mark II test rig, and validated its performance. It was found that the axial load fluctuated by $\pm 5\%$, while the error in the speed control was about 1%, frictional losses in the system were assumed negligible.

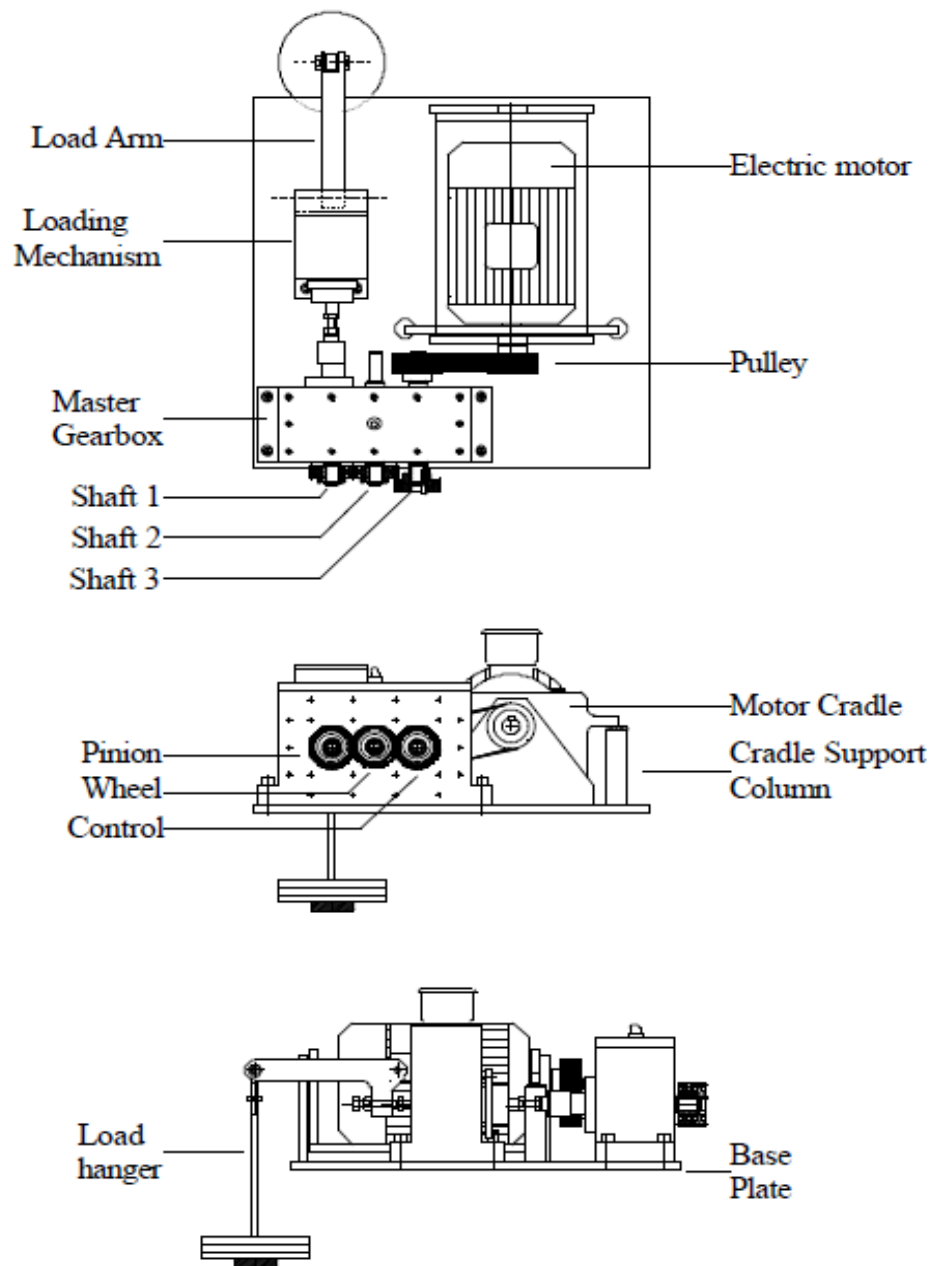


Figure 3.17: Mark II test rig, designed by White, 1999 [84].

3.4.5.3 Wear Mechanism of Gear Test Rig

The wear was measured by the mass loss of the gears. To do this the mass of the gear was measured before and after the test. In some tests, the gears were stopped at set times, their positions recorded, they were removed, weighed, and then replaced as closely as could be to their initial positions. This procedure minimised both the loss of transfer film and disturbance to the meshing of individual gear teeth.

However, Kono [4] has suggested using surface replication techniques so that disruption is minimised because measurements can be made without the gears being removed from the rig. Materials such as used in dental procedures, i.e., hydrophilic vinyl polysiloxane precision impression material supplied by Mydent International.

Hoskins [2] used surface replication techniques to measure the depth wear for gear tooth by using CharmFlexRPutty hydrophilic vinyl polysiloxane vinyl impression material (Denkist, Inc., South Korea).

Basler ace Camera Software Suite version 6.0.0 used, the test was stopped, and scan for the tooth surface was table. It was mall, affordable and highly productive, in addition to take fixe scale. Figure 3.18 shows the Basler ace cameras for the images tooth profiles.

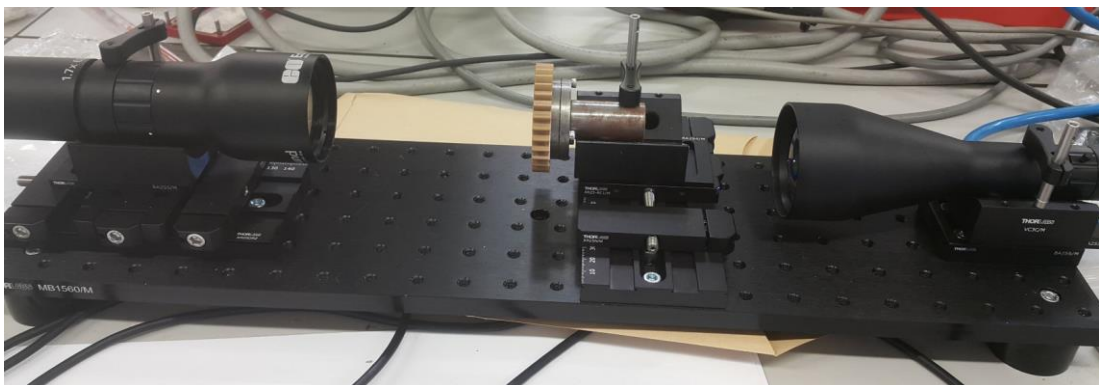


Figure 3.18: The Basler ace cameras.

3.5 Physical Properties of Polymers (Surface Microscopy)

Normally, any of polymer's mechanical properties will give an indication of its operating capacity and a preliminary indication of the surface contact.

3.5.1 Scanning Alicona Microscopes

A topographical method was used to measure the three-dimensional wear scar volumes with different finishing processes. The Alicona G5 infinite focus light microscope was used for the three-dimensional measurements of the surfaces.

Three-dimensional surface profiling provided the physical appearance of the sample surfaces (in terms of three-dimensional co-ordinates) before and after the tests. The loss of volume was then calculated. This allowed not only measurement of wear but also the weight loss of the teeth.

3.5.2 Scanning Electron Microscopes (SEM)

Surface observations of the surfaces tested in this work were also made using Scanning electron microscopy (SEM). In this project the SEM used was a JEOL 6060 combined with energy-dispersive X-ray spectroscopy. To enable the polymer surface to be imaged, the polymer samples should be electrically conductive; therefore, an ultra-thin layer of gold needed to be sputtered onto the polymer surfaces.

3.5.3 Thermal Camera

Thermal Camera was used to measured temperature profile variation during disc rotation Relative Thermal Index (RTI) in chapter 4.

3.5.4 Crystallinity

Differential Scanning Calorimetry (DSC) was used to ascertain whether the surface of a polymer test specimen underwent any thermal ageing during a test, in particular the crystallinity of the surface. The crystallinity test surface needs about (12- 9 mg) weighed from the contact area and placed in an aluminium pan. The heat flow to the

pan containing the sample was compared to the heat flow from an empty reference pan. In this research a Perkin Elmer DSC 7 was used. Each pan had its own heater and temperature measuring sensor and the power required to sustain each pan at a given temperature was recorded [85, 86]. The measured heat flows provide valuable information that enabled the crystallinity% of the samples to be determined using Equation 3.25:

$$\text{Crystallinity}\% = \Delta H_{\text{measured}} / \Delta H_{\text{fusion}} \quad \text{Equation 3.25}$$

where ΔH is the enthalpy.

The calibration of the calorimeter was carried out using high purity Zinc and Indium whose melting points ($T_{mZ} = 419.53^{\circ}\text{C}$ and $T_{mI} = 156.63^{\circ}\text{C}$) are accurately known. The correction for thermal lag was found using extrapolation.

3.6 Materials

These grades of PEEK were chosen because they have important properties desirable for components in high-performance machines including: a relatively high thermal index with retention of mechanical properties at elevated temperatures, good corrosion resistance, and a natural resistance to thermal degradation [87].

3.6.1 Injection model

PEEK (Direct Plastics, Sheffield, UK) and PMC (450CA30%, supplied by Victrex, Lancs, UK) (a reinforced grade of PEEK containing 30 % carbon fibres by weight). Mechanical properties of the PEEK, PMCS and AISI 52100 steel are shown in table 3.3.

Table 3.3: Mechanical properties of the PEEK and PMCS and AISI 52100 steel.

Material	Young modulus (GPa)	Tensile strength (MPa)	Poisson's ratio
PEEK	4.2	116	0.4
PMC	11	265	0.4
AISI 52100 steel alloy	210	2240	0.3

3.6.2 Selective Laser Sintering

Generally, polymer components have been injection moulded (IM) but advances in additive methods of manufacturing mean those geometric shapes that were very complicated and expensive to manufacture using layer deposition, colloquially referred to as “3-D printing”. Today, High temperature selective laser sintering (HT-SLS) is predominantly used in the medical and aerospace industries [88]. This, broadly, is a process by which laser sintering combined with digitised 3-D design data is used to produce the module by fusing together one layer of deposited powdered material at a time. Each deposited layer is fused to the previous one, building up the finished form, see Figure 3.19.

Such a process has greatly improved design flexibility by enabling production of highly complex specialist parts without the requirement for costly re-tooling, increasing interest in laser sintering of high temperature semi-crystalline materials. Thermoplastics of high performance (e.g., polyamide 12, (PA12)) have been laser sintered for some years, to manufacture component elements with superior mechanical durability [89-94], but these still have relatively low glass transition temperatures and melting temperatures values which limit their applications.

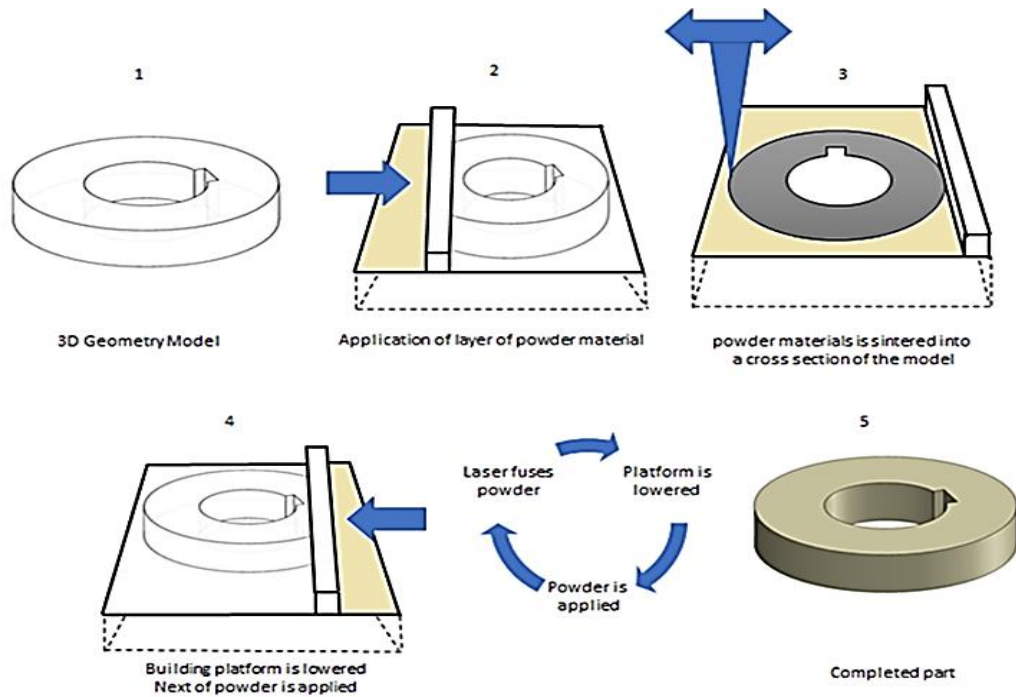


Figure 3.19: selective laser sintering process

Electro Optical Systems [EOS GmbH., Munich, Germany] and Victrex have developed a semi-crystalline thermoplastic, EOS PEEK HP3, a material belonging to poly-aryl-ether-ketones (PAEK), specifically for use on their EOS P800 HT- LS machine, see Figure 3.20. The P800 contains a CO₂ laser that operates at 385°C to build 3-D structures in layers 0.1 mm thick.



Figure 3.20: Electro Optical Systems (EOS) P800 High Temperature Laser Sintering (HTLS) system, (source EOS)²

² (https://www.eos.info/systems_solutions/plastic/systems_equipment/eosint_p_800)

Because the P800 operates at such a high temperature it can sinter high performance polymers like PEEK and PAEK, where a process cannot be done by traditional (LS). Figure 3.21 presents published data on the mechanical behaviour of five laser sintered polymers. The advantage of PEEK over the other polymers is obvious. for example, its modulus of elasticity is almost 20% greater than for POM and almost 80% greater than for PA12 [90].

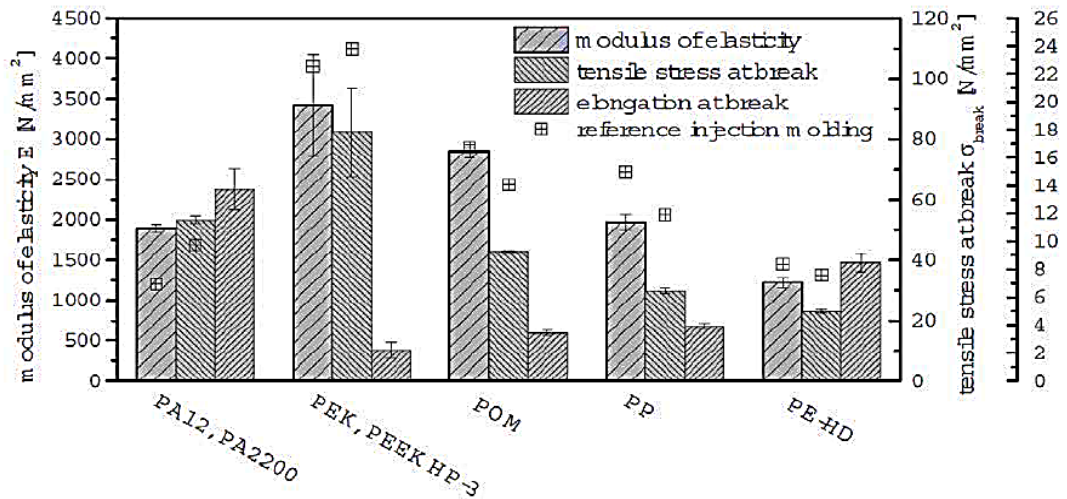


Figure 3.21: the mechanical properties of various selectively laser sintered polymeric materials [90].

At present, there is little independent published information on the application of EOS PEEK HP3. The EOS website reports PEEK HP3 as exhibiting “excellent wear resistance” based on its own research [90]. Several papers have been presented describing the selective laser sintering applied to high performance polymers, though with limited examination of material properties [88, 95]. Only a few works have been found that have attempted to describe the mechanical properties of components made from EOS PEEK HP3 [96-99]. Ghita et al., reported that the inherent anisotropy resulting from HT-LS meant the sintering mechanism made a significant difference to the component’s mechanical properties [97].

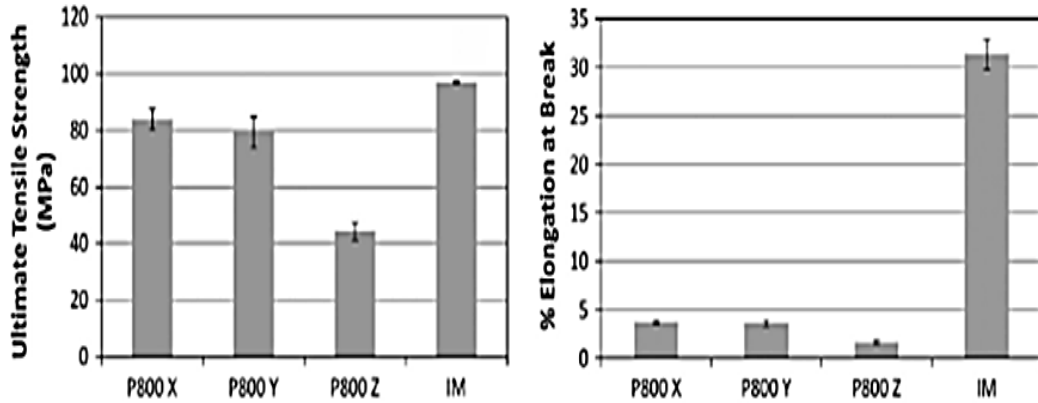


Figure 3.22: Effect of (X,Y,Z) orientations on ultimate tensile strength, and percentage elongation-to-break, for HT-LS EOS PEEK HP3 compared with IM PEEK specimens [98].

Ghita et al., demonstrated that HT-LS manufactured components exhibited different properties in different directions. The X and Y axes are in the plane of the component (say horizontal), and the Z axis is normal to that plane (say vertical). We see from the results presented in Figure 3.22 [98], that tensile strength and elongation to failure were much the same for the X and Y directions, but that in the Z direction the tensile strength was reduced by almost half, while the elongation-to-breaking point decreased by just over 50%. Such anisotropy is not unusual with parts produced by additive layer manufacturing. Previous reports [93], have described reductions in, e.g., tensile strength of Nylon of up to 20% in the Z direction. All the samples tested showed brittle failure, with the samples built with horizontal layers this presented as propagation of cracks from the skin, while for the Z samples there was boundary layer fracturing.

We see from Figure 3.22 that the elongation-to-break for the PEEK components manufactured by IM was some fifteen times higher than for the corresponding components manufactured by HT-LS. This was ascribed to the anisotropy of the samples, and the problems in obtaining a completely homogeneous sample [89, 96, 98].

In addition, Ghita et al., included up to 30% of used powder in their samples (the remaining percentage was virgin) and the inclusion of previously used powder was shown to decrease tensile strength by as much as 17% [97].

Berretta et. al. have also reported the effects on components build orientation. These researchers investigated the effect of horizontal, inverted horizontal and vertical build orientations on the properties of LS PEEK cranial implants. The differences between the component produced at each orientation was compared to the specified design; in particular dimensional accuracy and density, and the compressive strength measured using a simple uniaxial static compression test. The results showed that least deviation in measurements and density, and the greatest compressive strength was for the two horizontal orientations. The component built vertically had a significantly lower accuracy, and its measured compressive strength at first failure was 70% less than the value for the horizontally built components [100].

There is only a modest amount of independent data accessible regarding the mechanical properties of EOS PEEK HP3 and the majority of that information is manufacturer's data, where the relevance to a specific application may not be immediately evident [90]. Gears and Stok, and Schmidt et al. have described the use of selective laser sintering for high performance polymers but with limited information provided on the properties of the materials used [88, 95]. Beard et al., and Ghita et al. are the only researchers found to have attempted to describe the properties of EOS PEEK HP3 but the data they provided was limited [96-99].

Hoskins et al. have demonstrated that EOS PEEK HP3 performs substantially better than materials previously used with laser sintering, similar to high performance IM materials. It was found that the failure mechanisms were largely governed by how the sample was loaded; tensile tests showed secondary fractures, while compressive tests with higher loads produced delamination. The surfaces of samples that had failed the compressive test showed partial sintering; this process needs to be investigated as it could improve material properties by refining the process parameters. Because of the tendency to brittleness EOS PEEK HP3 was not recommended for impact loading as it could fail suddenly [99].

The work of Hoskins et al. has presented important mechanical characteristics of EOS PEEK HP3 and can indicate the HT-SLS materials suitability for specific applications. However, the use of software tools to optimise the load distribution over the component's surface is advocated to enhance component and system performance.

Because each application can be specific the particular design requirements will require analysis to assess the precise material properties [2].

Table 3.4 displays PEEK 450G and EOS PEEK HP3 the material properties.

Table 3.4: Mechanical Properties summary[2, 92, 95, 96, 98, 106]

Material	EOS PEEK HP3	PEEK 450G
Tensile Modulus (EN ISO 527)	2.76 ± 0.15 GPa	3.7 GPa
Tensile Strength (EN ISO 527)	88.7 ± 1.5 MPa	100 MPa
Elongation at Break (EN ISO527)	4.2 ± 0.2 %	34 %
Compressive Strength	184 ± 15 MPa	125 MPa
Flexural Modulus (EN ISO178)	3.26 ± 0.7 GPa	4.1 GPa
Glass Transition Temperature (DSC)	174.5 °C	143 °C
Fracture Toughness, KIC	1.40 ± 0.2MPa/m ²	5.4 - 7.5MPa/m ²
Glass Transition Temperature DMTA, $\tan\delta$)		
@1Hz	186.8 °C	165.8 °C
@3Hz	189.3 °C	
@10Hz	192.3 °C	
@30Hz	195.1 °C	
Density: Bulk (DIN 53466)	0.43 ± 0.01 g/cc	1.30 g/cc
Density: Laser sintered part (DIN EN ISO 1183)	1.307 ± 0.01g/cc	N/A
Porosity (BS ISO 15901)	4.359 %	N/A
Melting point (DSC)	372 °C	343 °C
Crystallinity (DSC)	35.4 %	30 %

Chapter Four
4



4

“The science of today is the technology of tomorrow”

Edward Teller

Tribological Properties of Twin Discs Simulation Additive Manufacture Gears

This chapter observes the influence of contact pressure, sliding/rolling velocity and working temperature on the tribological properties of PEEK, and EOS PEEK HP3. Through simulating polymer gear contact unlubricated and lubricated.

4.1 Twin Disc Testing

The tribological properties of PEEK and EOS PEEK HP3 were investigated by the twin disc test rig to explore the effects of contact pressure, temperature and slide-roll velocity. The tests were conducted with and without lubrication over a range of contact pressures and slip ratios in addition to lubrication (surface lubricated)

Table 4.1. showed the list of test conditions. During the tests, the friction, wear and temperature data for the system were collected. The loads of tests were equivalent the gear torques: 13.5, 10.1 and 6.4 Nm.

Table 4.1: Test conditions for disc twin discs tests, equivalent: 13.5, 10.1, and 6.4 torque gears /Nm

Max. Contact Pressure / MPa	Slip Ratios		
	3.9%	14.29%	28.59%
56	√	√	√
48		√	√
39			√

4.2 Friction Coefficient and Temperatures Results for un-lubricated tests

Each test was repeated three times which could be related to the friction profiles, wear and surface temperature. Figure 4.1, Figure 4.2, & Figure 4.3, show the average results obtained for a 14.29% slip ratio and 56 MPa contact pressure for EOS PEEK HP3 disc vs. EOS PEEK HP3 disc, EOS PEEK HP3 disc vs. steel disc, and a PEEK disc vs. steel disc, respectively. Melting Point (T_m) 343°C, Glass Transition (T_g) 143°C for the unfilled PEEK and Melting Point (T_m) 372°C, Glass Transition (T_g) 174.5°C for the EOS PEEK HP3 as in Table 3.4 in Chapter 3.

The mechanical response of EOS PEEK HP3 discs running against the EOS PEEK HP3 discs counterface in a rolling contact is shown in Figure 4.1. It can be seen that the temperature increased rapidly to a value of about 275°C during the first 5 min., after which there was a linear increase with time to a temperature 319°C after 100 min. We also see a rapid rise in the coefficient of friction to a maximum of about 0.35 after about 15 min., the trace then showed some fluctuation before settling down, after about 40 min to a steady level of 0.33. Wear rises monotonically with time, more or less linearly to about 80 min, after which the wear accelerates.

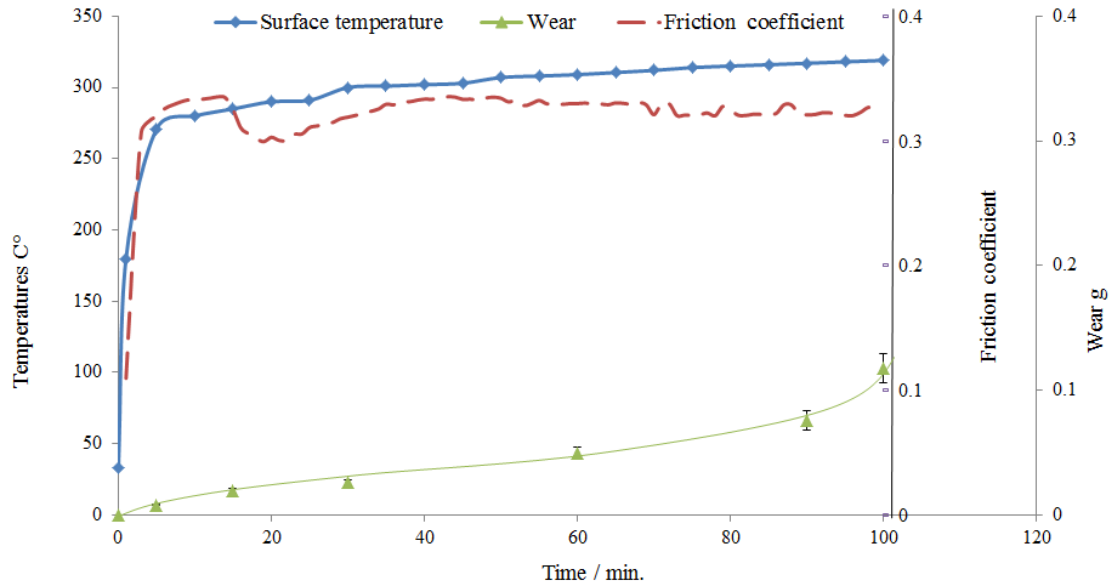


Figure 4.1 : Results obtained for surface temperature, wear and friction coefficient for EOS PEEK HP3 disc running against EOS PEEK HP3, contact pressure 56 MPa and slip ratio 14.29%.

Figure 4.2, shows the results obtained for EOS PEEK HP3 discs running against steel under the same conditions above (contact pressure 56 MPa and slip ratio 14.29%). It was observed that, as previously, the temperature rose rapidly but to only about 60°C during the first 5 min., after which it rose gradually to 90.8°C at 100 min. During the test after about 10 min., the friction profile was more or less constant at a value of 0.21. The wear shows a somewhat inconsistent pattern, except after about 80 min., as in the previous test, there was a rapid increase in its value.

Figure 4.3, shows an unfilled PEEK disc running against steel under the same conditions above (contact pressure 56 MPa and slip ratio 14.29%). As previously, a rapid initial rise in temperature was observed during the first 5 min., followed by a gradual increase to a value of about 101.8°C after 100 min. After a short initial period of about 10 min., the friction coefficient settled down to a value of 0.24, wear rises relatively rapidly initially, then increases more or less linearly with time, and after about 80 min., the wear accelerates.

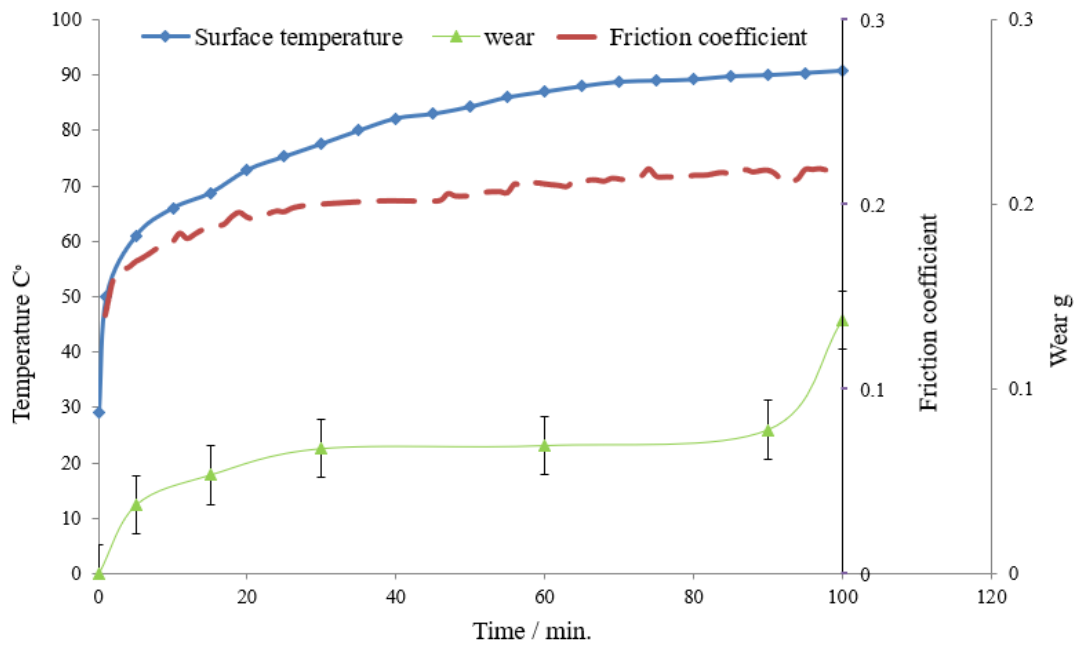


Figure 4.2: Results obtained for surface temperature, wear and friction coefficient for EOS PEEK HP3 disc running against steel disc under contact pressure of 56 MPa and slip ratio of 14.29%.

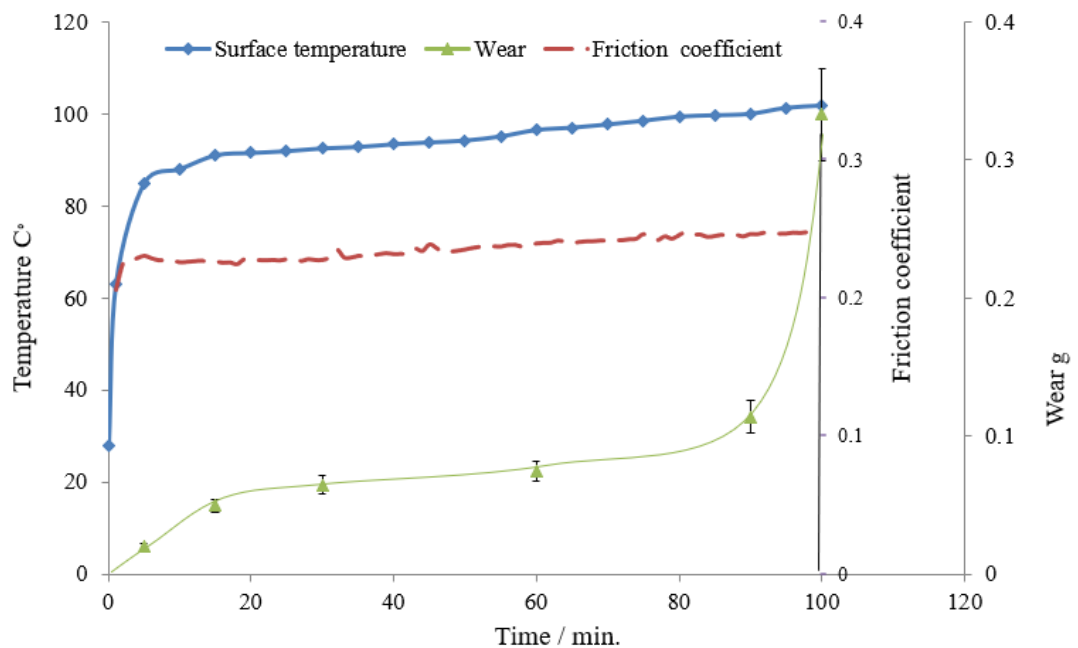


Figure 4.3: Results obtained for surface temperature, wear and friction coefficient for PEEK disc running against steel disc under contact pressure of 56 MPa and slip ratio of 14.29%.

Each Figure 4.1, Figure 4.2 & Figure 4.3, could be divided into three general areas which could be related to temperature, friction coefficient and wear. We see a short initial 5

min. “running-in” period in which each of the three parameters increases rapidly, then a period of more-or-less steady-state running. With wear there is a final period of wear accelerating and in the final period of increased wear leading (sometimes quickly) to specimen failure [14, 47, 50, 53, 54, 68, 79, 101, 102]. The best result was obtained for EOS PEEK HP3 discs running against steel, the temperature of disc of EOS PEEK HP3 was less than any tests due to the higher thermal conductivity of the steel disc, therefore acting as a heat sink and taking heat away from the interface of contact [81, 103].

Comparing the above result with previous work [14] under the same parameters, contact pressures and slip ratios, the mechanical response of unfilled PEEK when run against a PEEK counterface in a rolling contact by twin disc, reported that the temperature of around 340°C near melting point 343°C, and friction profiles around 0.47 and there was no steady state under contact pressure 56 MPa and slip ratio 14.29% during 100 min [14], all the results in Table 4.2.

Table 4.2: Friction coefficient, wear and surface temperatures under contact pressure of 56 MPa and slip ratio of 14.29%.

Materials of disc	Friction Coefficient	Wear/g	Temperatures (°C)
EOS PEEK HP3 vs EOS PEEK HP3	0.33	0.0588	319
EOS PEEK HP3 vs STEEL	0.21	0.0294	90.6
PEEK disc vs STEEL	0.2	0.0665	101.8
PEEK vs PEEK [14]	0.47	1.2845	340

4.3 The Steady State Friction Coefficient: Non-lubricated Tests

The time steady state average friction coefficients as a function of the contact pressures and slip-ratio are shown in Figure 4.4. The time steady state vs. coefficient of friction for all test conditions EOS PEEK HP3 disc vs. EOS PEEK HP3 disc.

The time steady state average friction coefficient as a function of the contact pressures and slip-ratio are shown in Figure 4.5 for the EOS PEEK HP3 disc vs. steel disc test conditions.

Figure 4.6 shows the time steady state average friction coefficient as a function of the contact pressures and slip-ratio for the results PEEK vs. steel test.

It was found that, generally, the higher the contact pressure and the higher the slip ratio, the longer it took to reach the steady state. At the maximum slip-ratio of 28.57% and the maximum contact pressure 56 MPa, the time for the EOS PEEK HP3 disc vs. steel disc to reach a steady state was 50 min. However, for the lowest contact pressure, 39 MPa and low slip ratio tests created the lowest temperature and wear, where this considered being the least severe.

The friction coefficient increases with increasing slip ratio. An increase in friction value causes temperature increase. Besides, thermal conductivity of polymer is low, as a result, the surface of polymer at higher temperatures has more plastic deformation generating higher surface roughness.

The higher contact pressure in these non-lubricated tests meant adhesion between the surfaces became prominent. Adhesion in the contact region, and increased pressure meant increased asperities deformation on the surface of polymer, resulting in an increase in the real region of contact, increasing adhesion and thus increasing the friction coefficient [14, 81, 103].

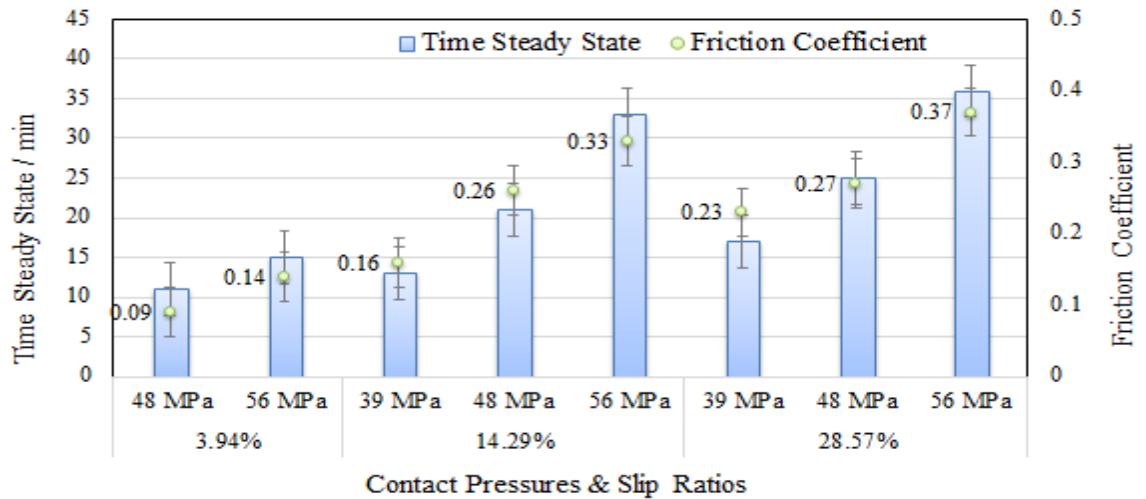


Figure 4.4: The time steady state average friction coefficient EOS PEEK HP3 vs. EOS PEEK HP3 disc for three applied pressures (39, 48, and 56 MPa), three slip values (3.94, 14.29, and 28.57%) showing the test duration at which peak value was attained.

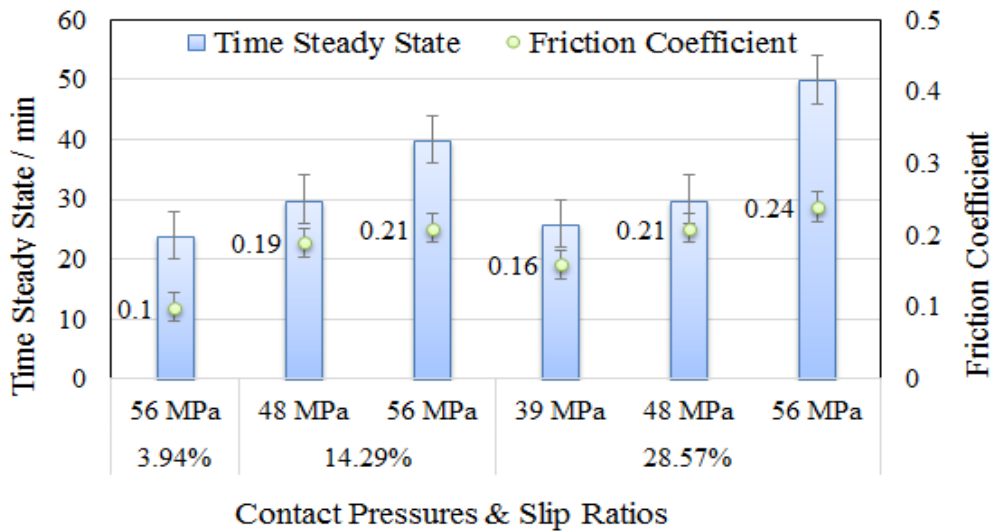


Figure 4.5: The time steady state average friction coefficient EOS PEEK HP3 disc vs. steel disc for three applied pressures (39, 48, and 56 MPa), three slip values (3.94, 14.29, and 28.57%) showing the test duration at which peak value was attained

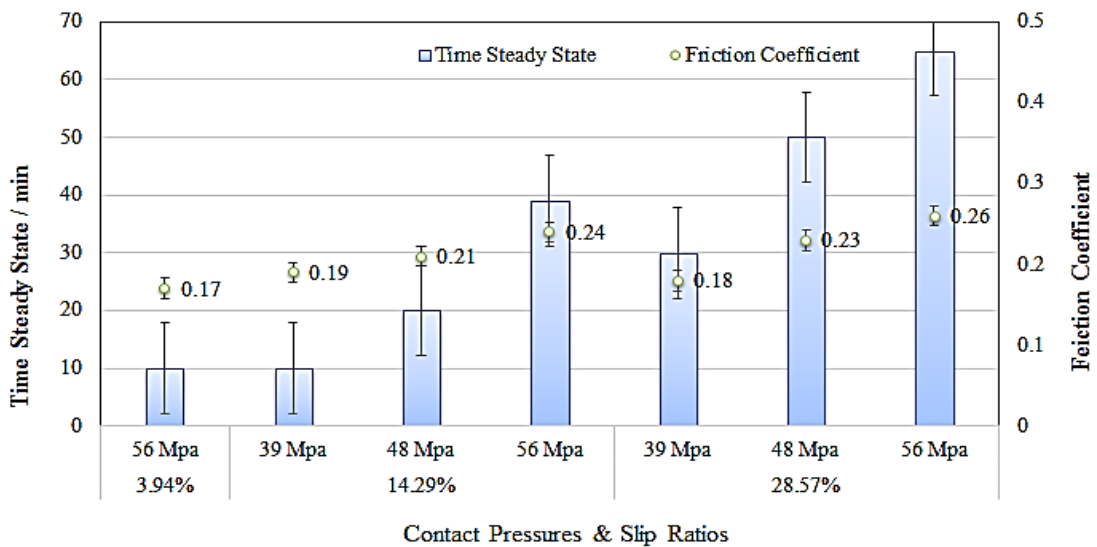


Figure 4.6: The time steady state average friction coefficient for PEEK vs. steel disc for three applied pressures (39, 48, and 56 MPa), three slip values (3.94, 14.29, and 28.57%) showing the test duration at which peak value was attained.

4.4 Wear Mechanisms and Topographical Analysis: Non-lubricated Tests

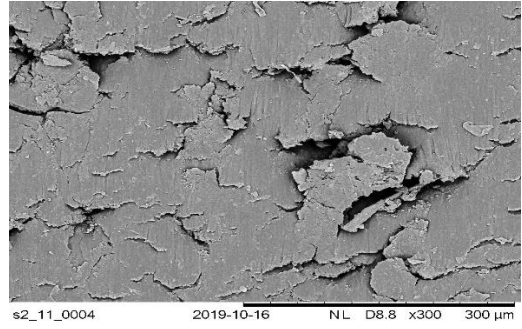
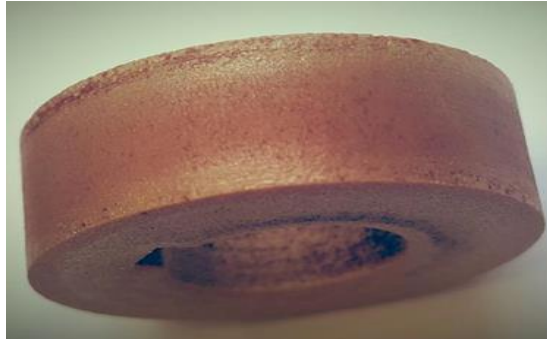
The Alicona microscope images in Figure 4.7 shows the disc surfaces under contact pressure 56 MPa and slip ratio 14.29% test during 100 min. Where Figure 4.7-a, b, c and d. shows the surface of the disc for the samples EOS PEEK HP3 vs. EOS PEEK HP3, EOS PEEK HP3 vs. steel, PEEK vs. steel and PEEK vs. PEEK [14] respectively.

Slight localised damage could be seen on the surface of the disc for the samples EOS PEEK HP3 vs. EOS PEEK HP3, EOS PEEK HP3 vs. steel and PEEK vs. steel. Where it could be seen the damage on the surface of the disc PEEK vs. PEEK under the same condition and its effect on friction and wear in Figure 4.7-d [14].

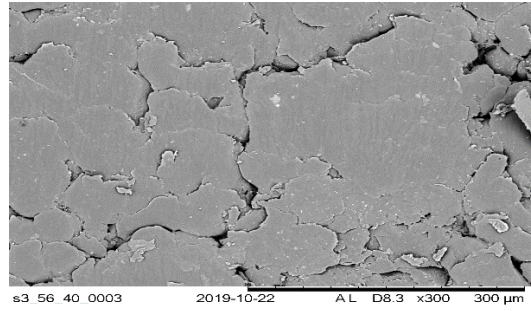
Figure 4.7-a shows the surface of the test disc for EOS PEEK HP3 vs. EOS PEEK HP3. The discolouration of the samples, they became darker, was due to a thin region adjacent to the surface of the EOS PEEK HP3 disc being oxidised as a consequence of the high temperature generated at the point of contact, near 319°C [104].

In addition, we also get pitting on the surface of the disc because of the high temperature of the surfaces in contact. It may be that thermal overload led to superficial layers to change their crystalline structure, which is a form of permanent deformation. It is thought that at the contact point the high temperatures generated forced expulsion of wear debris, a proportion of which was then trapped in the gear mesh, damaging the surface of the disc. Subsequent adhesion and cyclic fatigue related to this failure could be seen on the surface of the disc.

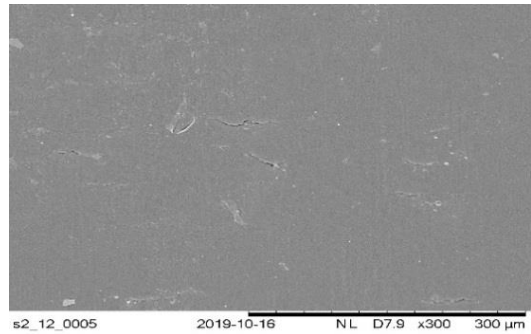
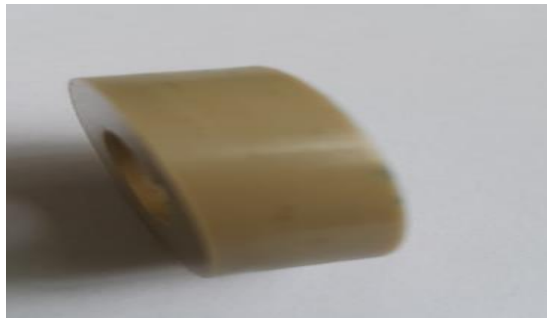
The results for EOS PEEK HP3 vs. a steel disc are shown in Figure 4.7-b. The surface contact temperature was 50.8°C (as shown in Table 4-2, and Figure 4.2), and slight damage was observed on the surface of the disc. The lower surface contact temperature is due to both a lower friction coefficient and the steel disc having a higher conductivity than EOS PEEK HP3. Figure 4.7-c shows the results for PEEK vs. a steel disc, the temperate of surface contact was 91°C, and some small pitting can be seen on the surface of the PEEK disc.



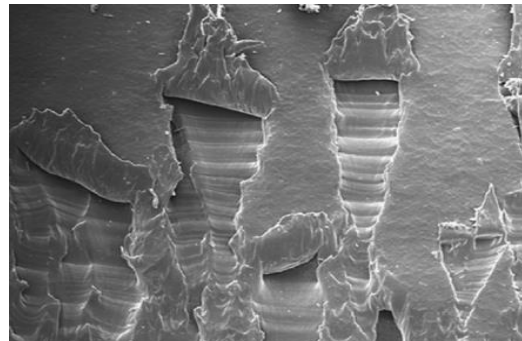
a- EOS PEEK HP3 disc vs. EOS PEEK HP3 disc.



b- EOS PEEK HP3 disc vs. Steel disc.



c- PEEK disc vs. steel disc.



d- PEEK disc vs. PEEK disc [14].

Figure 4.7: Surface damage incurred in EOS PEEK HP3 vs. EOS PEEK HP3, EOS PEEK HP3 vs. steel, PEEK vs. steel and PEEK vs. PEEK tests with 14.29% slip-ratio and contact pressure 56 MPa.

4.5 Wear Tracks

Wear track results by an Alicona microscopic after the polished sample can be seen in Figure 4.8, displayed EOS PEEK HP3 disc vs. EOS PEEK HP3 disc the depth of the wear tracks results. There is a definite change in depth of the wear track across the sectioned disc. Here the three plots are for a contact pressure of 56 MPa and slip-ratios of 28.57% (red), 14.29% (green), and 3.9% (blue).

Figure 4.9 shows the depth of the wear tracks for EOS PEEK HP3 disc vs. steel disc, after tests under contact pressure of 56 MPa and slip ratios of 28.57%, 14.29% and 3.9%, as seen by an optical microscopic. It can be seen that the wear of the track in the middle of the contact area with slip ratio 28.59%, was generally greater than those for the other slip ratios.

In Figure 4.10 presents the results for PEEK disc vs. steel disc, the wear tracks results, again as seen by an Alicona microscope after polishing the sample. Contact pressure was 56 MPa and slip-ratios were 28.57%, 14.29% and 3.9%. We see a small but significant increase in the depth of wear across around the centre of the sectioned disc.

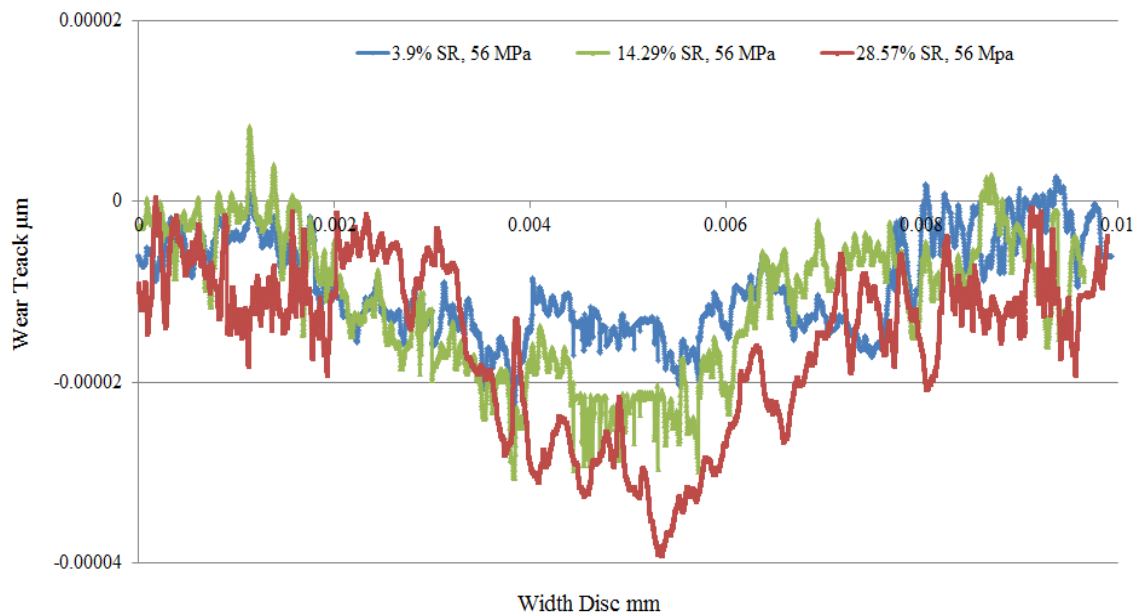


Figure 4.8: Wear as seen by an Alicona microscope for EOS PEEK HP3 disc vs. EOS PEEK HP3 disc, for contact pressure of 56 MPa and three slip-ratios, 28.57%, 14.28% and 3.9%.

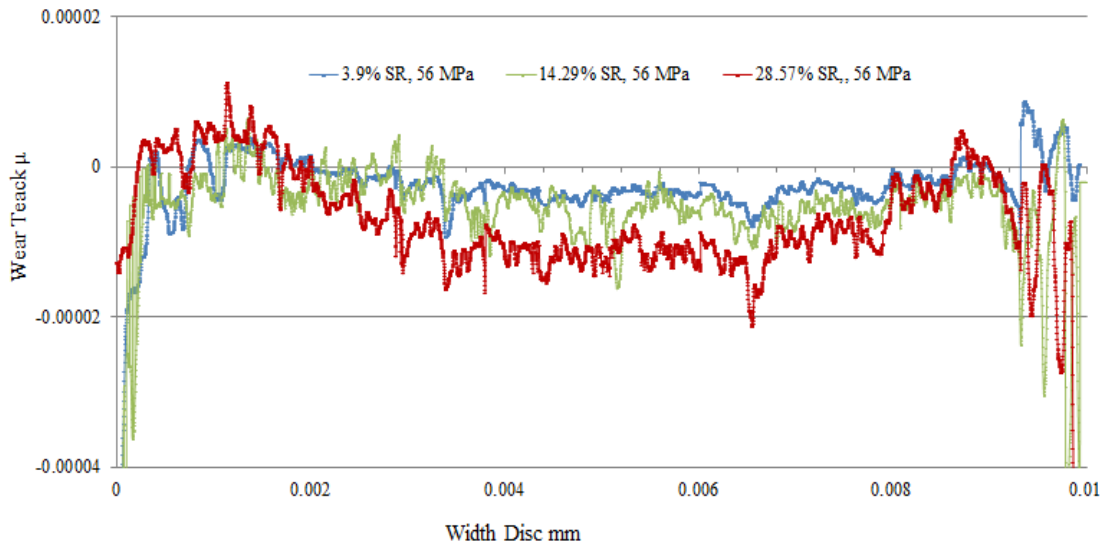


Figure 4.9: Wear as seen by an Alicona microscope for EOS PEEK HP3 disc vs. steel disc, for contact pressure of 56 MPa and three slip-ratios, 28.57%, 14.28% and 3.9%.

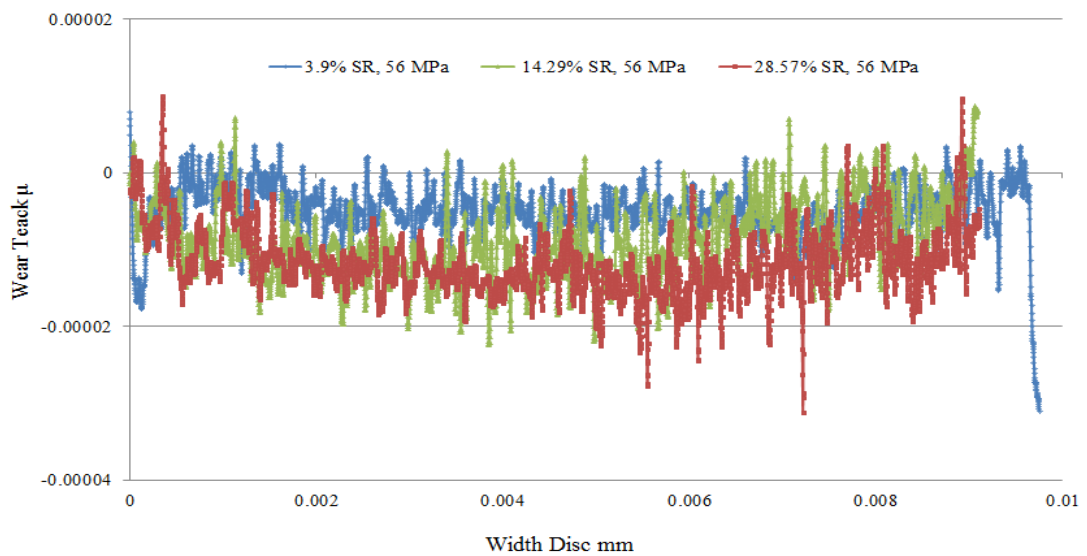


Figure 4.10: Wear as seen by an Alicona microscope for PEEK disc vs. steel disc, for contact pressure of 56 MPa and three slip-ratios, 28.57%, 14.28% and 3.9%.

For all the tests, there is a definite change in the depth of wear in the material across the face of the disc, with greatest wear around the centre of the sectioned disc, an area related to the highest temperatures (as in paragraph 4.7) during running and is symptomatic of cohesive wear [14, 81].

Under severe contact pressures operational conditions, EOS PEEK HP3 vs. steel produced significantly less wear than other materials and lower temperatures [79, 105].

In addition, because the glass transition temperature of EOS PEEK HP3 is relatively high, 172°C, it retained its mechanical strength over the period of the test, its surface softening when the temperature increased to approximately 300°C [14].

4.6 Average wear rate versus test severity

During the first 5 mins of the tests, high temperatures were generated at the line of contact rapidly; it is supposed that this was a result of the forced ejection of wear debris. Temperature/time plots for all the tests carried out to show the average wear rate correlated with the relative test severity were. The severity of the test was calculated as the average time-integrated thermal output from the touch, allowing quantification of wear rates based on operating conditions of slip ratios of 28.57%, 14.29%, and 3.9% and contact pressures 56, 48 and 39 MPa.

Figure 4.11 shows the relatively strong relating of the average wear rate and the integral measure of temperature for EOS PEEK HP3 disc vs. EOS PEEK HP3 disc. Figure 4.12 shows the relatively strong relating of the average wear rate and the integral measure of temperature for EOS PEEK HP3 disc vs. steel disc and Figure 4.13 shows the relatively strong relating of the average wear rate and the integral measure of temperature for PEEK disc vs. steel disc.

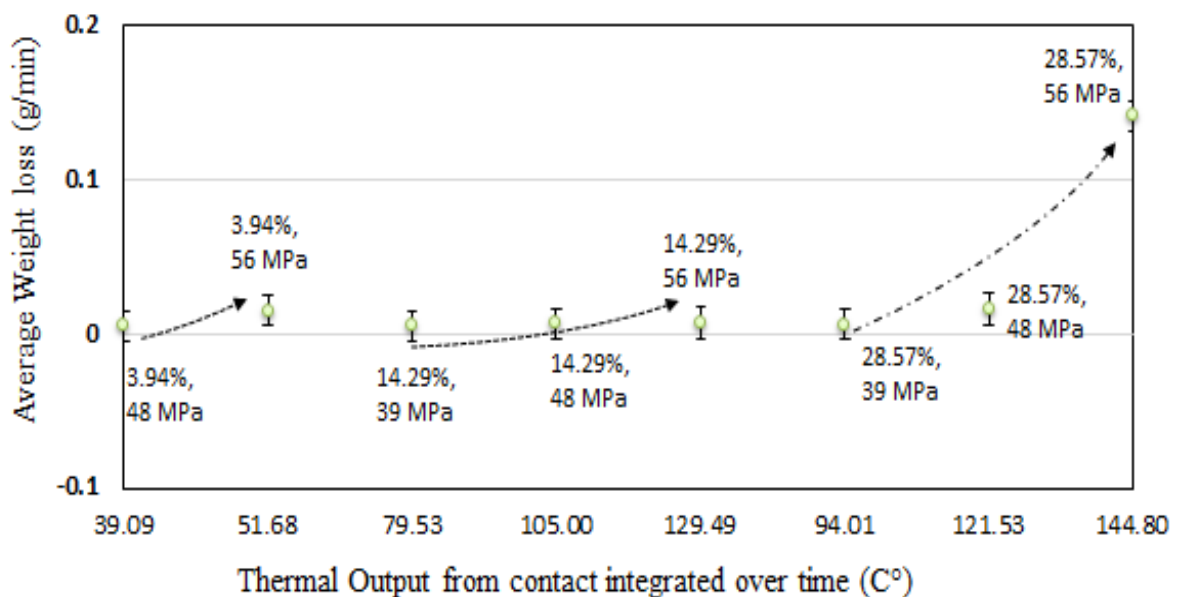


Figure 4.11: Average wear rate versus test severity for EOS PEEK HP3 disc vs. EOS PEEK HP3 disc twin disc tests.

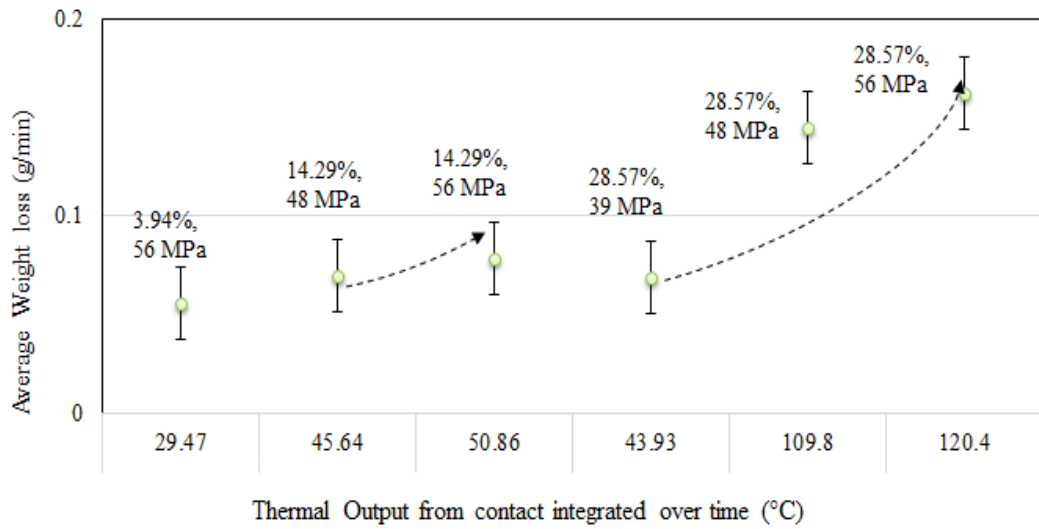


Figure 4.12: Average wear rate versus test severity for EOS PEEK HP3 disc vs. steel disc twin disc tests.

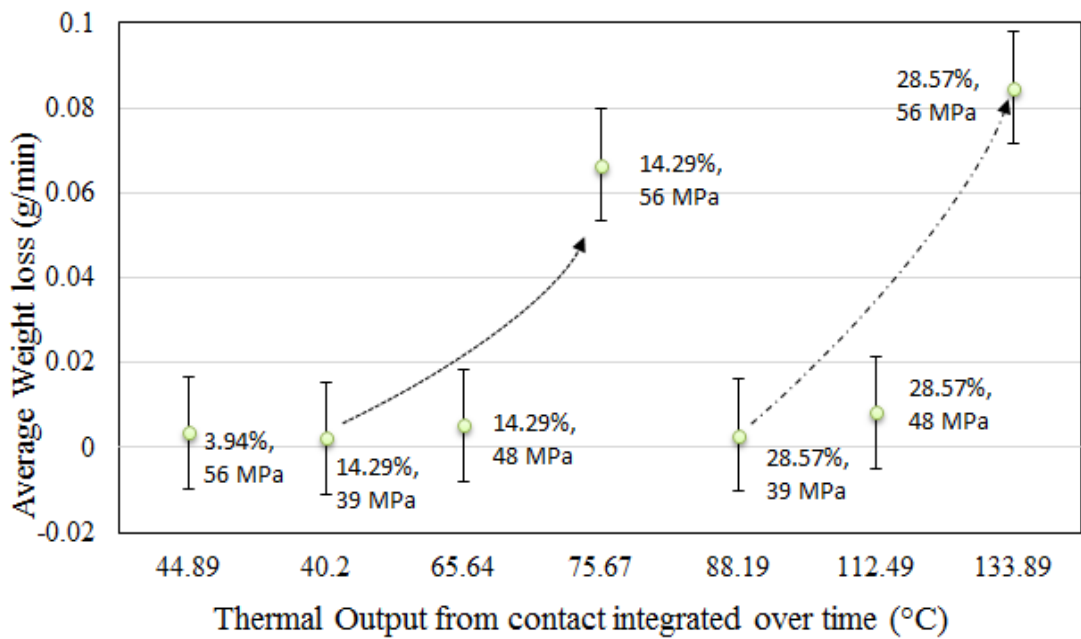


Figure 4.13: Average wear rate versus test severity for PEEK disc vs. steel disc twin disc tests.

It can be seen that the high slip-ratio, high contact pressures tests yielded most temperature increased and produced the highest wear rate and were thus considered to be the most severing. The low slip ratio and low contact pressures tests were the least severe and thus produced the lowest wear rate.

Overall, EOS PEEK HP3 vs. steel demonstrated significantly lower wear than other reported materials, with a lower surface temperature (for a 28.57% slip ratio and contact pressure 48 MPa the wear was approximately $2.8 \cdot 10^{-4}$ $\mu\text{m}/\text{cycle}$). Where EOS PEEK HP3 vs. EOS PEEK HP3 confirmed wear was approximately $4.7 \cdot 10^{-4}$ $\mu\text{m}/\text{cycle}$, (for a 28.57% slip ratio and contact pressure 48 MPa).

This is comparable to where PEEK and other maternal has shown considerable wear in other published results (for a 28.57% slip ratio and a 300N load contact pressure 48 MPa the wear was approximately 10^{-4} $\mu\text{m}/\text{cycle}$ [14]; for slip ratios above 11% Acetal discs were reported to have a wear rate 10^{-4} $\mu\text{m}/\text{cycle}$ [47], while Nylon 6-6, for slip ratio of 28% and a load of 200N showed wear rates exceeding 10^{-2} $\mu\text{m}/\text{cycle}$ [71].

Though the wear rates are high in the most severe tests, there was very little visible wear at lower temperatures.

The extreme harshness of the test was calculated as the average thermal output from the contact over time, allowing the wear rates to be put into numbers based on the operating conditions. It was found that the high contact pressure, high slip-ratio tests were the worst and so produced the greatest wear rate, temperature and friction increase. The low contact pressure and low slip-ratio tests produced the lowest wear rate and temperature increase and were considered to be the least extreme.

This can be correlated to the temperatures more than the Relative Thermal Index (RTI) of polymer for mechanical use with impact (180°C) [1, 70].

This is related to the interfacial wear in the thin region adjacent to the surface, where due to contact the energy from the friction component is dissipated.

4.7 Measured Temperature, Non-lubricated Tests

The temperature profile of the EOS PEEK HP3 disc when in contact with a second similar EOS PEEK HP3 disc under operating conditions of contact pressure 56 MPa and slip-ratio of 14.29 %, is shown in Figure 4.14, The maximum measured temperature attained at the meshing point was 319°C the time of this profile was taken 100 min after the start of the test.

Figure 4.15 shows the measured temperature variation at the end disc rotation profile, when the contact pressure is 56 MPa and the slip ratio is 14.29 %, the maximum generated temperature at the meshing point was (90.8°C).

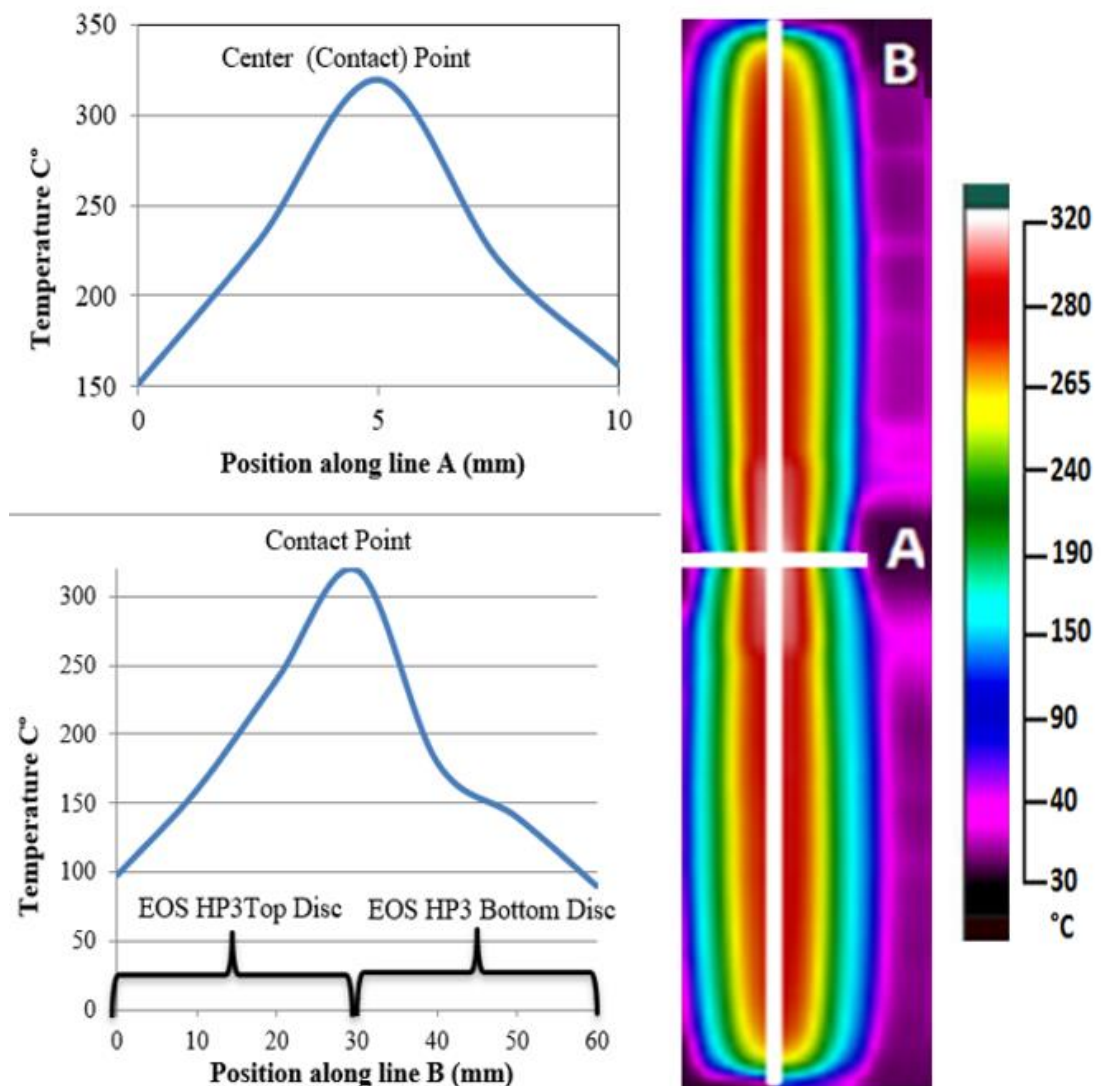


Figure 4.14: Infrared temperature profile for EOS PEEK HP3 disc vs. EOS PEEK HP3 disc, along lines A and B measured at the end of the test under the conditions of 14.29% slip-ratio and contact pressure 56 MPa.

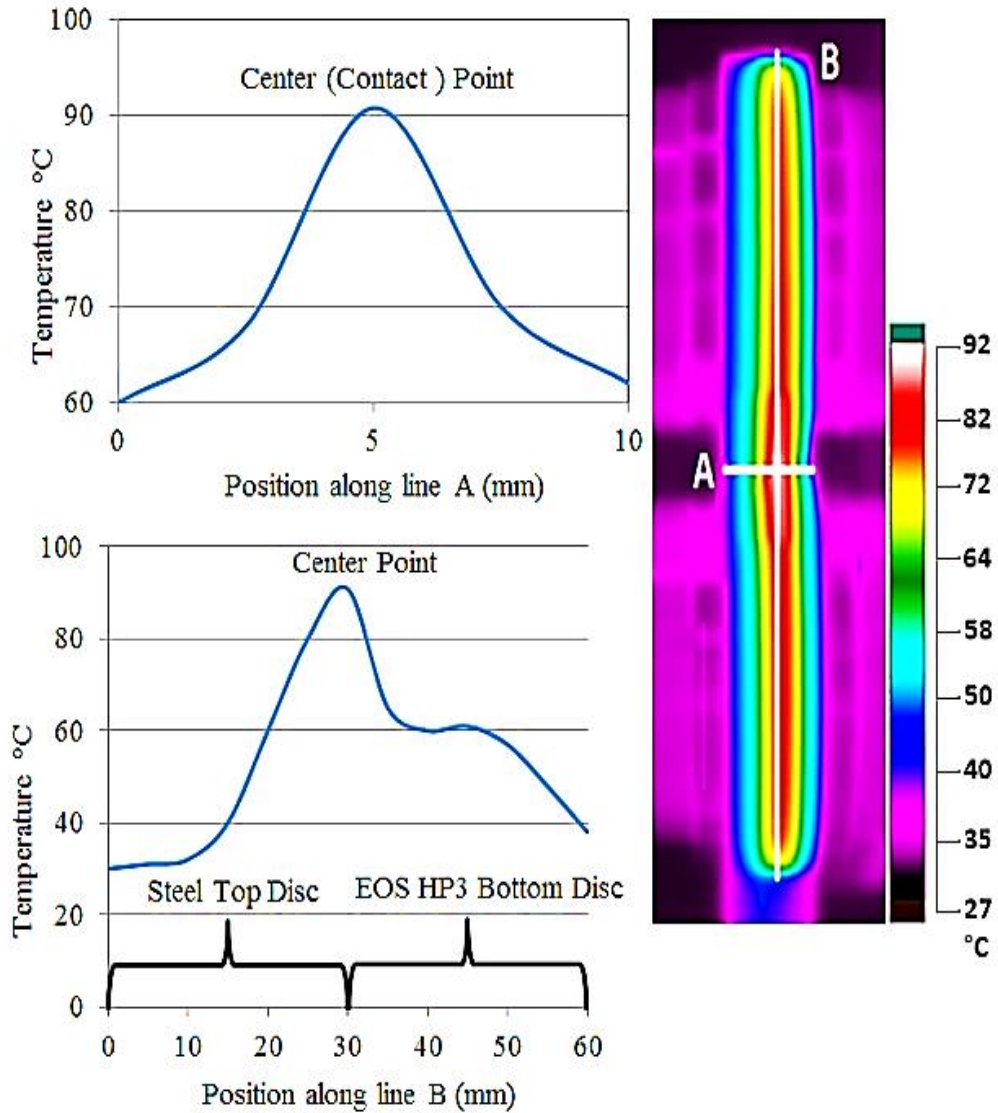


Figure 4.15: Infrared temperature profiles for EOS PEEK HP3 disc vs. steel disc along lines A and B measured at the end of the test under the conditions of 14.29% slip-ratio and contact pressure 56 MPa.

Line A (length 10 mm) presents the temperature variation from the centre line across the face of the disc to the outer edge. The temperature at any point is due to combined heat generation due to friction forces and heat transfer due to conduction, convection and radiation from the disc surface to the surroundings [79].

Line B (length 60 mm) shows the variation of temperature around the circumference in a direction parallel to the direction of rotation. The contact causes a flash increase in temperature (see Section 4.8), which is clearly a maximum at the point where the discs meet but will also depend on the heat loss from the disc to the surroundings as it rotates. With the temperature profiles of the EOS PEEK HP3 disc vs. steel disc, it was observed that the upper steel disc was cooler than the lower EOS PEEK HP3 disc despite the upper disc rotating at a higher speed.

4.8 Bulk Temperature

The mechanical behaviour of polymers is very much influenced by the properties of the surfaces that are interacting. This, in turn, means the polymer's properties will be a function of surface operating conditions.

Frictional heating is assumed to take place instantaneously as one surface slides over a specific point on the other; the consequent flash increase in temperature is assumed to dissipate rapidly. Thus the actual temperature at any point of contact between the surfaces is the sum of the material's bulk temperature and the flash temperature [29].

The maximum flash temperature (T_f) and interface temperature (T_i) for the tests for EOS PEEK HP3 disc vs. EOS PEEK HP3 disc (see Section 2.2.3), was calculated and the results presented in Table 4.3.

Table 4-3: Interfacial temperature (T_i) and associated flash temperature rise (T_f) for EOS PEEK HP3 vs. EOS PEEK HP3.

Contact Pressures MPa	Slip Ratios		
	3.9%	14.29%	28.57%
56	$T_f= 23^{\circ}\text{C}$, $T_i= 216^{\circ}\text{C}$	$T_f= 33^{\circ}\text{C}$, $T_i= 325^{\circ}\text{C}$	$T_f= 31^{\circ}\text{C}$, $T_i= 381^{\circ}\text{C}$
48	$T_f= 32^{\circ}\text{C}$, $T_i=144^{\circ}\text{C}$	$T_f= 26^{\circ}\text{C}$, $T_i= 284^{\circ}\text{C}$	$T_f= 25^{\circ}\text{C}$, $T_i= 293^{\circ}\text{C}$
39		$T_f= 29^{\circ}\text{C}$, $T_i= 173^{\circ}\text{C}$	$T_f= 32^{\circ}\text{C}$, $T_i= 187^{\circ}\text{C}$

Table 4.4 presents the interfacial temperatures (T_i) and associated flash temperature rises (T_f) for EOS PEEK HP3 disc vs. steel disc.

Table 4-4: Interfacial temperature (T_i) and associated flash temperature rise (T_f) for EOS PEEK HP3 vs. steel.

Contact pressures MPa	Slip Ratios		
	3.9%	14.29%	28.57%
56	$T_f = 24^\circ\text{C}, T_i = 64^\circ\text{C}$	$T_f = 24^\circ\text{C}, T_i = 91^\circ\text{C}$	$T_f = 21^\circ\text{C}, T_i = 184^\circ\text{C}$
48		$T_f = 23^\circ\text{C}, T_i = 80^\circ\text{C}$	$T_f = 27^\circ\text{C}, T_i = 120^\circ\text{C}$
39			$T_f = 23^\circ\text{C}, T_i = 70^\circ\text{C}$

Table 4.5 presents the interfacial temperatures (T_i) and associated flash temperature rises (T_f) for PEEK disc vs. steel disc.

Table 4-5: Interfacial temperature (T_i) and associated flash temperature rise (T_f) for PEEK disc vs. steel disc.

Contact pressures MPa	Slip Ratios		
	3.9%	14.29%	28.57%
56	$T_f = 24^\circ\text{C}, T_i = 74^\circ\text{C}$	$T_f = 23^\circ\text{C}, T_i = 121^\circ\text{C}$	$T_f = 23^\circ\text{C}, T_i = 224^\circ\text{C}$
48		$T_f = 25^\circ\text{C}, T_i = 135^\circ\text{C}$	$T_f = 26^\circ\text{C}, T_i = 143^\circ\text{C}$
39			$T_f = 25^\circ\text{C}, T_i = 98^\circ\text{C}$

The results for interfacial temperature (T_i) and associated flash temperature rise dT_{flash} are summarised in Figure 4.16, Figure 4.17, and Figure 4.18. Importantly, it can be seen that as slip-ratio and the contact pressure was increased, dT_{flash} was also increased. Temperature dominates all characteristics about the performance and design of elements of polymer machine; that has an effect on the failure modes found in components as gears, limiting the process to lower temperatures. On behalf of the tested PEEK discs. Heat is generated and dissipated through complex combinations of mechanisms:

1. Heat generation through hysteresis losses, viscoelastic deformations that are mainly converted into heat.
2. Frictional heating caused by the slip ratio applied to the test discs.
3. Heat conducted through drive shafts and discs.
4. Heat loss through ambient radiation and convection.

Koffi, et al., modelled aspects of heat generation for a polyamide 6/6 gear [106]. It was shown that frictional heating (energy dissipated by friction) was responsible for the largest proportion of the heat generated that raises the temperature of the discs [47, 50]. This was found to be generally the case except for pure rolling (i.e. at the pitch point of the gears, where sliding velocities are zero) and during tooth contact outside the line of action where tooth deformation is increased [27]. Hooke, et al., and Kukureka, et al., have confirmed by twin disc tests that this is the case for polyamide roll/slide [14, 50, 107].

The relationship between measured peak temperature and friction coefficient is plotted in Figure 4.16 for EOS PEEK HP3 disc vs. EOS PEEK HP3 disc for twin-disc tests under the specified conditions.

Figure 4.17: shows the maximum measured temperature and coefficient of friction for all test conditions for EOS PEEK HP3 disc vs. steel disc, and Figure 4.18 shows the maximum measured temperature and corresponding friction coefficient for all test conditions for PEEK disc vs. steel disc

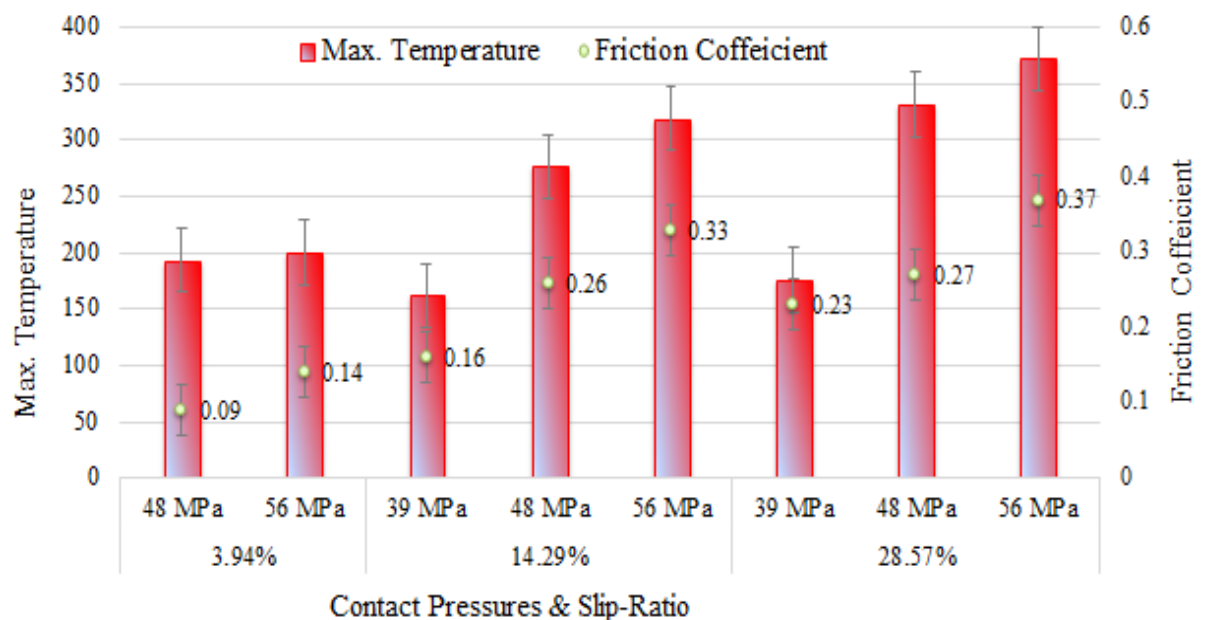


Figure 4.16: Maximum measured temperature and coefficient of friction for all test conditions: EOS PEEK HP3 disc vs. EOS PEEK HP3 disc.

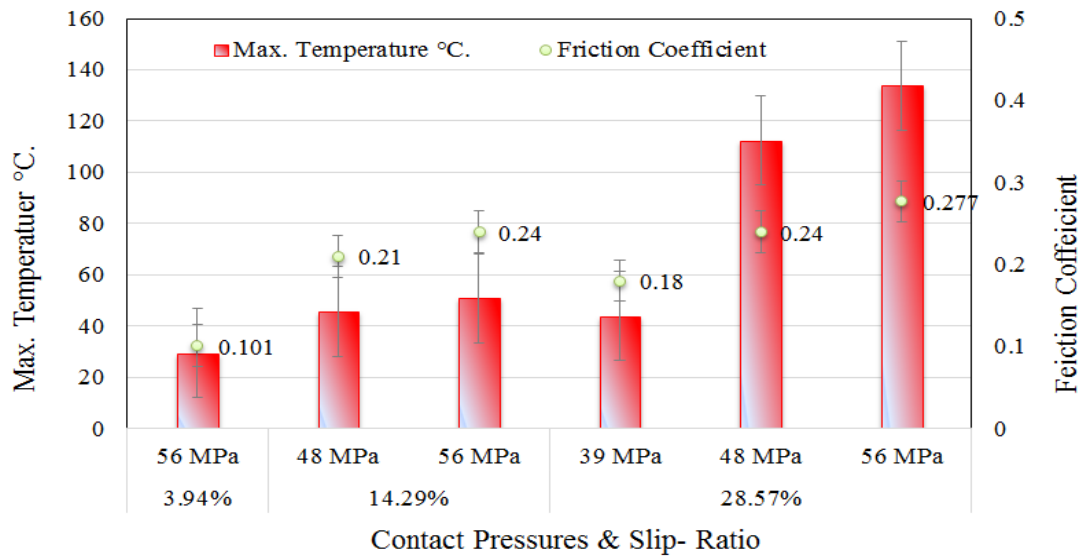


Figure 4.17: Maximum measured temperature and coefficient of friction for all test conditions: EOS PEEK HP3 disc vs. steel disc.

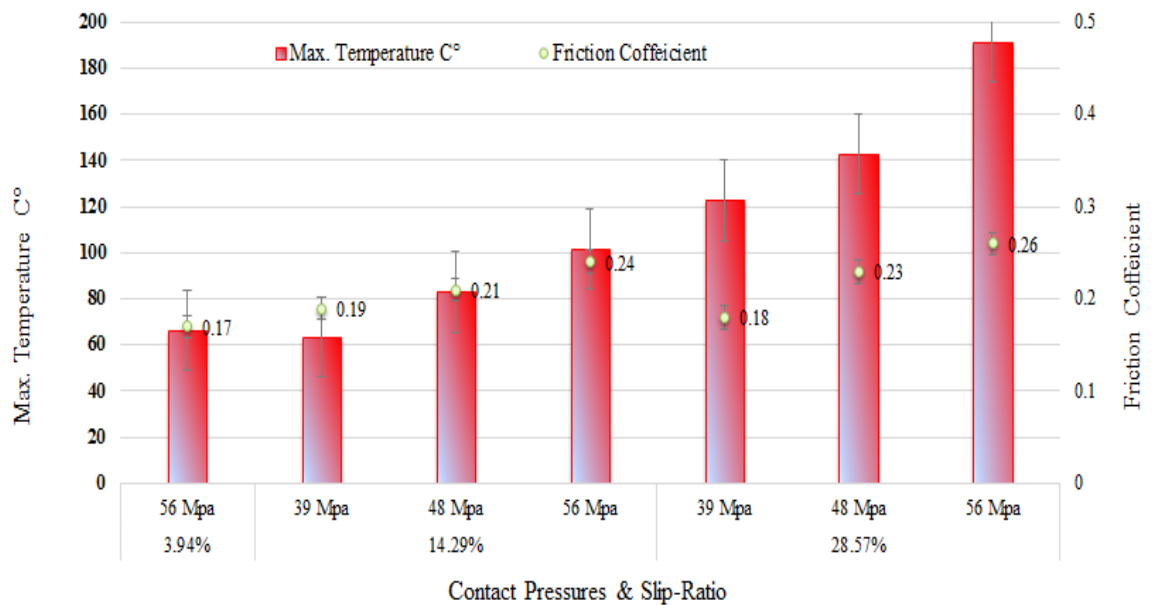


Figure 4.18: Maximum measured temperature vs. coefficient of friction for all test conditions: PEEK disc vs. steel disc.

The relationship between measured maximum temperature and friction coefficient was shown in three figures above for every twin-disc test. Energy dissipated by friction is the major source of heat that raised the temperature of the discs [47, 50].

It is accepted that frictional heating is the major contributing factor generating heat in the discs and a rapid increase in the friction coefficient can be observed as the temperature of the material increases to the value of the glass transition temperature. This took place in the first 5 or so mins of the test, see Figure 4.1, Figure 4.2 & Figure 4.3. The very clear effect of the transition temperature on wear and friction has been previously noted for polymer twin discs and fretting tests [14, 50, 108]. Subsequent to discolouration of the samples, the observed friction coefficient and wear rate significantly increased.

4.9 Crystallinity Measures

Crystallinity refers to the degree of structural order in a solid. In a crystal, the atoms or molecules are arranged in a regular, periodic manner. The degree of crystallinity has a significant influence on hardness, density, transparency and diffusion.

When the operation temperature is larger than the glass transition temperature of EOS PEEK HP3 (174.5°C) and at the same time is less than the principle crystalline melt transition (380°C) enthalpic relaxation will occur in polymer gears or discs. Therefore, crystallinity values were measured experimentally after the twin disc tests and found to be in the range of about 39-42%. For EOS PEEK HP3 vs. EOS PEEK HP3, the value was 36-39%, for the tests of EOS PEEK HP3 vs. steel and for the PEEK vs. steel tests its value was about 35-37%. In all tests the maximum generated temperature exceeded the glass transition temperature of the material. Crystallinity values measured on samples previously tested using the twin disc test are typically 3-8% higher than those obtained using untested samples. The results are presented in Table 4.6.

This point is similar to that made by Ostberg and Seferis [109] and it means that annealing above the glass transition temperature will have an effect on the crystallinity of PEEK [14, 109]. Additionally, high shearing friction forces due to the tests will also effect the molecular orientation of PEEK to produce additional enthalpic relaxation [110].

Table 4.6: Crystallinity results samples.

Slip ratios %	The contact pressures MPa	Crystallinity % for EOS PEEK HP3 vs EOS PEEK HP3	Crystallinity % for EOS PEEK HP3 vs steel	Crystallinity % for PEEK vs steel
3.9	56	39.54	37.50	35.46
14.29	48	41.14	38.16	35.78
14.29	56	41.87	39.11	37.75
28.59	39	40.09	36.33	37.10
28.59	48	41.69	37.14	37.45
28.59	56	42.64	38.05	37.83

In other words, enthalpic relaxation can be produced due to:

- 1- Increasing the maximum generated temperature above the glass transition temperature of the material.
- 2- High shear friction forces.

Because of the increased wear rate that occurred towards the end of the tests, much of the surface material was removed. Thus, the crystallinity values are a good way to present useful information related to this stage of the testing.

Assuming that it is significant to comprehend the effect of crystallinity on the wear mechanisms the discolouration of test samples was useful. When the crystallinity is changed as indicated by discolouration, or the severity at the point exceeds that required, the efficiency of the gear system could be improved by changing the slip ratio or loading to reduce the temperature at the point. The twin-disc test simulated position of the gear tooth relates with a specific contact condition.

It is important to understand the effect of crystallinity on the wear mechanisms one indication observed in the tests was discolouration of the test samples. When the crystallinity changes, or the severity at a point exceeds that permissible for the

continued efficient operation of a gear system, as seen by discolouration of the surface, then the slip ratio or loading should be reduced to lower the temperature at this point.

4.10 The Properties of Lubricated EOS PEEK HP3

Laser sintered EOS PEEK HP3 is known to have a porous surface due to the incomplete sintering of the powder [96], however, this can be minimized through careful parameter selection [111]. Surface porosity can have a significant influence on the surface lubricant retention and therefore on the friction and wear mechanisms observed.

Liquid lubricants are widely used to reduce the friction between, and wear of, mechanical components. Silicone oil was used here to investigate its effectiveness in the lubrication of polymers. Specifically, the aim was to assess the reduction in friction obtained by using silicone oil under minimum lubrication conditions (intend the silicone oil to flow into the pores).

Silicone oil lubricants can be easily recycled, and they are comprised of relatively non-hazardous chemicals [112, 113]. Also, silicone oil lubricants are well known for their thermally stable properties. They have a relatively high flash point temperature and a high auto-ignition point temperature [112, 113]. Friction experiments were performed using silicone oil as the lubricant for EOS PEEK HP3 and PEEK specimens.

To maximize the amount of lubricant stored in the pores, the samples were (immersed) submerged in silicone oil for one month, see Figure 4.19. The aim of immersing the samples in the silicone oil was to deposit a thin layer of lubricant on the surface and inside the preliminary layers of the specimen. The aim of immersing the samples in the silicone oil was to deposit a thin layer of lubricant on the surface and inside preliminary layers of the specimen (inside Organizational Structure) as (surface lubricated).

Preliminary tests showed that the amount of lubricant coating the specimen's surface and present inside the samples would vary with the porosity of the surface of the samples. By using this method, a thin layer of silicone oil lubricant was coated onto the surface and inside the preliminary layers of the EOS PEEK HP3 disc specimens around (0.0045- 0.0050 g).

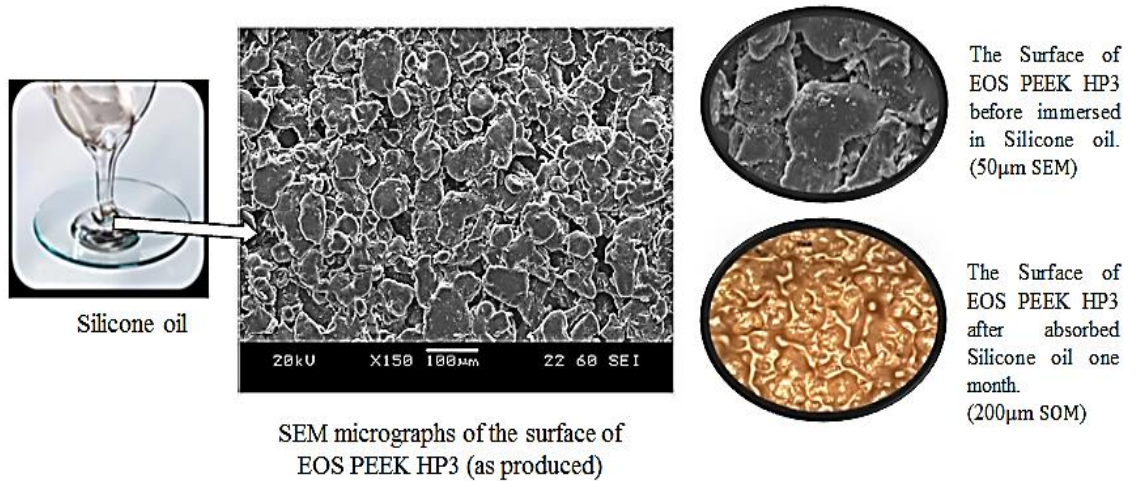


Figure 4.19: SEM micrographs of the surface of EOS PEEK HP3 (as produced). Where SEM is the Scanning Electron Microscope), and SOM is the Scanning Optical Microscope

The tribological characteristics of EOS PEEK HP3 was established lubricated samples have been tested by the twin disc rig at slip ratio 28.59%, and contact pressures (39 and 56) MPa; see Table 4.7.

Table 4.7: Test lubricated conditions for disc twin discs tests, calculated equivalent gear torques were 13.5 and 6.4 Nm.

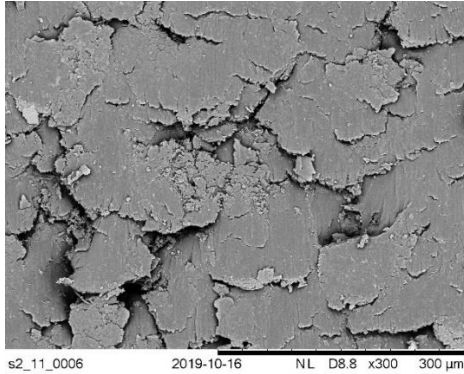
Max. Contact Pressure / MPa	Slip Ratio
	28.59%
56	√
39	√

To allow preferential friction coefficient stability of the EOS PEEK HP3 vs EOS PEEK HP3 sample and EOS PEEK HP3 vs steel, measurement of wear and temperature of the area contact was made over a two-hour period.

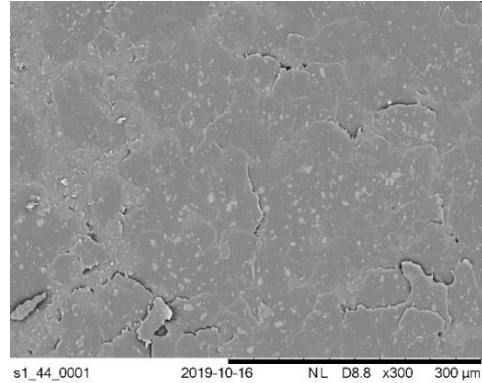
4.11 Wear Mechanisms and Topographical Analysis: Lubricated Tests

Figure 4.20 shows SEM micrographs of the surface EOS PEEK HP3 disc were rolled/ slid against an EOS PEEK HP3 disc, and then EOS PEEK HP3 and PEEK discs were rolled/ slid against a steel disc in the friction tests.

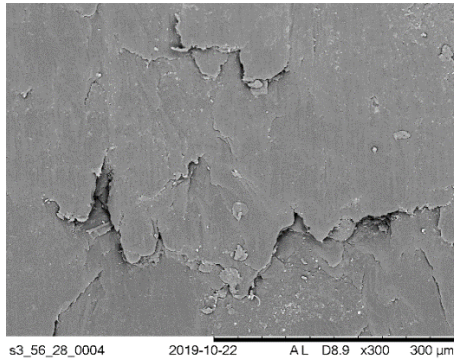
Un-Lubricated



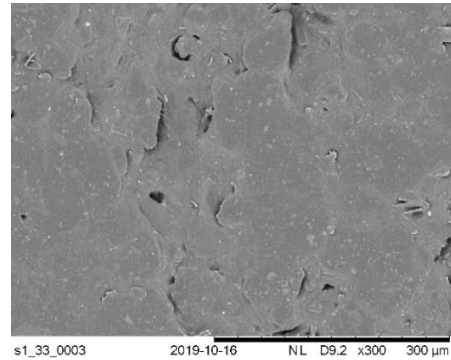
Lubricated



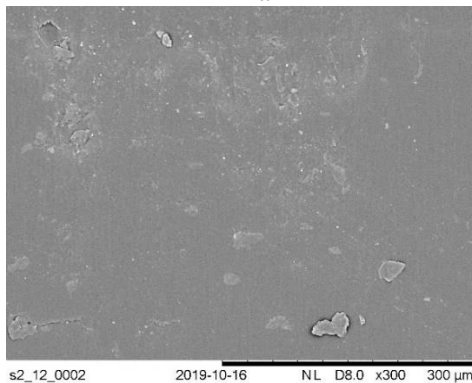
EOS PEEK HP3 vs EOS PEEK HP3 - 28.59% -56 MPa



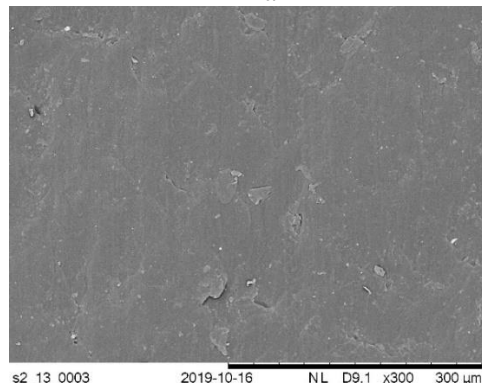
EOS PEEK HP3 vs EOS PEEK HP3 - 28.59% -56 MPa



EOS PEEK HP3 vs Steel - 28.59% -56 MPa



EOS PEEK HP3 vs Steel - 28.59% -56 MPa



PEEK vs Steel - 28.59% -56 MPa

PEEK vs Steel - 28.59% -56 MPa

Figure 4.20: SEM micrographs of the surface of EOS PEEK HP3.

The results of the wear experiments showed that a minimum amount silicone oil lubricant was very effective in reducing the wear of the EOS PEEK HP3 and PEEK samples as shown in Table 4.8. It was noted that the greater the contact pressure the greater, proportionally, the reduction in wear in the presence of lubrication.

Table 4.8: Wear under non-lubricated and lubricated conditions, slip ratio 28.59%.

Materials	Lubricated		Non-lubricated	
	Wear/g		Wear/g	
	39 MPa	56 MPa	39 MPa	56 MPa
EOS PEEK HP3 vs EOS PEEK HP3	0.0018	0.0052	0.0063	0.1414
EOS PEEK HP3 vs Steel	0.0011	0.0069	0.0039	0.0102
PEEK vs Steel	0.0015	0.0192	0.0033	0.0847

Figure 4.21 shows the result of energy dispersive spectroscopy (EDS) spectrum of the EOS PEEK HP3 disc surface which characterise the silicone oil observed on the surface of the EOS PEEK HP3 disc. From EDS, major amounts of silicone oil was observed as Figure 4.22A. where Figure 4.22B showed mixed map: Silicon Ka1 (red), Iron Ka1 (green).

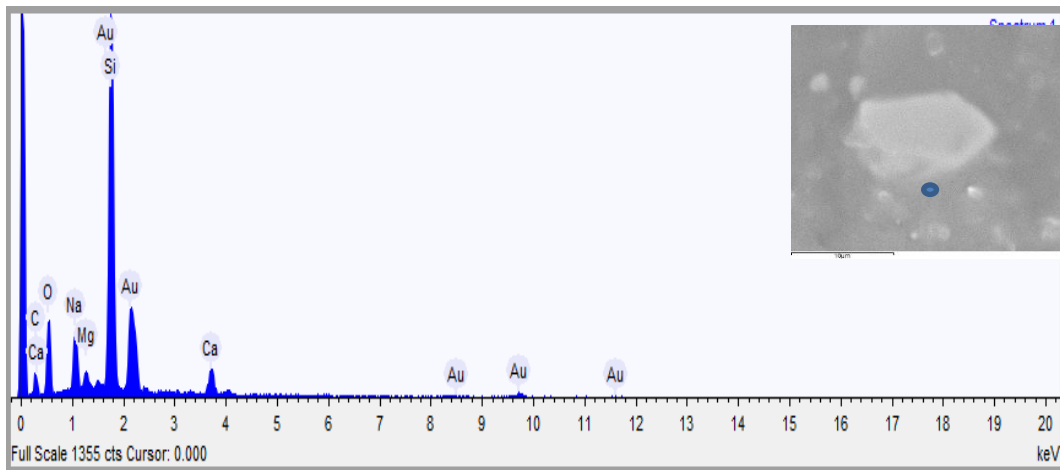


Figure 4.21: Measured EDS spectrum on the surface of the disc EOS PEEK HP3

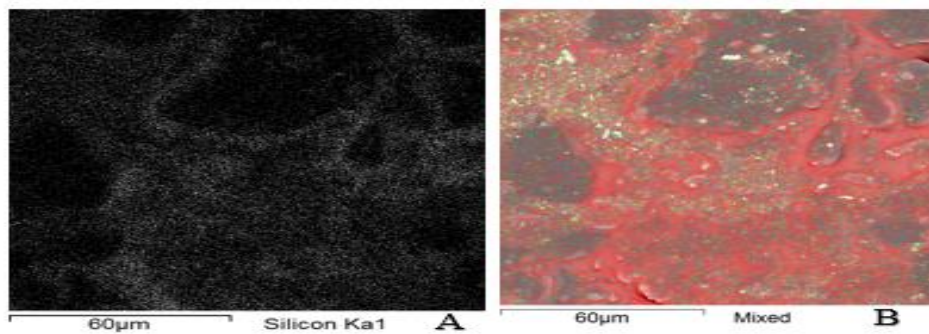


Figure 4.22: shows the location of silicone oil on the surface of the disc EOS PEEK HP3
Mixed map: Silicon (red), Iron (green) by EDS,

Table 4.10 shows amounts (weight %) of silicone oil, measured using EDS spectrum (the 13 points random) on the EOS PEEK HP3 disc surface, the silicone oil observed on the disc surface. This amount (weight %) of silicone oil was significant reduced the wear and friction coefficient at higher sliding rolling speed and contact pressure on the surface contact of the EOS PEEK HP3.

Table 4.10: Wear under non-lubricated and lubricated conditions, slip ratio 28.59%. (All spectra (displaying weight %))

Name	C	O	Na	Mg	Al	Si	Ca
Spectrum 1	24.175	31.785	6.505	1.447		31.469	4.619
Spectrum 2	30.571	19.895	4.832	1.475		36.520	6.708
Spectrum 3	31.265	22.400	3.955	1.442		34.123	6.817
Spectrum 4	29.754	22.800	5.346	2.008		34.625	5.466
Spectrum 5	22.843	32.382	6.520	1.924	0.472	31.103	4.755
Spectrum 6	27.157	26.511	5.830	1.598	0.665	33.115	5.123
Spectrum 7	70.525	18.267	1.135			10.072	
Spectrum 8	62.800	22.605				14.595	
Spectrum 9	64.665	23.405				11.930	
Spectrum 10	52.190	23.664				24.146	
Spectrum 11	55.065	22.602				22.333	
Spectrum 12	62.338	25.733				11.929	
Spectrum 13	61.781	24.210				14.008	

4.12 Friction Coefficient Properties for EOS PEEK HP3: Lubricated

Conditions

Figure 4.23 presents results for the frictional coefficient for EOS PEEK HP3 discs running against an EOS PEEK HP3 disc under lubricated and non-lubricated conditions, with contact pressures of 56 and 39 MPa, and slip ratio of 28.57%.

Figure 4.24 presents the results for the frictional coefficient for EOS PEEK HP3 discs running against steel in lubricated and non-lubricated tests, with contact pressure 56 and 39 MPa, and slip ratio 28.57%. It can be seen that the friction coefficient for the lubricated condition was more stable and of lower value than that for the non-lubricated condition. This confirms the possible benefits of using a minimum level of lubrication for friction coefficient reduction of EOS PEEK HP3.

Figure 4.25 shows the measured frictional coefficient for PEEK discs running against steel, lubricated and non-lubricated tests, when contact pressure was 56 and 39 MPa, and slip ratio 28.57%.

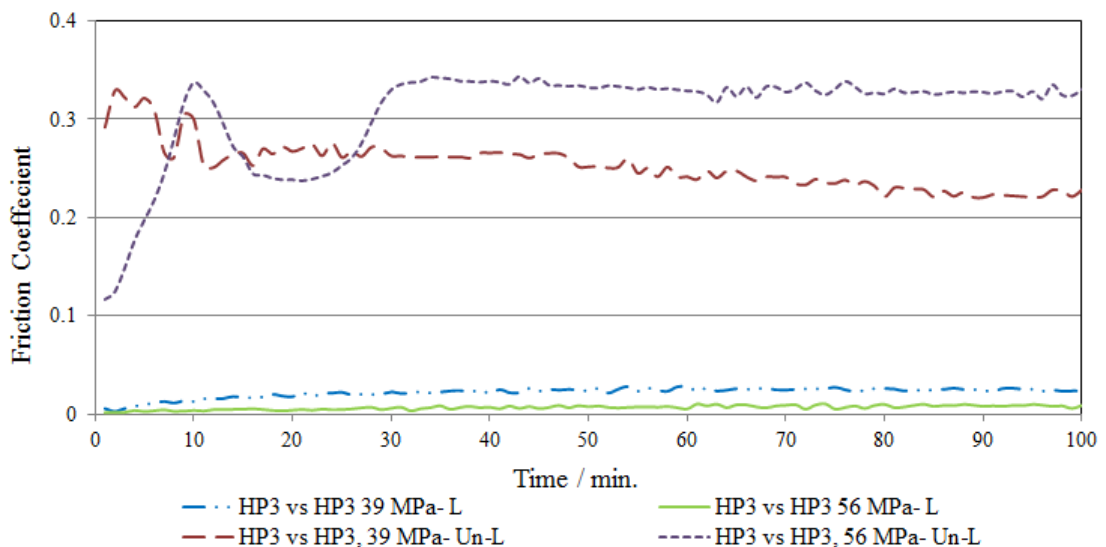


Figure 4.23: Frictional coefficient for EOS PEEK HP3 vs. EOS PEEK HP3, for contact pressures 56 and 39 MPa, with slip ratio 28.57% for lubricated (L) and non-lubricated conditions (Un-L).

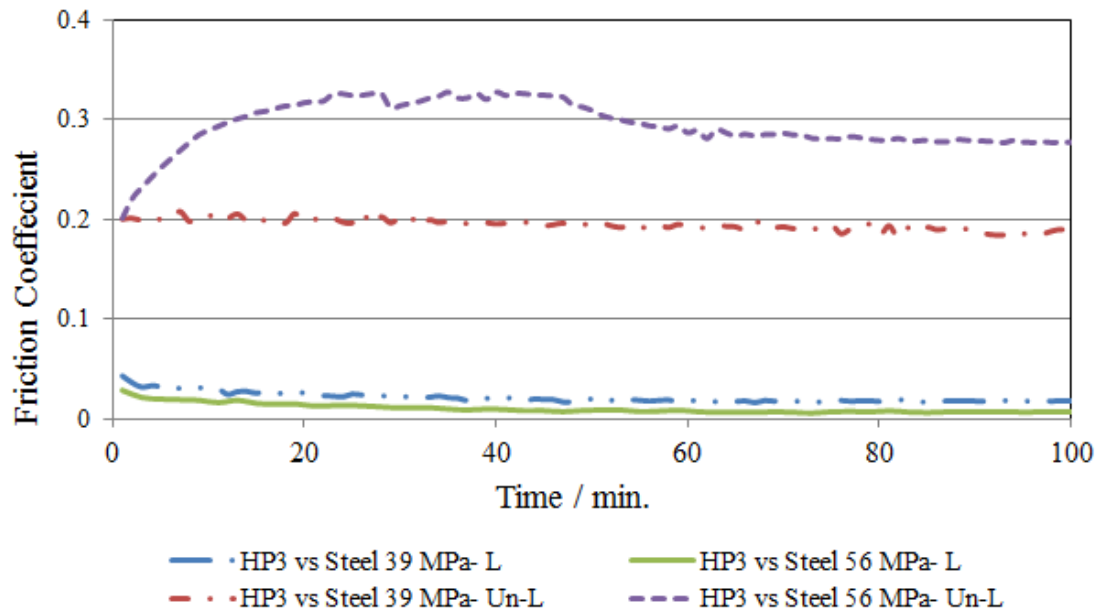


Figure 4.24: Frictional coefficient for EOS PEEK HP3 vs. steel, with contact pressures 56 and 39 MPa, and slip ratio 28.57%, lubricated (L) and non-lubricated (Un-L) conditions.

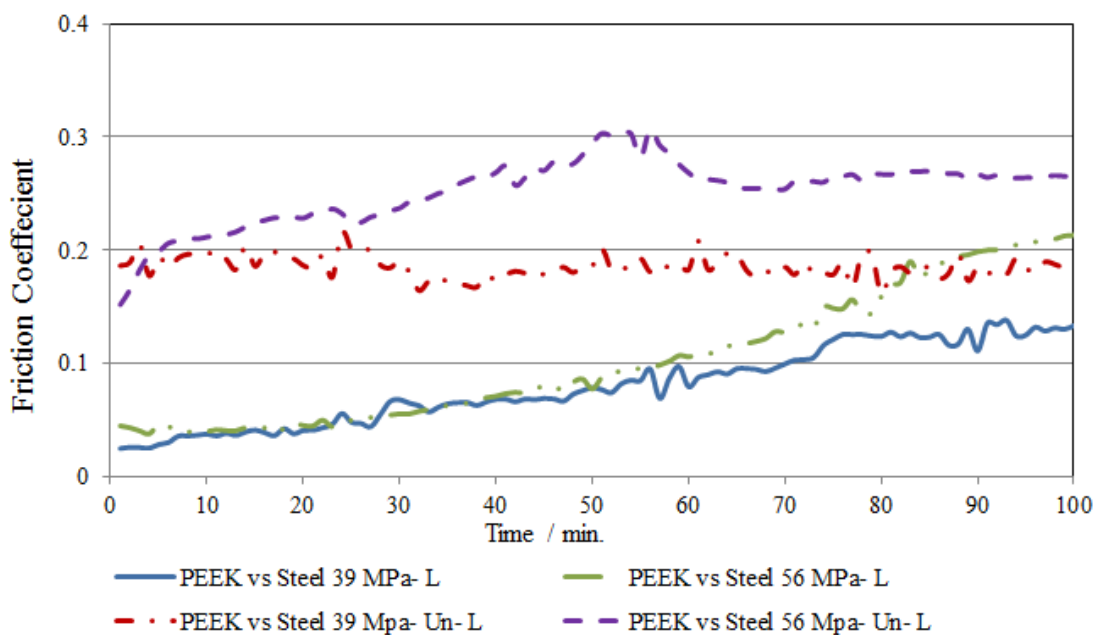


Figure 4.25: Frictional coefficient for PEEK vs. steel, with contact pressures 56 and 39 MPa, and slip ratio 28.57%, lubricated (L) and non-lubricated (Un-L) conditions.

From Figure 4.23, Figure 4.24 & Figure 4.25 above, we see that the coefficient of friction was consistently much lower for EOS PEEK HP3 when lubricated (approximately 50% apart from Figure 4.25). In addition the significant variations in the friction coefficient that occurred in the non-lubricated case during bedding-in have been eliminated. The

presence of the lubrication is particularly effective in reducing the friction coefficient at the higher pressure (56 MPa).

However, for PEEK vs steel, the friction coefficient starts much lower in the lubricated case but increased steadily until at the end of the test (100 min.) it was approaching the values obtained in the non-lubricated tests. This behaviour is likely to be due to the PEEK being injection moulded and not having the porosity of EOS PEEK HP3.

Due to the reduced adhesion the friction coefficient was reduced, and the lubricant film acted to support the load, reducing the material contact stresses. The effectiveness of the lubricant in reducing the coefficient of friction under high load is explained thus: the increase in contact pressure results in an increase in lubricant viscosity which will greatly enhance the ability of the lubricant to support the load without being compressed out of the contact area.

It was observed that the friction coefficient reaches steady state for lubricated test after an initial period (but not for PEEK). Where it could be analysed the tribological properties and determine the component usable life, when the tested approach to steady state conditions. The friction coefficient was reduced with higher contact pressure.

Table 4.11, shows friction coefficient and temperatures for the results of all materials (EOS PEEK HP3 vs EOS PEEK HP3, EOS PEEK HP3 vs steel and PEEK vs steel) under un-lubricated and lubricated conditions.

Table 4.11: Measured friction coefficients for both non-lubricated and lubricated conditions.

Materials	Lubricated		Non-lubricated		Reduction in Friction Coefficient	
	Friction Coefficient		Friction Coefficient			
	39 MPa	56 MPa	39 MPa	56 MPa	39 MPa	56 MPa
EOS PEEK HP3 vs EOS PEEK HP3	0.0175	0.0068	0.0612	0.3734	71 %	97 %
EOS PEEK HP3 vs Steel	0.0237	0.0075	0.1864	0.2447	87%	97%
PEEK vs Steel	0.1333	0.213	0.1927	0.2788	30%	23 %

4.13 Measured contact temperature

The thermal imager was used to measure the maximum contact temperature for the different materials tested under 28.57% slip ratio and contact pressures 39 and 56 MPa. It was assumed that the maximum temperature measured at a particular time was the contact temperature of the two discs, and was indicated as the color white A.

Table 4.12 shows the measured contact temperatures for EOS PEEK HP3 discs running against EOS PEEK HP3, and steel, and PEEK running against steel, for contact pressures 56 and 39MPa and slip ratio 28.57% for both lubricated and non-lubricated conditions. We see a substantial decrease in contact temperature whenever lubrication is used.

Table 4.12: Contact temperatures under lubricated and non-lubricated conditions

Materials	Lubricated		Non-lubricated		Reduction in Contact Temperature	
	Temperature C°		Temperature C°			
	39 MPa	56 MPa	39 MPa	56 MPa	39 MPa	56 MPa
EOS PEEK HP3 vs EOS PEEK HP3	83.3	189.6	176	372	52%	49%
EOS PEEK HP3 vs Steel	48.9	64.6	76.8	191	36%	32%
PEEK vs Steel	123.8	175	166.5	199	25%	8%

4.14 Conclusions

The wear mechanisms of EOS PEEK HP3 have been studied using a twin disc rig with a range of the contact pressures and slip-ratios, in non-conformal, lubricated and non-lubricated rolling-sliding contact. The use of EOS PEEK HP3 disc vs EOS PEEK HP3 disc, EOS PEEK HP3 disc vs steel disc and PEEK disc vs steel disc has been tested under both low and high contact pressures. It was shown that high temperature operation was possible despite some increase in wear, friction and surface temperature as the slip-ratio and the contact pressures increased.

Generally, the wear rates of EOS PEEK HP3 are significantly lower than those of PEEK when measured using the twin-disc configuration. Here the failure mechanisms of EOS PEEK HP3 were observed on the surfaces of contact, involved contact fatigue failures and surface melting, especially higher slip-ratios, and high contact pressures.

In lubricated contact, it was found that the friction coefficient of the lubricated surface was more stable and lower than that of the non-lubricated condition. The results of this work demonstrate the possibility of lubrication for reduction of the friction coefficient of EOS PEEK HP3.

The results of the wear experiments showed that the minimum silicone oil lubricant was effective in reducing the wear and the temperatures areas contact of EOS PEEK HP3 samples. The minimum silicone oil lubricant implies lower oil levels so less cost and it will be reducing the weight.

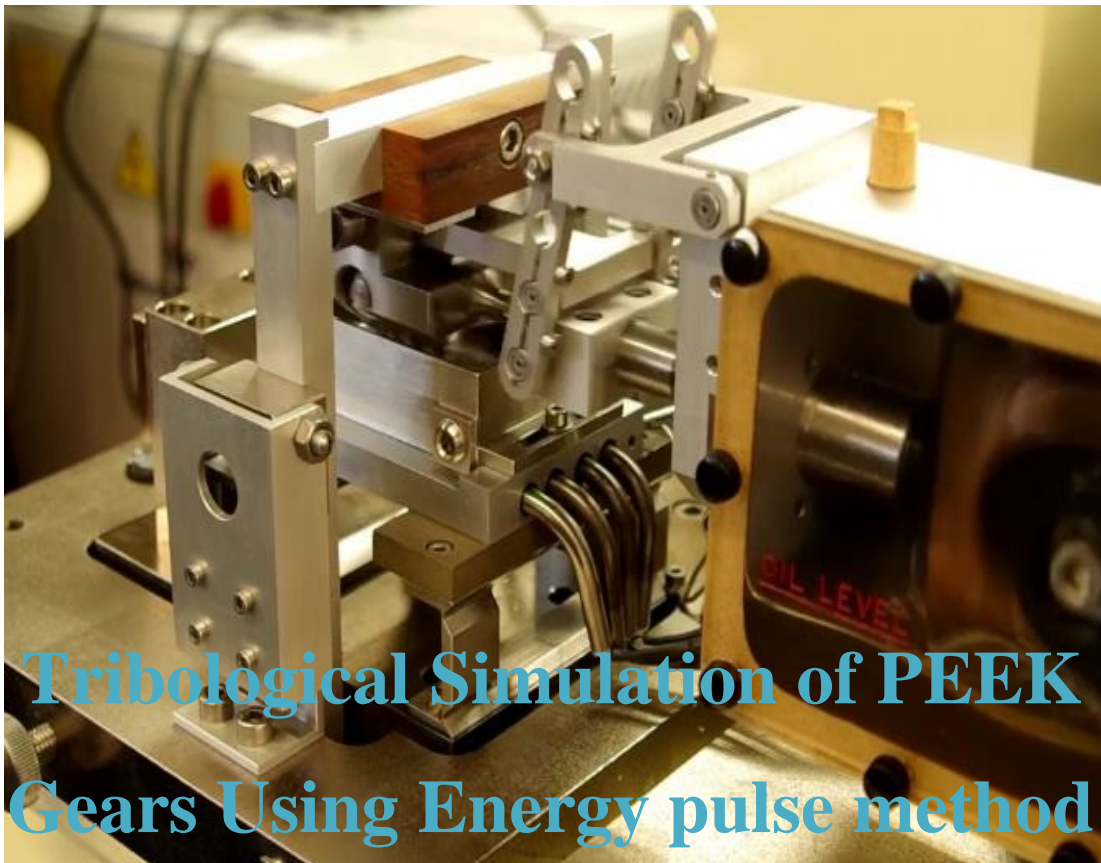
These results can be used to aid the design of high contact polymeric gear systems making them more effective. The results show that the generated contact surface temperature between gear tooth surfaces can be reduced by reducing the contact pressures, slip-ratios and adding lubrication, with an associated effect around the pitch-point and in the contact region of a gear pair.

This opens the possibility of optimizing the tooth geometry of polymeric gears in such a way as to reduce slip-ratio away from the pitch point. Such a development has the potential to increase service life of the gear, also decrease the amount of wear as demonstrated in the tests with high slip-ratios.

The thin layer of the silicone oil that was stored in the pores inside the preliminary layers and the surface specimen; it was worked as a good lubricant.

Chapter Five

5



5

“All ideas in science were born in the dramatic conflict between reality and our attempt to understand it”.

Albert Einstein, scientist (1879-1955)

Tribological Simulation of PEEK Gears Using Energy pulse method

A High Frequency Friction Machine (TE 77) fitted with an energy pulse (EP) adaptor has been used to simulate polymer gears, and in particular the rolling–sliding type of movement and wear behaviour of

1. Poly-Ether-Ether-Ketone (PEEK) plate running against AISI 52100 STEEL discs.
2. PMC (Victrex, 450CA30) plate against AISI 52100 STEEL discs.
3. Selective Laser Sintering (EOS PEEK HP3) plate running against AISI 52100 STEEL discs, and
4. Poly-Ether-Ether-Ketone (PEEK) plate running against PEEK discs.

The TE 77 Energy Pulse (EP) Slide/Roll Adapter (EP-Gear slide/roll adaptor) was used to perform tests with high slide/roll ratios (25%, 43% and 83%) and under a variety of lubrication conditions including silicone, base oil and water.

This chapter describes the minimum film thickness of the lubricant (silicone, base oil and water) was calculated theoretically. Also, investigated series of experiments conducted to assess a range of slide/roll conditions beyond the traditional limitations found in twin-disc testing, and so replicating a wider range of kinematic conditions found typically in machine elements. Tests were conducted with a range of lubricants and slide/roll ratios.

5.1 Materials & Methods

Unfilled PEEK 450G was used in this study, filled PEEK 450G with carbon fibre 30% (MPCs) in addition to EOS PEEK HP3. This grade of PEEK possesses several key properties that make it desirable for use in high-performance machine elements. These include maintaining mechanical properties at high temperatures, an inherent resistant to stress and thermal degradation, high corrosion resistance and a high relative thermal index for mechanical contact [87].

The slide ratio tests were conducted under externally lubricated conditions where 15 ml of the following lubricants were added to the specimen bath, encasing the test specimens on the main test rig:

1. Deionised water with a dynamic viscosity of 0.89 mPa.s at 25°C
2. Silicone oil (WACKER® AK 100) with a dynamic viscosity of 1000 mPa.s at 25°C
3. SN100 base oil with a dynamic viscosity of 95 mPa.s at 25°C

The lubricants represent a wide range of viscosities. The motivation to use water as a lubricant was determined by environmental and economic reasons [114, 115]. Silicone oil was selected as it has been shown to be resistant to chemical and heat oxidation over a wider temperature range compared to hydrocarbon-based lubricants, as a reference [116, 117] and SN100 base oil was selected as the control.

5.2 Tribological tests

The TE 77 with EP - Gear Slide/roll adaptor fitted, when configured in this manner, the upper specimen disc rotates under load against a lower specimen plate. The load is varied by adding mass to, or removing mass from, the load bridge. Additionally, a sinusoidal rocking motion can be induced by a link age mechanism. The full experimental parameters used in the experiments are given in Table 5.1.

Table 5.1 Experimental parameters used during the tribological testing.

Parameter	
Contact pressure	39 MPa
Stroke	10 mm
Reciprocation frequency	2 Hz
Temperature	22±20 °C
Test duration	2 Hours

5.3 Theoretical Estimation of Film Thickness for The EP Kinematic Conditions

From Figure 5.1 shows the film thicknesses are dependent on the rolling velocity (entrainment speed) that was dependant on the slip ratio [23]. Figure 5.1 shows the theoretically determined film thickness generated under the slide/ roll ratio 83%, Figure 5.2 displays the film thickness under the slide/ roll ratio 43%, and Figure 5.3 illustrations the film thickness created under the slide/ roll ratio 25%, for the three lubricants. Those figures offer an indication of the effect of slide/ roll ratio on generated lubricant film thicknesses for different types of lubrication by the TE77 EP/Gear adaptor during a single reciprocating stroke. The experimental conditions have been selected to simulate a PEEK/steel gear contact of the Birmingham standard benchmark geometry as defined in [27] transmitting a torque of (7 - 6.4)Nm and 39 MPa contact pressure. As the slide/ roll ratio was increased so the film thicknesses and the entrainment velocities decreased.

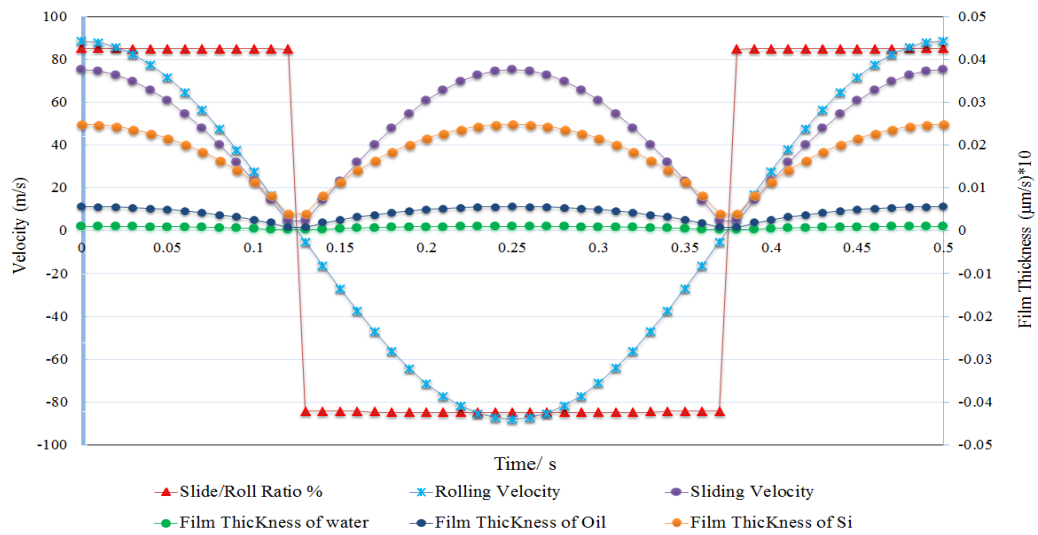


Figure 5.1: showing the film thicknesses for the three lubricants tested for the slide/roll ratio 83% using the TE77 EP/Gear adaptor during a single reciprocating stroke 10mm, 2 Hz.

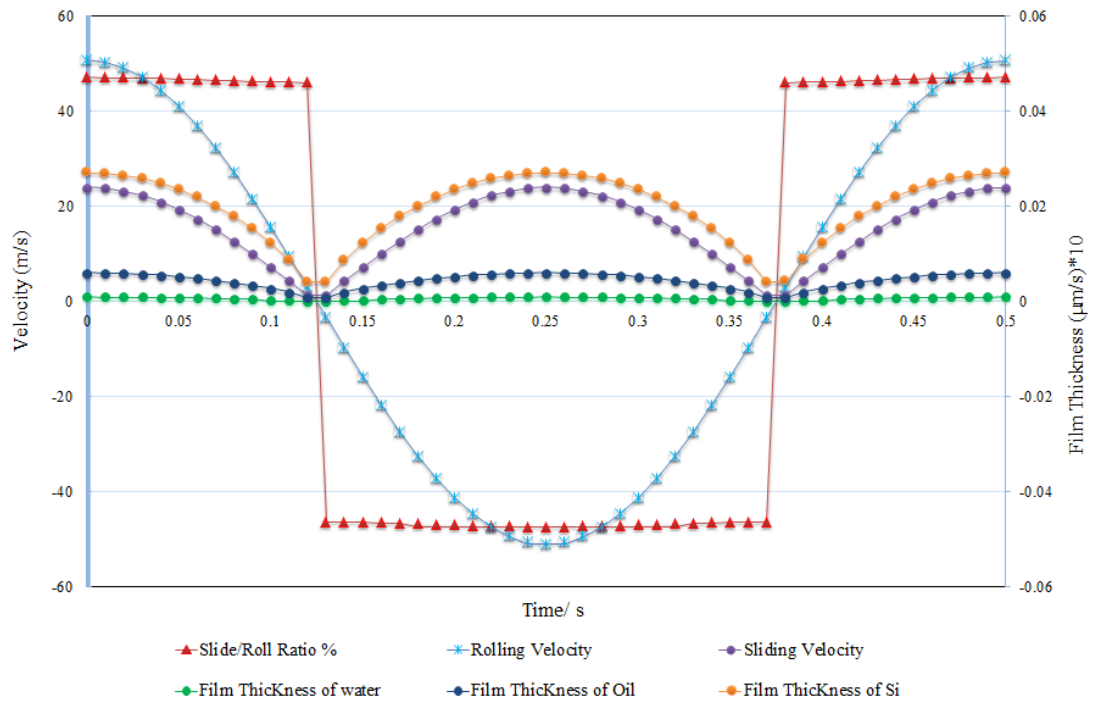


Figure 5.2: showing the film thicknesses for the three lubricants tested for the slide/roll ratio 43%, using the TE77 EP/Gear adaptor during a single reciprocating stroke 10mm, 2 Hz.

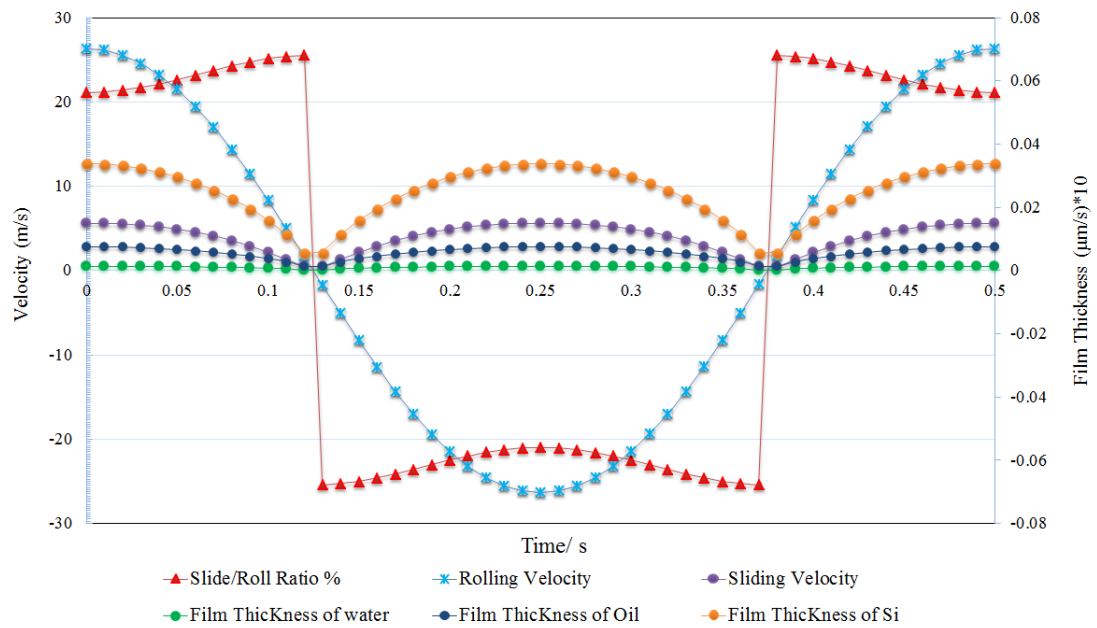


Figure 5.3: showing the film thicknesses for the three lubricants tested for the slide/roll ratio 25%, using the TE77 EP/Gear adaptor during a single reciprocating stroke 10mm, 2 Hz.

5.3.1 Effect of the Slide/ Roll Ratios on the Film Thickness for the EP Kinematic Conditions

Figure 5.4 displays effect the slide/roll ratios on the film thickness for oil lubricants tested using the TE77 EP/Gear adaptor during a single reciprocating stroke 10mm, and 2 Hz. At sliding rolling contact the EP Kinematic Conditions the calculated film thickness value reduced at high slip slide/roll ratio, similar behaviour were found in [24, 25].

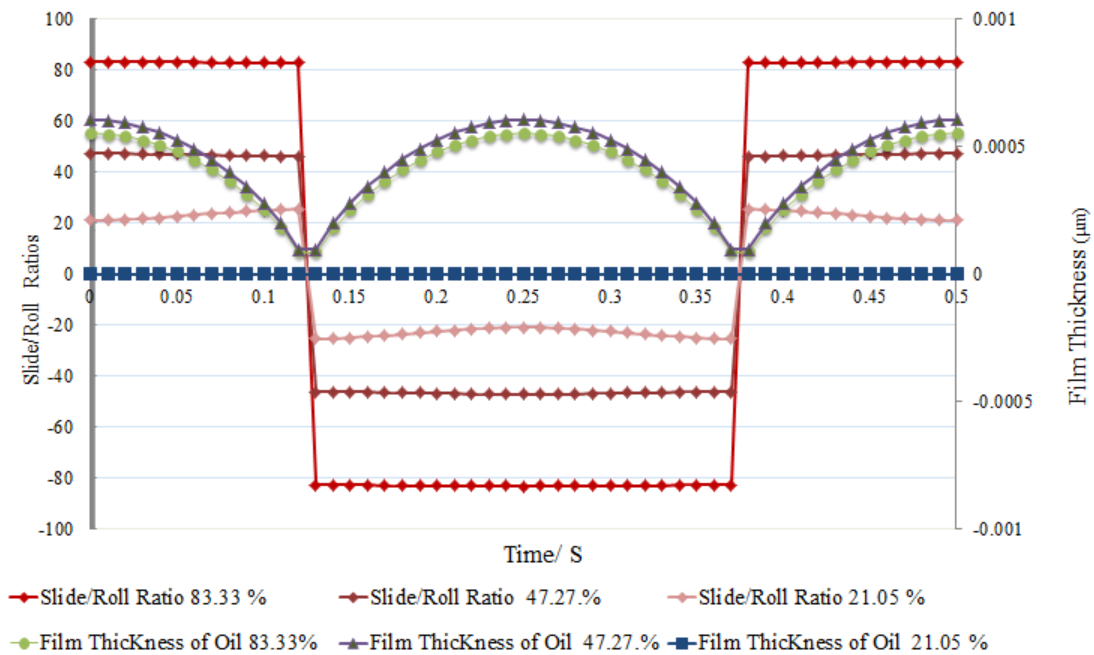


Figure 5.4: showing the film thicknesses for the three slide/roll ratios for oil lubricants tested using the TE77 EP/Gear adaptor during a single reciprocating stroke 10mm, and 2 Hz.

5.3.2 Effect of the Frequency on the Film Thickness for the EP Kinematic Conditions

The pioneering work of Hamrock and Dowson [21] and Dowson [22] and Dearn [19] contributed to tribological literature and the design of rules for machine elements have been shown on the EHL contact problem.

Building on their results other solvers have emerged, currently in this paragraph calculating the phenomena of film thicknesses with different frequencies combinations for oil lubricants with the slide/ roll ratio 83.8% by using the TE77 EP/Gear adaptor during a single reciprocating stroke 10 mm in Figure 5.5.

The size of the loops film thicknesses grew with increasing test frequency, it was the same behaviour shown in [19, 24].

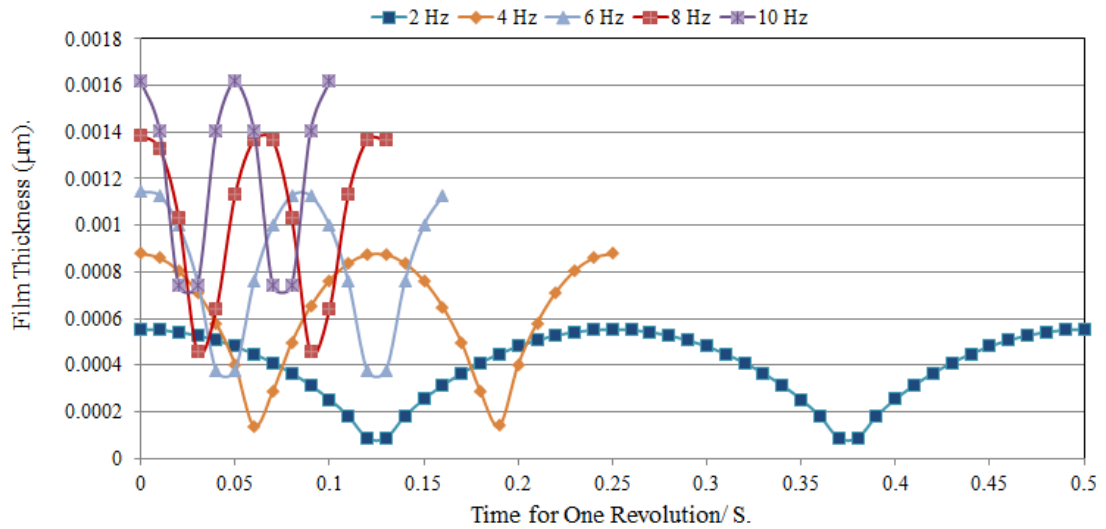


Figure 5.5: showing effect the different frequency on the film thicknesses oil lubricants for the slide/ roll ratio 83.8% by using the TE77 EP/Gear adaptor during a single reciprocating stroke 10 mm.

5.3.3 Effect of the Loads on the Film Thickness for the EP Kinematic Conditions

Figure 5.6 displays the load effect on film thicknesses where the film thickness with load decreases as predicted. Remember that the curves are shown for all film thickness estimates, assuming optimal load sharing [19, 24].

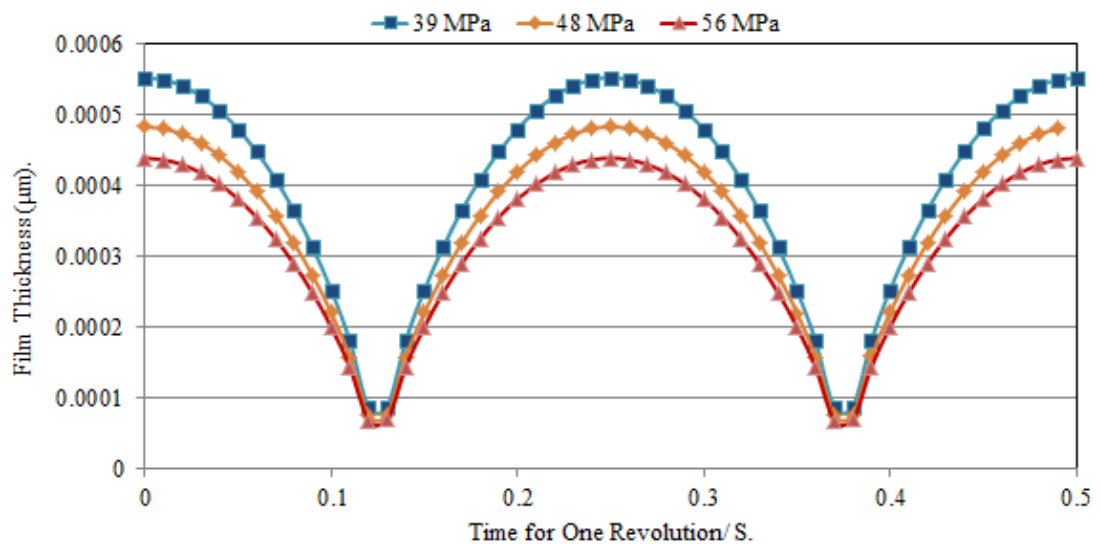


Figure 5.6: showing effect the contact pressures on the film thicknesses oil lubricants for the slide/ roll ratio 83.8% by using the TE77 EP/Gear adaptor during a single reciprocating stroke 10 mm, 2Hz.

5.3.4 Effect of Stroke Length on the Film Thickness for the EP Kinematic Conditions.

Figure 5.7 displays the effect of the slide/roll ratios on the film thickness for oil lubricants polymer/steel tested using the TE77 EP/Gear adaptor during a single reciprocating cycle for contact pressure 39 Nm, and 2Hz. At sliding rolling contact the EP Kinematic Conditions the film thickness value was increased with increase length of strokes and it was reduced at low slip slide/roll ratio, similar behaviour was found in [24].

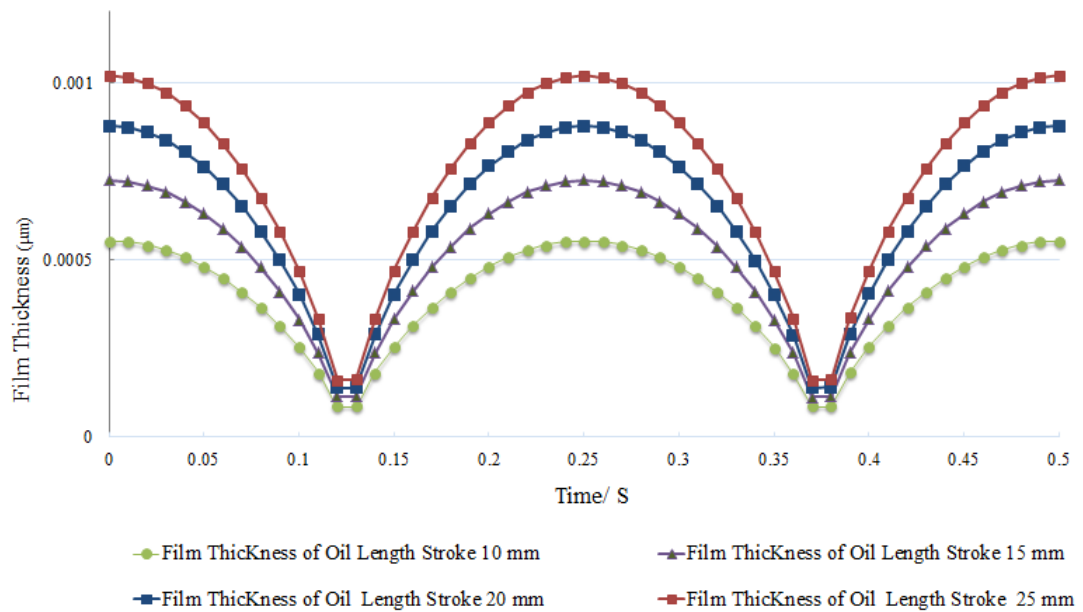


Figure 5.7: showing effect the load on the film thicknesses oil lubricants for the slid/ roll ratio 83.8% by using the TE77 EP/Gear adaptor during a single reciprocating for contact pressure 39 Nm, and 2Hz.

5.4 Tribological Properties of Polymer vs. Steel Simulation of lubricated Gear.

This section will investigate the rolling–sliding wear behaviour of PEEK 450G disc running against steel, and the use of this as a simplified method of analysing the dynamic response of high-performance polymeric gear teeth.

5.4.1 Frictional Results of PEEK lubricated.

Figure 5.8 shows the friction coefficients measured during the PEEK-on-steel tests for the three slide/roll ratios and each of the lubricants. The friction coefficient in the water lubricated tests at a slide/roll ratio of 83.3% was by far the highest of those measured and did not reach the pre-defined steady-state conditions within the test time. The friction trace for these parameters developed rapidly for the first 1500 seconds after which it increased more slowly until the end of the test at 7000 seconds. For all of the friction results, the general trend was that the friction coefficient increased with increasing slide/roll ratio, agreeing with [14, 73]. The oil lubricated tests produced the most precise results and showed the least dependence on slide/roll ratio. The lowest friction data occurred with the silicone oil, with a friction coefficient approaching super-lubricity levels at the lowest ratio of 25.3%.

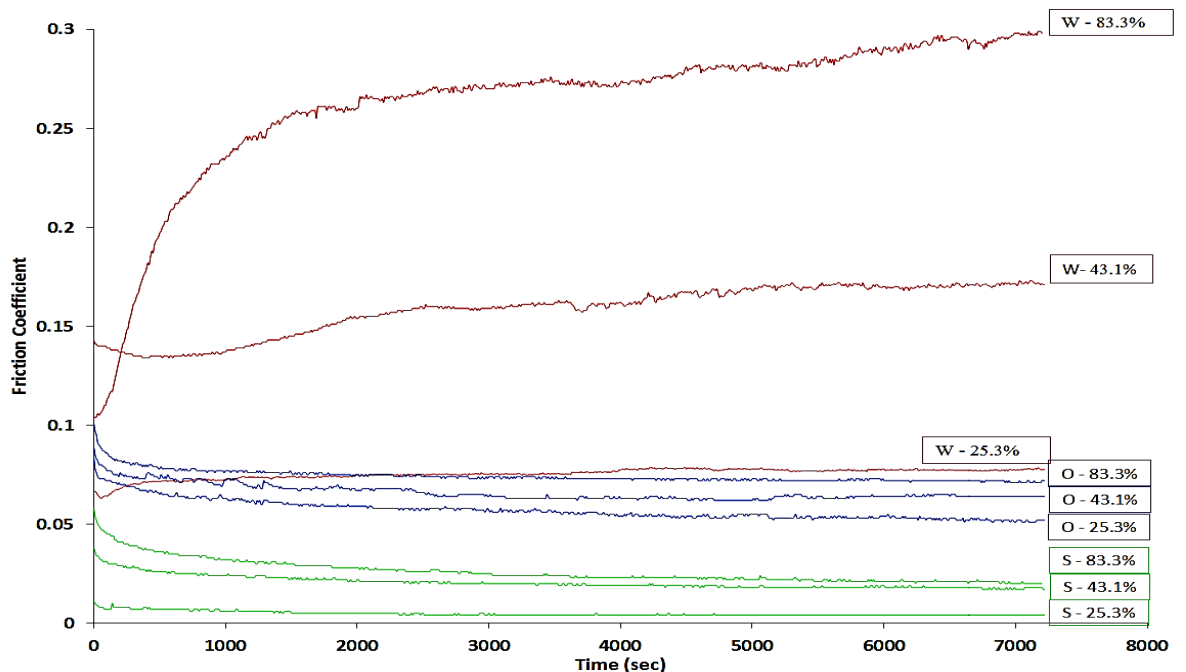


Figure 5.8: showing the average friction coefficient plotted against time for PEEK-Steel, where the initial represents the lubricants (W- deionised water, O- SN100 base oil and S-Silicone oil), and the percentage is the slide/roll ratio.

The average time for the recorded frictional forces to reach a steady state is shown in Figure 5.9 confirms the trends shown in Figure 5.8. It provides the maximum and minimum error in the measured values and that the frictional response of the water lubricated specimens were much less stable compared with the other results. The frictional response of both the base oil and silicone oil tests were all, relative to the water lubricated tests, characterised by low levels of friction, with steady conditions reached rapidly, characterized by highly stable frictional readings, all of which are indicative of the formation of stable lubricant films throughout the contact.

For the base oil and silicone lubricant, the friction coefficients were generally very low and reached a steady state in a short period of time. When water was used to lubricate the samples the friction coefficient was higher than other lubricants. The water lubricated tests at the higher slide/roll ratios offered no steady state condition as shown in Figure 5.9, and this was a result of the low viscosity leading to low lubrication film thickness. Only the friction force measured during the water lubricated tests at the lowest slide/roll ratio of 25.3% tended towards a steady-state conditions, and displayed frictional properties similar to those values measured with the highest slide/roll ratio base oil tests. These same tests also showed more stability relative to the high slide/roll ratios (43.1% and 83.3%). Generally, at the lowest ratio, the kinematic conditions are driven by the higher rolling velocities relative to that of the sliding speed and enabled a more robust fluid film to develop in Figure 5.9.

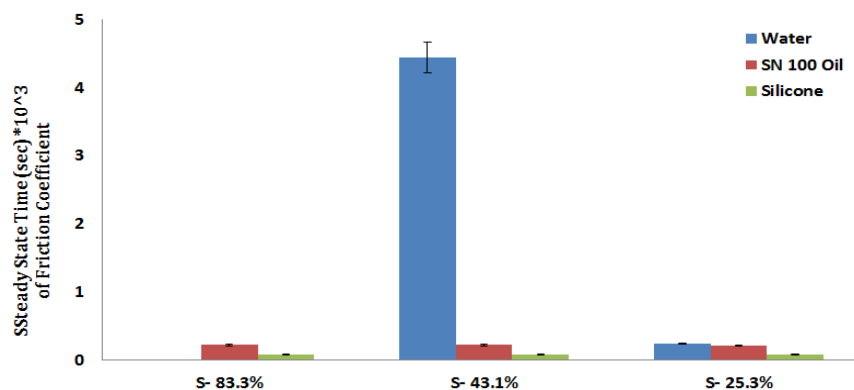


Figure 5.9: showing the average time taken to reach steady-state frictional conditions for each of the three lubricants and three slide/roll ratios for PEEK-Steel Contact

The silicone oil produced near super-lubricity conditions with the lowest average friction coefficient of 0.004 at a ratio of 25.3%, silicone also possessed the highest

viscosity facilitating a greater loading capacity through the formation of more robust lubricant films.

5.4.2 Results of Wear and Energy Pulse

The weight of all samples was measured both before and after testing and in addition to this a polymer control sample was used throughout each test to account for moisture uptake. The wear scar of each sample was observed and then the topography measured from the surface profile using an Alicona G5 Infinite Focus. An example of a measured surface is presented in Figure 5.10 (a). The wear scar comprised the geometry of the surface profile and with the stroke, which when combined could be used to calculate a volume of wear. These values correlated with wear measured gravimetrically for the full range of results are summarised in Table 5.2.

Figure 5.10 (b) provides an example of the lateral wear scar profile from X1 to X2 (representing the full reciprocating stroke length) in the direction of motion. It has a clear ‘bath-tub’ profile tending towards zero at the ends stroke and is a maximum at the middle stroke. The kinematics of the system means that rolling velocity tends to zero at the beginning and end of the stroke, and minimum film conditions prevail, hence the increased wear. Conversely, at the centre of the stroke, velocity and lubricating film thickness should be at a maximum, as is also shown in Figure 5.1, Figure 5.2 & Figure 5.3.

Table 5.2: The wear Volume for the test conditions.

Slide/roll ratio (%)	Wear Volume by scale mm ³			Wear Volume by (geometry of the surface *width (6mm)) mm ³		
	W	O	S	W	O	S
83.3	1.52	0.91	0.68	1.85	0.97	0.64
43.1	1.25	0.68	0.61	1.56	0.71	0.51
25.3	1.21	0.53	0.45	1.38	0.62	0.47

Where W: water, O: SN 100 Oil, S: Silicone

All of the tested samples possessed similar wear characteristics; however, the depth and severity of wear was highly dependent on a combination of the lubrication viscosity, the rolling velocity and the ratio of this to the sliding velocity. Generally, the depth of the wear scar reduced at low Slide/roll ratio and as the lubricant viscosity increased, so the silicone oil produced the smallest wear scar and the water the largest for each of the three slide/roll ratios.

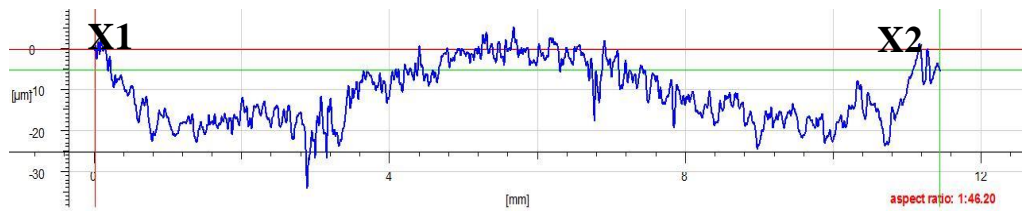
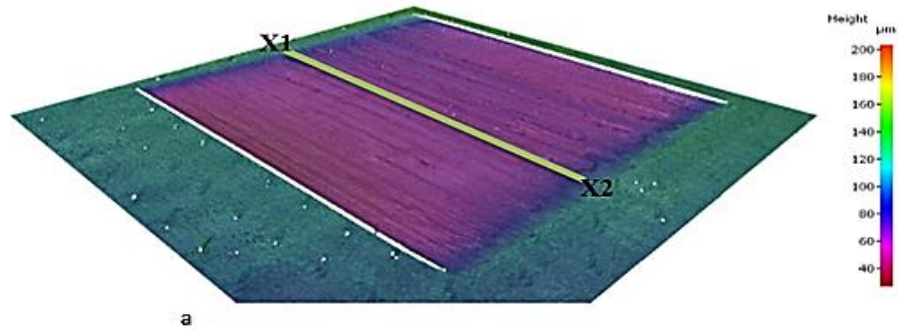


Figure 5.10: showing (a) a sample of the measured wear track and (b) the profile of the same wear scar, generated on the PEEK plate at a slide/roll ratio of 83.3% and lubricated with deionised water.

The energy pulse (J/mm^2) of the plate samples under lubricated conditions was calculated using (Eq 3.20& Eq3.21 in p. 56) and was plotted against wear volume (mm^3) as shown in Figure 5.11. Like the friction results, high wear rates were measured in the highest slide/roll ratios, decreasing to the minimum wear at the lowest ratio. This is again is a kinematic effect, as the higher slide/roll ratio induced a reduction in the rolling velocity, whilst also an increased sliding velocity similarly to the results described by Chan and Li [26].

When calculating the EP for the system in the tests conducted, only the EP of the PEEK plate was considered as it was from these samples that all of the wear occurred. There was no measurable change in the weight of the steel test discs. Figure 5.11 shows that the EP criterion increases with similar trends and the full range of results is summarised in Table 5.3. Water lubrication showed a significant variation in friction coefficient and wear. The water, because of its relatively low viscosity, cannot support the applied pressures and the process of sliding-rolling will generate more frictional heat as a result of surface contact. This will raise the temperature of the contact area, affecting the mechanical properties of the PEEK test specimens.

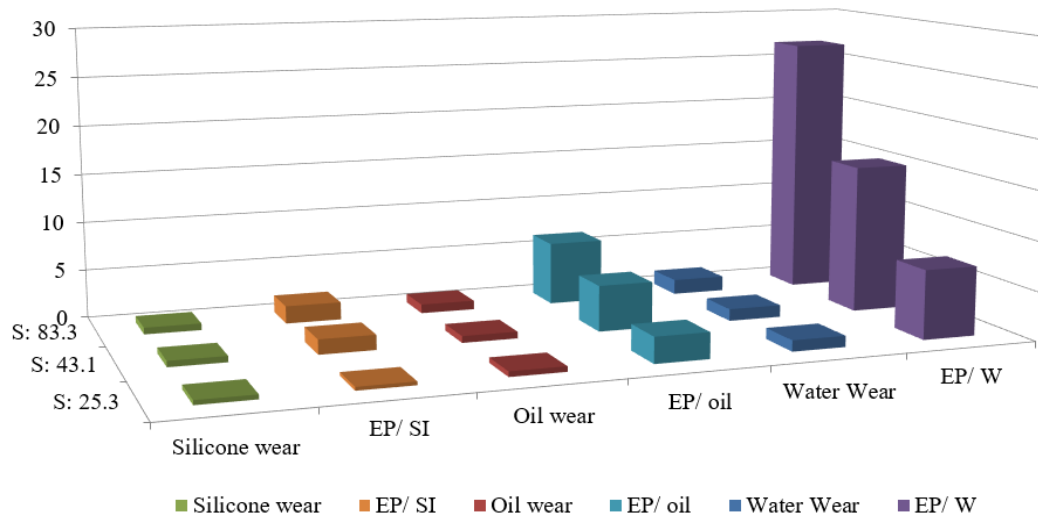
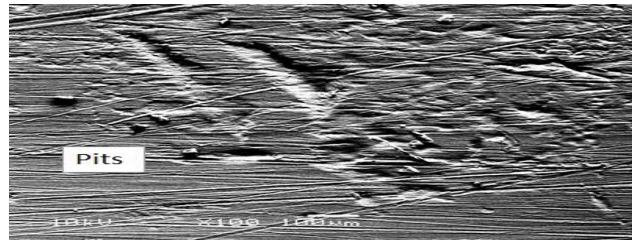


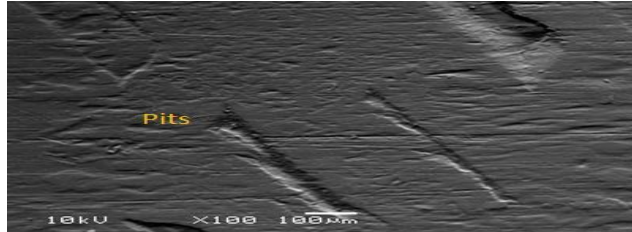
Figure 5.11: showing the calculated energy pulse with volume of wear during the two hours.

From the micrographs SEM microscopy examinations of the surfaces shown in Figure 5.12 (a), there is significant surface damage including small pits, some larger spalling type damage as well as detached debris. This debris on the PEEK surfaces may also be the root cause of some of the observed ploughing [114, 118]. Silicone, with its high viscosity and the theoretical film analysis shown in Table 5.3, is likely to be able to support high contact pressures with a reduction in the volume of the material removed from the surface. The average volume of wear from each of the lubricants is given in Table 5.2. Generally, these indicate that wear volume is still dependent on the slide/roll ratio, rolling velocity and viscosity of the lubricant used, despite the kinematics of the EP/ Gear adaptor. Since the same conditions were used, it is the viscosity of lubricant which predominantly affects the wear mechanisms. In order to understand this effect, the film thickness of lubricant in the test conditions was calculated and shown in Figure 5.8. This figure predicts under idealised, theoretical conditions the effect of lubricant type (i.e. viscosity of lubricant) on the film thickness and then on the wear as shown in Tables 5.2 & 5.3.

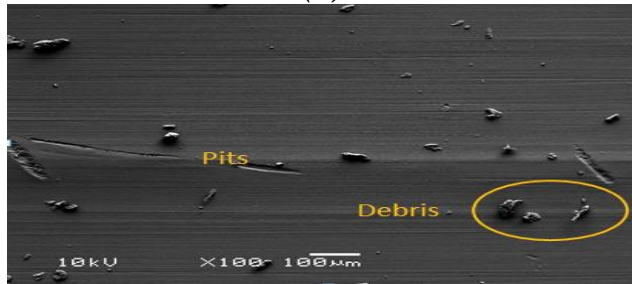
Generally, at the lowest ratio, the kinematic conditions are driven by the higher rolling velocities relative to that of the sliding speed enabling a more robust fluid film to develop, as indicated by the theoretical values for film thickness shown in table 5.3.



(a)



(b)



(c)

Figure 5.12: showing SEM micrographs of the worn PEEK surfaces at a slide/roll ratio of 83.3%, when lubricated with (a) deionised water, (b) SN100 base oil, and, (c) silicone oil. Note: images were taken from the centre of the wear scar from each sample

Table 5.3: The EP for each of the test conditions.

Slide/roll ratio (%)	Rolling Velocity mm/s	Sliding Velocity mm/s	Film Thickness μm			energy pulse J/mm^2		
			W	O	S	W	O	S
83.3	88.71	73.92	1.62E-03	3.65E-02	1.75E-01	26.79	6.47	1.79
43.1	101.65	48.05	1.78E-03	4.00E-02	1.92E-01	15.20	4.69	1.51
25.3	140.46	29.57	2.45E-03	5.51E-02	2.65E-01	7.04	2.63	0.35

Where W: water, O: SN 100 Oil, S: Silicone

5.5 Tribological Properties of Polymer Vs. Steel in the Simulation of Gear Un-Lubricated.

The frictional fundamental and wear behaviour were investigated for (PEEK 450G, PEEK CA30% and EOS PEEK HP3), discs running against steel, and this was used as a simplified method of analysing the dynamic response of high-performance polymeric gear teeth. EOS PEEK HP3 was described to show “excellent wear resistance”. For polymers, the wear mechanism was revealed to be considerably affected by roughness of the surface.

To establish the tribological properties of (PEEK 450G, PEEK CA30% and EOS PEEK HP3) lubricated and unlubricated, a TE77- EP - Gear Slide/roll adaptor was used, the test parameters are 39 MPa contact pressure and 2 Hz frequency and the slide/ roll ratio was 83.3% .

5.5.1 Results – Friction Coefficients

Figure 5.13 shows the friction coefficients results during the EOS PEEK HP3 vs. steel, PEEK vs. steel and PEEK CA 30% (CMPs) vs. steel tests for the higher slide/roll ratio 83.3%, unlubricated. The friction coefficient was steady state during the first period of the test for EOS PEEK HP3 samples and PEEK CA30%, whereas were the PEEK friction coefficient was increasing. It could be seen the best results were with EOS PEEK HP3 materials friction coefficient had been steady during the first minutes of the test in addition to minimum values.

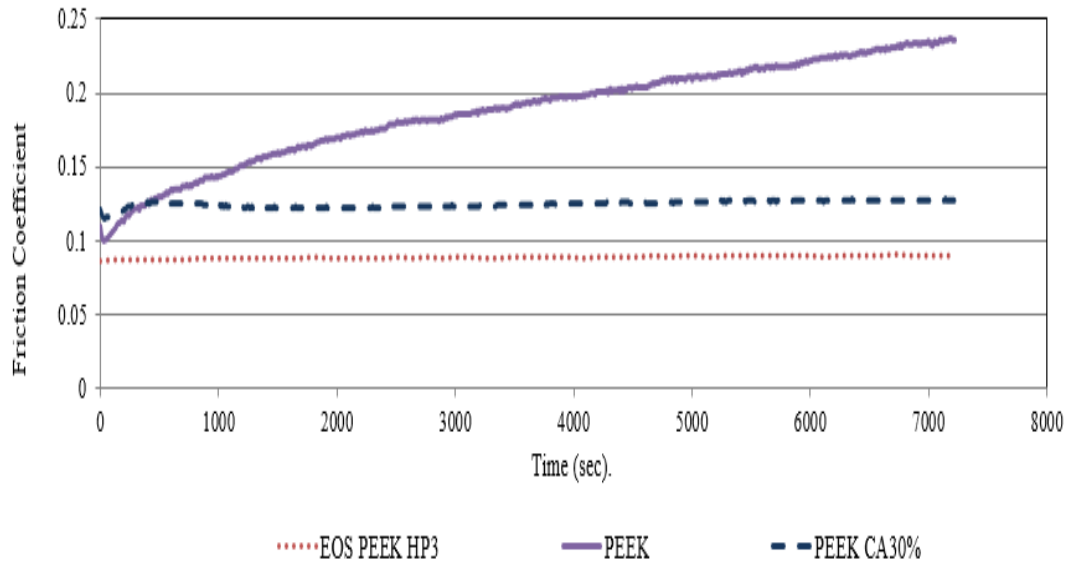


Figure 5.13: showing the average friction coefficient plotted against time for EOS PEEK HP3 - Steel, PEEK-Steel, and PEEK CA30%-Steel, where the slide/roll ratio was 83.3% , contact pressure 39 MPa and 2 Hz, unlubricated .

Figure 5.14 shows the friction coefficients measured during the EOS PEEK HP3 vs. steel unlubricated TE77 EP - Gear Slide/roll adaptor results.

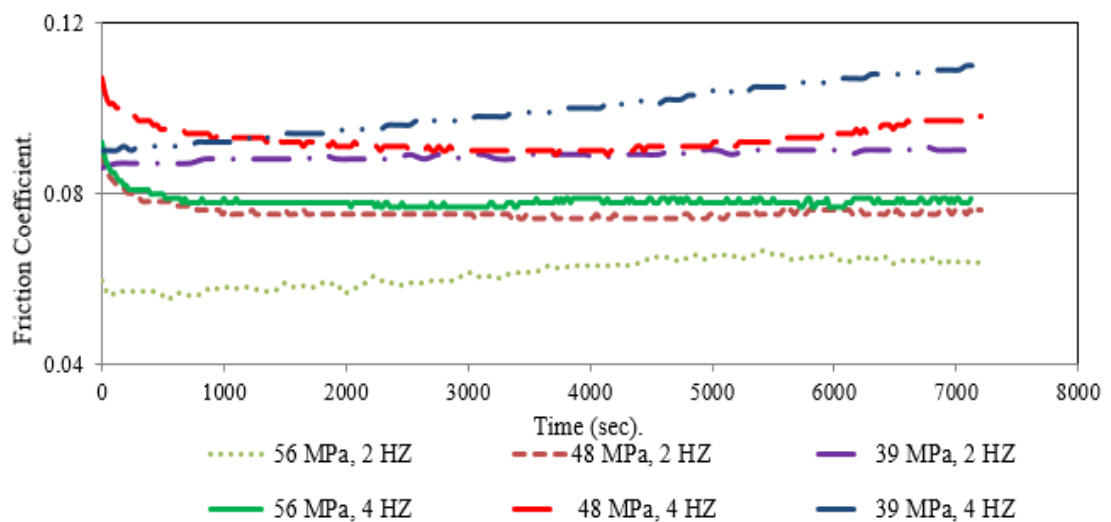


Figure 5.14: Friction coefficient (EOS PEEK HP3 vs Steel) unlubricated

The results showed that the friction coefficient decreased with the load applied but increased with frequency. Therefore, the role of adhesion became more prominent in heavily loaded unlubricated tests. This is clear from the oscillation in the friction coefficient trace. Furthermore, because adhesion is to the connected region, asperity

deformation resulted in increased adhesion on the polymer surface in the actual contact field.

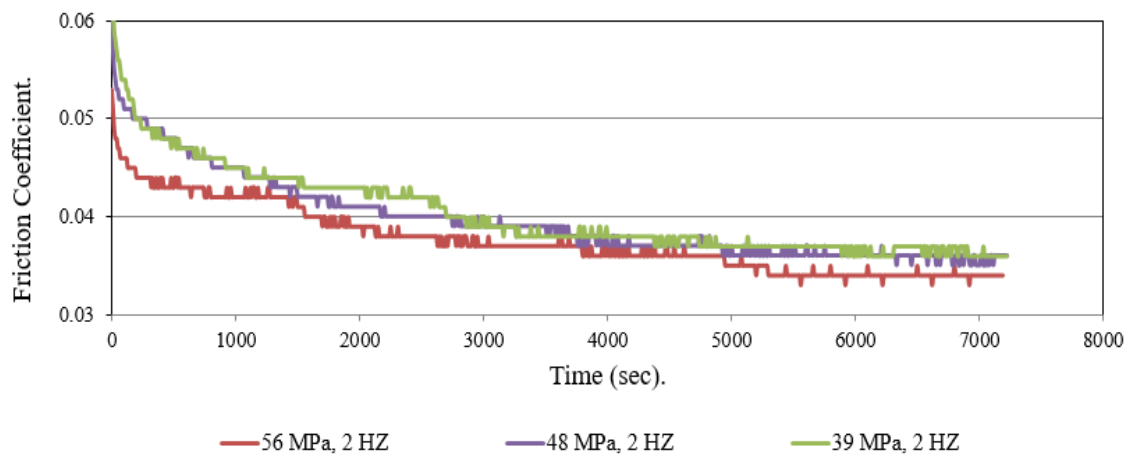


Figure 5.15: friction Coefficient (Steel vs. EOS PEEK HP3 – lubricated)

Figure 5.15 displays the results of TE77 EP - Gear Slide/roll lubricated tests. The friction coefficient was much lower in the lubricated tests (about 50%). The decrease in the friction coefficient was due to decreased adhesion and the load-supporting lubricant film, reducing the material's contact. In addition, the increased contact pressure under high loads there will be increase the viscosity of the lubricant.

In as much as viscosity is a degree of fluid flow resistance to; this improvement significantly increased ability of the lubricant to support load without being compressed out of the contact area.

5.5.2 Results – Wear

After slide/roll tests of TE77 EP, the scars generated by the wear were inspected. The observed scars for EOS PEEK HP3 were less than for those detected on the PEEK and PEEK CA 30%. Figure 5.16 shows the surface wear scars of the depth for the three materials with a contact pressure of 39 MPa and a frequency of 2 Hz.

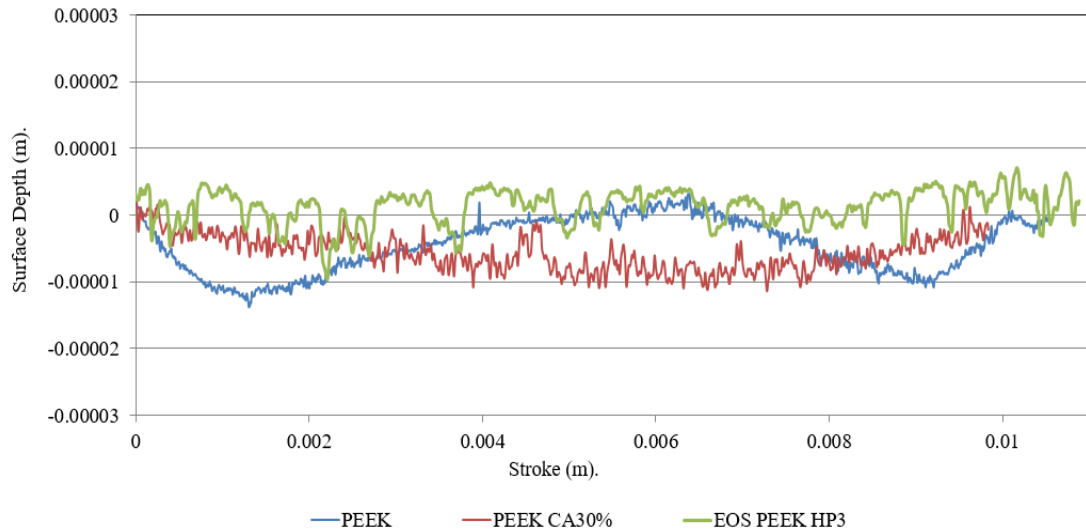


Figure 5.16: Profile of surface depth of scars generated on non-lubricated EOS PEEK HP3, PEEK, and PEEK CA 30% plates (frequency 2 Hz, contact pressure 39 MPa, and slide/roll ratio 83.3%).

However, in the tests carried out without lubrication the wear was relatively much greater than lubricated tests. Table 5.4 presents wear determined for the non-lubricated and lubricated tests.

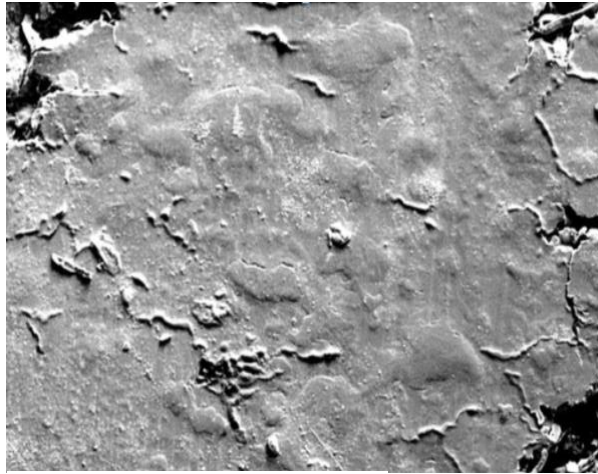
It could be seen the wear increase with both contact pressure and speed for both non-lubricated and lubricated conditions, though of course it was lower for the lubricated condition

Table 5.4: EOS PEEK HP3 vs. steel, apparent wear, for contact pressures 56, 48 and 39 MPa and frequency 2 Hz

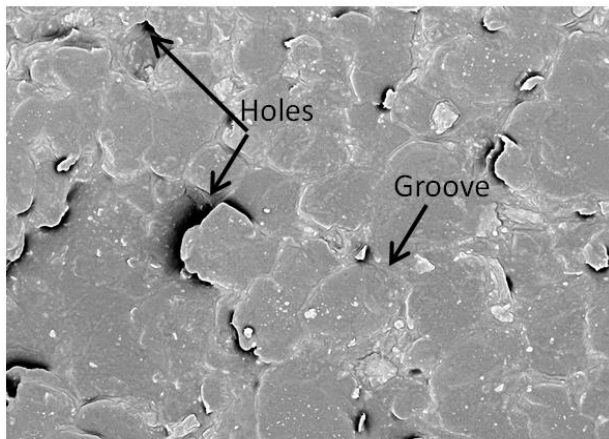
Contact Pressure	Wear (g)	
	Unlubricated	Lubricated
56 MPa	0.0372	0.0296
48 MPa	0.0358	0.02653
39 MPa	0.0321	0.0246

Figure 5.17 shows the wear of non-lubricated and lubricated surfaces for different contact pressures. The harder steel counterface ploughed through the softer EOS PEEK HP3 and we see preferential wear of the surface asperities with a consequential smearing of material forming the asperities. The smearing increased with increase in contact pressure, significantly reducing surface roughness but increasing the wear scar

area, see Table 4 and Figure 5.17 A. In Figure 5.17 C, fatigue tearing, and grinding can be discerned in the deformed region. Comparing Figure 5.17 A and Figure 5.17 B we see these effects are more prominent under higher load. In fact, the effects are only detected under high loads, i.e., high contact pressures. In the given tests, asperity wear dominated the contact and the impact of fatigue tearing and grinding on the tribological properties of the surface was minimal.

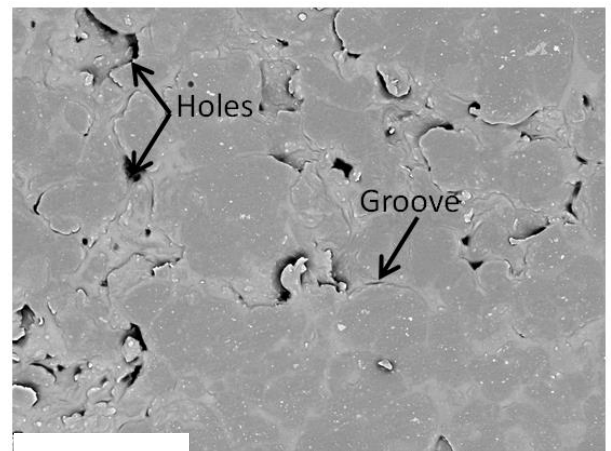


A



B

AL D8.2 x300 300 μm



C

2019-12-03 AL D8.1 x300 300 μm

Figure 5.17: Smearing of the surface asperities of EOS PEEK HP3: A) contact pressure 39 MPa, frequency 2 Hz, non-lubricated, B); as A but lubricant added; and C) contact pressure 56 MPa and frequency 2 Hz with lubricant added.

Figure 5.18 shows the preferential asperity wear for the unlubricated and lubricated tests. It was noted that in all tests where lubrication was applied, the degree of roughness of the test surfaces meant the film of lubricant was not thick enough to preventing asperity wear. This means that one outcome of the test was to polish the

surface of the material. This reduced surface roughness and improved wear characteristics.

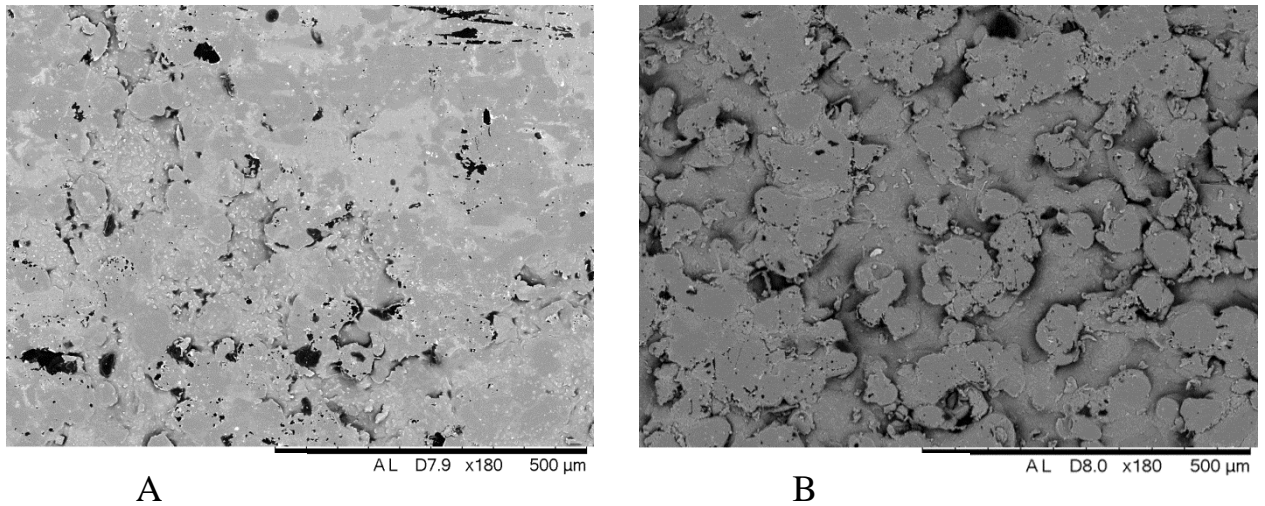


Figure 5.18: Wear of surface asperities of EOS PEEK HP3 for A) unlubricated and B) lubricated tests; contact pressure 56 MPa and frequency 2 Hz.

5.6 CONCLUSIONS

Theoretically, elastohydrodynamic lubrication theory was used to determine the effects of viscosity on lubricant film thickness, for a small surface contact area (Hertzian region), at the sliding and rolling speeds. The outcomes of the current work can be used in the design process in order to increase the efficiency of the contact conditions for gears of PEEK, for any application.

The EP was associated with film thickness at the three lubrication conditions. It was found that the EP approach, as a global factor, can be used to indicate the real operating conditions of wear, and can also provide experimental results to help in the design of sliding-rolling motion.

The transient tribological behaviour of PEEK against steel was investigated experimentally for lubricated sliding/rolling (non-conformal) contact. Friction coefficient and wear mechanisms were measured at three sliding/rolling ratios and with 3 lubricants with varying viscosities. The aim was to determine if the Energy Pulse, as a means of providing a transient profile of sliding/rolling (non-conformal) contact could be used to model wear mechanisms, frictional properties of polymer/

steel contacts and if the EP criterion could be used as a valid performance measure. It was shown that: friction coefficients were highest with water lubrication followed by base oil with friction of about 0.08 and 0.004 for silicone oil.

The highest wear rates were also measured in this order, water, 100 SN base oil and silicone oil. The most severe tribological conditions were found in the highest slide/roll ratios. The wear appears to be closely linked to the EP parameter. The presence of lubricant improved wear behaviour with silicone the best lubricant of those tested.

The EP parameter can be used to successfully relate real operating circumstances to wear under lubricated conditions. Furthermore, experimentally, this parameter is a valuable addition to support and connect laboratory tests to real life contact conditions. The current results can help in improving polymeric gear systems when high slide/roll ratio and more efficient velocity transmission can be achieved.

The friction coefficient of EOS PEEK HP3 was much lower in the lubricated tests (about 50%). The decrease in the friction coefficient was due to decreased adhesion and the load-supporting lubricant film.

Chapter Six

6



6

“An experiment is a question which science poses to Nature, and a Measurement is the recording of Natures answer”

Max Planck

THE SUITABILITY OF LASER-SINTERED PEEK FOR GEAR APPLICATIONS

The key advantage of additive layer manufacturing (ALM) is that it can be used when and where traditional manufacturing methods have reached their limits. However, it has been suggested [99] that although, generally, the tribological properties of EOS PEEK HP3 compares well with injection moulded PEEK, its mechanical strength and failure limit, impose limits on its applications.

This part of the thesis studies the application EOS PEEK HP3 to power transmission gears.

6.1 Gear Production

Traditionally, polymer gears to power transmit were produced by injection moulding have been made with a central steel hub to prevent coupling failures between the gears and enabling the shafts to be properly located. The design of the gear body has been changed, due to the difficulty of sintering around a steel coupling, to accommodate the polymer stresses and to avoid failures in the body [2].

There have been two model variations, Figure 6.1, and Figure 6.2 shows the developed test geometry:

- Steel hub was removed; the internal keyway instead has been manufactured as a feature of polymer gear.
- Multiple external couples of faces.

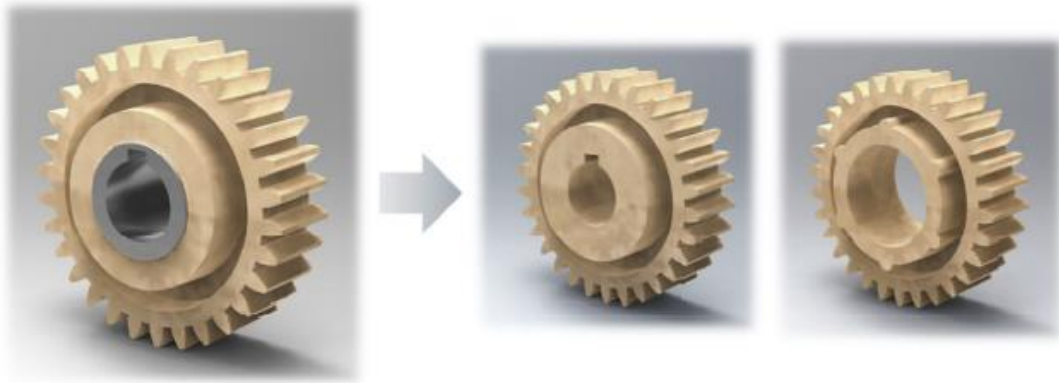


Figure 6.1: Keyway re-design to allow for removal of the steel hub [after [2]].

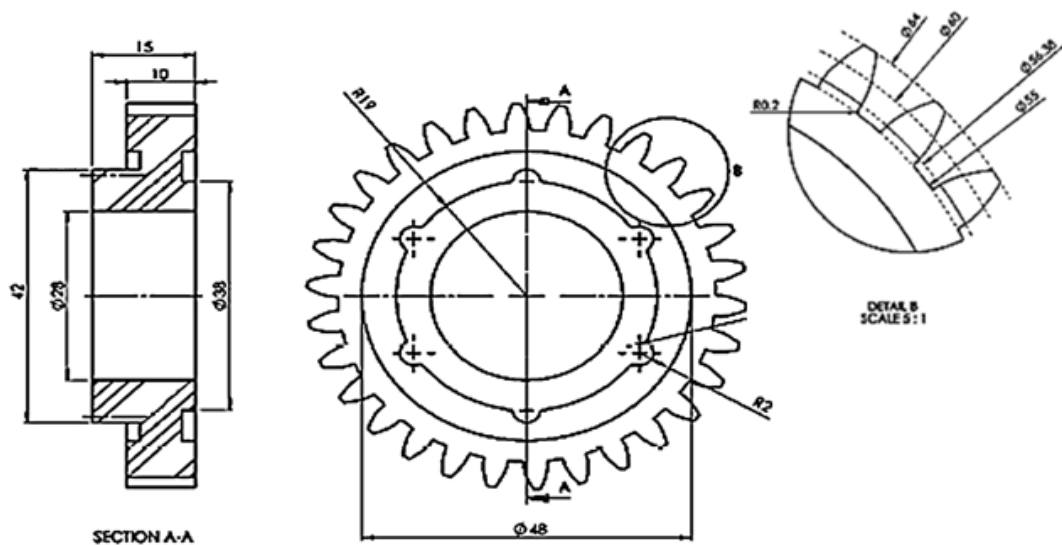


Figure 6.2: Manufactured gear geometry [after [2]].

Figure 6.3. shows the EOSINT P 800 laser sintering system at the University of Exeter, where the geometric design was produced by the Centre Additive Layer Manufacturing (CALM).

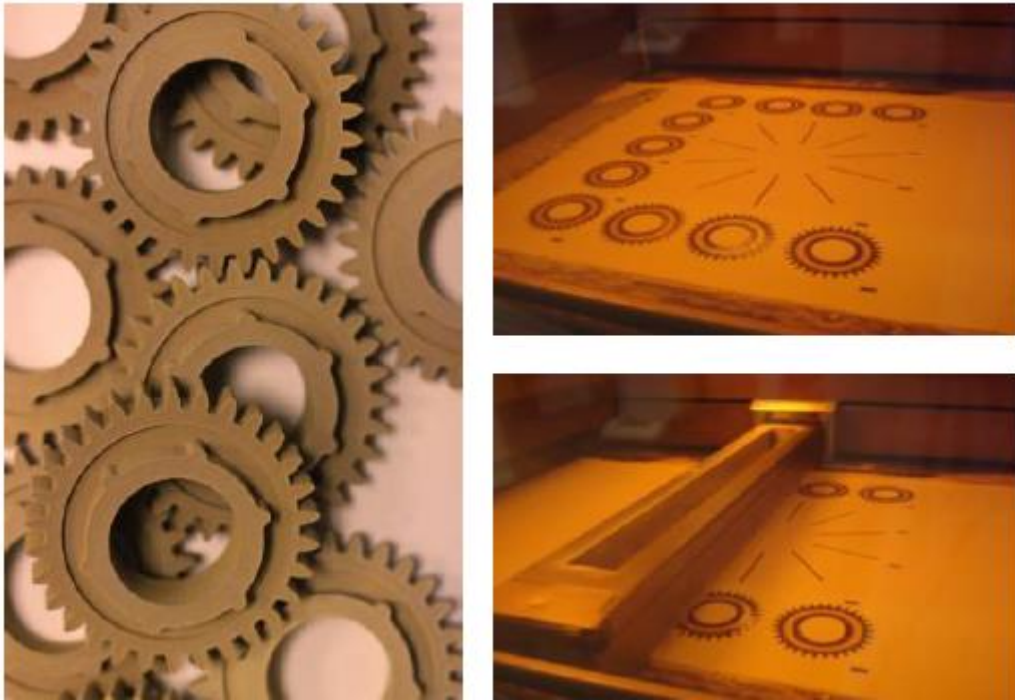


Figure 6.3: EOSINT P800 laser-sintering machine.

6.1 Test Methods

The gear test rig MK II was updated to permit mounting of the different design of the gear hub on the gear test rig; Figure 6.4 displays the hub assembly [2].



Figure 6.4: Hub assembly.

The gear tests were taken at a variety of loads and velocities, as shown in Table 6.1, surface lubricated tests were also achieved to evaluate the influence of the (silicone oil) to material wear and tribological properties.

Table 6.1: Gear test conditions.

No.	Test	Lubrication	Load (Nm)	Speed (rpm)
1	Steel vs. HP3	√	6.3	500
2	Steel vs. HP3	√	8.2	500
3	HP3 vs. HP3	√	8.2	500
4	Steel vs. HP3	√	8.2	750
5	Steel vs. HP3	√	8.2	1000
6	HP3 vs. HP3	√	8.2	1000
7	Steel vs. HP3	-	12.2	1000
8	Steel vs. HP3	-	8.2	1000
9	HP3 vs. HP3	-	8.2	1000

6.2 Results

Gears of EOS PEEK HP3 materials have been tested to evaluate the reaction to the effect of the tribological properties on the contact of polymer gears.

6.2.1 Gear Failure

Bending fatigue has been found to be the predominant mode of failure in the EOS PEEK HP3 gears. On the other hand, samples have been shown to be sensitive to fluctuations in speed of rotation and applied load.

Figure 6.5 shows two typical examples of the geometry of gear failure. Specific teeth were broken off the gear body.



EOS PEEK HP3 vs Steel, test 9



EOS PEEK HP3 vs EOS PEEK HP3, test 8

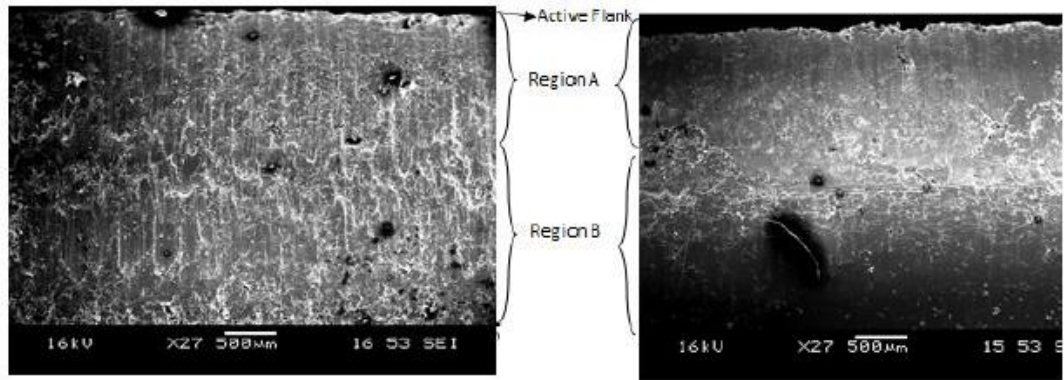
Figure 6.5: Root failures of EOS PEEK HP3 with dry running

There were two different regions of failure discovered on the broken gear tooth, see Figure 6.6.



Figure 6.6: Regions of failure: Region A and Region B, surface fracture

Progressive failure was observed to advance into the material up to 2 ~ 3 mm before tooth fracture occurred. Usually, the failures occurred at the tooth flank in the pitch point and extended outwards, see Figure 6.7.



EOS PEEK HP3 vs EOS PEEK HP3

EOS PEEK HP3 vs Steel

Figure 6.7: Regions of failure: Region A, and; Region B.

Figure 6.8 shows delamination in the samples occurred where the surfaces ruptured. It is most probable that at the boundary between the sintered layers, void nucleation and coalescence induced crack propagation in the sample.

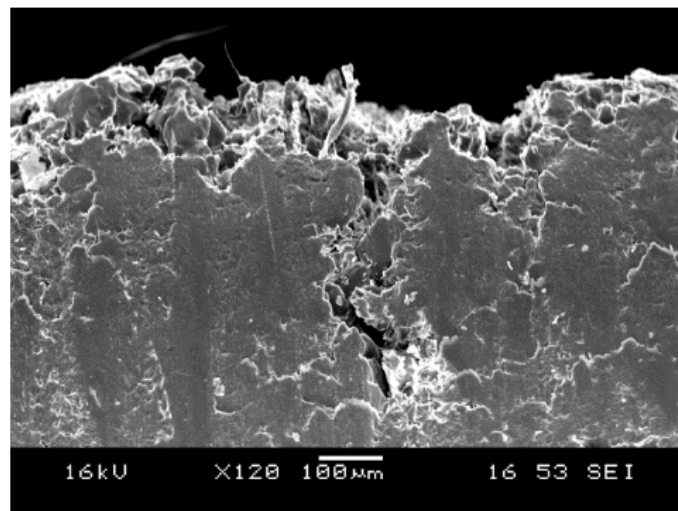


Figure 6.8: Failure surface fracture on the boundary surface for EOS PEEK HP3 vs steel test at 1000 rpm and load 8.2 Nm.

Figure 6.9 shows the failure surface of the partial sintered material. It can be seen that in the progressive region of failure, parts of the sintered material were more evident. Thus, the stress direction in the progressive failure region was assumed to be controlled

by partial sintering at the boundaries of the layers of powder that formed the polymer gear.

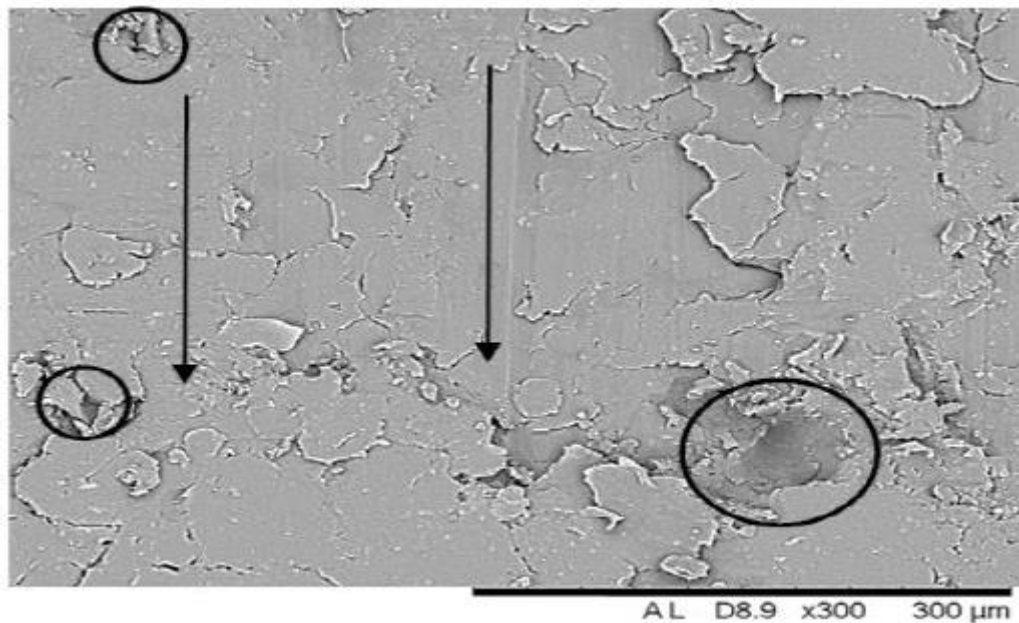


Figure 6.9: Failure surface (Region A).

From Figure 6.10, EOS PEEK HP3 surface of been partially sintered, it can be seen that the direction of the manufacture of plane; focussed to the regions adjacent of the planes. Again, this suggests the material was only partially sintered and, as a result, there was a degree of porosity at the interface between the layers occurring during manufacture, where the process of sintering was not fully completed. The same results were observed and discussed in [99].

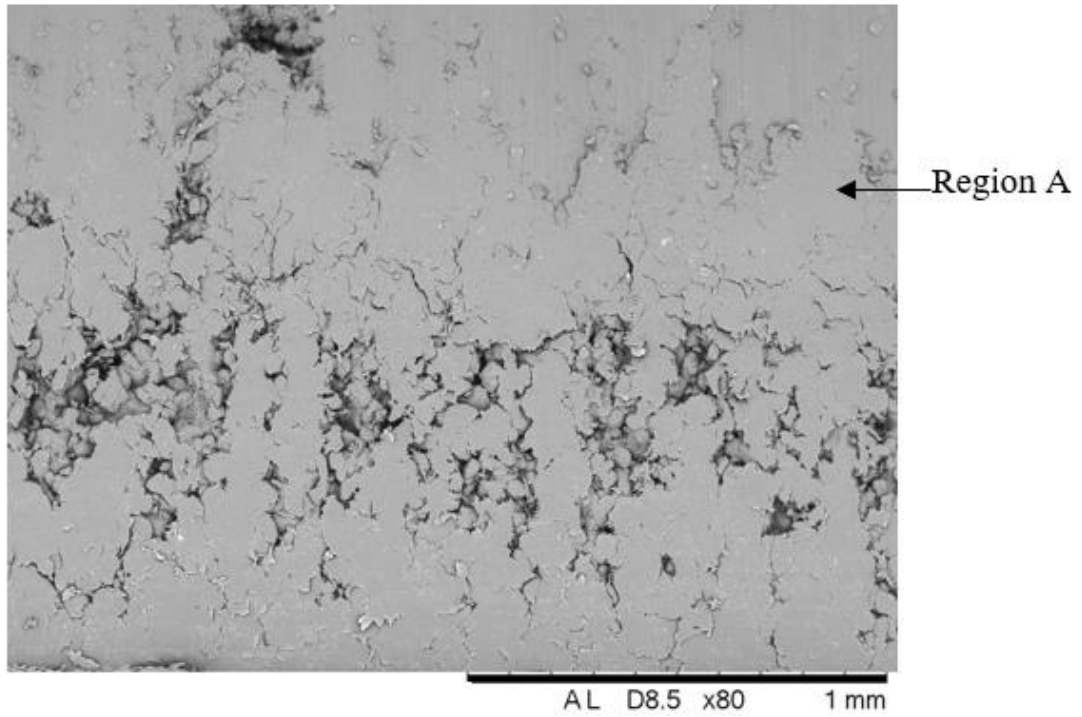


Figure 6.10: Partially sintered on the surface. (Region A)

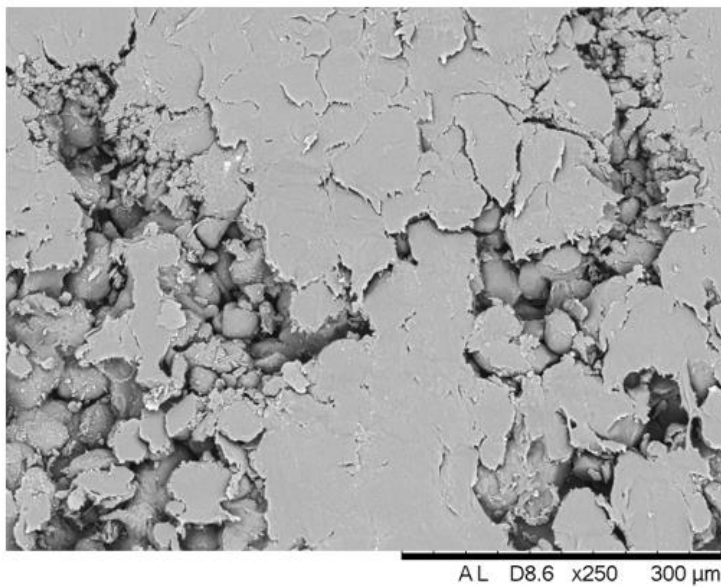


Figure 6.11 shows the gear flank has the progress of partially sintered material. The surface of failure showed a progression ruled by loading of the tooth. Furthermore, a smearing wear can again be seen on the surface.

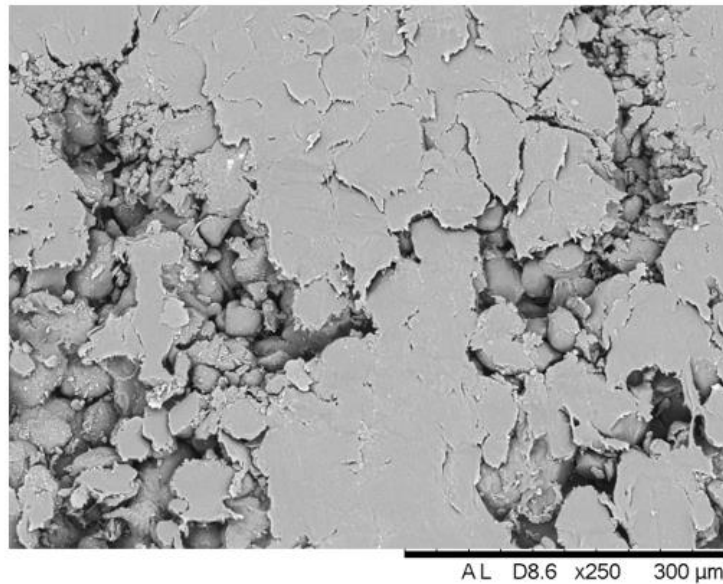


Figure 6.11: Failure surface gear teeth at Region B.

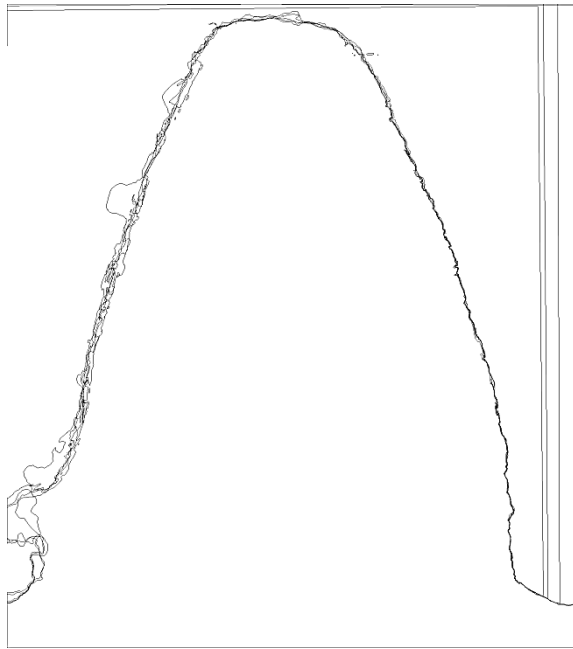
6.2.1 Gear Wear

Using Pylon 6 Camera Software Suite version 6.0.0 was used to show the differential wear for gear tooth. The test was stopped, and a scan taken for the tooth in question, the gear was weighed, and the test then continued. Figure 6.12 shows the superimposed tooth profiles by opencv-python image processing.

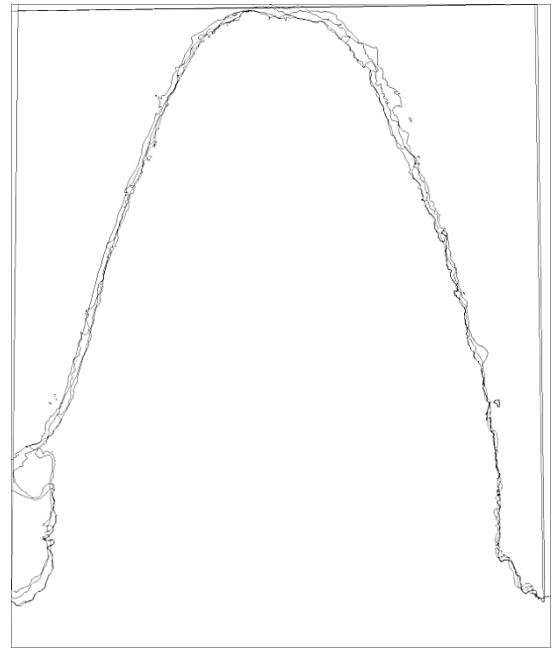
The performance EOS PEEK HP3 gears in conjunction with a steel pinion was found to be poor, when compared with the results obtained from similar tests conducted on EOS PEEK HP3 vs EOS PEEK HP3 gear pairs. Figure 6.12 (a, b, c, d) illustrate this difference for gears of EOS PEEK HP3, where Figure 6.12 (a, c) show lubricated and unlubricated both tooth profiles of gears tested in like/like combinations, while Figure 6.12 (b, d) shows EOS PEEK HP3 gears lubricated and unlubricated tested in conjunction with a steel pinion. The difference is stark; no wear could be detected in EOS PEEK HP3/ EOS PEEK HP3 composite gear

pairs, a substantial portion of the tooth flanks were eroded when tested against a steel pinion.

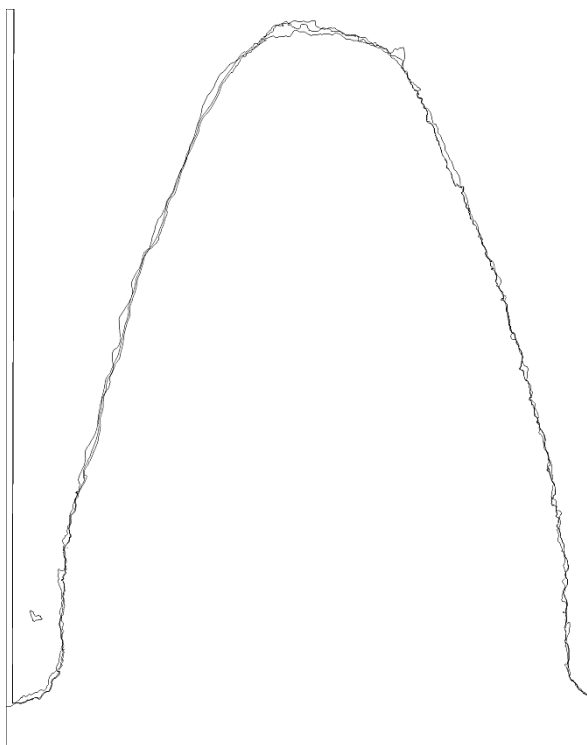
For example, Figure 6.12 -d shows the wear profiles of a gear tooth of EOS PEEK HP3 vs. steel test, measured at specific intervals during a test conducted at 8.2Nm and 1000 revs/min. From this it can be seen that a large radius was formed in the lower portion of the wear profile, in addition to the fact that the tooth showed a significant degree of thinning in this region. By the end of the test a crack had developed in the lower wear profile. The same behaviour was shown for the polymer vs. steel in [30].



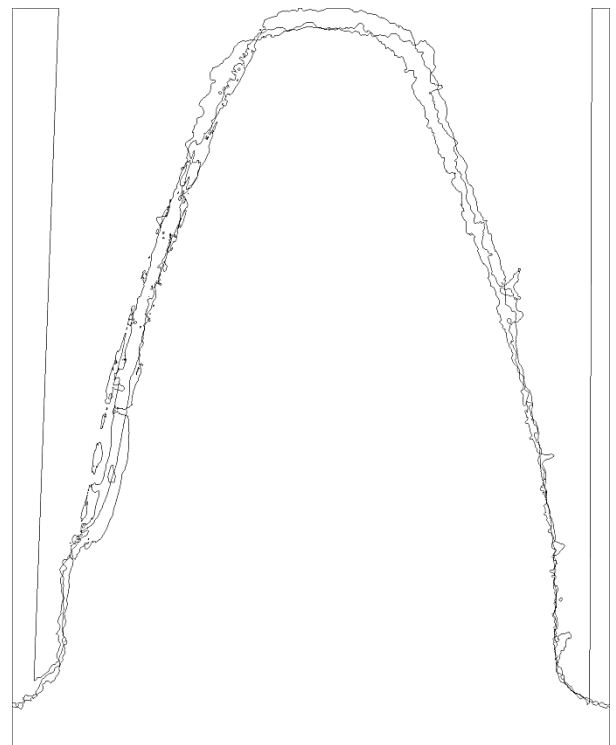
a- EOS PEEK HP3 vs. EOS PEEK HP3- L



b- EOS PEEK HP3 vs. Steel -L



c- EOS PEEK HP3 vs. EOS PEEK HP3 - UNL



d- EOS PEEK HP3 vs. Steel - UNL

Figure 6.12: Differential wear scan using pylon 6 Camera, the direction of rotation clockwise

Figure 6.13 displays the wear loss of EOS PEEK HP3 vs. EOS PEEK HP3 gears during number of cycles for the lubricated tests.

From Table 6.2, determined that limits were imposed on transmitted load and the gear's speed of rotation by the presence of partially sintered particles in the bulk of the material.

Table 6.2: Gear test conditions and the results.

No.	Test	Lubrication	Load (Nm)	Speed (rpm)	Cycles	Time (hours)
1	Steel vs. HP3	√	6.3	500	$4.5 \cdot 10^6$	150
2	Steel vs. HP3	√	8.2	500	$4.5 \cdot 10^6$	150
3	HP3 vs. HP3	√	8.2	500	$4.5 \cdot 10^6$	150
4	Steel vs. HP3	√	8.2	750	$4.5 \cdot 10^6$	104
5	Steel vs. HP3	√	8.2	1000	$4.5 \cdot 10^6$	77
6	HP3 vs. HP3	√	8.2	1000	$4.5 \cdot 10^6$	77
7	Steel vs. HP3	-	12.2	1000	$120 \cdot 10^3$	2
8	Steel vs. HP3	-	8.2	1000	$1.2 \cdot 10^6$	20
9	HP3 vs. HP3	-	8.2	1000	$1.8 \cdot 10^6$	30

Figure 6.14 shows the wear losses of EOS PEEK HP3 vs. steel gears with number of cycles for the lubricated tests.

For the EOS PEEK HP3 vs. EOS PEEK HP3 and EOS PEEK HP3 vs. Steel unlubricated tests, wear losses vs. number of cycles, the failure has suddenly happened, indicating the influence of wear in inducing failures of teeth was limited Figure 6.15.

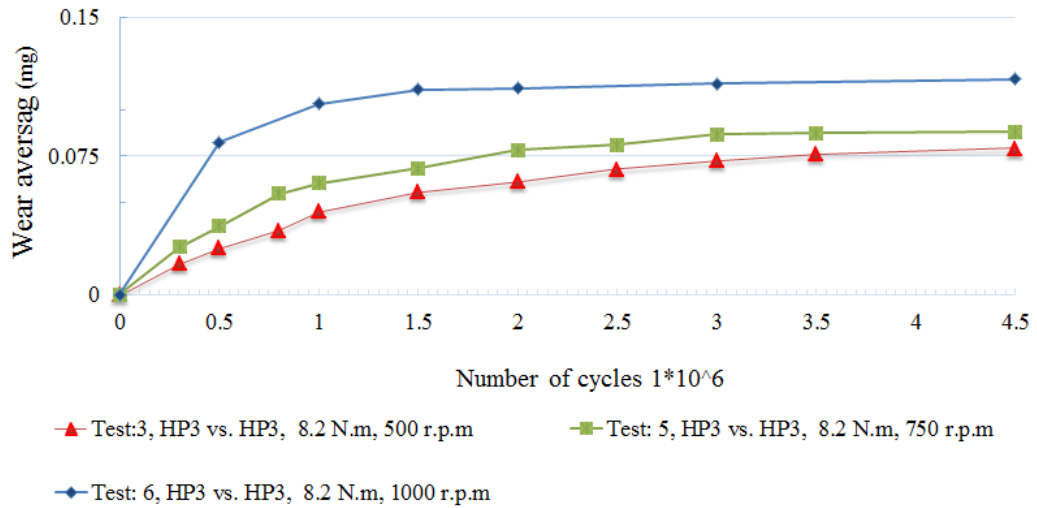


Figure 6.13: wear loss for the EOS PEEK HP3 vs. EOS PEEK HP3 gears lubricated.

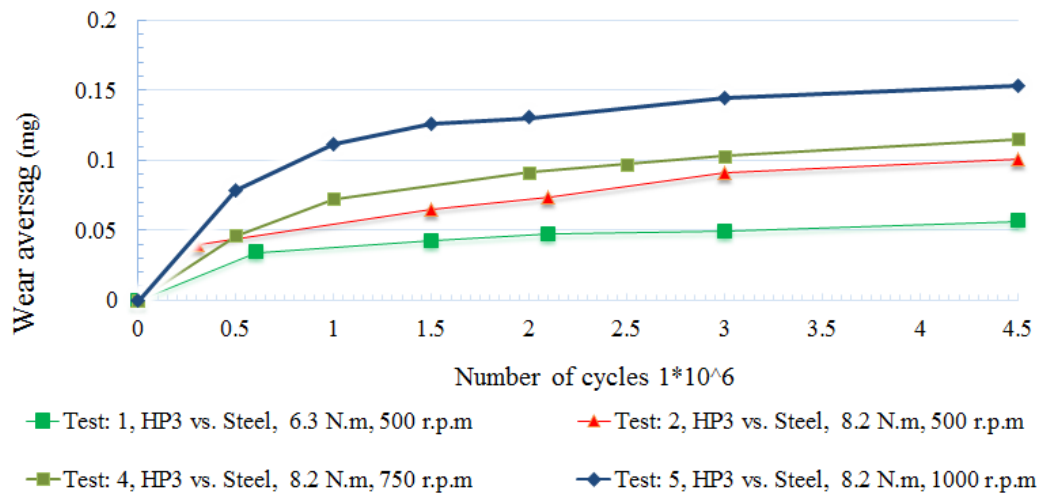


Figure 6.14: wear loss of the EOS PEEK HP3 vs. Steel gears lubricated.

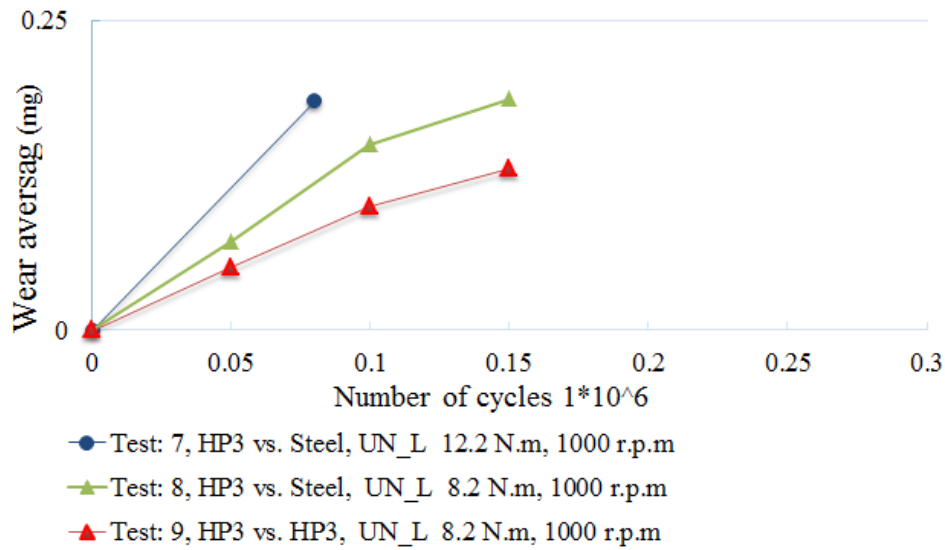


Figure 6.15: wear loss for the un-lubricated.

From Figure 6.13, Figure 6.14 & Figure 6.15, it was very clear that the lubricated surface performance was better. It was noted that the presence of lubrication significantly improved the lifetime of the gear under a given load. When lubricated EOS PEEK HP3 was run against itself, it was seen that the rate of wear was less than EOS PEEK HP3 against steel gears, and in all the tests running until 4.5×10^6 cycles.

EOS PEEK HP3 gears, when run un-lubricated has higher wear and fast failure before 0.2×10^6 cycles.

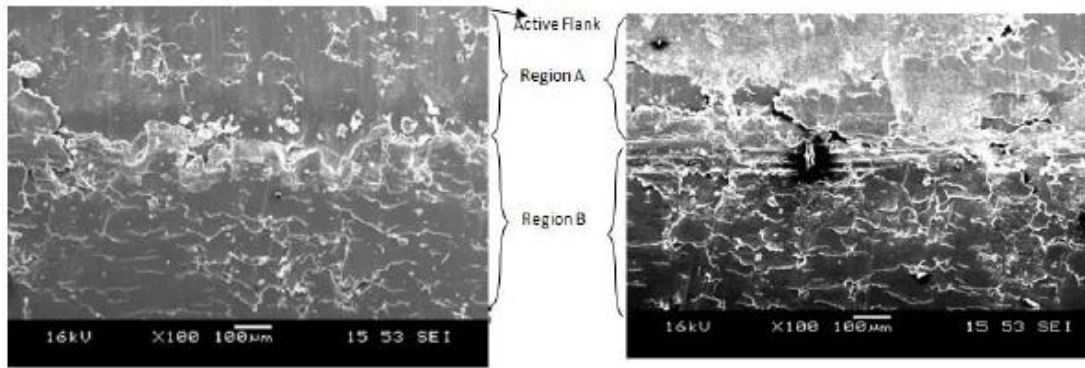
6.2.1.1 Un-lubricated Wear (SEM)

In the unlubricated tests, the levelling of the asperities in EOS PEEK HP3 was shown to decrease the roughness of the surface. However, the only way to determine the specific properties of the gear material accurately is through practical application. From Figure 6.16 for unlubricated tests, there is significant scuffing on the EOS PEEK HP3 gears flanks, growing towards the contact ends where the sliding velocities are highest.



Figure 6.16: scuffing on addenda of gear tooth

Figure 6.17 illustrates the elevated contact line for EOS PEEK HP3 gears at pitch point. The pitch line was raised due to the build-up of debris in the contact area due to the direction of the sliding velocity. Furthermore, as a result of high localised contact stresses; surface fatigue near the pitch point could shown.

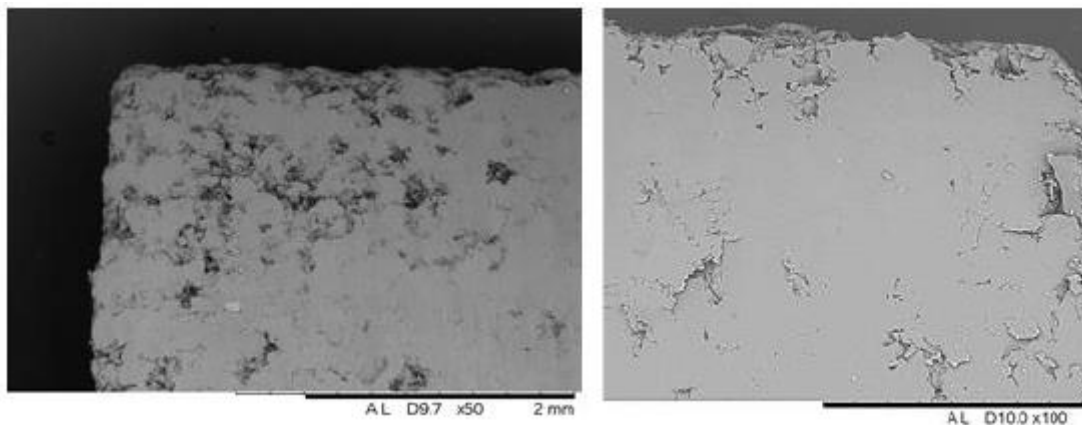


EOS PEEK HP3 vs EOS PEEK HP3

EOS PEEK HP3 vs Steel

Figure 6.17: EOS PEEK HP3 gear the pitch line

From Figure 6.18, shows that material was built-up at the end of the mesh, similar to the findings reported in [99].



EOS PEEK HP3 vs EOS PEEK HP3

EOS PEEK HP3 vs Steel

Figure 6.18: material build-up and smearing at the end of the mesh

During the period of initial bedding, the wear was mostly abrasion; but, as the temperature rose, the effect of adhesion between gear surfaces became more important. The influence of adhesive wear was particularly important when EOS PEEK HP3 were running against steel gears and there was a transfer of EOS PEEK HP3 material to the steel gear, see Figure 6.19.

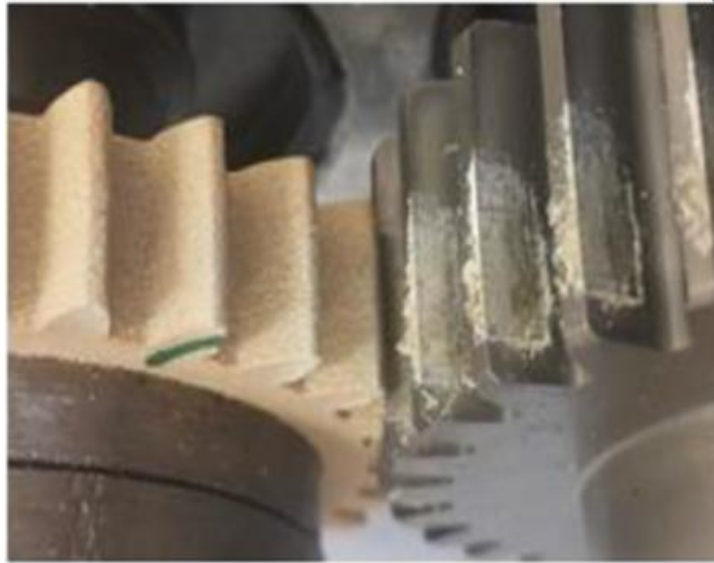


Figure 6.19: EOS PEEK HP3 transfer to the metal (non-lubricated conditions)

The transferred EOS PEEK HP3 on the steel gear is shown in Figure 6.19. This effectively created an EOS PEEK HP3 transfer layer, strengthening the contact's tribological properties, reducing the steel counterface surface roughness and subsequent abrasive wear. It was concluded that the increase of EOS PEEK HP3 transfer was a result of the decreasing roughness of the counterface and the increased durability of the transferred material.

6.2.1.2 Lubricated Wear

Lubricated significantly improves EOS PEEK HP3 tribological properties (see Chapters 4 and 5). However, lubrication was shown to significantly reduce adhesion. Figure 6.20 & Figure 6.21 show the surfaces that were worn. It can be seen that on the steel counterface there are no evidence layer transfer. Furthermore, it can be seen that the silicone oil was a good lubricant, forming a thin layer over the entire polymer and steel surfaces, stored in the pores in the preliminary layers of (EOS PEEK HP3) on surface of the polymer specimen.



A) Steel

B) HP3- low speed define

C) HP3-high speed

Figure 6.20: EOS PEEK HP3 vs. Steel gear teeth lubricated.

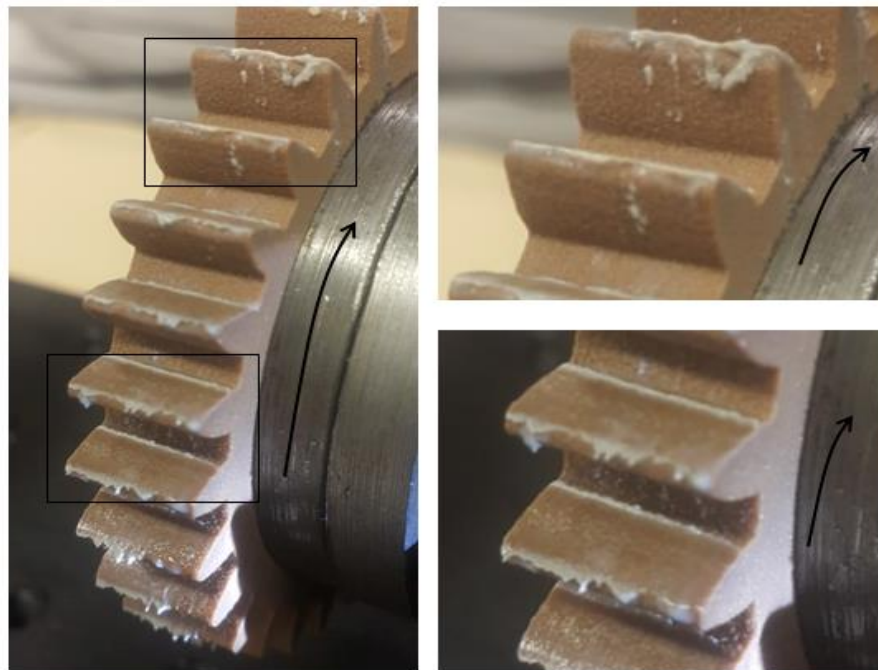


Figure 6.21: Lubricated wear of EOS PEEK HP3 vs. EOS PEEK HP3 gear teeth.

EDS was used to discern the silicone oil and other material present on the EOS PEEK HP3 surface, and significant quantities of both iron and silicone oil were detected (Figure 6.22 & Figure 6.23). It was shown that the silicone oil particle on the teeth surface; the most of the particle was popular found located in the cavities surface (may be pores caused it) while important quantities were besides showed on the surface. In addition there were significant amounts of silicone oil under the pitch line for the both

tests 5 and 6 in Table 6.1. It was concluded that when the pitch line was raised as a result of EOS PEEK HP3 partials was build-up due to both the sliding speed and the high stress, some particles have been removed from the EOS PEEK HP3 gear teeth surface and stuck up with the silicone oil. Consequently, more silicone oil was found below the pitch point than above.

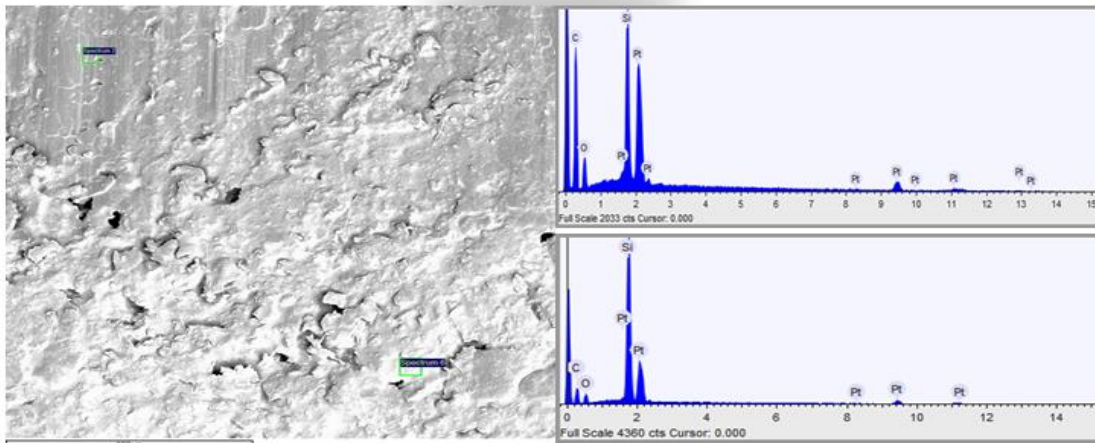


Figure 6.22: EDS of the surface EOS PEEK HP3 gear for Test 6, around the pitch line [Platinum coating]

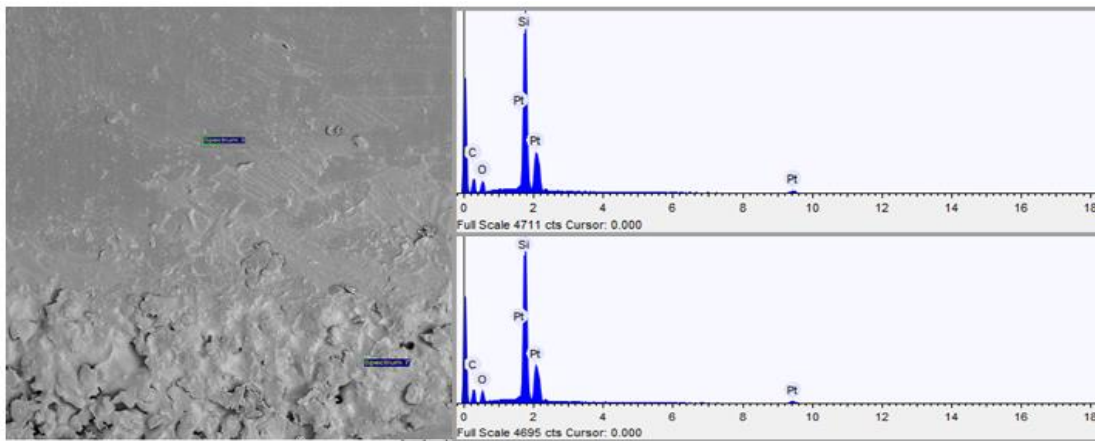


Figure 6.23: EDS of the surface EOS PEEK HP3 surface tooth for the Test 5, around the pitch line [Platinum coating]

Figure 6.24 & Figure 6.25 shows the EOS PEEK HP3 tooth surface of the gear has little abrasion, through decreased asperity of the smearing substance for both tests 5 and 6.

After running the tests for 4,500,000 cycles, small scale pitting could be seen at the single tooth of first point contact. This is due to high contact stresses and the low compliance of the material.

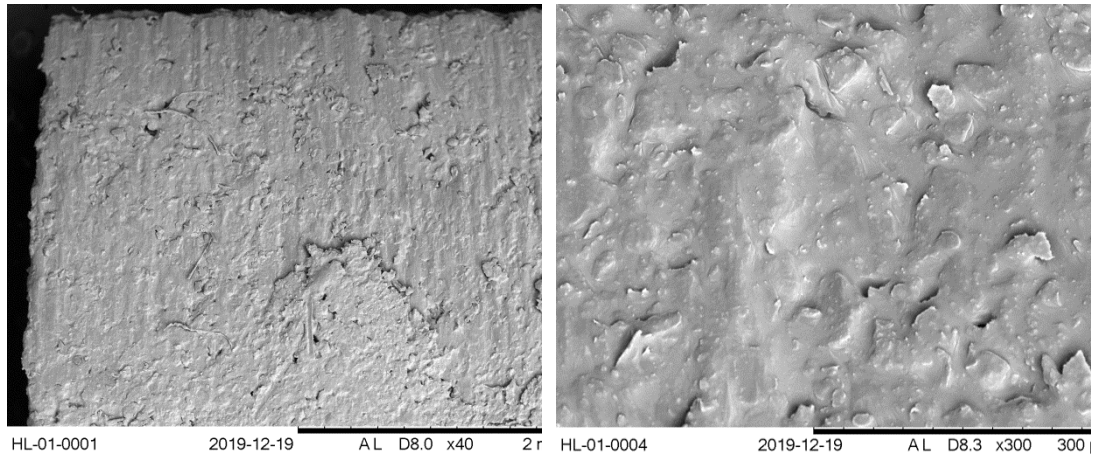


Figure 6.24: EOS PEEK HP3 gear tooth lubricated, Test 6.

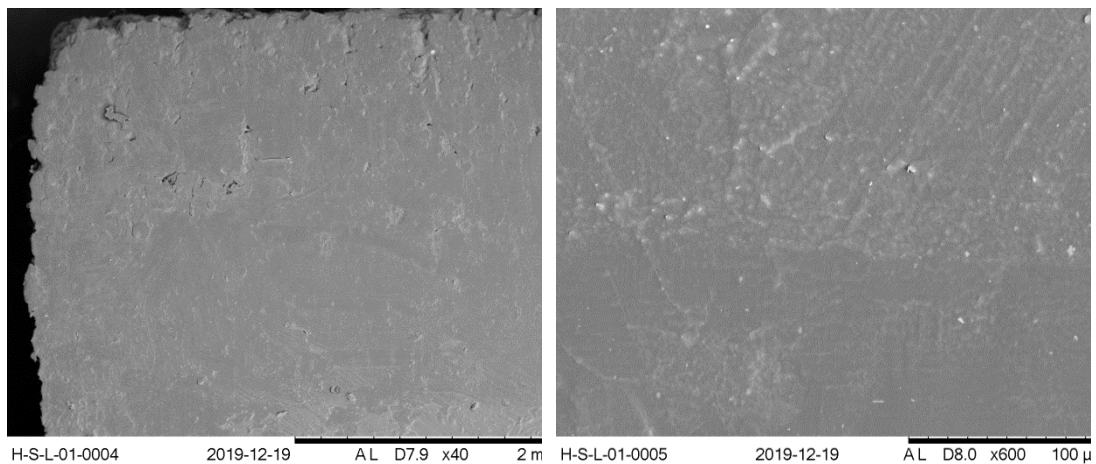


Figure 6.25: EOS PEEK HP3 of gear tooth lubricated Test 5.

It could be observed there was macro-pitting of larger scale on EOS PEEK HP3 teeth surface near the pitch point of the tooth, as (Figure 6.26 & Figure 6.27). After 4,500,000 cycles, a build-up of surface material was seen; this was due to the propagation of sintered particles on the surface.

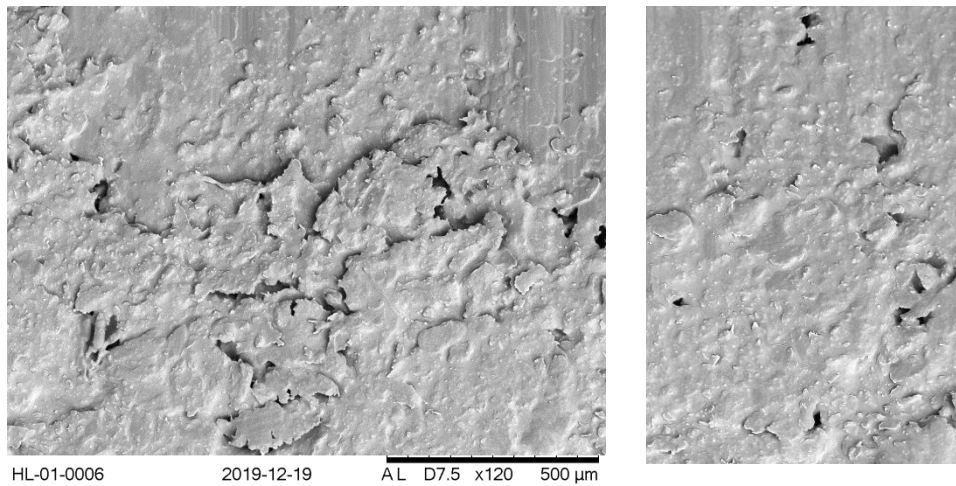


Figure 6.26: EOS PEEK HP3 gear in Test 6 (with lubricant).

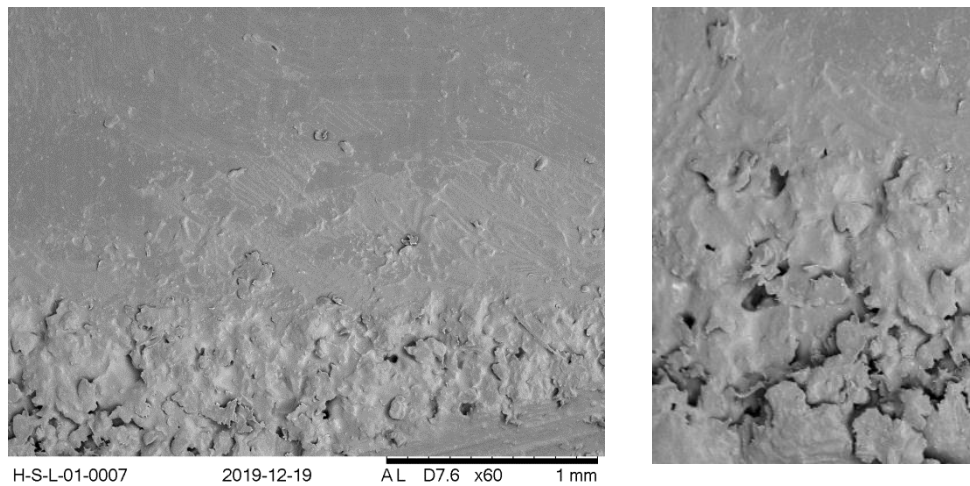


Figure 6.27: the pitch line of EOS PEEK HP3 gear in Test 5 (with lubricant)

The partly sintered layer borders on the ground surface were also evident in the bulk of the sample (Figure 6.26 & Figure 6.27). The progression of the material failure from cyclic stress, with and without lubrication, is concentrated partly on boundaries of sintered particles and thus the subsequent abstraction of the substance depends on the sintering phase.

After surface analysis, it was observed that the progression of failure was based on progression through the boundaries of particles between the layers formed.

It has been shown that the importance of this partly sintered material on porosity is small; however, wear mechanisms could change drastically when these particles were removed.

6.3 CONCLUSIONS

While identifying a specific polymer for such gears applications, it is essential to include consideration of the friction properties, type of lubrication and the manner in which the presence of the lubricant affects the surface's fatigue response will need to be considered.

This section investigated the gears for power transmission designed from EOS PEEK HP3, and the likely occurrence of, and mechanism leading to, bending failure and all the PEEK tests was depended on the results previous tests at university of Birmingham [2].

Bending fatigue was the chief failure of in the EOS PEEK HP3 gear tests, and the failed surfaces did show regions of fast fracture and progressive failure.

EOS PEEK HP3 gears, when run in non-lubricated conditions, demonstrated the following wear mechanisms: adhesion, asperity spread, fatigue and fretting, and with EOS PEEK HP3 vs. steel gears, polymer was relocated onto the conforming steel gear forming a layer. The layer is significantly more noticeable for low speeds and lowered subsequent contact abrasion.

As expected, the presence of lubrication lowered adhesion with no layer of polymer visible on the steel counterface. However, it was observed that steel gear's surface has layer from the silicone oil that was transferred from the

polymer surface. Again, as expected, because the silicone lubricant dampened tooth impacts the working life of the EOS PEEK HP3 gears increased.

After prolonged running, even in the presence of lubricant, the EOS PEEK HP3 gear surface has evident fatigue, and adjacent to the gear's pitch point this progressed into pitting on a large scale. The porosity of the polymer had a noticeable effect on the endurance of a gear; with failure paths, both for contact fatigue and bending, travelling along the boundaries between the layers laid down during manufacture.

These corresponded to the boundaries between the layers laid down during laser-sintering, and the presence of partially sintered particles on the polymer surface. The obvious conclusion is that the sintering process needs to be optimized to improve the durability of the manufactured component.

The relatively low toughness and ductility of laser-sintered polymers mean that with high power transmission, the presence of high shock loads will significantly affect its bending strength and fatigue. Thus, although such materials can be, and are, used for gears for low power transmission, their performance is often less than that of injection moulded counterparts.



CONCLUSIONS AND FUTURE WORK

7

“You will never do anything in this world without courage. It is the greatest quality of the mind next”

Aristotle

CONCLUSIONS AND FUTURE WORK

Machine parts of polymer are a growing research area and development; polymers capable of high performance, with lower density and requiring less lubrication would have significant advantages over traditional components. Despite this, there is a sense of wariness, even suspicion, attached to the use of these materials, possibly because their material properties and performance are neither well-documented nor well-understood.

Here we present the major findings of this research and make references for work in the future that could further enhance the knowledge of the properties and behaviour of polymers for use as machine elements in power transmission systems.

7.1 Chapter 4 Conclusion

The wear mechanisms of EOS PEEK HP3 have been studied using a twin disc rig with a range of the contact pressures and slip-ratios, in non-conformal, lubricated and non-lubricated rolling-sliding contact. The use of EOS PEEK HP3 disc vs EOS PEEK HP3 disc, EOS PEEK HP3 disc vs steel disc and PEEK disc vs steel disc has been tested under both low and high contact pressures. It was shown that high temperature

operation was possible despite some increase in wear, friction and surface temperature as the slip-ratio and the contact pressures increased under non-lubricated conditions.

In lubricated contact, it was found that the friction coefficient of the lubricated condition was lower and more stable than that of the non-lubricated condition. The results of this work demonstrated the possibility of surface lubrication reducing friction with EOS PEEK HP3. The results of the wear experiments showed that minimum silicone oil lubricant was effective in reducing the wear and the temperatures of the contact areas of the EOS PEEK HP3 samples.

The results of the wear experiments showed that the silicone oil surface lubricant was effective in reducing the wear and the area contact temperatures of EOS PEEK HP3 samples. The silicone oil surface lubrication implies lower oil levels so less cost and it will also reduce the weight.

The thin layer of the silicone oil that was stored in the pores inside the preliminary layers and the surface specimen; worked as good lubrication.

7.2 Chapter 5 Conclusion

Nevertheless, it was not easy to fully control the conditions of the tests. The High Frequency Friction Machine (TE77) energy pulse (EP) adaptor tests required a constant load and the obtained pressure profiles were derived from a given loading of the gear teeth.

The wear mechanisms for EOS PEEK HP3, PEEK CA30%, and PEEK were tested against steel, for a range of slip-ratios and applied loads in non-conformal roll/slide contact, both lubricated and non-lubricated conditions were explored, to investigate how the temperature of the roll/slide interaction affected the tribological properties of

the materials. However, the friction and wear all increase with load and slip ratio. Importantly, the wear rates obtained EOS PEEK HP3 using the TE77 apparatus were significantly lower than those obtained for PEEK CA30%, and PEEK.

Simplified geometry disc on plate has been a great help in indicating the likely performance of polymer materials for particular gear applications, showing much the same wear under specified sliding/ rolling speeds and loads. These results could be incorporated into the design process, and may help develop more effective, polymer gear systems that can sustain high loads. Experimental testing of polymer gears is advocated for a more complete appreciation of their in-situ response, because their kinematics is so very complex.

7.3 Chapter 6 Conclusion

While identifying a specific polymer for such gears applications, it is essential to include consideration of the friction properties, type of lubrication and the manner in which the presence of the lubricant affects the surface's fatigue response.

This section has investigation gears for power transmission designed from EOS PEEK HP3, the likely occurrence of, and mechanism leading to, bending failure.

The bending fatigue chief failure observed in the EOS PEEK HP3 gear tests, and the failed surfaces did show regions of fast fracture and progressive failure.

EOS PEEK HP3 gears, when run in non-lubricated conditions, demonstrated the following wear mechanisms: adhesion, asperity spread, fatigue and fretting, and when EOS PEEK HP3 were run against steel gears, polymer was relocated onto the conforming steel gear forming a layer. It was significantly more noticeable for low speeds and lowered subsequent contact abrasion.

As expected, the presence of lubrication lowered adhesion with no layer of polymer visible on the steel counterface. However, it was observed that the steel gear's surface has layer from the silicone oil that was transferred from the polymer surface. Again, as expected, because the silicone lubricant dampened tooth impacts the working life of the EOS PEEK HP3 gears increased.

After prolonged running, even in the presence of lubricant, surface fatigue was evident on the EOS PEEK HP3 gears, and adjacent to the gear's pitch point this progressed into pitting on a large scale. The porosity of the polymer had a noticeable effect on the endurance of a gear; with failure paths, both for contact fatigue and bending, travelling along the boundaries between the layers laid down during manufacture.

It was determined that limits were imposed on transmitted load and the gear's speed of rotation by the presence of partially sintered particles in the bulk of the material. These corresponded to the boundaries between the layers laid down during laser-sintering, and the presence of partially sintered particles on the polymer surface. The obvious conclusion is that the sintering process needs to be optimized to improve the durability of the manufactured component.

The relatively low toughness and ductility of laser-sintered polymers mean that with high power transmission, the presence of high shock loads will significantly affect its bending strength and fatigue. Thus, although such materials can be, and are, used for gears for low power transmission, their performance is often less than that of injection moulded counterparts.

7.4 Summary

This thesis has described on the relative dynamic performances of laser-sintered and injection-moulded poly-ether-ether-ketone (EOS PEEK HP3) gears and discusses the possibility of producing high performance polymer gears, manufactured by laser-sintering. Using Twin Disc test rig and TE77 EP-GEAR DYNAMICS test rig high frequency reciprocating tribometer to simulate polymer gears contact unlubricated and lubricated in addition to gears direct testing.

The wear rates and failure mechanisms, including contact fatigue and surface melting of laser-sintered and injection-moulded EOS PEEK HP3 were tested under conditions of relatively high loads and high slip-ratios.

It was observed that the coefficient of friction and wear rates were significantly below that of injection moulded PEEK. However, when using of laser sintered EOS PEEK HP3 for gears for transmission of power, the predominant failure mechanism was bending fatigue, and this meant using this material limited power transmission to low levels.

The improvement in tribological properties EOS PEEK HP3 with laser-sintering is better than the improvement of EOS PEEK HP3 and EOS PEEK HP3 with laser-sintering can be used for gears in power transmission.

Despite the advances made in laser-sintering of EOS PEEK HP3 further advances are required before it can be used for gears in power transmission.

7.5 Future Work

Outlined below are suggested research topics that could help increase the loads transmitted by laser-sintered polymer gears, and better the understanding of such materials. These suggestions are listed under the headings: tribological testing methods and specific application-based problems.

7.5.1 Tribological Testing and Mechanical

To further investigate the tribological responses and mechanical properties of selected laser-sintered polymers, to better our understanding of these materials. Ongoing research in this topic will lead to a better understanding of material-specific affects. Possible areas could be:

- The use of water and low viscosity lubricants.
- The relative wear of polished and unpolished surfaces. Material transfer was demonstrated to decrease the abrasive wear of non-lubricated gears of EOS PEEK HP3, thus for non-lubricated polymer and steel gears the effect of counterface roughness should be investigated.
- Noise emissions from working gears as a means to better understand the tribological responses of the materials in contact, could be investigated.
- Characterization of adhesion as a function of temperature for, in particular, EOS PEEK HP3 for a better understanding of the effect of temperature on the wear characteristics of it.
- Measured and calculated depth wear for the gear teeth during the test and without effect on the thermal efficiency of the EOS PEEK HP3 materials.

7.5.2 Gear Design

It is generally accepted that the only sure way to be confident when specifying a polymer for use as a gear is to test it experimentally. Thus, the design of laser-sintered

polymer gears should go hand-in-hand with experimental testing to be sure of the suitability of the design for its intended application.

Future research and development of polymer gears could include internal features such as, for example, cooling holes for temperature control, or to enhance control of shrinkage rates of the geometry of product gears, also, to investigate the advantages of tooth profile asymmetry.

Finally, there could be further investigation of the thermal gears properties for laser-sintered, such as quantifying the effect high temperatures on long-term fatigue.

REFERENCES

- [1] J. W. Humphrey, J. P. Oleson, A. N. Sherwood, and M. Nikolic, *Greek and Roman technology: a sourcebook: annotated translations of Greek and Latin texts and documents*. Psychology Press, 1998.
- [2] T. J. Hoskins, "The mechanical and tribological properties of PEEK gears," University of Birmingham, 2015.
- [3] H. Ono and N. J. Wade, "Depth and motion in historical descriptions of motion parallax," *Perception*, vol. 34, no. 10, pp. 1263-1273, 2005.
- [4] S. Kono, "Increase in power density of plastic gears for automotive applications," University of Birmingham, 2002.
- [5] R. J. Drago, *Fundamentals of gear design*. Butterworths Boston, 1988.
- [6] K. D. Dearn, "An investigation into tribological and performance related aspects polymeric gearing," The University of Birmingham, 2009.
- [7] D. Koffi, R. Gauvin, and H. Yelle, "Heat generation in thermoplastic spur gears," *Journal of Mechanisms, Transmissions, and automation in Design*, vol. 107, no. 1, pp. 31-36, 1985.
- [8] PLC Ticona. A guide to polymer gearing. Ticona company literature, Telford: Ticona PLC, (2006).
- [9] M. G. Rosato and D. V. Rosato, *Plastics design handbook*. Springer Science & Business Media, 2013.
- [10] R. G. Budynas and J. K. Nisbett, *Shigley's mechanical engineering design*. McGraw-Hill New York, 2008.
- [11] H. E. Merritt, *Gear Engineering*. London: Pitman. (1971).
- [12] K. D. Dearn, S. N. Kukureka, and D. Walton, "Engineering polymers and composites for machine elements, ," vol. in: S.K. Sinha B.J. Briscoe Ed. *Polym. Tribol.*, Imperial College Press, London, 2009: pp. 470–505., 2009.
- [13] J. Brandrup, E. Immergut, and E. A. Grulke, "Polymer handbook. 4th," *Edn. New York: A Wiley-Interscience publication*, 1999.
- [14] T. Hoskins, K. Dearn, Y. Chen, and S. Kukureka, "The wear of PEEK in rolling–sliding contact–Simulation of polymer gear applications," *Wear*, vol. 309, no. 1-2, pp. 35-42, 2014.
- [15] R. O. Ebewele, *Polymer science and technology*. CRC press, 2000.
- [16] D. G. Eckold, "Spinal implants-the problems of debris," University of Birmingham, 2016.
- [17] G. Stachowiak and A. W. Batchelor, *Engineering tribology*. Butterworth-Heinemann, 2013.
- [18] O. Reynolds, "IV. On the theory of lubrication and its application to Mr. Beauchamp tower's experiments, including an experimental determination of the viscosity of olive oil," *Philosophical Transactions of the Royal Society of London*, vol. 177, pp. 157-234, 1886.
- [19] K. Dearn, T. Hoskins, L. Andrei, and D. Walton, "Lubrication regimes in high-performance polymer spur gears," *Advances in Tribology*, vol. 2013, 2013.
- [20] K. Johnson, "Regimes of elastohydrodynamic lubrication," *Journal of Mechanical Engineering Science*, vol. 12, no. 1, pp. 9-16, 1970.
- [21] B. J. Hamrock and D. Dowson, "Isothermal elastohydrodynamic lubrication of point contacts: Part 1—Theoretical formulation," *Journal of Lubrication Technology*, vol. 98, no. 2, pp. 223-228, 1976.
- [22] Z. Jin, D. Dowson, and J. Fisher, "Analysis of fluid film lubrication in artificial hip joint replacements with surfaces of high elastic modulus," *Proceedings of*

- the Institution of Mechanical Engineers, Part H: Journal of Engineering in Medicine*, vol. 211, no. 3, pp. 247-256, 1997.
- [23] *Phenoce TE77 High Frequency Friction Machine Specification*. (2013) [Online]. Available from: <http://www.phoenix-tribology.com/cat/at2/spec/te77.htm> [Accessed 15/07/2018].
- [24] E. Ciulli, K. Stadler, and T. Draexl, "The influence of the slide-to-roll ratio on the friction coefficient and film thickness of EHD point contacts under steady state and transient conditions," *Tribology International*, vol. 42, no. 4, pp. 526-534, 2009.
- [25] M. Smeeth and H. Spikes, "The influence of slide/roll ratio on the film thickness of an EHD contact operating within the mixed lubrication regime," in *Tribology Series*, vol. 31: Elsevier, 1996, pp. 695-703.
- [26] C. Chan and L. Li, "An analysis of the effect of slide-to-roll ratio and surface velocity on wear using energy pulse and mean surface temperature approaches," *Wear*, vol. 236, no. 1-2, pp. 276-284, 1999.
- [27] M. Karimpour, K. Dearn, and D. Walton, "A kinematic analysis of meshing polymer gear teeth," *Proceedings of the Institution of Mechanical Engineers, Part L: Journal of Materials: Design and Applications*, vol. 224, no. 3, pp. 101-115, 2010.
- [28] J. D. Ferry and J. D. Ferry, *Viscoelastic properties of polymers*. John Wiley & Sons, 1980.
- [29] H. Blok, "The flash temperature concept," *Wear*, vol. 6, no. 6, pp. 483-494, 1963.
- [30] A. B. Cropper, "The failure mode analysis of plastic gears," University of Birmingham, 2003.
- [31] O. T.L., "Properties Influencing Wear of Metals," vol. J. Met. , no. 3, pp. 438-439, 1951.
- [32] I. Hutchings, "Tribology: Friction and Wear of Engineering Materials—CRC Press," *Boca Raton*, p. 137, 1992.
- [33] B. J. Briscoe and S. K. Sinha, "Tribological applications of polymers and their composites: past, present and future prospects," in *Tribology and Interface Engineering Series*, vol. 55: Elsevier, 2013, pp. 1-14.
- [34] B. Briscoe, "Wear of polymers: an essay on fundamental aspects," *TRIBOLOGY international*, vol. 14, no. 4, pp. 231-243, 1981.
- [35] K. Laux and C. Schwartz, "Influence of linear reciprocating and multi-directional sliding on PEEK wear performance and transfer film formation," *Wear*, vol. 301, no. 1-2, pp. 727-734, 2013.
- [36] H. Koike, K. Kida, E. C. Santos, J. Rozwadowska, Y. Kashima, and K. Kanemasu, "Self-lubrication of PEEK polymer bearings in rolling contact fatigue under radial loads," *Tribology International*, vol. 49, pp. 30-38, 2012.
- [37] S. Bahadur, "The development of transfer layers and their role in polymer tribology," *Wear*, vol. 245, no. 1-2, pp. 92-99, 2000.
- [38] P. L. Menezes, S. V. Kailas, and M. R. Lovell, "Friction and transfer layer formation in polymer–steel tribo-system: role of surface texture and roughness parameters," *Wear*, vol. 271, no. 9-10, pp. 2213-2221, 2011.
- [39] E. E. Nunez and A. A. Polycarpou, "The effect of surface roughness on the transfer of polymer films under unlubricated testing conditions," *Wear*, vol. 326, pp. 74-83, 2015.

- [40] W. Wieleba, "The mechanism of tribological wear of thermoplastic materials," *archives of civil and mechanical engineering*, vol. 7, no. 4, pp. 185-199, 2007.
- [41] T. Hoskins, K. Dearn, S. Kukureka, and D. Walton, "Acoustic noise from polymer gears—A tribological investigation," *Materials & Design*, vol. 32, no. 6, pp. 3509-3515, 2011.
- [42] A. Moore and D. Tabor, "Some mechanical and adhesive properties of indium," *British Journal of Applied Physics*, vol. 3, no. 9, p. 299, 1952.
- [43] J. Lancaster, "Basic mechanisms of friction and wear of polymers," *Plastics & polymers*, vol. 41, no. 156, pp. 297-306, 1973.
- [44] J. Lancaster, "Abrasive wear of polymers," *Wear*, vol. 14, no. 4, pp. 223-239, 1969.
- [45] N. Wright and S. Kukureka, "Wear testing and measurement techniques for polymer composite gears," *Wear*, vol. 251, no. 1-12, pp. 1567-1578, 2001.
- [46] Y. Chen, S. Kukureka, and C. Hooke, "The wear and friction of short glass-fibre-reinforced polymer composites in unlubricated rolling-sliding contact," *Journal of materials science*, vol. 31, no. 21, pp. 5643-5649, 1996.
- [47] D. Gordon and S. Kukureka, "The wear and friction of polyamide 46 and polyamide 46/aramid-fibre composites in sliding-rolling contact," *Wear*, vol. 267, no. 1-4, pp. 669-678, 2009.
- [48] H. Ruckdäschel, J. K. Sandler, and V. Altstädt, "On the friction and wear of carbon nanofiber-reinforced PEEK-based polymer composites," in *Tribology and Interface Engineering Series*, vol. 55: Elsevier, 2008, pp. 149-208.
- [49] R. Schroeder, F. Torres, C. Binder, A. Klein, and J. de Mello, "Failure mode in sliding wear of PEEK based composites," *Wear*, vol. 301, no. 1-2, pp. 717-726, 2013.
- [50] C. Hooke, S. Kukureka, P. Liao, M. Rao, and Y. Chen, "The friction and wear of polymers in non-conformal contacts," *Wear*, vol. 200, no. 1-2, pp. 83-94, 1996.
- [51] S. Nak-Ho and N. P. Suh, "Effect of fiber orientation on friction and wear of fiber reinforced polymeric composites," *Wear*, vol. 53, no. 1, pp. 129-141, 1979.
- [52] T. Ovaert and H. Cheng, "Counterface topographical effects on the wear of polyetheretherketone and a polyetheretherketone-carbon fiber composite," *Wear*, vol. 150, no. 1-2, pp. 275-287, 1991.
- [53] S. Kukureka, Y. Chen, C. Hooke, and P. Liao, "The wear mechanisms of acetal in unlubricated rolling-sliding contact," *Wear*, vol. 185, no. 1-2, pp. 1-8, 1995.
- [54] S. Kukureka, C. Hooke, M. Rao, P. Liao, and Y. Chen, "The effect of fibre reinforcement on the friction and wear of polyamide 66 under dry rolling-sliding contact," *Tribology International*, vol. 32, no. 2, pp. 107-116, 1999.
- [55] A. Avanzini, G. Donzella, A. Mazzù, and C. Petrogalli, "Wear and rolling contact fatigue of PEEK and PEEK composites," *Tribology international*, vol. 57, pp. 22-30, 2013.
- [56] T. Sinmazçelik and T. Yılmaz, "Thermal aging effects on mechanical and tribological performance of PEEK and short fiber reinforced PEEK composites," *Materials & design*, vol. 28, no. 2, pp. 641-648, 2007.
- [57] M. Buggy and A. Carew, "The effect of thermal ageing on carbon fibre-reinforced polyetheretherketone (PEEK)," *Journal of materials science*, vol. 29, no. 7, pp. 1925-1929, 1994.

- [58] M. Berer, Z. Major, and G. Pinter, "Elevated pitting wear of injection molded polyetheretherketone (PEEK) rolls," *Wear*, vol. 297, no. 1-2, pp. 1052-1063, 2013.
- [59] B. Bhushan, "Adhesion and stiction: mechanisms, measurement techniques, and methods for reduction," *Journal of Vacuum Science & Technology B: Microelectronics and Nanometer Structures Processing, Measurement, and Phenomena*, vol. 21, no. 6, pp. 2262-2296, 2003.
- [60] G. Jintang, "Tribocchemical effects in formation of polymer transfer film," *Wear*, vol. 245, no. 1-2, pp. 100-106, 2000.
- [61] E. Letzelter, M. Guingand, J.-P. De Vaujany, and P. Schlosser, "A new experimental approach for measuring thermal behaviour in the case of nylon 6/6 cylindrical gears," *Polymer testing*, vol. 29, no. 8, pp. 1041-1051, 2010.
- [62] K. Terashima, N. Tsukamoto, N. Nishida, and J. Shi, "Development of Plastic Gear for Power Transmission: Abnormal Wear on the Tooth Root and Tooth Fracture near Pitch Point," *Bulletin of JSME*, vol. 29, no. 251, pp. 1598-1604, 1986.
- [63] H. Düzcükoğlu, R. Yakut, and E. Uysal, "The use of cooling holes to decrease the amount of thermal damage on a plastic gear tooth," *Journal of failure analysis and prevention*, vol. 10, no. 6, pp. 545-555, 2010.
- [64] J.-g. Zhang, S.-j. Liu, and T. Fang, "Determination of surface temperature rise with the coupled thermo-elasto-hydrodynamic analysis of spiral bevel gears," *Applied Thermal Engineering*, vol. 124, pp. 494-503, 2017.
- [65] Y. Wang, W. Tang, Y. Chen, T. Wang, G. Li, and A. D. Ball, "Investigation into the meshing friction heat generation and transient thermal characteristics of spiral bevel gears," *Applied Thermal Engineering*, vol. 119, pp. 245-253, 2017.
- [66] A. Bravo, L. Toubal, D. Koffi, and F. Erchiqui, "Gear fatigue life and thermomechanical behavior of novel green and bio-composite materials VS high-performance thermoplastics," *Polymer Testing*, vol. 66, pp. 403-414, 2018.
- [67] W. Zhen, Y.-j. WANG, J.-j. WANG, S.-r. WANG, and K. Mao, "Study on the Instantaneous Temperature and Life Prediction of Polymer Gear Based on ANSYS/LS-DYNA," *DEStech Transactions on Computer Science and Engineering*, no. mso, 2018.
- [68] M. Rao, C. Hooke, S. Kukureka, P. Liao, and Y. Chen, "The effect of PTFE on the friction and wear behavior of polymers in rolling-sliding contact," *Polymer engineering & science*, vol. 38, no. 12, pp. 1946-1958, 1998.
- [69] A. Breeds, S. Kukureka, K. Mao, D. Walton, and C. Hooke, "Wear behaviour of acetal gear pairs," *Wear*, vol. 166, no. 1, pp. 85-91, 1993.
- [70] K. Mao, "A numerical method for polymer composite gear flash temperature prediction," *Wear*, vol. 262, no. 11-12, pp. 1321-1329, 2007.
- [71] Y. Chen, O. Modi, A. Mhay, A. Chrysanthou, and J. O'sullivan, "The effect of different metallic counterface materials and different surface treatments on the wear and friction of polyamide 66 and its composite in rolling-sliding contact," *Wear*, vol. 255, no. 1-6, pp. 714-721, 2003.
- [72] A. Harsha, R. Wäsche, and M. Hartelt, "Tribological studies on polyetherketone composite under reciprocating sliding condition against steel cylinder," *Proceedings of the Institution of Mechanical Engineers, Part J: Journal of Engineering Tribology*, vol. 229, no. 7, pp. 795-806, 2015.

- [73] M. Mbarek, S. Rhaiem, M. Kharrat, and M. Dammak, "Experimental simulation of the friction, temperature, and wear distributions for polyamide–steel gear contact using twin-disc setup," *Proceedings of the Institution of Mechanical Engineers, Part J: Journal of Engineering Tribology*, vol. 230, no. 9, pp. 1127-1138, 2016.
- [74] M. Kalin and A. Kupec, "The dominant effect of temperature on the fatigue behaviour of polymer gears," *Wear*, vol. 376, pp. 1339-1346, 2017.
- [75] P. K. Singh and A. K. Singh, "An investigation on the thermal and wear behavior of polymer based spur gears," *Tribology International*, vol. 118, pp. 264-272, 2018.
- [76] J. Moder, F. Grün, F. Summer, M. Kohlhauser, and M. Wohlfahrt, "Application of high performance composite polymers with steel counterparts in dry rolling/sliding contacts," *Polymer Testing*, vol. 66, pp. 371-382, 2018.
- [77] F. J. Ferfecki and A. Hale, "Polymer Gear Development to Improve Efficiency and NVH Performance of an Engine Mass Balance System," SAE Technical Paper0148-7191, 2011.
- [78] L. Snyder, "At the "PEEK" of the polymer food chain," *Gear Technology*. Available: http://www.geartechnology.com/articles/0610/At_the_PEEK_of_the_Polymer_Food_Chain, 2010.
- [79] K. Dearn, T. Hoskins, D. Petrov, S. Reynolds, and R. Banks, "Applications of dry film lubricants for polymer gears," *Wear*, vol. 298, pp. 99-108, 2013.
- [80] "Hertz, Über die Berührung fester elastischer Körper, J. Für Die Reine U. Angew. Math. 92 (1882) 156–171.."
- [81] K. Dearn, S. Kukureka, and D. Walton, "Engineering polymers and composites for machine elements," in *Polymer Tribology*: World Scientific, 2009, pp. 470-505.
- [82] "Slide-Roll Ratio versus Slip - Phoenix Tribology Ltd www.phoenix-tribology.com/wp.../Guidance-Slide-Roll-Ratio.pdf."
- [83] M. Plint and A. Alliston-Greiner, "The energy pulse: A new wear criterion and its relevance to wear in gear teeth and automotive engine valve trains," *Lubrication Science*, vol. 8, no. 3, pp. 233-251, 1996.
- [84] J. White, "The design and evaluation of polymer composite spur gears," University of Birmingham, 1999.
- [85] J. Atkinson, J. Hay, and M. Jenkins, "Enthalpic relaxation in semi-crystalline PEEK," *Polymer*, vol. 43, no. 3, pp. 731-735, 2002.
- [86] M. Jenkins, "Crystallisation in miscible blends of PEEK and PEI," *Polymer*, vol. 42, no. 5, pp. 1981-1986, 2001.
- [87] V. PLC, "Vitrex PEEK polymer properties guide," Lancashire, UK, 2009.
- [88] J. Greses and C. Stotko, "EOS innovations for e-manufacturing: High performance polymers and integrated quality management system," in *Innovative Developments in Design and Manufacturing*: CRC Press, 2009, pp. 677-682.
- [89] D. Drummer, D. Rietzel, and F. Kühnlein, "Development of a characterization approach for the sintering behavior of new thermoplastics for selective laser sintering," *Physics Procedia*, vol. 5, pp. 533-542, 2010.
- [90] "EOS, Material Data Sheet (preliminary) EOS PEEK HP3, 49 (n.d.) 1–2.."
- [91] G. Salmoria, J. Leite, R. Paggi, A. Lago, and A. Pires, "Selective laser sintering of PA12/HDPE blends: Effect of components on elastic/plastic behavior," *Polymer Testing*, vol. 27, no. 6, pp. 654-659, 2008.

- [92] B. Van Hooreweder, D. Moens, R. Boonen, J.-P. Kruth, and P. Sas, "On the difference in material structure and fatigue properties of nylon specimens produced by injection molding and selective laser sintering," *Polymer Testing*, vol. 32, no. 5, pp. 972-981, 2013.
- [93] U. Ajoku, N. Saleh, N. Hopkinson, R. Hague, and P. Erasenthiran, "Investigating mechanical anisotropy and end-of-vector effect in laser-sintered nylon parts," *Proceedings of the Institution of Mechanical Engineers, Part B: Journal of Engineering Manufacture*, vol. 220, no. 7, pp. 1077-1086, 2006.
- [94] R. Goodridge, C. Tuck, and R. Hague, "Laser sintering of polyamides and other polymers," *Progress in Materials Science*, vol. 57, no. 2, pp. 229-267, 2012.
- [95] M. Schmidt, D. Pohle, and T. Rechtenwald, "Selective laser sintering of PEEK," *CIRP Annals-Manufacturing Technology*, vol. 56, no. 1, pp. 205-208, 2007.
- [96] M. Beard, O. Ghita, J. Bradbury, S. Flint, and K. Evans, "Material characterisation of additive manufacturing components made from a polyetherketone (PEK) high temperature thermoplastic polymer," *Innovative Developments in Virtual and Physical Prototyping*, pp. 329-332, 2011.
- [97] O. Ghita, E. James, R. Trimble, and K. E. Evans, "Physico-chemical behaviour of poly (ether ketone)(PEK) in high temperature laser sintering (HT-LS)," *Journal of Materials Processing Technology*, vol. 214, no. 4, pp. 969-978, 2014.
- [98] O. Ghita *et al.*, "High Temperature Laser Sintering (HT-LS): An investigation into mechanical properties and shrinkage characteristics of Poly (Ether Ketone)(PEK) structures," *Materials & Design*, vol. 61, pp. 124-132, 2014.
- [99] T. Hoskins, K. Dearn, and S. Kukureka, "Mechanical performance of PEEK produced by additive manufacturing," *Polymer Testing*, vol. 70, pp. 511-519, 2018.
- [100] S. Berretta, K. Evans, and O. Ghita, "Additive manufacture of PEEK cranial implants: Manufacturing considerations versus accuracy and mechanical performance," *Materials & Design*, vol. 139, pp. 141-152, 2018.
- [101] Y. Chen, S. Kukureka, C. Hooke, and M. Rao, "Surface topography and wear mechanisms in polyamide 66 and its composites," *Journal of materials science*, vol. 35, no. 5, pp. 1269-1281, 2000.
- [102] D. Walton, A. Cropper, D. Weale, and P. K. J. P. o. t. I. o. M. E. Meuleman, Part J: *Journal of Engineering Tribology*, "The efficiency and friction of plastic cylindrical gears Part 1: Influence of materials," vol. 216, no. 2, pp. 75-78, 2002.
- [103] J. Sukumaran *et al.*, "Modelling gear contact with twin-disc setup," vol. 49, pp. 1-7, 2012.
- [104] P. Rae, E. Brown, and E. J. P. Orler, "The mechanical properties of poly (ether-ether-ketone)(PEEK) with emphasis on the large compressive strain response," vol. 48, no. 2, pp. 598-615, 2007.
- [105] H. J. T. I. Ìmrek, "Performance improvement method for Nylon 6 spur gears," vol. 42, no. 3, pp. 503-510, 2009.
- [106] D. Koffi, R. Gauvin, H. J. J. o. M. Yelle, Transmissions,, and a. i. Design, "Heat generation in thermoplastic spur gears," vol. 107, no. 1, pp. 31-36, 1985.
- [107] C. Hooke, S. Kukureka, P. Liao, M. Rao, and Y. J. W. Chen, "Wear and friction of nylon-glass fibre composites in non-conformal contact under combined rolling and sliding," vol. 197, no. 1-2, pp. 115-122, 1996.

- [108] F. E. Kennedy and X. Tian, "The effect of interfacial temperature on friction and wear of thermoplastics in the thermal control regime," in *Tribology Series*, vol. 27: Elsevier, 1994, pp. 235-244.
- [109] G. M. Ostberg and J. C. J. J. o. A. P. S. Seferis, "Annealing effects on the crystallinity of polyetheretherketone (PEEK) and its carbon fiber composite," vol. 33, no. 1, pp. 29-39, 1987.
- [110] S. Mukherjee, S. A. J. P. E. Jabarin, and Science, "Aging characteristics of oriented ply (ethylene terephthalate)," vol. 35, no. 14, pp. 1145-1154, 1995.
- [111] M. Schmidt, D. Pohle, and T. J. C. a. Rechtenwald, "Selective laser sintering of PEEK," vol. 56, no. 1, pp. 205-208, 2007.
- [112] S.-S. Yoo, D.-E. J. I. J. o. P. E. Kim, and Manufacturing, "Minimum lubrication technique using silicone oil for friction reduction of stainless steel," vol. 14, no. 6, pp. 875-880, 2013.
- [113] B. Gerjets, "THERMOPLASTIC ELASTOMERS • STRUCTURAL • WEAR CONDUCTIVE • COLOR • FLAME RETARDANT," *Product Development Engineer*, vol. rtpcompany.com rtp@rtpcompany.com., 2014.
- [114] J. G. Zhang and C. L. Cai, "Friction and wear properties of carbon fiber reinforced PEEK composites under water lubrication," in *Applied Mechanics and Materials*, 2011, vol. 66, pp. 1051-1054: Trans Tech Publ.
- [115] N. Khare and P. RJ, "Friction and wear characteristics of PEEK and PEEK composites in water lubricated slow speed sliding," *Tribology Online*, vol. 10, no. 1, pp. 84-90, 2015.
- [116] S.-S. Yoo and D.-E. Kim, "Minimum lubrication technique using silicone oil for friction reduction of stainless steel," *International Journal of Precision Engineering and Manufacturing*, vol. 14, no. 6, pp. 875-880, 2013.
- [117] A. Abdelbary, *Wear of polymers and composites*. Woodhead Publishing, 2015.
- [118] S. Wu and H. Cheng, "A sliding wear model for partial-EHL contacts," *Journal of Tribology*, vol. 113, no. 1, pp. 134-141, 1991.